IL
NUOVO CIMENTO
ORGANO DELLA SOCIETÀ ITALIANA DI FISICA
SOTTO GLI AUSPICI DEL CONSIGLIO NAZIONALE DELLE RICERCHE

VOL. VI, N. 4 *Serie decima* 1° Ottobre 1957

Interaction non locale séparable et matrice de collision (*).

M. GOURDIN et A. MARTIN

Laboratoire de Physique, Ecole Normale Supérieure - Université de Paris

(ricevuto il 5 Aprile 1957)

Summary. — The problem of determining a two body (e.g. nucleon-nucleon) interaction in the S state from the energy dependence of the experimental phase shift is studied with the assumption of a non-local separable central interaction. It is shown that, under this hypothesis, the interaction is given, in momentum space, by the solution of a Fredholm inhomogeneous integral equation of second kind. General properties of this equation enable one to show that, if the physical system has no bound state there exists at most one solution; if the system has one bound state there may exist a one parameter set of solutions. Explicit solutions are obtained when the energy dependence of the phase shift is exactly given by the shape-independent approximation. This treatment is extended to the case where $k \operatorname{tg} \delta$ is a rational function of the energy. In this case, existence and multiplicity of the solutions are related to the number of roots of an algebraic equation that are located in the upper complex half plane. Further, when the phase-shift remains between 0 and π or between 0 and $-\pi$ in the whole range of variation of the energy, our results are similar to those obtained when a local interaction is assumed: if the system has no bound state, the solution is unique; if the system has one bound state there exists a one-parameter set of solutions. On the other hand, if the energy dependence of the phase shift is no longer restricted as above, the problem can only be solved provided the values of the energy where δ goes through $n\pi$ satisfy certain inequalities. The solutions then obtained are correct in a mathematical sense, but their physical interest is questionable, because, in this case, there is no longer stability of the phase shift with respect to small variations of the interaction.

(*) Ce travail a été réalisé en partie grâce à une subvention de l'« United States Air Force, European Office, Air Research and Development Command ».

Introduction.

Il est interessant d'étudier dans quelle mesure l'interaction de deux particules peut être déterminée à partir de la matrice de collision correspondante. Celle-ci est supposée connue par analyse des sections efficaces expérimentales et des mesures de polarisation. Un tel problème est particulièrement important dans l'étude de la diffusion nucléon-nucléon. Plusieurs auteurs l'ont traité en supposant l'interaction « locale », c'est-à-dire représentable par un potentiel ([1-3]). Mais il est permis d'envisager, comme l'a suggéré WHEELER ([4]), une interaction plus générale appelée « non locale ». Le potentiel est alors remplacé par un opérateur intégral $V(\boldsymbol{r}, \boldsymbol{r}')$ et l'équation de Schrödinger de deux particules s'écrit, en coordonnées relatives:

$$\left(-\frac{\Delta}{2M_r} - E \right) \psi(\boldsymbol{r}) = -\int V(\boldsymbol{r}, \boldsymbol{r}') \psi(\boldsymbol{r}') \, \mathrm{d}^3 r' ,$$

où $\hbar = 1$, et $M_r =$ masse réduite des deux particules $= M/2$ dans le cas de deux nucléons.

L'interaction « locale » apparaît alors comme un cas particulier pour lequel:

$$V(\boldsymbol{r}, \boldsymbol{r}') = V(\boldsymbol{r}) \, \delta(\boldsymbol{r} - \boldsymbol{r}') .$$

Dans cet article nous considérerons uniquement des forces centrales. Les conditions d'invariance par rotation imposent alors à $V(\boldsymbol{r}, \boldsymbol{r}')$ la forme:

$$V(\boldsymbol{r}, \boldsymbol{r}') = \sum_{l=0}^{\infty} V_l(|\boldsymbol{r}|, |\boldsymbol{r}'|) \, P_l(\cos(\boldsymbol{r}, \boldsymbol{r}')) .$$

Un cas très simple est celui où $V_l(r, r')$ est le produit d'une fonction de r seulement par une fonction de r'. La condition d'hermiticité impose la forme suivante:

$$V_l(r, r') = \varepsilon_l u_l^*(r) \, u_l(r') \qquad \text{où} \qquad \varepsilon_l = \pm 1 .$$

Une telle interaction, appelée « séparable », permet une résolution exacte, au moyen de quadratures, de l'équation de Schrödinger du problème à deux

---

([1]) N. LEVINSON: *Dan. Mat. Fys. Medd.*, **25**, 9 (1949).

([2]) R. JOST et W. KOHN: *Phys. Rev.*, **87**, 977 (1952); **88**, 382 (1952); *Dan. Mat. Fys. Medd.*, **27**, (1953).

([3]) I. M. GEL'FAND et B. M. LEVITAN: *Dokl. Akad. Nauk URSS*, **77**, 557 (1951).

([4]) J. A. WHEELER: *Phys. Rev.*, **50**, 643 (1936).

corps. Elle a été proposée pour la première fois par WIGNER [5] et appliquée depuis par divers auteurs aux problèmes nucléon-nucléon [6,7]. Récemment P. C. MARTIN et C. DE DOMINICIS l'ont utilisée dans l'étude des propriétés de la matière nucléaire [8].

Nous nous sommes posé un problème analogue à celui qu'ont traité LEVINSON, JOST et KOHN, GEL'FAND et LEVITAN qui postulaient l'existence d'un potentiel: est-il possible de trouver une interaction séparable conduisant à une matrice de collision en accord avec les données expérimentales. Cette interaction est-elle unique [9]? Nous traiterons ces questions pour les états S. Mais l'étude des états de moment angulaire différent de zéro se fait d'une manière analogue sans nouvelles difficultés.

Notre hypothèse impose certaines restrictions au système des deux particules. Celui-ci ne peut admettre qu'un état lié au plus, ce qui est acceptable si ces particules sont des nucléons. D'autre part il est généralement admis qu'une interaction séparable conduit à un déphasage qui reste constamment compris dans un intervalle d'amplitude maximum π. Ceci est strictement vrai si la transformée de Fourier $v(p)$ de la fonction $u(r)$ n'admet aucun zéro. Si $v(p)$ s'annule pour une valeur p_0 de la quantité de mouvement il est généralement possible de fixer l'intensité de l'interaction de telle façon que la tangente du déphasage s'annule et change de signe à l'énergie $E_0 = p_0^2/2M_r$.

Les conditions à imposer au déphasage pour que le problème posé admette une solution sont donc moins restrictives que celles indiquées ci-dessus; nous les étudierons en détail dans l'h pothèse où $k \operatorname{tg} \delta$ est représentable par une fraction rationnelle en fonction de l'énergie. Nous déterminerons alors explicitement l'interaction séparable cherchée: elle est unique si le système n'admet aucun état lié; s'il existe un état lié la solution dépend d'un paramètre arbitraire. Ces résultats sont à rapprocher de ceux obtenus dans la recherche d'un potentiel phénoménologique [1-3] qui contient autant de paramètres arbitraires qu'il existe d'états liés.

Un compte rendu préliminaire de l'essentiel de ces résultats a déjà été publié [10].

---

[5] E. P. WIGNER: non publié, cité par BLATT et WEISSKOPF, p. 139.

[6] A. BLOCH, M. GELL-MANN et M. L. GOLDBERGER: non publié, cité par Y. YAMAGUCHI.

[7] Y. YAMAGUCHI: *Phys. Rev.*, **95**, 1628 (1954); Y. YAMAGUCHI et Y. YAMAGUCHI: *Phys. Rev.*, **95**, 1635 (1954).

[8] P. C. MARTIN et C. DE DOMINICIS: *Phys. Rev.*, **105**, 1419 (1957).

[9] Cette question posée au cours d'un séminaire par A. M. L. MESSIAH a été le point de départ de ce travail.

[10] M. GOURDIN et A. MARTIN: *Compt. Rend.*, **244**, p. 1153, 1329, 1469 (1957).

1. – Etude des solutions de l'équation de Schrödinger avec une interaction séparable (état S).

1·1. *Conditions d'existence d'une solution.* – Pour que l'équation de Schrödinger admette une solution il est nécessaire, comme dans le cas d'un potentiel local, d'imposer certaines restrictions à l'interaction « séparable » au voisinage de $r = 0$ et $r = +\infty$. Si $\varepsilon u(r)u(r')$ est l'interaction séparable agissant dans l'état S, l'équation radiale correspondante s'écrit:

$$W''(r) + k^2 W(r) = \varepsilon M(4\pi) \int r u(r) r' u(r') W(r') \, \mathrm{d}r' \,, \tag{1.1}$$

où $W(r)$ est la fonction d'onde réduite, $r\varphi(r)$. L'intégrale portant sur la variable r' étant indépendante de r, on est ramené aux deux équations suivantes:

$$\begin{cases} W''(r) + k^2 W(r) = C r u(r) \,, \\ C = \varepsilon M(4\pi) \int_0^\infty r' u(r') W(r') \, \mathrm{d}r' \,. \end{cases}$$

Si $u(r)$ se comporte comme $r^{-\alpha}$ au voisinage de $r = 0$, $W(r)$ se comporte comme $r^{3-\alpha}$ (le cas $\alpha = 2$ sera traité plus loin), et pour que C soit une quantité finie il est nécessaire que l'intégrale $\int_0^A r'^{4-2\alpha} \mathrm{d}r'$ soit convergente. Nous imposerons à α d'être strictement inférieure à $\frac{5}{2}$.

Une seconde condition apparaît si l'on veut que la section efficace à l'énergie zéro, c'est à dire le carré de la longueur de diffusion, reste finie (dans toute la suite nous supposerons qu'il n'y a pas de résonance à l'énergie zéro). Pour $k = 0$ la fonction d'onde réduite s'écrit:

$$W(r) = Ar + B - C \int_0^r \mathrm{d}r' \int_{r'}^\infty r'' u(r'') \, \mathrm{d}r'' \,.$$

La longueur de diffusion est liée au comportement asymptotique de l'intégrale écrite ci-dessus. Pour qu'elle soit finie on doit imposer qu'à grande distance $u(r)$ se comporte comme $r^{-\beta}$ avec $\beta > 3$.

1·2. *Calcul du déphasage S.* – Ce calcul du déphasage se fait plus aisément dans l'espace des moments. Nous définissons la transformation de Fourier

par les formules réciproques:

$$\psi(\boldsymbol{p}) = \int \exp\left[-i\boldsymbol{p}\boldsymbol{r}\right]\psi(\boldsymbol{r})\,\mathrm{d}^3r\,,$$

$$\psi(\boldsymbol{r}) = (2\pi^{-3})\int \exp\left[i\boldsymbol{p}\boldsymbol{r}\right]\psi(\boldsymbol{p})\,\mathrm{d}^3p\,,$$

et l'équation de Schrödinger dans l'état S prend la forme:

$$\varphi(p) = \frac{\delta(p-k)}{k^2} - \frac{1}{p^2-k^2}\,\frac{\varepsilon M}{2\pi^2}\int_0^\infty V(p,p')\varphi(p')p'^2\,\mathrm{d}p'\,,$$

la fonction d'onde radiale S étant définie par:

$$\varphi(p) = \int \psi(\boldsymbol{p})\,\mathrm{d}\Omega_p\,.$$

Le noyau $V(p, p')$ est séparable lui aussi:

$$V(p,p') = \varepsilon v(p)v(p')$$

avec

$$\text{(1.2)}\qquad \begin{cases} ru(r) = (2\pi^2)^{-1}\displaystyle\int_0^\infty pv(p)\sin pr\,\mathrm{d}p\,, \\ pv(p) = 4\pi\displaystyle\int_0^\infty ru(r)\sin pr\,\mathrm{d}r\,. \end{cases}$$

Dans ces conditions l'équation (1.1) se résout de manière exacte. Le retour dans l'espace de configuration et l'étude de la forme asymptotique de la solution permettent de définir le déphasage:

$$\text{(1.3)}\qquad -\frac{2}{\pi}\,k\,\mathrm{tg}\,\delta = \frac{f(k)}{1 + P\displaystyle\int_0^\infty \frac{f(p)\,\mathrm{d}p}{p^2-k^2}}\,,$$

où la fonction $f(p)$ est déduite du potentiel par la relation

$$f(p) = \frac{\varepsilon M}{2\pi^2}\,p^2v^2(p)\,.$$

Notons que $f(p)$ garde un signe constant. La formule que nous avons obtenue montre que $\operatorname{tg}\delta$ ne peut changer de signe en s'annulant que si le numérateur et le dénominateur de l'expression (1.3) s'annulent simultanément. Le plus souvent $\operatorname{tg}\delta$ change de signe en passant par un pôle et par suite δ reste constamment compris entre 0 et π ou 0 et $-\pi$.

Néanmoins il ne nous est pas possible d'exclure le cas où un zéro du numérateur et du dénominateur coïncident.

Les restrictions imposées à $u(r)$ se répercutent sur $f(p)$ et finalement sur $\operatorname{tg}\delta$.

— La condition $u(r) \sim 1/r^{\alpha}$ avec $\alpha < \frac{5}{2}$ pour $r \to 0$ fournit par transformation de Fourier (formule (1.2)) le comportement asymptotique de $p\,v(p)$ et par suite de $f(p)$:

$$f(p) \sim p^{1-\varepsilon'} \qquad \text{avec} \qquad \varepsilon' > 0\,. \tag{1.4}$$

Ceci permet de montrer que:

$$\lim_{k\to 0} P \int \frac{f(p)\,\mathrm{d}p}{p^2 - k^2} = 0\,,$$

c'est-à-dire $-(2k/\pi)\operatorname{tg}\delta \sim f(k)$ pour $k \to \infty$.

— La condition $u(r) \sim 1/r^{\beta}$, $\beta > 3$ pour $r \to \infty$ nous assure de la même manière que:

$$\frac{f(p)}{p^2} < B\,, \quad \text{pour } p \to 0, \tag{1.5}$$

et par conséquent:

$$\lim_{k\to 0} P \int_0^{\infty} \frac{f(p)\,\mathrm{d}p}{p^2 - k^2} = \int_0^{\infty} \frac{f(p)}{p^2}\,\mathrm{d}p\,.$$

On en déduit qu'au voisinage de $k = 0$

$$-\frac{2}{\pi}\frac{\operatorname{tg}\delta}{k} \simeq \frac{f(k)}{k^2}\left[1 + \int_0^{\infty} \frac{f(p)}{p^2}\,\mathrm{d}p\right]^{-1}.$$

2. – Equation intégrale donnant le potentiel. Théorèmes généraux.

En posant $-(2k/\pi)\operatorname{tg}\delta = g(k)$, on peut réécrire l'équation (1.3) sous la forme:

$$f(k) = g(k)\left[1 + P\int_0^{\infty} \frac{f(p)\,\mathrm{d}p}{p^2 - k^2}\right]. \tag{2.1}$$

Si nous supposons désormais $g(k)$ donné, cette équation est une équation intégrale de Fredholm de deuxième espèce déterminant $f(k)$, donc $v(k)$ et, par transformation de Fourier, l'interaction séparable dans l'espace de configuration. Les seules solutions physiquement intéressantes sont les solutions qui gardent un signe constant, continues et dérivables.

Les conditions trouvées à la Sect. 1 imposent:

$$\lim_{k\to 0}\frac{g(k)}{k^2} < B\,, \qquad \lim_{k\to\infty}\frac{g(k)}{k} = 0\,,$$

et

$$\left|\begin{array}{l} \lim\limits_{k\to 0}\dfrac{f(k)}{g(k)} = 1 + \displaystyle\int \frac{f(p)\,\mathrm{d}p}{p^2}\,, \\ \lim\limits_{k\to\infty}\dfrac{f(k)}{g(k)} = 1\,. \end{array}\right. \tag{2.2}$$

Les équations précédentes permettent d'énoncer le théorème suivant:

Théorème I. Si $g(+\infty) > 0$, $g(+0) < 0$ [11] l'équation (1.4) n'admet aucune solution acceptable.

En effet $f(k)$ est du signe de $g(+\infty)$, donc positif; il en est de même de $1 + \int f(p)\,\mathrm{d}p/p^2$. Pour que les égalités (1.2) soient vérifiées, il faudrait que $g(+0)$ soit positif, ce qui est contraire à l'hypothèse.

L'étude de la multiplicité des solutions se fait par examen de l'équation homogène:

$$\Phi(k) = g(k) P \int_0^\infty \frac{\Phi(p)\,\mathrm{d}p}{p^2 - k^2}\,, \tag{2.3}$$

où Φ est la différence entre deux solutions f_1 et f_2 de l'équation inhomogène. Les hypothèses faites sur les (1.4), (1.5) permettent d'affirmer que

$$\Phi(k) \quad \text{et} \quad P\int_0^\infty \frac{\Phi(p)\,\mathrm{d}p}{p^2 - k^2}\,,$$

existent dans tout l'intervalle $0 \mapsto +\infty$ pour k.

Nous allons démontrer le théorème suivant:

Théorème II. Toute solution physiquement acceptable de l'équation homogène garde un signe constant.

Nous utiliserons à cet effet plusieurs lemmes.

---

[11] On désigne par $g(+0)$ la quantité $g(\varepsilon)$, $\varepsilon > 0$ infiniment petit.

Lemme I. Si $\Phi(k)$ s'annule en changeant de signe au point $k = k_i$ alors l'intégrale $P\int\Phi(p)\,dp/(p^2 - k_i^2)$ est nulle.

En vertu de l'équation (2.3) ceci est trivial si $g(k_i) \neq 0$ ou si $g(k)$ s'annule sans changer de signe pour $k = k_i$.

Si $g(k)$ s'annule en changeant de signe, $1 + P\int f_1(p)\,dp/(p^2 - k_i^2) = 0$ et $1 + P\int f_2(p)\,dp/(p^2 - k_i^2) = 0$ afin que f_1 et f_2 ne changent pas de signe au point $k = k_i$. Par différence, on en déduit qu'ici encore $P\int(\Phi(p)\,dp)/(p^2 - k_i) = 0$.

Lemme II. La fonction $\Phi(k)$ ne peut pas s'annuler en changeant de signe en un nombre fini de points.

Supposons un instant que $\Phi(k)$ s'annule et change de signe aux points $k_1, k_2, \ldots, k_n$. La quantité

$$\frac{\Phi(p)}{(p^2 - k_1^2)(p^2 - k_2^2) \ldots (p^2 - k_n^2)},$$

conservera un signe constant et son intégrale ne pourra être nulle. Or, par décomposition de cette fraction rationnelle en élements simples, elle est nulle:

$$P\int_0^\infty \frac{\Phi(p)}{(p^2 - k_1^2) \ldots (p^2 - k_n^2)}\,dp = \sum_i a_i P\int \frac{\Phi(p)}{p^2 - k_i^2}\,dp = 0,$$

ce qui démontre par l'absurde le lemme II.

Nous excluons pour des raisons physiques la possibilité d'un point d'accumulation de tels zéros à distance finie.

Lemme III. La fonction $\Phi(p)$ ne peut pas s'annuler en changeant de signe en une suite infinie de points k sans point d'accumulation à distance finie.

Soient $k_1 k_2 \ldots k_n k_{n+1} \ldots$ la suite croissante, infinie de ces points. Considérons la quantité

$$u_n(p) = \frac{\Phi(p)(k_{n+1} - p^2)^{n-2}}{(k_1^2 - p^2)(k_2^2 - p^2) \ldots (k_n^2 - p^2)}.$$

Comme précédemment, en décomposant le coefficient de $\Phi(p)$ en éléments simples, nous montrons que l'intégrale $\int u_n(p)\,dp$ est nulle. Nous pouvons par ailleurs borner inférieurement en module cette intégrale si nous remarquons que l'intégrant garde un signe constant de $p = 0$ à $p = k_{n+1}$.

$$\left|\int_0^\infty u_n(p)\,dp\right| > \int_0^{k_2} |u_n(p)|\,dp - \int_{k_{n+1}}^\infty |u_n(p)|\,dp,$$

d'autre part

$$\text{pour} \quad 0 \leqslant p \leqslant k_2 \qquad |u_n(p)| > \left| \frac{\Phi(p)}{(k_2^2 - p^2)(k_1^2 - p^2)} \right| ,$$

$$\text{pour} \quad p \geqslant k_{n+1} \qquad |u_n(p)| < \left| \frac{\Phi(p)}{(k_2^2 - p^2)(k_1^2 - p^2)} \right| ,$$

par suite la première intégrale est bornée inférieurement par une quantité non nulle indépendante de n. La seconde est bornée supérieurement par

$$\int_{k_{n+1}}^{\infty} \frac{|\Phi(p)|}{(p^2 - k_2^2)(p^2 - k_1^2)} \mathrm{d}p .$$

Cette intégrale est convergente parce que $\int_0^{\infty} \Phi(p)\,\mathrm{d}p/(p^2 - k^2)$ a un sens.

En choisissant n assez grand, donc k_{n+1} assez grand, on peut rendre cette seconde intégrale aussi petite que l'on veut. On aboutit ici encore à une contradiction.

La réunion des lemmes II et III démontre le théorème II.

Théorème III. L'équation homogène admet au plus une solution physiquement acceptable.

Soient $\Phi_1(p)$ et $\Phi_2(p)$ deux solutions linéairement indépendantes de l'équation homogène. Il existe au moins un point k_0 tel que

$$\frac{\Phi_1'(k_0)}{\Phi_1(k_0)} \neq \frac{\Phi_2'(k_0)}{\Phi_2(k_0)} ,$$

la solution $\Phi_3 = \Phi_1(p)\,\Phi_2(k_0) - \Phi_2(p)\,\Phi_1(k_0)$ s'annule en changeant de signe pour une série de valeurs de k_i qui comprend au moins le point k_0. Etudions l'intégrale $P \int_0^{\infty} \Phi_3(p)/(p^2 - k_i^2)\,\mathrm{d}p$. Deux cas se présentent:

— ou bien $g(k)$ ne change pas de signe au point k_i et il est clair que

$$P \int_0^{\infty} \frac{\Phi_3(p)}{p^2 - k_i^2} \mathrm{d}p = 0 ,$$

— ou bien $g(k)$ s'annule en changeant de signe au point k_i et il a été démontré que

$$P \int \frac{\Phi_1(p)}{p^2 - k_i^2} \mathrm{d}p = P \int \frac{\Phi_2(p)}{p^2 - k_i^2} \mathrm{d}p = 0 .$$

Il suffit alors de reprendre les méthodes des lemmes II et III; mais ici nous savons qu'il existe au moins un point k_0 dans la suite des k_i et l'absurdité n'est levée qu'en prenant $\Phi_3 \equiv 0$.

Théorème IV. Si $g(+0)$ et $g(+\infty)$ sont de même signe l'équation homogène n'admet aucune solution.

Ce théorème utilise les deux propriétés suivantes:

a)
$$\lim_{k\to 0} P\int \frac{\Phi(p)\,dp}{p^2-k^2} = \int \frac{\Phi(p)\,dp}{p^2}\,.$$

Cette égalité vraie pour $f_1(p)$ et $f_2(p)$ l'est pour leur différence $\Phi(p)$.

b)
$$\lim_{k\to\infty} k^2 P\int_0^\infty \frac{\Phi(p)\,dp}{p^2-k^2} = \int_0^\infty \Phi(p)\,dp\,.$$

Pour établir cette propriété il faut étudier le comportement asymptotique de Φ. On peut montrer que si $g(k) \sim k^{1-\varepsilon}$, $\Phi(k) \sim k^{-1-\varepsilon}$. Il est alors aisé d'obtenir l'égalité ci-dessus.

Les limites *a)* et *b)* ont pour conséquence

$$\lim_{k\to 0}\left(\frac{\Phi(k)}{g(k)}\right) = \int_0^\infty \frac{\Phi(p)\,dp}{p^2}\,,$$

et

$$\lim_{k\to\infty}\left(\frac{\Phi(k)}{k^2 g(k)}\right) = -\int_0^\infty \Phi(p)\,dp.$$

Φ gardant un signe constant, en vertu du théorème III, ces deux équations ne sont compatibles que si $g(+0)$ et $g(+\infty)$ sont des signes contraires.

Théorème V. Si $\Phi(k)$ est solution de l'équation homogène, la solution générale de l'équation inhomogène est

$$-\frac{\Phi(k)}{\int_0^\infty \Phi(p)\,dp}\,[k^2+\lambda]\,.$$

En effet

$$\frac{k^2\Phi(k)}{g(k)} = -\int_0^\infty \Phi(p)\,dp + P\int_0^\infty \frac{p^2\Phi(p)\,dp}{p^2-k^2}\,.$$

L'intégrale $\int_0^\infty \Phi(p)\,dp$ n'est ni nulle ni infinie parce que $\Phi(p)$ a un signe constant et se comporte comme $p^{-1-\varepsilon}$ à l'infini. Ceci démontre que $k^2\Phi(k)/(-\int_0^\infty \Phi(p)\,dp)$ est une solution particulière de l'équation inhomogène.

Nous pouvons regrouper les résultat obtenus:

1) $g(+0) < 0$, $g(+\infty) > 0$: aucune solution.

2) $g(+0)\cdot g(+\infty) > 0$: l'équation homogène n'admet aucune solution. L'équation inhomogène a au plus une solution.

3) $g(+0) > 0$, $g(+\infty) < 0$: l'équation homogène admet au plus une solution (à un facteur multiplicatif près). Si cette solution existe la solution générale de l'équation inhomogène s'écrit:

$$-\Phi(k)[k^2+\lambda]\left[\int \Phi(p)\,dp\right]^{-1}.$$

L'étude des états liés du système va nous permettre de caractériser les divers cas précédents.

Théorème VI. Si $g(+0)\cdot g(+\infty) > 0$ le système n'admet aucun état lié. Si $g(+0) > 0$, $g(+\infty) < 0$ le système admet un état lié.

L'équation donnant les états liés du système s'écrit $1+\int_0^\infty f(p)dp/(p^2+x^2) = 0$. $f(p)$ ayant un signe constant, la fonction $F(x) = 1+\int_0^\infty f(p)\,dp/(p^2+x^2)$ est une fonction monotone de x qui varie de $1+\int_0^\infty f(p)dp/p^2$ à 1 lorsque x varie de 0 à ∞. Par conséquent le système admettra un état lié unique si $1+\int_0^\infty f(p)\,dp/(p^2) < 0$ et n'admettra aucun état lié si $1+\int_0^\infty f(p)\,dp/p^2 > 0$. Or la relation (2.2) montre que le signe de cette quantité est celui du produit $f(+0)g(+0)$ qui est aussi le signe de $g(+\infty)g(+0)$, puisque f est du signe de $g(+\infty)$, ce qui démontre le théorème.

On peut alors réécrire les conclusions sous la forme suivante:

1) $g(+\infty) > 0$, $g(+0) < 0$: pas de solution.

2) Si le système n'admet aucun état lié, l'équation inhomogène admet au plus une solution.

3) Si le système a un état lié l'équation homogène peut admettre au plus une solution, et l'équation inhomogène admet au plus une famille de solutions à un paramètre.

4) Si le système a plus d'un état lié, il n'est pas possible de représenter l'interaction par un potentiel non local séparable.

Nous n'avons jusqu'ici démontré en aucune manière l'existence de solutions, mais les théorèmes d'unicité que nous avons établis nous garantissent que, dans la suite de cette étude, nous ne laissons échapper aucune solution.

3. – Approximation indépendante de forme dans la diffusion nucléon-nucléon.

Nous supposons l'approximation indépendante de forme valable à toutes les énergies et nous représentons le déphasage par la relation:

$$k \operatorname{ctg} \delta = -\frac{1}{a} + \frac{1}{2} r_0 k^2 ,$$

a étant la longueur de diffusion et r_0 la portée. La fonction $g(k)$ correspondante s'écrit alors

$$g(k) = \frac{-(4/\pi r_0)k^2}{k^2 - (2/a r_0)} .$$

Nous distinguerons le cas singulet pour lequel la longueur de diffusion étant négative nous poserons $\alpha^2 = -2/a r_0$ et le cas triplet où cette fois la longueur de diffusion étant positive nous écrirons $\gamma^2 = 2/a r_0$. Avec ces notations nous pourrons exprimer $g(k)$ comme suit:

$$(3.1) \qquad \begin{cases} a) \quad g(k) = \dfrac{Ck^2}{k^2 + \alpha^2} \quad \text{pour l'état singulet} , \\ b) \quad g(k) = \dfrac{Ck^2}{k^2 - \gamma^2} \quad \text{pour l'état triplet} , \end{cases}$$

C est une constante négative égale à $-4/\pi r_0$.

Nous traiterons successivement les deux problèmes en commençant par le cas singulet.

3·1. *Etat singulet.* – La fonction inconnue $f(p)$ est une solution paire à signe constant — par sa définition — de l'équation intégrale:

$$(3.2) \qquad f(k) = \frac{Ck^2}{k^2 + \alpha^2} \left\{ 1 + P \int_0^\infty \frac{f(p)}{p^2 - k^2} \, \mathrm{d}p \right\} .$$

Nous allons essayer, pour $f(p)$, une fonction de même forme que $g(p)$, satisfaisant la condition (2.2):

$$f(p) = \frac{Cp^2}{p^2 + \beta^2},$$

où β est un nombre complexe à partie réelle strictement positive.

Si nous portons une telle expression dans l'équation (3.2), le calcul de l'intégrale se fait élémentairement et nous obtenons par identification, la relation suivante entre α, C, β:

$$\beta^2 + \frac{\pi C}{2}\beta - \alpha^2 = 0 . \tag{3.3}$$

Cette équation a toujours deux racines réelles, une positive et une négative. Il existe toujours une valeur et une seule de β, solution de cette équation, vérifiant les restrictions ci-dessus; nous avons donc déterminé une fonction $f(p)$ solution de notre problème. L'étude faite dans la seconde partie nous assure qu'il n'existe pas d'autre solution que celle que nous venons d'obtenir.

Il est alors facile de calculer explicitement l'interaction dans l'espace de configuration par transformation de Fourier (relation (1.2)); C étant négatif, on doit prendre $\varepsilon = -1$, ce qui correspond à un attraction dans l'état singulet S:

$$\varepsilon \cdot u(r)u(r') = \frac{-2}{\pi^3 r_0 M}\frac{\beta^2}{rr'} K_1(\beta r)K_1(\beta r') , \tag{3.3}$$

où K_1 est une fonction de Bessel du second type.

Aux données expérimentales de la diffusion neutron proton à basse énergie, $a_s = -23.7 \cdot 10^{-13}$ cm, $r_{0_s} = 2.5 \cdot 10^{-13}$ cm, correspond une portée

$$1/\beta = 1.19 \cdot 10^{-13} \text{ cm} .$$

Dans ces conditions la fonction radiale $w(r) = r\varphi(r)$, obéit à l'équation

$$\left(\frac{\mathrm{d}^2}{\mathrm{d}r^2} + k^2\right) w(r) + \frac{8\beta^2}{\pi^2 r_0} K_1(\beta r) \int_0^\infty K_1(\beta r')w(r')\,\mathrm{d}r' = 0 .$$

L'intégrale qui apparait ici est une constante indépendante de r. Il s'en suit que, puisque $K_1(\beta r)$ est équivalent, au voisinage de zéro, à $1/\beta r$, la solution $w(r)$, nulle à l'origine, se comporte comme $r \operatorname{Log} r$. On vérifie a postériori que l'intégrale apparaissant dans l'équation est bien convergente. La fonction d'onde $\varphi(r)$ diverge logarithmiquement à l'origine. Mais cette solution est

néanmoins parfaitement acceptable. En effet, d'une part elle est de carré sommable, d'autre part l'intégrale $\int (H - E)\varphi(r)\,\mathrm{d}^3r$ étendue à un petit volume entourant l'origine est rigoureusement nulle. Ces conditions sont suffisantes ([12]).

Il est intéressant de comparer cette situation à celle des potentiels locaux envisagés par K. M. Case ([13]). A une énergie donnée nous pouvons définir un potentiel local équivalent par la relation

$$V(r) = \varepsilon \frac{u(r)}{\Phi(r)} \int u(r')\Phi(r')4\pi r'^2\,\mathrm{d}r'.$$

Dans le cas présent, le potentiel local équivalent est donc en 1 (r^2 Log r) à l'origine. Il est par conséquent moins singulier que $1/r^2$ qui correspond à la singularité maximum permise où suivant l'intensité du potentiel attractif il existe ou n'existe pas de solution de l'équation de Schrödinger.

3.2. *Etat triplet*, – Le cas de l'état triplet S se traite d'une manière analogue avec une fonction d'essai de même forme. Nous sommes alors conduits à une équation du second degré en β:

$$\beta^2 + \frac{\pi C}{2}\beta + \gamma^2 = 0\,, \tag{3.4}$$

dont les deux racines distinctes ou confondues ont toujours une partie réelle positive ($C < 0$).

Examinons d'abord le cas de deux solutions:

$$f_1(p) = \frac{Cp^2}{p^2 + \beta_1^2}\,, \qquad f_2(p) = \frac{Cp^2}{p^2 + \beta_2^2}\,,$$

pour lesquelles β_1 et β_2 sont réelles. La quantité $f_1(p) - f_2(p)$ est alors solution de l'équation intégrale homogène, et nous savons qu'en vertu des théorèmes généraux (2ème partie) c'est la seule. La solution générale s'écrira donc

$$f(p) = \lambda f_1(p) + (1 - \lambda) f_2(p)\,.$$

λ est une constante, réelle dans ce cas où β_1 et β_2 sont réels afin que $f(p)$ soit également réel. Par un changement de paramètre simple nous mettons $f(p)$ sous le forme:

$$f(p) = \frac{Cp^2(p^2 + \varrho)}{(p^2 + \beta_1^2)(p^2 + \beta_2^2)}\,,$$

([12]) P. A. M. Dirac: *Quantum Mechanics* (3ème édition), p. 156.
([13]) K. M. Case: *Phys. Rev.*, **80**, 797 (1950).

le paramètre ϱ étant positif pour que $f(p)$ conserve un signe constant quel que soit p.

Soient maintenant deux racines imaginaires conjuguées β et β^*. Formons à nouveau la combinaison $\lambda f_1+(1-\lambda)f_2$. Si nous prenons $\lambda=\frac{1}{2}+i\mu$, la solution f est réelle et s'écrit:

$$f(p) = \frac{Cp^2(p^2+\varrho)}{(p^2+\beta^2)(p^2+\beta^{*2})}.$$

Enfin l'équation en β peut avoir une racine double lorsque $\gamma = -\pi C/4$. Nous essayons alors une solution

$$f(p) = \frac{Cp^2(p^2-\varrho)}{(p^2+\gamma^2)^2},$$

et vérifions, par identification, que l'équation intégrale est bien satisfaite dans ce cas particulier.

En conclusion, nous avons trouvé pour $f(p)$, une solution à un paramètre continu qui peut s'écrire, à l'aide des fonctions symétriques des racines de l'équation (3.4):

$$f(p) = \frac{Cp^2(p^2+\varrho)}{p^4+p^2[(\pi^2C^2/4)-2\gamma^2]+\gamma^4}, \tag{3.5}$$

ϱ ne prendra que des valeurs positives afin que $f(p)$ puisse garder un signe constant.

En général le calcul de $u(r)$ à partir de cette expression de $f(p)$ ne peut se faire que numériquement. Seules les solutions particulières f_1 et f_2 conduiront à des calculs analytiques.

Les singularités de l'interaction et de la fonction d'onde au voisinage de $r=0$ sont les mêmes que précédemment, soit respectivement r^2 et $\mathrm{Log}\, r$.

4. – La tangente du déphasage est une fraction rationnelle fonction de l'énergie.

Nous nous proposons de trouver une classe de fonctions $f(p)$ solutions de l'équation intégrale (2.1) dans le cas où $g(k)$ est une fraction rationnelle réelle. L'équation de Schrödinger étant invariante par changement de k en $-k$, le déphasage $\delta(k)$ prolongé par les valeurs négatives de k est une fonction impaire de k et par suite la fonction $g(k)$ est paire par rapport à k. Nous supposerons que $g(k)$ possède $2n$ pôles complexes $\pm i\alpha_n[\mathrm{Re}\,\alpha_n>0]$ et $2r$ pôles purement réels $\pm\gamma_q(\gamma_q>0)$.

Les conditions imposées d'une manière générale (1ère partie) aux déphasages:

$$\lim_{\substack{k\to 0\\ k\to\infty}} \frac{g(k)}{k} = 0\,,$$

entraînent pour la décomposition de $g(k^2)/k^2$ en éléments simples la forme suivante

$$g(k^2) = 2k^2\left[\sum_1^n \frac{A_p}{k^2+\alpha_p^2} + \sum_1^r \frac{C_q}{k^2-\gamma_q^2}\right]. \tag{4.1}$$

4·1. *Forme de la fonction* $f(p)$. – La fonction $f(p)$ doit être solution de l'équation intégrale

$$f(k) = g(k)\left[1 + P\int_0^\infty \frac{f(p)}{p^2-k^2}\,\mathrm{d}p\right], \tag{4.2}$$

et nous pourrons appliquer la méthode des résidus pour calculer l'intégrale en valeur principale puisque $f(p)$ satisfait aux conditions suivantes:

a) $f(p)/p \to 0$ quand $p \to \infty$ et dans le demi-plan supérieur du plan complexe de p. On appelle z la variable complexe correspondante.

b) $f(p)$ n'a aucun pôle sur l'axe réel.

c) On suppose que $f(z)$ satisfait à une condition de symétrie dans le plan complexe qui est du type de celle imposée à la matrice S et par conséquent à $g(z)$:

$$f(-z^*) = f^*(z)\,. \tag{4.3}$$

Nous nous limiterons à une fonction $f(z)$ méromorphe, sans pôles multiples pour l'instant. Soit β_j un pôle situé dans le demi-plan supérieur ($\mathrm{Re}\,\beta_j > 0$). La fonction $f(z)$ est réelle sur l'axe réel; elle admet donc également le pôle β_j^*; la condition de symétrie (4.3) nous montre qu'existent également les pôles $-\beta_j$ et $-\beta_j^*$. Compte tenu des conditions limites (1.4), (1.5) pour $p = 0$ et $p = +\infty$, nous obtenons pour $f(p)$ le développement

$$f(p) = 2p^2 \sum_{j=1}^m \frac{b_j}{\beta_j}\,\frac{1}{p^2-\beta_j^2}\,. \tag{4.4}$$

Il reste alors à porter l'expression (4.4) dans l'équation (4.2), ce qui conduit à l'identité

$$\sum_j \frac{b_j}{\beta_j}\,\frac{1}{k^2-\beta_j^2} \equiv \left[\sum_1^n \frac{A_p}{k^2+\alpha_p^2} + \sum_1^r \frac{C_q}{k^2-\gamma_q^2}\right]\left[1 - i\pi\sum_j \frac{b_j}{k^2-\beta_j^2}\right]. \tag{4.5}$$

4.2. *Degré d'indétermination du problème.* – Une égalité de fractions rationnelles nous permet d'avoir des renseignements sur le degré des polynômes qui composent ces fractions rationnelles. Nous supposerons les deux membres de (4.5) mis sous la forme de quotients de polynômes dont on spécifie le degré en k^2

$$f(k^2) = \frac{2k^2 P_{m-1}}{Q_m}, \qquad g(k^2) = \frac{2k^2 R_{n+r-1}}{S_{n+r}}.$$

L'identité (4.5) devient

$$\frac{P_{m-1}}{Q_m} = \frac{R_{n+r-1}}{S_{n+r}} \frac{T_m}{Q_m}. \tag{4.6}$$

Les fractions P/Q, R/S, T/Q sont irréductibles et le coefficient du terme de plus haut degré de Q, S et T est l'unité. L'identité (4.6) impose que S divise T:

$$T_m \equiv S_{n+r} V_t . \tag{4.7}$$

Ceci définit un polynôme V, de degré t en k^2 qui a lui aussi comme coefficient du terme de plus haut degré 1. Le problème n'a de sens que si:

$$t \geqslant 0 .$$

Dans ces conditions il est facile de déterminer P à partir de R:

$$P_{m-1} \equiv R_{n+r-1} V_t . \tag{4.8}$$

Nous avons au total $m+n+r$ relations (m provenant de (4.7) et $(n+r)$ de (4.8)) pour déterminer $2m$ quantités (les b_j et les β_j). Le problème admet donc t paramètres arbitraires et ce sont les coefficients du polynôme V_t.

Il est possible de tirer des relations (4.6, 7, 8) des renseignements généraux sur le comportement de $f(p)$. En effet, les β_j étant complexes, le polynôme Q conserve un signe constant. Le signe de $f(p)$ est le même que celui de P, c'est-à-dire celui du produit $R \cdot V$. D'où les conséquences suivantes:

a) les zéros de $f(k)$ sont les mêmes que ceux de $g(k)$ et de $V_t(k)$.

b) $f(k)$ garde un signe constant au voisinage d'un pôle de $g(k)$.

Or, nous cherchons des solutions $f(p)$ de signe constant. Si $g(k)$ possède un zéro d'ordre impair, on imposera donc à $V_t(k)$ d'avoir au même point un zéro d'ordre impair.

4.3. *Equation permettant de trouver* β_j. – Développons le second membre de (4.5) en éléments simples. Si nous identifions les termes en $1/(k^2+\beta_j^2)$ dans

les deux membres nous obtenons:

$$1 = -i\pi\beta_j \left[\sum_{p=1}^{n} \frac{A_p}{\alpha_p^2 + \beta_j^2} + \sum_{q=1}^{r} \frac{C_q}{\beta_j^2 - \gamma_q^2} \right]. \tag{4.9}$$

Cette égalité, qui peut encore s'écrire

$$g(\beta_j^2) = \frac{2i}{\pi} \beta_j ,$$

devient une fois rendue entière, une équation algébrique en β_j, de degré $2(n+r)$, dont nous cherchons les racines à partie imaginaire positive. Considérons une équation auxiliaire dépendant d'un paramètre réel positif λ:

$$\lambda g(z_\lambda^2) = \frac{2i}{\pi} z_\lambda , \tag{4.10}$$

identique à l'équation (4.9) pour $\lambda = 1$. Tout d'abord il est clair qu'une valeur z_λ réelle n'est jamais solution de (4.10), le premier membre étant alors réel et le second imaginaire pur. Donc, lorsque λ varie, une racine z_λ ne traversera pas l'axe réel et il est suffisant d'étudier la position des z_λ lorsque λ est infiniment petit. Nous partirons des valeurs z_0 pour classer les racines z_λ.

a) Les solutions construites à partir de $z_0 = i\alpha_p$ seront dans le demi-plan supérieur, celles construites à partir de $z_0 = -i\alpha_p$ dans le demi-plan inférieur. Il y en a n de ce type dans chaque demi-plan.

b) Pour les racines se déduisant des $z_0 = \pm\gamma_q$ réels le problème est plus délicat. Posons $\mathrm{Im}\,(z_\lambda) = \mathrm{Im}(z_\lambda - \gamma_q) = \sigma$. Au voisinage de $\lambda = 0$ l'équation (4.10) ne peut être vérifiée que si $C_q\sigma < 0$. Les deux solutions correspondant à $\pm\gamma_q$ sont dans le demi-plan supérieur ($\sigma > 0$) si le coefficient C_q est négatif et dans le demi-plan inférieur ($\sigma < 0$) dans le cas contraire.

En conclusion, si s est le nombre de coefficients du développement (4.1) négatifs, l'équation (4.9) admet $(n+2s)$ racines β_j dans le demi-plan supérieur. Nous avons alors $m = n + 2s$, ce qui d'après (4.7) s'écrit:

$$r + t = 2s .$$

Le problème n'est possible que si $2s - r \geqslant 0$.

L'équation (4.9) peut avoir une ou plusieurs racines doubles, purement imaginaires. On peut voir aisément que l'adjonction au développement (4.4) d'un terme du type

$$p^2 \frac{d_j}{(p^2 - \beta_j^2)^2} ,$$

entraîne pour β_j une condition supplémentaire, celle de vérifier l'équation dérivée par rapport à β_j de (4.9); β_j est donc bien une racine double de (4.9). L'introduction d'un terme supplémentaire laisse alors inchangé le nombre de paramètres arbitraires, t.

4·4. *Réduction de l'indétermination t.* – Il nous faut utiliser le fait que $f(p)$ doit être de signe constant, donc imposer à $V_t(k^2)$ d'avoir les mêmes zéros impairs que $g(k^2)$. Commençons par examiner le cas où $g(k^2)$ n'a aucun zéro impair.

Traduisons cette condition en examinant la représentation graphique de $g(k)$. Nous avons $2r$ pôles réels $\pm\gamma_q$ et l'allure de la courbe au voisinage d'un pôle est déterminée par le signe du coefficient C_q. Nous avons deux positions possibles (Fig. 1). Une condition nécessaire pour que $g(k^2)$ n'ait aucun zéro impair est donc que les signes des C_q, rangés dans l'ordre croissant des γ_q, soient alternés. Le signe du dernier, C_r étant celui de $g(+\infty)$. Nous avons donc trois seules possibilités:

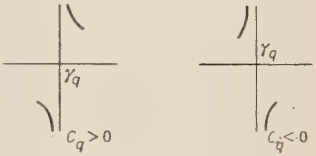

Fig. 1

a) *r est pair* et $s = r/2$ donc $t = 0$: le problème ne comporte aucun arbitraire, $f(p)$ admet la solution unique

$$f(p) = 2p^2 \frac{R_{n+r-1}(p^2)}{\prod_1^{n+r} (p^2 - \beta_j^2)} ,$$

les β_j sont les solutions situées dans le demi-plan supérieur de l'équation (4.9), prises avec leur ordre de multiplicité. Remarquons que, puisque $s = r/2$, $g(+0)$ et $g(+\infty)$ ont le même signe.

b) *r est impair* et $s = (r+1)/2$; dans ce cas $t = 1$: le problème admet une solution à un paramètre $f(p)$ que l'on peut écrire

$$f(p) = 2p^2 \frac{(p^2 + \varrho) R_{n+r-1}(p^2)}{\prod_1^{n+r+1} (p^2 - \beta_j^2)} ,$$

le paramètre ϱ ne pourra prendre que des valeurs positives afin que $f(p)$ conserve un signe constant. D'autre part, nous avons $C_r < 0$ et ceci entraîne pour g les signes suivants:

$$g(+\infty) < 0 , \qquad g(+0) > 0 .$$

c) *r est impair* et $s = (r-1)/2$: nous avons $t = -1$ et le problème n'admet pas de solution $f(p)$ de signe constant. Comme nous avons $C_r > 0$, g possède les signes suivants

$$g(+\infty) < 0\,, \qquad g(+0) > 0\,.$$

Nous retrouvons la propriété générale (Théorème I) qu'il est impossible dans ce cas de trouver une solution physique au problème.

Ces situations sont illustrées par la Fig. 2.

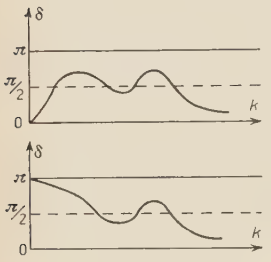

Fig. 2.

a) $r = 4 \quad t = 0 \quad s = 2$
b) $r = 3 \quad t = 1 \quad s = 2$

Supposons maintenant que $g(k)$ s'annule et change de signe en un nombre σ de points k_i. Nous imposons alors à $V_t(k^2)$ d'avoir en ces points k_i un zéro simple. Par conséquent $f(k^2)$ aura un zéro d'ordre pair n'entraînant aucun changement de signe. Nous aurons ainsi σ conditions supplémentaires à vérifier et l'indétermination sera en réalité $\tau = t - \sigma$; le problème n'aura de solution physique que si $\tau > 0$.

Nous associons à chaque zéro d'ordre impair k_i de $g(k)$ la dérivée $h_i = g'(k_i)$ et ordonnons la suite des C_q et h_i dans l'ordre croissant des σ_q et k_i correspondants. Il est aisé de voir sur la représentation graphique de $g(k)$ que cette suite est alternée. Appelons σ_1 le nombre de h_i négatifs. Nous avons cette fois encore trois possibilités:

a) $r+\sigma$ *est pair*, soit $r+\sigma = 2(s+\sigma_1)$: l'indétermination τ vaut alors $-2\sigma_1$. Le problème n'est possible que si $\sigma_1 = 0$; la solution est alors unique et elle s'écrit:

$$f(p) = \frac{2p^2(p^2-k_1^2)(p^2-k_2^2)\ldots(p^2-k_\sigma^2)R_{n+r-1}(p^2)}{\prod_1^{m=n+r-\sigma}(p^2-\beta_j^2)}\,.$$

$g(+\infty)$ et $g(+0)$ sont dans ce cas de même signe.

b) $r+\sigma$ *est impair* avec $r+\sigma = 2(s+\sigma_1)-1$: l'indétermination vaut alors $1-2\sigma_1$. Il nous faut cette fois encore $\sigma_1 = 0$: la solution du problème contient un paramètre arbitraire; elle s'écrit:

$$f(p) = \frac{2p^2(p^2+\varrho)(p^2-k_1^2)\ldots(p^2-k_\sigma^2)R_{n+r-1}(p^2)}{\prod_1^{m=n+r+\sigma+1}(p^2-\beta_j^2)}\,.$$

Les signes correspondants de g sont alors:

$$g(+\infty) < 0\,, \qquad g(+0) > 0\,.$$

c) $r+\sigma$ *est impair* avec $r+\sigma = 2(s+\sigma_1)+1$: l'indétermination étant égale à $-1-2\sigma_1$, le problème est impossible et ceci correspond au cas où $g(+\infty)>0$ et $g(+0)<0$.

4·5. *Relation entre les déphasages et les états liés.* – Nous avons montré que les solutions à un paramètre décrivaient des systèmes possédant un état lié et que les solutions définies de manière unique étaient relatives à des systèmes n'admettant pas d'état lié.

Etudions maintenant la variation globale du déphasage δ entre $k=0$ et $k=+\infty$. Puisque $\sigma_1=0$, tous les h_i sont positifs et nous obtenons:

a) $g(+0)g(+\infty)>0$ pas d'état lié, solution unique:

$$\delta(0)-\delta(+\infty)=\sigma\pi\,.$$

b) $g(+0)>$, $g(+\infty)<0$ un état lié, solution à un paramètre:

$$\delta(0)-\delta(+\infty)=\pi+\sigma\pi\,.$$

c) $g(+0)<0$, $g(+\infty)>0$ pas de solution au problème:

$$\delta(0)-\delta(+\infty)=-\pi+\sigma\pi\,.$$

La Fig. 3 montre des exemples de ces différents cas.

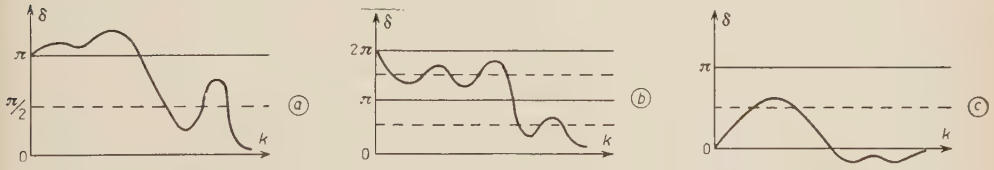

Fig. 3. *a)* $r=3$ $s=2$ $t=1$ $\sigma=1$ $\tau=0$ $\sigma_1=0$
b) $r=8$ $s=5$ $t=2$ $\sigma=1$ $\tau=1$ $\sigma_1=0$
c) $r=2$ $s=1$ $t=0$ $\sigma=1$ $\tau=-1$ $\sigma_1=0$

5. – Discussion des résultats et conclusion.

Lorsque la tangente du déphasage ne s'annule pas en changeant de signe (passage du déphasage par les valeur $h\pi$), nos résultats sont bien en accord avec ceux de LEVINSON [1] établis pour une classe de potentiels locaux: si $\delta(+0)-\delta(+\infty)$ est égal à $n\pi$ (ou $(n+\frac{1}{2})\pi$ pour le cas d'une résonance à l'énergie zéro, circonstance que nous avons écartée) on a n états liés et si $\delta(+0)-\delta(+\infty)$ est inférieur à π, le potentiel correspondant est unique. La condition pour que la donnée du déphasage en fonction de l'énergie, $\delta(k)$,

détermine biunivoquement le potentiel est donc qu'il n'existe pas d'états liés. D'autre part, comme JOST et KOHN [2] nous avons montré que si le système admet un état lié nous obtenons une solution à un paramètre. Enfin, la détermination de l'interaction lorsque les déphasages sont fonctions de l'énergie sous forme de fractions rationnelles se ramène à la résolution d'une équation algébrique. Mais nous avons également trouvé des solutions mathématiques lorsque le déphasage varie d'un multiple de π entre $k = 0$ et l'infini, sans passer deux fois par une même valeur $h\pi$. Soit k_i une valeur de l'énergie où $v(p)$ s'annule. La fonction $f(p)$ a alors un zéro double et la quantité

$$R(k) = 1 + P \int_0^\infty \frac{f(p)}{p^2 - k^2} \, \mathrm{d}p \,,$$

change de signe en s'annulant au point k_i. Faisons varier l'intensité de l'interaction, ce qui revient à considérer des functions $f_\lambda(p) = \lambda f(p)$, λ étant une constante voisine de l'unité. Au point $p = k_i$, il est évident que $f_\lambda(p)$ possède toujours un zéro double mais $R_\lambda(k_i)$ n'est plus nul: il vaut $(1 - \lambda)$ et le zéro de $R_\lambda(k)$ est décalé. Décrivons graphiquement la situation au point de vue déphasage (Fig. 4).

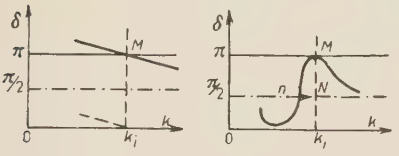

Fig. 4. - *a*) $\lambda = 1$; *b*) $\lambda \neq 1$.

Pour $\lambda \neq 1$, le déphasage ne traverse pas la valeur π et la comparaison des Fig. 3 *a*) et 3 *b*) montre clairement qu'il n'y a pas continuité des déphasages par rapport au paramètre λ pour la valeur $\lambda = 1$. On peut aussi faire cesser la situation anormale que nous venons d'étudier par addition au Hamiltonien d'une interaction supplémentaire aussi petite soit elle, en particulier un potentiel local. Lorsque l'équation de Schrödinger avec ce seul potentiel local se résout exactement, on peut calculer le déphasage associé à l'interaction non locale par des quadratures. Inversement, sachant qu'entre deux particules existe une interaction locale connue et une interaction non locale séparable inconnue on peut à partir des déphasages déterminer cette dernière interaction.

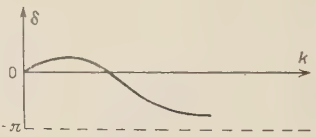

Fig. 5.

Si comme l'indique l'expérience, le déphasage ^1S proton proton s'annule en changeant de signe à une certaine énergie [11], il lui correspond une interaction unique séparable pourvu que $\delta(0) - \delta(+\infty) = \pi$ (Fig. 5). Cependant, si nous postulons l'indé-

---

[14] O. CHAMBERLAIN, E. SEGRÈ, R. D. TRIPP, C. WIEGAND et T. YPSILANTIS: *Phys. Rev.*, **105**, 288 (1957).

pendance de charge des forces nucléaires, l'interaction obtenue conduit à un déphasage ^1S du système neutron proton qui ne change plus de signe entre 0 et $+\infty$ ($\delta(0) - \delta(+\infty) = 0$). Ce fait semble difficile à concilier avec les résultats expérimentaux à haute énergie ([15]).

([15]) C. KLEIN: *Nuovo Cimento*, **2**, 38 (1955).

RIASSUNTO (*)

In base all'ipotesi di un'interazione centrale separabile non locale si studia il problema di determinare un'interazione di due corpi (ad es. nucleone nucleone) nello stato S a partire dalla dipendenza dello spostamento di fase sperimentale dall'energia. Si dimostra che con questa ipotesi l'interazione è data, nello spazio dei momenti, dalla soluzione di un'equazione integrale di Fredholm non omogenea di seconda specie. Le proprietà generali di questa equazione ci consentono di dimostrare che, se il sistema fisico non ha stati legati può esistere un sistema di soluzioni a un parametro. Soluzioni esplicite si ottengono quando la dipendenza dello spostamento di fase dall'energia è data esattamente dall'approssimazione indipendente dalla forma. Questo procedimento si estende al caso in cui $k\,\mathrm{tg}\,\delta$ è una funzione razionale dell'energia. In questo caso l'esistenza e la molteplicità delle soluzioni sono in relazione al numero delle radici di un'equazione algebrica poste nel semipiano complesso superiore. Inoltre, quando lo spostamento di fase resta tra 0 e π o tra 0 e $-\pi$ nell'intero campo di variazione dell'energia, i nostri risultati sono simili a quelli ottenuti assumendo un'interazione locale: se il sistema non ha stati legati, la soluzione è unica; se il sistema ha uno stato legato, esiste un sistema di soluzioni a un parametro. D'altro lato se la dipendenza dello spostamento di fase dall'energia non ha più le restrizioni indicate sopra, il problema si può risolvere solo se i valori dell'energia ai quali δ passa per $n\pi$ soddisfano determinate disuguaglianze. Le soluzioni così ottenute sono corrette in senso matematico, ma è dubbio il loro significato fisico, perchè, in questo caso, non si ha più stabilità dello spostamento di fase rispetto alle piccole variazioni dell'interazione.

(*) *Traduzione a cura della Redazione.*

Production en paire des mésons positifs par un méson.

R. Omnes

CERN - Geneva

(ricevuto il 5 Giugno 1957)

Summary. — We establish a system of generalized Low equations in the model of Chew. The cross-section for production of two positives π-mesons in a P-state is deduced by a one-meson approximation. The corresponding integral equation is numerically solved by using the experimental phase-shifts and the invalidity of an iteration solution is showed. Every numerical approximation done in the text has been tested.

1. – Introduction.

Nous avons déterminé la section efficace de production de deux mésons positifs par collision d'un méson positif et d'un proton à l'aide du modèle statique de Chew, Low [1] et Wick [2]. On peut compter obtenir ainsi des informations sur l'ordre de grandeur de la section efficace jusqu'à des énergies totales de l'ordre de 300 ou 400 MeV dans le système du centre de masse.

Dans la Sect. 2 nous donnons une méthode, fondée sur l'étude de la structure des états physiques, pour obtenir des équations du type de Low pour les processus de création. Le résultat est mis sous une forme simple dans le cas de la production d'une paire de mésons à l'aide de propriétés spécifiques du modèle de Chew. Les équations ainsi obtenus vérifient les conditions d'unitarité, de causalité et de croisement.

La Sect. 3 est consacrée à la réduction d'une approximation à un méson sur l'équation qui définit la production en paires. Nous obtenons ainsi une équation intégrale linéaire dont le noyau est fonction des phase-shifts de dif-

(1) G. F. Chew et F. E. Low: *Phys. Rev.*, **101**, 1570 (1956).
(2) G. C. Wick: *Rev. Mod. Phys.*, **27**, 339 (1955).

fusion. La résolution numérique sur machine (non par itération) de cette équation nous donne des sections efficaces de production plus importantes que ce qui a été calculé jusqu'ici à l'aide de méthodes respectant l'unitarité de la matrice S [3]. Nous donnons ces sections efficaces différentielles et totales.

2. – Généralités.

En théorie statique du nucléon, l'hamiltonien du système méson-nucléon est donné par

$$H = H_0 + H_1 , \tag{1}$$

$$H_0 = \sum_k n_k \omega_k , \qquad H_1 = \sum_k a_k V_k + a_k^+ V_k^+ . \tag{2}$$

$$V_k = V_{ki\lambda} = (3\pi)^{-\frac{1}{2}} f k^{\frac{3}{2}} v(k) \sigma_i \tau_\lambda , \tag{3}$$

où l'indice k désigne tous les nombres quantiques nécessaires à la définition d'un méson: nombre d'ondes (k), polarisation ou valeur de la projection du moment angulaire du méson, qui est dans un état P, sur un axe fixe (i), charge (λ)·$\omega = (k^2 + 1)^{\frac{1}{2}}$ est l'énergie du méson (nous prenons $\hbar = c = \mu = 1$). L'opérateur vertex V_k contient la fonction de coupure $v(k)$. Sa normalisation a été fixée en posant pour condition que le nombre d'états d'un méson de polarisation et de charge déterminées et d'énergie comprise entre ω et $\omega + \mathrm{d}\omega$ soit précisément égal à $\mathrm{d}\omega$.

Notons les relations de commutation

$$\begin{cases} [H, a_k] = -\omega_k a_k - V_k^+ , \\ [H, a_k^+] = \omega_k a_k^+ + V_k . \end{cases} \tag{4}$$

Nous désignerons dans la suite par $|\alpha a\rangle$ ou plus simplement $\rangle$ l'état physique d'un nucléon dont les indices de spin et de charge sont a et α, par $|p\alpha +\rangle$ ou $|p +\rangle$ l'état physique du système d'un nucléon et d'un méson sortant, par $|n\rangle$ un système complet d'états.

Nous allons maintenant donner un certain nombre de formules nécessaires pour la suite. Leurs démonstrations ne présentent pas en général de difficulté, mais nous ne les donnerons pas ici à cause de leur volume important.

---

[3] J. Franklin: *Phys. Rev.*, **105**, 1101 (1957); M. Nelkin: *Phys. Rev.*, **104**, 1150 (1956); J. Fukuda et J. S. Kovacs: *Phys. Rev.*, **104**, 1784 (1956); S. Barshay: *Phys. Rev.*, **103**, 1102 (1956); L. S. Rodberg: *Phys. Rev.*, **106**, 1090 (1957). Le calcul de Nelkin est effectué par la méthode Tamm-Dancoff, celui de Barshay, par la méthode de Chew et Low, ne respecte pas la condition d'unitarité.

Tout d'abord, on a la formule

$$a_q \frac{1}{x+H} = \frac{1}{x+\omega_q+H} a_q - \frac{1}{x+\omega_q+H} V_q^+ \frac{1}{x+H}, \tag{5}$$

qui permet de permuter un opérateur annihilation a_q et un propagateur. (5) a été donnée par Wick (2), x est un nombre réel pouvant éventuellement avoir une partie imaginaire infinitésimale de sorte que les inverses d'opérateurs écrits dans la formule aient un sens.

L'action d'un opérateur création sur un état physique peut s'écrire

$$a_q^+ |n+\rangle = |qn+\rangle + \frac{1}{H-\omega_q-E_n-i\varepsilon} V_q |n+\rangle, \tag{6}$$

cette équation est la généralisation de

$$a_q^+ \rangle = |q+\rangle + \frac{1}{H-\omega_q-i\varepsilon} V_q \rangle, \tag{7}$$

qui a été démontrée par Wick. Elle peut être démontrée de façon analogue ainsi que l'équation suivante

$$|p_1 p_2 \dots p_s +\rangle = a_1^+ a_2^+ \dots a_s^+ \rangle - \frac{1}{H-E-i\varepsilon} \Big(\sum_{i=1}^{s} a_1^+ \dots a_{i-1}^+ V_i a_{i+1}^+ \dots a_s^+\Big)\rangle, \tag{8}$$

où

$$E = \omega_1 + \omega_2 + \dots + \omega_s .$$

L'action d'un opérateur annihilation sur un état physique peut s'écrire

$$a_\lambda |n+\rangle = \sum_1^n \delta_{q p\lambda} |n_\lambda +\rangle - \frac{1}{H+\omega_q-E_n-i\varepsilon} V_q^+ |n+\rangle, \tag{9}$$

Ce qui généralise l'équation de Wick

$$a_q \rangle = -\frac{1}{H+\omega_q} V_q^+ . \tag{10}$$

Dans (9) $|n+\rangle$ est un état à n mésons, p_λ un quelconque de ces mésons et $|n_\lambda+\rangle$ l'état physique à ondes sortantes comprenant les mêmes mésons que l'état n, sauf le méson p_λ. (9) peut être démontrée par récurrence à l'aide de (5), (6) et (10).

Nous nous proposons maintenant d'établir la structure générale de l'élé-

ment de matrice de réaction entre un état initial quelconque i à s mésons $p_1, p_2, ..., p_s$ d'énergies $\omega_1, \omega_2, ..., \omega_s$ et un état final également quelconque f à r mésons $q_1, q_2, ..., q_r$ d'énergies $\omega'_1, \omega'_2, ..., \omega'_r$.

L'élément de matrice de S entre i et f est défini par

$$(f|S|i) = \langle f - | i + \rangle \tag{11}$$

et l'on définit la matrice de réaction T par

$$(f|S|i) = \delta_{fi} - 2\pi i\,\delta(E_i - E_f)T_i(f)\,. \tag{12}$$

D'après (8) et l'équation analogue pour les états à ondes entrantes, on peut écrire

$$|p_1 p_2 \dots p_s +\rangle = |p_1 p_2 \dots p_s -\rangle - 2\pi i\,\delta(H - E)\Big(\sum_{i=1}^{s} a_1^+ \dots V_i \dots a_s^+\Big)\rangle\,, \tag{13}$$

où nous avons utilisé la formule connue

$$\frac{1}{H - E - i\varepsilon} = \pi i\delta(H - E) + P\,\frac{1}{H - E}\,, \tag{14}$$

ici P représente la partie principale au sens de Cauchy. Introduisant (13) dans (11) et comparant à (12), il vient

$$T_{p_1 p_2 \dots p_s}(f) = \langle f - | \sum_{i=1}^{s} (a_1^+ \dots V_i \dots a_s^+)\rangle\,. \tag{15}$$

Dans le cas où f est constitué des r mésons $q_1 q_2 \dots q_r$ on peut développer $\langle f - |$ à l'aide de l'équation analogue à (8) pour obtenir

$$T_{p_1 p_2 \dots p_s (q_1 q_2 \dots q_r)} = \tag{16}$$
$$= \left\langle \left[a_{1'} \dots a_{r'} + \sum_{j'=1}^{r} (a_{1'} \dots V_{j'}^+ \dots a_{r'}) \frac{1}{E - H - i\varepsilon} \right] \Big(\sum_{i=1}^{s} a_1^+ \dots V_i \dots a_s^+\Big) \right\rangle .$$

Considérons le second terme du second membre; en introduisant le système complet d'états $|n -\rangle$ à ondes entrantes, il s'écrit, en posant $E = \omega_1 + \omega_2 + \dots + \omega_s = \omega'_1 + \omega'_2 + \dots + \omega'_r$

$$\sum_n \langle \sum_{j'=1}^{r} (a_{1'} \dots V_{j'}^+ \dots a_{r'}) | n - \rangle \frac{1}{E - E_n - i\varepsilon} \langle n - | \sum_{i=1}^{s} (a_1^+ \dots V_i \dots a_s^+)\rangle\,,$$

soit, en tenant compte de (15)

$$\sum_n \frac{T^*_{q_1 q_2 \dots q_r}(n) T_{p_1 p_2 \dots p_s}(n)}{E - E_n - i\varepsilon} . \tag{17}$$

Le premier terme du second membre de (16) peut être mis sous une forme plus explicite à l'aide de (10), de (6) et des relations de commutation des opérateurs a et a^+. En fait, il s'écrit

$$\begin{aligned} C(p_1 p_2 \dots p_s ; q_1 q_2 \dots q_r) &= \\ &= \left\langle V^+_{1'} \frac{1}{H + \omega'_1} V^+_{2'} \frac{1}{H + \omega'_1 + \omega'_2} \dots V^+_{r'} \frac{1}{H + E} V_r \dots V_2 \frac{1}{H + \omega_1} V_1 \right\rangle + \\ &+ \delta_{11'} \left\langle V^+_{2'} \frac{1}{H + \omega'_2} V^+_{3'} \dots V^+_{r'} \frac{1}{H + E - \omega_1} V_r \dots V_3 \frac{1}{H + \omega_2} V_2 \right\rangle + \\ &+ \delta_{11'} \delta_{22'} \langle \dots \rangle + \text{Perm } (1\,2 \dots s)(1'\,2' \dots r') , \end{aligned} \tag{18}$$

où le symbole Perm $(1\,2 \dots s)(1'\,2' \dots r')$ signifie qu'il faut ajouter aux termes explicitement écrits de (18) tous ceux qui s'en déduisent par permutation des indices $1\,2 \dots s$ entre eux ou $1'\,2' \dots r'$ entre eux.

Il est possible d'écrire pour le second terme de (16) une formule analogue à (18) faisant intervenir la valeur moyenne de produits d'opérateurs vertex et de propagateurs (on peut alors aisément vérifier des relations de croisement généralisées). On sait d'autre part que de telles expressions correspondent biunivoquement à des graphiques du type de Feynman et, en fait, aux graphiques de la théorie des perturbations représentant l'ordre le plus bas du processus de réaction considéré. En particulier, on voit d'après (18) que le terme C correspond aux graphiques où les lignes mésoniques sont complètement croisées, alors que (17) correspond à l'ensemble de tous les autres graphiques.

Notons que (18) entraine

$$C(p_1 p_2 \dots p_s ; q_1 q_2 \dots q_r) = C^*(q_1 q_2 \dots q_r ; p_1 p_2 \dots p_s) \tag{19}$$

et que C est une quantité bien définie (les propagateurs qui y interviennent sont bien définis, sans l'artifice des infinitésimaux imaginaires). En regroupant (17) et (18), il vient (*)

$$T_{p_1 p_2 \dots p_s (q_1 q_2 \dots q_r)} = C_{(p_1 p_2 \dots p_s q_1 q_2 \dots q_r)} + \sum_n \frac{T^*_{q_1 q_2 \dots q_r (n)} T_{p_1 p_2 \dots p_s (n)}}{E - E_n - i\varepsilon} . \tag{20}$$

(*) Des équations analogues ont été publiées par J. Fukuda et J. S. Kovacs [3] mais elles font intervenir deux matrices T et S, l'interprétation physique de S n'étant pas claire.

Sur cette formule, les propriétés de causalité et d'unitarité de la matrice S sont évidentes. En effet, on peut étendre T aux valeurs complexes de l'énergie $E = z$ à l'aide de (20) et, d'après la forme (18) de C et (20) on constate que cette fonction est holomorphe dans le demi-plan complexe supérieur et y est bornée par une quantité de la forme $A/|z|$, ce qui constitue la forme mathématique de la condition de causalité. D'autre part, (20), (19) et (14) entrainent

$$T^*_{p_1 p_2 \dots p_s (q_1 q_2 \dots q_r)} - T_{q_1 q_2 \dots q_r (p_1 p_2 \dots p_s)} = 2\pi i \sum_n \delta(E_n - E) T^*_{p_1 p_2 \dots p_s (n)} T_{q_1 q_2 \dots q_r (n)} ,$$

ce qui n'est autre que la condition d'unitarité de S

$$\langle p_1 p_2 \dots p_s | S S^+ | q_1 q_2 \dots q_r \rangle = \delta_{p_1 p_2 \dots p_s ; \, q_1 q_2 \dots q_r} .$$

L'équation (20) est fortement analogue à l'équation de Low. En fait, elle s'y réduit pour $r = s = 1$. Nous nous proposons maintenant, dans le cas où r et s sont inférieurs à 3, de donner au terme C une forme qui mette plus encore en évidence cette analogie. Nous utiliserons pour cela des propriétés spécifiques du modèle de Chew pour étendre les éléments de matrice de T en dehors de la couche d'énergie et traiterons explicitement, pour plus de clarté, le cas $S = 1$, $r = 2$. Dans ce cas, l'on a:

$$C(p ; q_1 q_2) = \left\langle V_p \frac{1}{H + \omega_p} V^+_{q_2} \frac{1}{H + \omega_{q_1}} V^+_{q_1} \right\rangle + \text{Perm (12)} ,$$

que nous écrirons

$$\sum_n \langle V_p | n - \rangle \frac{1}{E_n + \omega_p} \left\langle n - | V^+_{q_2} \frac{1}{H + \omega_{q_1}} V^+_{q_1} \right\rangle + \text{Perm (12)} .$$

Or, d'après (15), on a

$$T_{q_1 q_2 (n)} = \langle n - | a^+_{q_1} V_{q_2} + a^+_{q_2} V_{q_1} \rangle ,$$

ce qui s'écrit à l'aide de (9)

$$\sum_\lambda \delta_{q_2 p_\lambda} \langle n_\lambda - | V_{q_1} \rangle - \left\langle n - | V_{q_2} \frac{1}{H + \omega_{q_2} - E_n - i\varepsilon} V_{q_1} \right\rangle + \text{Perm (12)} . \tag{22}$$

Notons maintenant que, d'après l'hermiticité de V_p, le premier facteur de (21) est $T^*_p(n)$. Le dernier facteur n'est pas sans analogie avec le second terme de (22). Introduisons donc, pour préciser cette analogie, deux mésons q'_1 et q'_2 ayant respectivement même polarisation et même charge que q_1 et q_2 mais des nombres d'ondes différents q'_1 et q'_2 correspondant à des énergies $\omega_{q'_1}$ et $\omega_{q'_2}$. D'après l'hermiticité des V et leur dépendance explicite en fonction de l'énergie

(équation (3)), on peut écrire

$$(23)\qquad \left\langle n-|\, V^{+}_{q_2}\frac{1}{H+\omega_{q_1}}\,V^{+}_{q_1}\right\rangle = \left\langle n-|\, V_{q_2}\frac{1}{H+\omega_{q_1}}\,V_{q_1}\right\rangle = \\ = \left\langle n-|\, V_{q_2'}\frac{1}{H+\omega_{q_1}}\,V_{q_1'}\right\rangle \frac{\Omega(q_1)\Omega(q_2)}{\Omega(q_1')\Omega(q_2')}\,,$$

où

$$(24)\qquad \Omega(q) = q^{\frac{3}{2}}v(q)\,.$$

Par comparaison avec (22), on voit qu'en choisissant les énergies $\omega_{q_1'}$ et $\omega_{q_2'}$ telles que

$$(25)\qquad \begin{cases} \omega_{q_1'} = \omega_{q_2} + E_n \\ \omega_{q_2'} = \omega_{q_1} + E_n \end{cases}$$

il vient

$$(26)\qquad C(p;\, q_1q_2) = -\sum_n \frac{T^{*}_{p(n)}T_{q_1'q_2'(n)}}{E+E_n}\,\frac{\Omega(q_1)\Omega(q_2)}{\Omega(q_1')\,\Omega(q_2')}\,,$$

(le terme en $\delta_{q_2'p_\lambda}$ de (22) disparait car (25) entraine $\omega_{q_2'} > E_n \geqslant \omega_\lambda$).

On démontre de la même façon

$$C(p_1p_2;\, q_1q_2) = -\sum_n \frac{T^{*}_{p_1'p_2'n(}T_{q_1'q_2'(n)}}{E_n+E}\,\frac{\Omega(p_1)\Omega(p_2)\Omega(q_1)\Omega(q_2)}{\Omega(p_1')\Omega(p_2')\Omega(q_1')\Omega(q_2')}\,.$$

Ainsi pour r et $s \leqslant 2$ avons-nous obtenu une équation beaucoup plus proche de l'équation de Low que (20) bien que ceci n'ait pu être réalisé que grâce à de propriétés spécifiques du modèle de Chew.

Notons qu'il est possible, en utilisant les méthodes récemment développées par N. N. Bogoliubov et ses collaborateurs (4), d'obtenir un système complet d'équation du type de Low, relativistes, quadratiques selon les éléments de matrice de S, mais que ces équations sont plus difficiles à aborder numériquement que (20) et (26) (5).

(4) N. N. Bogolioubov, Medvedev et Polivanov: présenté à la Conférence de Seattle de Physique théorique (Sept. 1956).

(5) R. Omnes: *Nuovo Cimento*, **5**, 983 (1957).

3. – Etude des termes à 2 mésons.

Récapitulons les équations obtenues dans le cas du passage de 1 à 2 ou de 2 à 1 mésons.

$$(1) \qquad T_{q(p_1p_2)} = -\sum_n \left[\frac{T^*_{q(n)} T_{p'_1p'_2(n)}}{E_n + E} \frac{\Omega(p_1)\Omega(p_2)}{\Omega(p'_1)\Omega(p'_2)} + \frac{T^*_{p_1p_2(n)} T_{q(n)}}{E_n - E - i\varepsilon} \right],$$

$$(2) \qquad T_{p_1p_2(q)} = -\sum_n \left[\frac{T^*_{p'_1p'_2(n)} T_{q(n)}}{E_n + E} \frac{\Omega(p_1)\Omega(p_2)}{\Omega(p'_1)\Omega(p'_2)} + \frac{T^*_{q(n)} T_{p_1p_2(n)}}{E_n - E - i\varepsilon} \right],$$

avec $\omega_1 + \omega_2 = \omega_q = E$.

Pour aborder numériquement l'étude de ces équations, nous limiterons la sommation dans le second membre à des états intermédiaires où le nombre de mésons est borné. On pourrait songer à adjoindre à (1) et (2) l'équation décrivant le passage de 2 à 2 mésons et limiter les sommations aux termes ayant au plus 2 mésons. Cependant, les termes (2-2) (2 mésons à 2 mésons) sont faibles devant les termes (2.1) et on les négligera en se limitant aux états intermédiaires à 0 ou 1 méson. Notons que l'équation ainsi obtenue est linéaire selon les termes (1-2) et permet d'estimer aisément par perturbation l'erreur commise en négligeant les termes (2-2).

Nous verrons ainsi apparaitre dans les équations des termes (1-0) (0-1) (1-1) (2-0) (1-2) (2-1) qu'il s'agit de ramener à la forme la plus simple. Pour cela, on réduit d'abord la dépendance en fonction des énergies en posant

$$(3) \qquad \begin{cases} T_{q(0)} = q^{\frac{3}{2}} v(q) T_{\mu m \beta b(\alpha a)} \\ T_{q(p)} = -(pq)^{\frac{3}{2}} v(p) v(q) T_{\mu m \beta b(\lambda m' \alpha a)} \\ T_{p_1p_2(0)} = -(p_1p_2)^{\frac{3}{2}} v(p_1) v(p_2) T_{\lambda_1\lambda_2 m_1 m_2 \beta b(\alpha a)} \\ T_{q(p_1p_2)} = -(p_1p_2q)^{\frac{3}{2}} v(p_1) v(p_2) v(q) T_{\mu m \beta b(\lambda_1\lambda_2 m_1 m_2 \alpha a)} \\ T_{p_1p_2(q)} = -(p_1p_2q)^{\frac{3}{2}} v(p_1) v(p_2) v(q) T_{\lambda_1\lambda_2 m_1 m_2 \beta b(\mu m \alpha a)} \end{cases}$$

où m, m_1, m_2, a, b et μ, λ_1, λ_2, α, β sont les indices de polarisation et de charge des mésons q, p_1 et p_2, du nucléon initial et du nucléon final.

On effectue la réduction en termes de spin isotopique et de moment angulaire en notant que les spins isotopiques de 2 mésons peuvent se coupler afin de donner une résultante $t = 0$, 1 ou 2 (3ème composante: t_3) laquelle se couple avec le spin isotopique du nucléon pour donner une résultante finale $I = \frac{1}{2}, \frac{3}{2}$ (le cas $I = \frac{5}{2}$ est exclu par conservation du spin isotopique dans la réaction).

D'après l'équivalence des rôles joués par les opérateurs σ et τ dans la théorie, la réduction en moment angulaire sera absolument semblable à celle

effectuée en termes de spin isotopique. C'est pourquoi dans les équations (4) suivantes, nous avons indiqué par (id.m.a.) la répétition de l'opération d'algèbre de Clebsch-Gordan indiquée, la seule modification étant le remplacement de μ, λ_1, λ_2, α, β, t, t_3 I, I_3 par m, m_1, m_2, a, b, L, L_3, J, J_3.

Nous posons donc

$$(4)\quad \begin{cases} T_{\mu m \beta b(\lambda a)} = C_{1\frac{1}{2}}(\frac{1}{2}\alpha\,|\,\mu\beta)\times(\text{id.m.a})T^0 \\ T_{\mu m \beta b(\lambda m' \alpha a)} = \sum_{IN} C_{1\frac{1}{2}}(IN\,|\,\mu\beta)\,C_{1\frac{1}{2}}(IN\,|\,\lambda\alpha)\times(\text{id.m.a})T^I_J \\ T_{\lambda_1\lambda_2 m_1 m_2 \beta b(\lambda a)} = \sum_{tt_3} C_{11}(tt_3\,|\,\lambda_1\lambda_2)\,C_{t\frac{1}{2}}(\frac{1}{2}\alpha\,|\,t_3\beta)\times(\text{id.m.a})T^t_L \\ T_{\mu m \beta b(\beta_1\lambda_2 m_1 m_2 \lambda a)} = \sum_{INtt_3} C_{11}(tt_3\,|\,\lambda_1\lambda_2)\,C_{t\frac{1}{2}}(IN\,|\,t_3\alpha)\,C_{1\frac{1}{2}}(IN\,|\,\mu\beta)\times(\text{id.m.a})T'^{It}_{JL} \\ T_{\lambda_1\lambda_2 m_1 m_2 \beta b(\mu m \alpha a)} = \sum_{INtt_3} C_{11}(tt_3\,|\,\beta_1\lambda_2)\,C_{t\frac{1}{2}}(IN\,|\,t_3\beta)\,C_{1\frac{1}{2}}(IN\,|\,\mu\alpha)\times(\text{id.m.a})T^{It}_{JL} \end{cases}$$

Le remplacement de (3) et (4) dans (1) et (2) limitées aux états intermédiaires à 1 méson donne les équations suivantes:

$$(5.1)\quad T^{It}_{JL} = (T^{It}_{JL})_\alpha + (T^{It}_{JL})_\beta + \\ + \pi i\{q^3v^2(q)(T^{It}_{JL}T^{*I}_J)_q + \sum_{I'I'J'L'} A^{It\ I'I'}_{JLJ'L'}[p_1^3v^2(p_1)(T'^{*\ II'}_{JL'}T^{I'}_{J'})_{p_1} + \text{Perm (12)}]\} + \\ + P\int_1^\infty d\omega_k k^3v^2(k)\left[\frac{(T^{It}_{JL}T^{*I}_J)_k}{\omega_k-\omega_q} + \sum_{I'I'J'L'} A^{It\ I'I'}_{JLJ'L'}(T'^{*\ II'}_{JL'}T^{I'}_{J'})_k\left(\frac{1}{\omega_k-\omega_2}+\frac{1}{\omega_k-\omega_1}\right)\right],$$

$$(5.2)\quad T'^{It}_{JL} = T^{*It}_{JL} + 2\pi i\{q^3v^2(q)(T^{It}_{JL}T^{*I}_J)_q + \\ + \sum_{I'I'J'L'} A^{It\ I'I'}_{JLJ'L'}[p_1^3v^2(p_1)(T'^{*It'}_{JL'}T^{I'}_{J'})_{p_1} + \text{Perm (12)}]\}.$$

Nous avons ici une équation intégrale linéaire inhomogène couplée à une équation algébrique.

Dans le noyau de cette équation apparait $T^I_J(\omega)$ qui est lié simplement à la fonction $g_{2I2J}(\omega)$ de Chew et Low et aux déphasages δ_{IJ} par

$$(6)\quad T^I_{J(\omega)} = \frac{1}{\pi}h_{2I2J}(\omega) = \frac{1}{\pi}\frac{\exp[i\delta]\sin\delta}{p\,v^2(p)}.$$

Le premier terme de l'intégrale de (5.1) provient du second terme de (2). Les termes croisés, précédés par $A^{It\ I't'}_{JL\,J'L'}$, proviennent également du second terme de (2), grâce aux propriétés particulières de $T_{p_1p_2}(n)$. En effet, dans la sommation faite dans (2) apparaissent des éléments de matrice $T_{p_1p_2}(n)$ hors

de la couche d'énergie. Si l'on se reporte à (2.15) et (2.9) on voit que, dans ce cas

$$T_{p_1 p_2}(n) = \sum_{\lambda} \delta_{p_1 p_\lambda} \langle n_\lambda - | V_2 \rangle + \text{Perm}\,(12) + T^{\text{Couche}}_{p_1 p_2 (n)}\,, \tag{7}$$

où $T^{\text{Couche}}_{p_1 p_2 (n)}$ est le prolongement explicite à l'aide de (3) et (4) de la matrice T définie sur la couche d'énergie.

Pour effectuer une approximation à 1 méson cohérente, nous avons ainsi été amenés à conserver des états n_λ à 1 méson dans le premier terme de (7) donc, partiellement, des états n à 2 mésons. Numériquement

$$A^{It\ I't'}_{JLJ'L'} = (-)^{t+t'}\big\{(2t+1)(2t'+1)^{\frac{1}{2}}(2I'+1)\cdot \cdot W(1tI'I\,|\,1\tfrac{1}{2})W(1t'I'I\,|\,1\tfrac{1}{2})\big\}\times\{\text{id.m.a}\}. \tag{8}$$

Les termes inhomogènes $(T)_\alpha$ et $(T)_\beta$ sont les analogues des termes à 0 méson de l'équation de Low. $(T)_\beta$ représente exactement la contribution des états intermédiaires à 0 méson aux 2 termes de (2) (noter que, pour $E_n = 0$, $p_1' = p_1$, $p_2' = p_2$),

$$(T^{It}_{JL})_\beta = \frac{4\delta_{I\frac{1}{2}}\delta_{J\frac{1}{2}} T_0 T^t_L}{E} - K_{JL}K_{It}\,\frac{T_0 T^{*t}_L}{E}\,. \tag{9}$$

Le premier terme de (9) est simple et provient du second terme de (2); le second, qui provient du terme de (2), est compliqué par des coefficients numériques dus au croisement des indices nucléoniques. Nous donnons la valeur des coefficients non nuls:

$$K_{\frac{1}{2}},\ 0 = 2/3\,, \qquad K_{\frac{1}{2}},\ 1 = 10/9\,, \qquad K_{\frac{3}{2}},\ 1 = 8/9\,. \tag{10}$$

Dans (9) on voit apparaitre T^0 qui, d'après (3) et (4), est un simple nombre égal au carré de l'élément de matrice réduit de l'opérateur tensoriel σ, multiplié par un coefficient proportionnel à la constante de couplage *renormalisée*. Cette renormalisation provient, comme de coutume, du passage de la valeur moyenne d'un opérateur $\sigma\tau$ entre états physiques du nucléon à sa valeur moyenne entre états nus,

$$T^0 = \sqrt{\frac{3}{\pi}}\, f_r\,. \tag{11}$$

T^t_L peut être calculé à l'aide de (3), (4) et de la formule non réduite

$$T_{p_1 p_2 b\beta}(a\alpha) = \langle a\alpha\,|\,a_1^+ V_2 + a_2^+ V_1\,|\,b\beta\rangle$$

qui est un cas particulier de (2.15). Elle s'écrit, à l'aide de (2.10):

$$-\left\langle a\alpha\left|V_1\frac{1}{H+\omega_1}V_2\right|b\beta\right\rangle + \text{Perm (12)}\,,$$

ou encore

$$-\sum_n \langle\alpha a|V_1|n\rangle\frac{1}{E_n+\omega_1}\langle n|V_2|b\beta\rangle + \text{Perm (1.2)}\,. \tag{12}$$

Nous avons calculé (12) en limitant la sommation sur les états n aux états à 1 méson, ce qui donne

$$T_L^t = (T_L^t)_0 + (T_L^t)_1 \tag{13}$$

où les deux termes représentent respectivement la contribution à (12) des états intermédiaires à 0 et 1 méson, soit

$$\left\{\begin{aligned}
&(T_L^t)_0 = \frac{3f_\pi^2}{\pi}\left(\frac{1}{\omega_1}+\frac{1}{\omega_2}\right)\frac{2^3}{[(2L+1)(2t+1)]^{\frac{1}{2}}}W(11\tfrac{1}{2}\tfrac{1}{2}|L\tfrac{1}{2})W(11\tfrac{1}{2}\tfrac{1}{2}|t\tfrac{1}{2})\,,\\
&(T_L^t)_1 = \sum_{IJ} -2[(-)^I(2I+1)W(\tfrac{1}{2}\tfrac{1}{2}11|tI)B_t]\cdot[\text{id.m.a}]\cdot\\
&\qquad\qquad\cdot\int_1^\infty \mathrm{d}\omega_k k^3 v^2(k)\,|T_J^I|_k^2\left\{\frac{1}{\omega_{k_1}+\omega_1}+\frac{1}{\omega_{k_2}+\omega_2}\right\},
\end{aligned}\right. \tag{14}$$

avec

$$B_0 = \frac{1}{3}\,,\qquad B_1 = -\frac{1}{\sqrt{3}}\,.$$

Quant au terme inhomogène $(T)_\alpha$, il provient des contributions au second terme de (2) des états n_λ à 0 méson (cf. (7)). En fait

$$(T_{JL}^{It})_\alpha = 2[(-)^t(2t+1)^{\frac{1}{2}}(2I+1)W(\tfrac{1}{2}I1t|1\tfrac{1}{2})][\text{id.m.a}]\,T^0 T^{*I}_{J(E)}\left\{\frac{1}{\omega_1}+\frac{1}{\omega_2}\right\}. \tag{15}$$

Finalement, on aura noté que dans le système (5) n'apparaissent plus de termes en p_1' et p_2'. Cela tient à ce que la contribution au premier terme de (2) des états intermédiaires d'énergie supérieure ou égale à 1 est très faible grâce à la petitesse du rapport $\Omega(p_1)\Omega(p_2)/\Omega(p_1')\Omega(p_2')$. En fait, l'étude numérique montre aisément que la contribution de ce terme est largement inférieure au centième de T_{JL}^{Jt}. Nous l'avons donc négligé dans l'équation finale.

Les équations (5) peuvent être aisément étudiées numériquement.

4. – Résolution numérique des équations.

Le système (III 5) se présente comme un système d'équations intégrales couplées dont les noyaux sont fonction des déphasages de diffusion. La méthode que nous avons suivie pour les dériver suggérerait d'utiliser une solution numérique des équations de Chew et Low pour les déphasages. Cependant, une telle solution dépend du choix de la fonction de coupure et nous avons préféré nous appuyer sur l'absence de cette fonctions dans les noyaux et introduire directement les déphasages expérimentaux.

Actuellement, seul le déphasage δ_3 est bien connu expérimentalement et les éléments de matrice réduits que nous pourrons calculer sans avoir besoin de δ_1 et δ_2 sont donc $T_{\frac{3}{2},2}$ et $T_{\frac{3}{2},1}$; la connaissance de ces éléments de matrice ne suffit pas pour estimer complètement la contribution des termes à 2 mésons dans les équations de Chew et Low, aussi la seule application que nous pourrons traiter sera-t-elle le calcul de la section efficace de production de 2 mésons dans un état de spin isobarique et de moment angulaire totaux $\frac{3}{2}$.

Considérons maintenant le terme inhomogène qui figure dans nos équations pour les cas intéressants. En se reportant aux expressions (9) et (15) de $(T)_\beta$ et $(T)_\alpha$, on constate que la dépendance de $(T)_\alpha$ en fonction des énergies est factorisable alors que celle de $(T)_\beta$ ne l'est pas. Si donc nous voulons calculer un processus auquel $(T)_\beta$ contribue, il nous faudra a priori résoudre une équation intégrale pour chaque couple de valeurs des énergies finales ω_1 et ω_2, ce qui rend le calcul rigoureux d'une section efficace long et difficile. D'autre part, le calcul pratique montre que la solution des équations est sensible au terme inhomogène et qu'il faut donc prendre de grandes précautions dans les approximations que l'on peut effectuer.

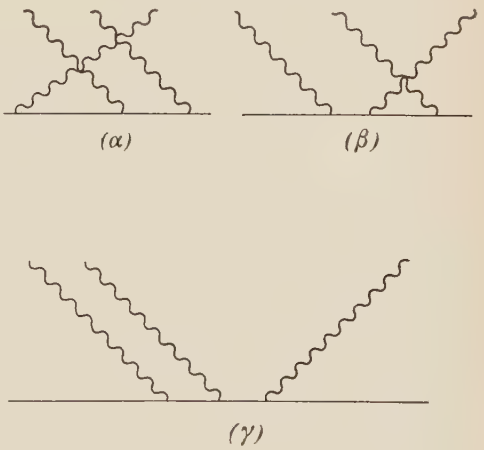

Fig. 1.

Une caractéristique intéressante du terme $(T)_\beta$ est son annulation lorsque t ou $L = 2$. Physiquement cela ressort de la Fig. 1; $(T)_\beta$ correspond en effet au calcul par perturbation des éléments de matrice décrits par les graphiques (α) et (γ), effectué à l'aide de la constante de couplage renormalisée: il est donc clair que le résultat est nul dans le cas considéré par suite de la conservation du moment angulaire et du spin isobarique.

On pourra donc faire le calcul complet de $T_{\frac{3}{2},2}$ par résolution d'une seule équation intégrale et c'est là précisément la seule quantité qui intervienne dans l'étude de la réaction

$$\pi^+ + \mathrm{P} \to \mathrm{N} + \pi^+ + \pi^+$$

elle-même facilement observable expérimentalement.

Cependant $T_{\frac{1}{2},2}$ est couplé aux autres éléments T par l'intermédiaire des termes croisés en $A_{JL,J'L}$: ceux-ci s'annulent, sauf pour $J' = \frac{3}{2}$, $L' = 1$ ou 2 où ils prennent des valeurs très petites (de l'ordre de 10^{-3}) et on les négligera. Nous avons d'ailleurs vérifié, après avoir résolu les équations ainsi obtenues que ces termes étaient effectivement petits et n'avaient pas d'influence sur la section efficace totale.

L'équation que nous avons résolue est donc

$$T_{(\omega_1\omega_2\omega_q)} = \text{const}\, h^*(\omega_j)\left(\frac{1}{\omega_1} + \frac{1}{\omega_2}\right) + \int_1^\infty \frac{(T^*h)_k}{\omega_k - \omega_q - i\varepsilon}\, k^3 v^2(k)\mathrm{d}\omega_k ,$$

puisqu'elle est linéaire, on peut poser

$$T_{(\omega_1\omega_2\omega_q)} = \text{const}\left(\frac{1}{\omega_1} + \frac{1}{\omega_2}\right) t(\omega_j) ,$$

où $t(\omega)$ est solution de

$$t(\omega) = h^*(\omega) + \int_1^\infty \frac{f(\omega')h^*(\omega')}{\omega' - \omega - i\varepsilon}\, k'^3 v^2(k')\, \mathrm{d}\omega' .$$

L'étude de cette dernière équation est particulièrement intéressante et présente des particularités qui peuvent être instructives dans de nombreux autres cas. On constate tout d'abord que la méthode de résolution par itérations successives ne converge pas, ce qui rend immédiatement douteux tout calcul fondé, explicitement ou implicitement, sur cette méthode. Nous avons donc remplacé l'intégrale par une somme, utilisant la méthode des différences finies, et le système linéaire obtenu a été résolu sur machine, nous avons pris des déphasages expérimentaux et une coupure à 5.5.

Trois constatations principales se dégagent des résultats obtenus:

1) La solution est nettement sensible aux variations du terme inhomogène, surtout dans la région des hautes énergies.

2) Elle est stable pour des variations faibles du noyau, ainsi avons-nous vérifié qu'il était légitime de négliger les termes croisés.

3) La solution diffère sensiblement du terme inhomogène, ce qui a une répercussion nette sur le calcul des sections efficaces. Cette différence est mise en évidence sur la Fig. 2 où nous avons porté pour comparaison le carré du module de l'élément de matrice de production $|T|^2$ et ce que donnerait le terme inhomogène $|T(B)|^2$. On s'explique ainsi que les calculs faits jusqu'ici aient toujours donné des sections efficaces de production petites par rapport

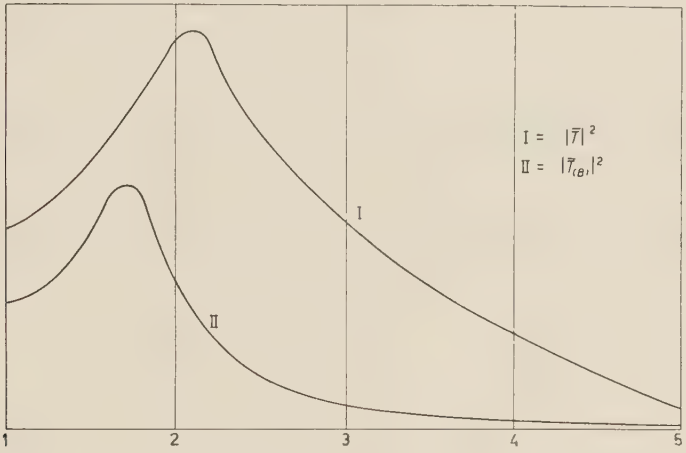

Fig. 2. – Composition des carrés des modules de $\bar{T}$ et $\bar{T}_{(B)}$.

aux premiers résultats expérimentaux. Toutes les méthodes utilisées à notre connaissance (à partir de théories respectant l'unitarité) supposaient en effet sous quelque forme la convergence de la méthode itérative et donnaient des résultats trop faibles, peu éloignés de l'approximation de Born.

La raison de ces difficultés d'ordre numérique semble demeurer dans la

TABLE I. – *Section efficace de production de deux mésons positifs par un méson positif et un proton.*

Energie en unité $\hbar = c = \mu = 1$	σ (mb)
$\omega_q = 2$	0
2.2	$6.7 \cdot 10^{-4}$
2.4	$7.7 \cdot 10^{-3}$
2.6	$2.4 \cdot 10^{-2}$
2.8	$7.5 \cdot 10^{-2}$
3.	0.122
3.5	0.428
4.	0.708
4.5	0.900

forte singularité de la distribution $Ph(\omega')/(\omega' - \omega)$ due à la fois au dénominateur et à la forte variation du numérateur. Nous avons vérifié que toutes les approximations faites, et en particulier l'approximation à un méson, étaient cohérentes avec le résultat final. Nous donnons dans la Fig. 3 et la Table I les valeurs de la section efficace totale en fonction de l'énergie de la réaction de production de deux mésons positifs.

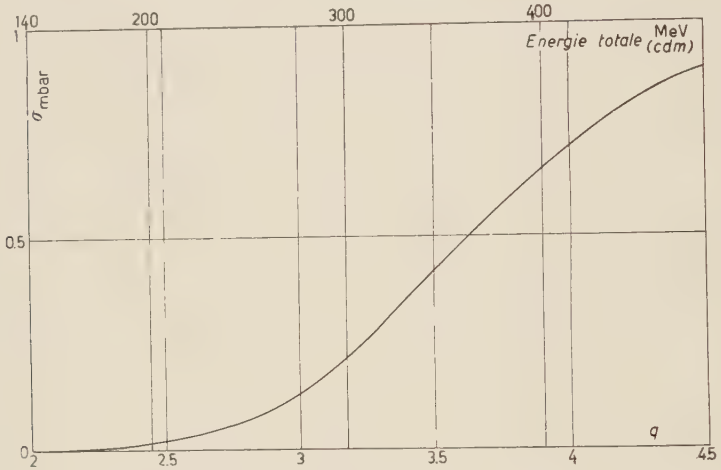

Fig. 3. – Section efficace totale de production de deux mesons positifs.

Dans l'hypothèse que nous avons adoptée, la forme de la section efficace différentielle a la forme simple (6)

$$\mathrm{d}\sigma = |\boldsymbol{n}_1(\boldsymbol{n}_2\cdot\boldsymbol{n}) + \boldsymbol{n}_2(\boldsymbol{n}_1\cdot\boldsymbol{n}) - \boldsymbol{n}(\boldsymbol{n}_1\cdot\boldsymbol{n}_2)|^2\,\mathrm{d}\Omega_1\,\mathrm{d}\Omega_2\,,$$

où $\boldsymbol{n}$ désigne un vecteur unitaire porté par l'impulsion du méson incident, $\boldsymbol{n}_1$ et $\boldsymbol{n}_2$ des vecteurs correspondants aux mésons sortants. Cette distribution possède de nombreuses symétries et leur observation permettrait en principe de déterminer l'influence des effets suivants: petits phase-shifts P, production dans l'état S, interaction méson-méson éventuelle.

5. – Conclusion.

Nous avons ainsi déterminé à l'aide du modèle de Chew et Low la section efficace de production de 2 mésons positifs jusqu'à des énergies totales dans le système du centre de masse de l'ordre de 400 MeV. Pour plus de brièveté,

(6) B. D'ESPAGNAT: *Mat. Fys. Medd.*, **28**, 11 (1954).

nous n'avons pas inclus ici de considérations sur les corrections relativistes et la production dans l'état S qui sont cependant faciles à établir d'après les équations de Low générales ([5]). La section efficace obtenue est nettement supérieure à ce qui a été déterminé jusqu'ici à l'aide de théories respectant la loi de conservation des probabilités, ce qui semble aller dans la direction des premiers résultats expérimentaux ([7]) et résulte d'un traitement exact des équations intégrales obtenues.

* * *

Je tiens à remercier ici le Professeur C. J. Bakker pour l'hospitalité qui m'a été offerte au CERN à Genève pendant l'accomplissement de ce travail, et à marquer ma reconnaissance envers messieurs Prentki et d'Espagnat, qui ont suggéré le sujet de cette étude. J'ai bénéficié de conversations avec les professeurs G. C. Wick et M. M. Lévy, ainsi que tous les membres de la section théorique du CERN à Genève et son directeur le professeur B. Ferretti. Je remercie le Commissariat à l'Energie atomique et monsieur le Haut-Commissaire F. Perrin pour leur appui.

([7]) A. E. Ignatenko: *Compt. Rend. du Symposium CERN*, tome 2, 313 (1956); J. Crussard, W. O. Walker et M. Koshiba: *Phys. Rev.*, **94**, 736 (1954); M. Blau et M. Caulton: *Phys. Rev.*, **96**, 150 (1954); A. V. Crewe, V. E. Kruse et H. D. Taft: *Bull. APS*, **1**, 150 (1956).

RIASSUNTO (*)

Costruiamo un sistema di equazioni di Low generalizzate nel modello di Chew. La sezione d'urto per la produzione di due mesoni π positivi in uno stato P si deduce con un'approssimazione a un mesone. La corrispondente equazione integrale si risolve numericamente usando gli spostamenti di fase sperimentali e si dimostra la non validità della soluzione per iterazione. Ogni approssimazione numerica fatta nel lavoro è stata verificata.

(* *Traduzione a cura della Redazione.*

Pleochroic Haloes and the Artificial Coloration of Biotites by α Particles.

S. Deutsch (*), P. Kipfer and E. Picciotto

Laboratoire de Physique Nucléaire - Université Libre de Bruxelles

(ricevuto il 6 Giugno 1957)

Résumé. — Nous avons donné dans ce travail les doses d'α nécessaires à la formation des halos pléochroiques dans des biotites de différents granites. Nous avons étudié seulement les halos résultant de l'action des α de la famille de l'Uranium et du Thorium en équilibre, émis en couche épaisse à partir d'inclusions grandes par rapport au parcours des α. Le début d'apparition du halo a lieu pour 10^{14} α émis par cm^2 de l'inclusion, la saturation pour environ $5 \cdot 10^{15}$ α/cm^2, le début d'inversion pour $5 \cdot 10^{17}$ α/cm^2. Les biotites des mêmes granites ont été irradiées, expérimentalement par une source de Rn + RaA + RaC', les α étant complètement absorbés dans la biotite. Les diverses biotites présentent des sensibilités très différentes aux irradiations des α, l'accroissement de densité pour une même dose pouvant varier d'un facteur 5. L'évolution de la coloration suit approximativement une loi de la forme

$$\Delta d_{\max} = \Delta d(1 - \exp[-\varrho\alpha]) ,$$

ϱ, $\Delta d_{\max}$ étant deux paramètres spécifiques et α la dose d'α par cm^2. Le début de la coloration apparaît pour une dose de $2 \cdot 10^{13}$ α/cm^2 en accord avec les anciens résultats de Joly et Rutherford sur des biotites de pegmatites. La saturation nécessite des doses de 7 à $10 \cdot 10^{14}$ α/cm^2 et l'inversion de la coloration n'apparaît pas encore pour des doses de $1.5 \cdot 10^{15}$ α/cm^2. Ces doses semblent plus faibles que celles qui sont nécessaires pour produire les mêmes effets dans les halos. Il n'est cependant pas possible de comparer directement ces doses à celles données pour les halos, à cause des différences dans le spectre d'énergie des α et dans les conditions géométriques d'irradiation. Si au lieu de comparer les doses en nombre d'α, on les compare en *nombre d'ions formés*, l'accroissement de la coloration reste plus rapide dans l'irradiation expérimentale que dans les halos. Les accroissements maxima de densité optique correspondant à la saturation de la coloration sont à peu près les mêmes dans les halos et dans les biotites irradiées expérimentalement. La comparaison des halos et

(*) Attachée à l'Institut Interuniversitaire des Sciences Nucléaires.

des biotites irradiées montre qu'il existe une correspondance au moins qualitative entre les sensibilités d'une biotite aux irradiations expérimentales et naturelles. Au point de vue des mesures d'âge, il n'est pas encore possible d'utiliser ces expériences de coloration artificielle pour une détermination d'âge absolue par les halos. Pour les déterminations relatives, il faut tenir compte des différences de sensibilité. Une méthode proposée consiste à comparer entre elles des biotites présentant la même sensibilité à l'irradiation expérimentale en supposant que cette similitude de sensibilité est valable aussi pour la formation des halos.

1. – Introduction.

In a previous work ([1,2]), we have studied the relation between the intensity of coloration of the pleochroic haloes in biotites, and the α-particle dose emitted by the inclusion responsible for the halo.

The intensity of the halo was expressed as a function of the mean optical density. The dose of α-particle irradiation was estimated, for rocks of known age, by measuring the specific α-activity of the inclusions by the nuclear emulsion method.

The possible determination of geological age by this method is based on the knowledge of the law relating the intensity of the halo with the total α irradiation for a given biotite and also on the assumption that the coloration formed does not fade with time.

The relationship between coloration and the α-particle dose may be established either by a study of haloes in rocks of known age, or by irradiation from an experimental α source. This second method is unique in enabling a determination of the absolute age to be carried out.

A study of the colour induced by experimental irradiation imparts important information regarding variations in the sensibility of biotites of diverse origins.

Finally, a comparison of the relations connecting the haloes and those connecting the results of experimental irradiation will permit the verification of the reciprocity law and the stability of the colour with respect to time, the fundamental hypothesis permitting a determination of age by this method.

The nuclear emulsion technique offers us, for the first time, the possibility of comparing the coloration due to the action of natural radioactive sources over a geological period with the coloration produced artificially by intensely active sources capable of delivering the same radiation dose in a period of the order of a few days. Our present work is based on this line.

([1]) S. Deutsch, D. Hirschberg and E. Picciotto: *Experientia*, **11**, 172 (1955).

([2]) S. Deutsch, D. Hirschberg and E. Picciotto: *Bull. Soc. Belge Géol.*, **65**, 267 (1956).

2. – Early work on pleochroic haloes.

In their earliest works, MÜGGE ([3,4]) and JOLY ([5]) have shown that the halo colorations in various minerals are artificially reproducible under α bombardment from a radium source.

These experiments indicated that the scale of geological time is spread over hundreds of millions of years. This early work established that, in the biotites of pegmatites, the coloration commenced after an irradiation of the order of 10^{13} α per cm^2 ([6]). JEDRZEJOWSKI ([7]) irradiated biotites from an intensely active radon source, and photometrically measured the optical density of the biotites as a function of the radiation dose received. His work indicates a general variation of the coloration as a function of the α dose without, however, giving the absolute value of the doses. His curve indicates, for the first time, the phenomenon of colour inversion.

HENDERSON and BATESON ([8]) have utilized the same technique and obtained the same type of result for two biotites of pegmatite. They observed that the curves corresponding to the two biotites, although presenting the same general form, show notable differences in the evolution of the coloration.

KÜRTI ([9]), using a collimated α beam from a polonium source, studied the coloration variations along the α particle path. He showed that, for weak doses, the different sections of the particle path do not contribute equally to the formation of the coloration. The most intense coloration is produced at the end of the α-particle path, following a law analogous to Bragg's law of ionization.

The evaluation of the naturally occurring α doses causing the pleochroic haloes was impossible prior to the development of the nuclear emulsion method. With the application of this method to the study of the radioactivity of rocks, it became possible to measure the α activity of the inclusions in the pleochroic haloes ([10-14]).

([3]) O. MÜGGE: *Zentrabl. f. Min.*, 397 (1907).
([4]) O. MÜGGE: *Zentrabl. f. Min.*, 65, 113, 142 (1909).
([5]) J. JOLY: *Phil. Mag.*, **13**, 381 (1907).
([6]) J. JOLY and E. RUTHERFORD: *Phil. Mag.*, **25**, 644 (1913).
([7]) H. JEDRZEJOWSKI: *Compt. Rend.*, **186**, 135 (1928).
([8]) G. H. HENDERSON and S. BATESON: *Proc. Roy. Soc.*, A **145**, 263 (1934).
([9]) G. KÜRTI: *Sitzungbericht. Akad. Wissenschaften*, Wien, II *a*, **147**, 402 (1938).
([10]) A. HEE: *Compt. Rend.*, **227**, 356 (1948).
([11]) E. PICCIOTTO: *Bull. Soc. Belge Géol.*, **58**, 75 (1949).
([12]) R. COPPENS: *Compt. Rend.*, **231**, 343 (1950).
([13]) I. HAYASE: *Ann. Min.*, **39**, 761 (1954).
([14]) O. HIEKE-MERLIN, E. PICCIOTTO and S. WILGAIN: *Geochim. et Cosmochim. Acta*, **11**, 171 (1957).

In our earlier work ([1,2]), we have estimated the natural doses necessary to produce the different stages of development of the haloes. These results are recapitulated in Table I.

TABLE I. – *Colour intensity of haloes and their radius of influence* τ *for various* α *doses.*

Aspect of the halo	$\bar{D}$	r_μ	α/cm^2
Very faint	3	10	10^{14}
Faint	7	20	$5 \cdot 10^{14}$
Medium	10	25	10^{15}
Intense	20	30	$4 \cdot 10^{15}$
Saturated Inversed	30	36 (RaC′) 42 (ThC′)	$5 \cdot 10^{17}$

The aim of this work was the comparison of the coloration produced by the experimental α irradiation with those produced by natural irradiations in equivalent doses, and also to compare the sensitivities of the various biotites, the haloes of which we had studied.

3. – Experimental technique.

As an α-particle source we used radon in equilibrium with its short life daughter elements. A thin sheet of biotite between $30 \div 40$ μm thickness was cloven from the granite under study and placed in a glass tube of 2 mm interior and 2.2 mm exterior diameter. This tube is attached, by means of a ground glass joint, to a radon extraction system (this apparatus built by the Union Minière du Haut Katanga and very kindly lent to us is of the well known MACDONALD and MARGOLESE ([15]) type) which permits the extraction of radon from a 100 millicurie solution of radium, its purification and its concentration to a volume of a few mm^3. The tubes containing the biotites are thus filled with radon, scaled, carefully washed and tested for radon leaks. They are then placed in a special support (see Fig. 1) designed to be fixed on a microscope stage, and enabling variations in the position and orientation of the biotite.

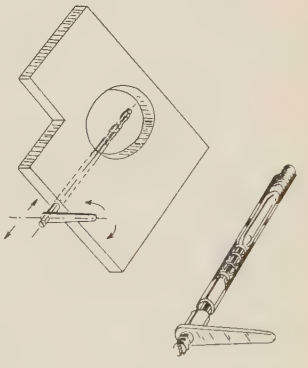

Fig. 1. – Special support for radon tubes.

The optical transmission across the biotite and the glass tube is measured with a micropho-

([15]) P. A. MAC DONALD and M. S. MARGOLESE: *Rev. Sci. Instr.*, **12**, 320 (1941).

tometer as described in our preceding work ([2]). The following modifications were, however, made:

The current produced in the photomultiplier is measured with the help of a galvanometer, in place of the usual method of recording on a potentiometer. A weakly magnifying objective (10×) is employed, the optical conditions being less stringent than for the measurement of pleochroic haloes; the diameter of the field covered by the photometer is 50 μm. The microscope was enclosed by a 30 cm thick steel protecting wall and the operations of adjusting and of varying the position of the object were carried out by remote control (Fig. 2).

In the conditions we employed, all tubes were about 1 cm long and contained one or two plates of biotite of an area of a few square mm each together with, at the start of the experiment, 20 to 40 millicuries of radon. Measurements of optical transmission were made at intervals of 3 or 4 hours over a period of several days.

The exact quantity of radon contained in each of the tubes was very kindly measured in the Radium Department of the Union Minière du Haut Katanga by comparing the γ activity of each tube with that of a standard Ra source, using an ionization chamber.

The total number of α-rays which has been emitted at time t is given by

$$N_\alpha = \frac{3 \cdot R \cdot 3.7 \cdot 10^{10}}{\lambda} (1 - \exp[-\lambda t]) ,$$

where $t = 0$ = time of filling of the tube,

R = amount of Rn (in Curies) contained in the tube at time $t = 0$,

t = time of measure, in s,

λ = radioactivity constant of Rn, in s^{-1}.

In order to estimate the dose received by the biotite we have assumed that there is no selfabsorption of α within the volume of the tube and that the flux of α radiation is constant for the whole tube, the edge effects thus being neglected.

The transmission across the biotite is always measured in the same region, located as well as possible for each measurement. It is expressed with respect to the transmission across the glass tube measured in the neighbourhood of the biotite, which eliminates the effect, caused by the coloration due to the α-particles, of the glass itself.

The increase in the optical density for a given biotite should be independent of the thickness of the sheet when this thickness is greater than the longest

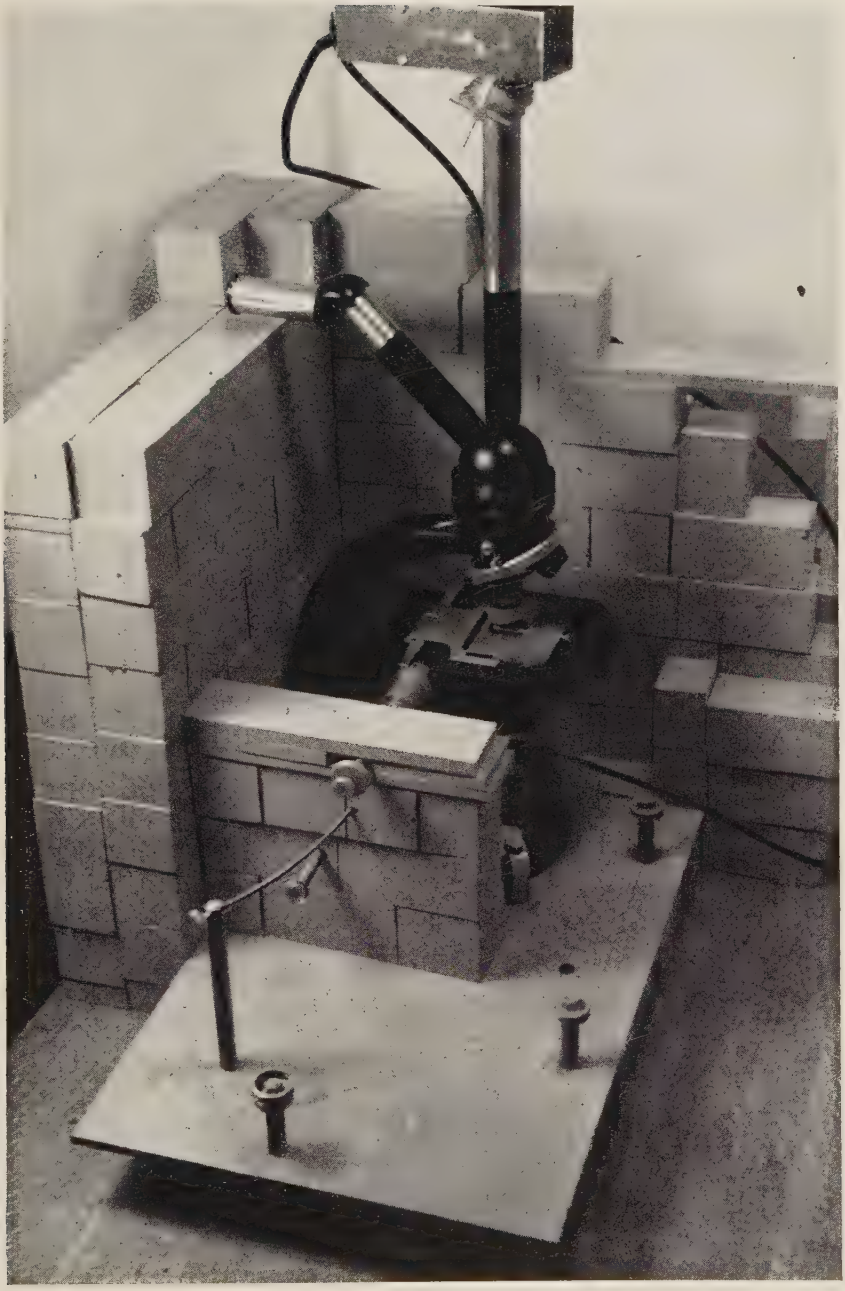

Fig. 2.

α-particle path (RaC′), to wit 36 μm. In fact, it can be shown that a thickness of 20 μm is sufficient to stop the particles. For a thin source of Rn+ +RaA +RaC′, the proportion of α which is not completely absorbed by 20 μm of mica, is less than a few percent.

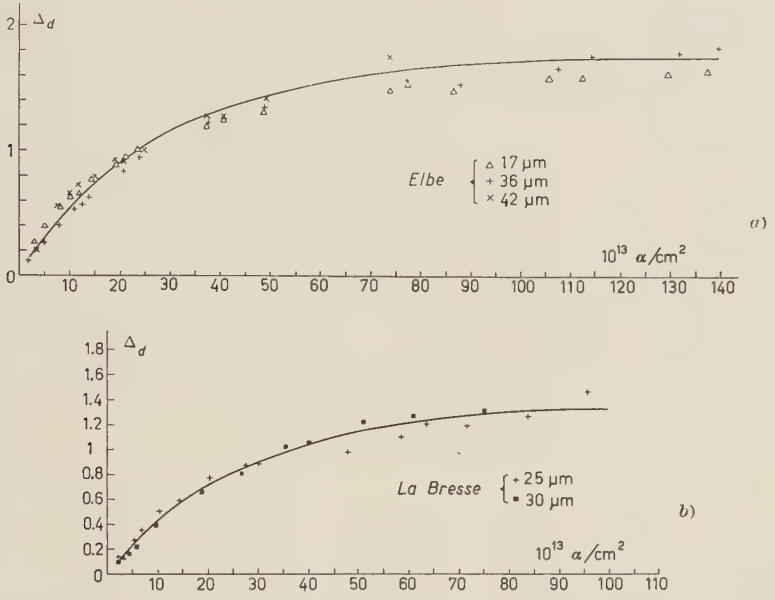

Fig. 3. – Increase in optical density as a function of the α dose for sheets of different thicknesses in two biotites.

Fig. 3 (*a* and *b*) shows the increase in optical density as a function of the α dose for sheets of different thicknesses of one biotite, placed in different tubes. We obtain an idea of the influence of thickness as well as the reproducibility of the measurements, the two series of measurements of the curve 2*b* having been carried out several months apart.

The necessity of measuring the optical transmission across the glass tube introduces an important distortion of the image, as well as an intensity of diffused light which prohibit measurements of feeble transmission. We have however, verified that for optical densities as high as 3, we obtain comparable results on measuring the biotite contained in the glass tube or the biotite placed on an object plate and immersed in oil.

4. – Results.

We have studied the biotites of 11 granites listed in Table II, of which we have studied the pleochroic haloes. The results concerning the haloes of some

of these biotites have already been published, the rest are in process of publication.

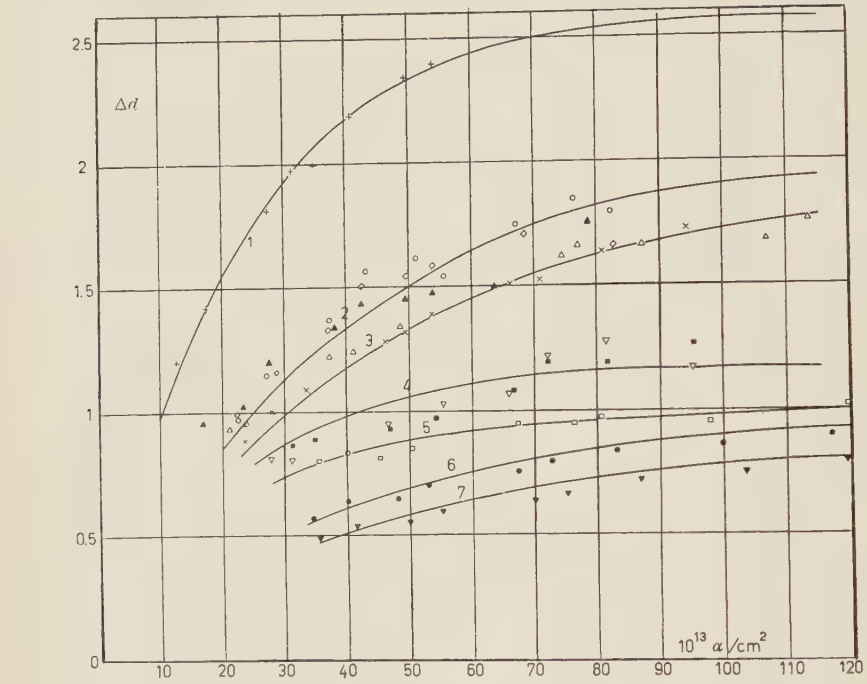

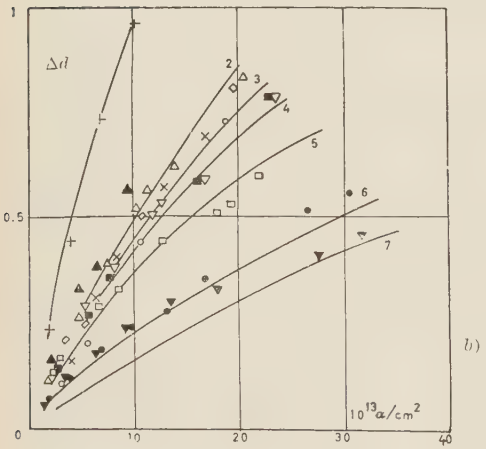

Fig. 4. – Increase in optical density as a function of the α dose for 11 granitic biotites.

1. Kalule +
2. Vire ◇, Lausitz ○, Causey ▲
3. Elbe △, Baveno x
4. La Bresse ■, St. Amarin ▽
5. S.te Marie □
6. Bonawe Quarry ●
7. Adamello ▼

The results are presented in Fig. 4 (including those of Fig. 3), which shows the increase in optical density Δd of the biotite (thickness 20 to 30 μm) as a function of the number of α from Rn + RaA + RaC′ per cm² totally absorbed

TABLE II.

Granitic Massif	Region	Age
Kalule	Kibara (Belgian Congo)	Kibarian
Chausey	Britain	Precambrian
Vire	Britain	
Bonawe Quarry	Scotland	Silurian
S.te Marie-aux-Mines	Vosges (France)	Lower Carboniferous
La Bresse		
St. Amarin		
Lausitz	Germany	
Baveno	Italy	
Monte Capanne	Elba Island	Upper eocene
Adamello	Italian Alps	Eocene

in the biotite. The optical density of the non-irradiated biotites is of the order of 1,2.

5. – Discussions of the results.

The general shape of the curves is the same for all the biotites. The commencement of a measurable coloration ($\Delta d = 0.1$) is provoked by a dose of 10^{13} α/cm^2 (in agreement with the observations of JOLY and RUTHERFORD), the optical density increases less and less until it reaches a plateau in the curve, for doses of the order of 10^{15} α/cm^2. The inversion stage is not reached for doses of less than $1.4 \cdot 10^{15}$ α/cm^2. One notes, however, pronounced individual variations in both the increase of density corresponding to the saturation, as well as the slope of the curves. Except for a few exceptions, the curves form a fairly close bundle with little divergence for doses less than $1.25 \cdot 10^{14}$ α/cm^2.

For a given biotite, it is possible to present, with fair approximation, the experimental points on a curve with an equation of the following type:

$$\Delta d = \Delta d_{max} (1 - \exp[-\varrho\alpha]) ,$$

where Δd_{max} is the value of Δd corresponding to the saturation plateau.

ϱ is a parameter characteristic of each biotite, representing the fraction formed per α, of the total number of colour centers.

α is the total dose of α per cm^2.

The sensitivity to coloration of a biotite by α-rays may then be defined by the two parameters Δd_{max} and ϱ. They may be easily estimated graphically. If we plot in semi-logarithmic co-ordinates $(\Delta d_{max} - \Delta d)/\Delta d_{max}$ against α, we obtain a straight line with a slope ϱ. When the experimental determination

of the value of Δd_{max} is not possible, it may be determined by iteration, by adjusting Δd_{max} so that the experimental points lie on a straight line. The values of Δd_{max} and ϱ thus found for various biotites are shown in Table III. The dose necessary to cause an increase in density equal to one half of Δd_{max} ($S_{\frac{1}{2}} = \log 2/\varrho$) are also given.

TABLE III. - *Parameters Δd_{max}, ϱ and $S_{\frac{1}{2}}$ (defining the law governing the increase of artificial coloration as a function of the α dose) for the biotites examined.*

Sample	Δd_{max}	ϱ 10^{-15}	$S_{\frac{1}{2}}$ 10^{+13}
Kalule	2.6	4.6	15
Chausey	2.1	2.6	27
Vire	2.1	2.6	27
Bonawe Quarry	1	2.3	29
S.te Marie-aux-Mines	1	4.5	15.2
La Bresse	1.2	4.3	16.2
St. Amarin	1.2	4.3	16.2
Lausitz	2.1	2.6	27
Baveno	1.9	2.5	28
Elba Island	1.9	2.5	28
Adamello	0.9	2	33

The curves passing through the experimental points of Fig. 3 have been calculated with these values of the parameter.

6. – Comparisons with the haloes.

The quantitative comparison of the colorations in the case of experimental irradiation and in the case of the haloes is complicated by two factors:

1) The energy spectrum of the α emerging from a thick inclusion containing U and Th is very different from that of the α emerging from a thin layer of radon.

2) The geometrical conditions of observation differ in both cases.

In the case of the biotite experimentally irradiated Δd (the increase in optical density) is measured at right angles to the surface of contact between the source and the biotite.

In the case of the haloes, the optical density is measured parallel to the surface of contact between the inclusion and the biotite, across a 25 μm thickness of biotite. The mean density increase across 25 μm, spread over

the whole radius of action η in (μm) of the halo is:

$$\frac{1}{r}\int_0^r D\,\mathrm{d}x = \frac{\overline{D}}{r}\,.$$

The same concentration of colour centers if measured at right angles to the surface of contact, would be seen across a thickness of r and would give an increase in density of

$$\Delta d_n = \frac{1}{r}\left\{\int_0^r D\,\mathrm{d}x\right\}\frac{r}{a} = \frac{D}{a}\,.$$

It must be remembered that D is measured across a standard thickness of 25 μm.

Δd_n represents the increase in density which would be measured were the halo photomeasured under the same geometrical conditions as the irradiated biotite.

We signify, by Δd_a, the increase in density as measured on experimentally irradiated biotites.

For doses corresponding to the same number of α per cm^2 we may expect to have $\Delta d_n < \Delta d_a$ for two reasons:

1) Δd is certainly a function of the total energy loss of the α-particles. in the case of emission from a thick layer (inclusions), the total energy expended in the biotite is less than that expended by an emission from a thin layer, for the same number of α per cm^2.

2) The increase in density is neither a linear function of the number of α nor of the energy loss, and presents a saturation effect. If we examine the distribution of ionization as a function of distance from the source ([16]), we find that the total ionization is distributed in a more homogeneous manner in the case of irradiated biotites than in the case of the haloes. For the same total energy expended, the haloes should blacken more slowly as certain regions are saturated more rapidly.

To clear the first difficulty, it seemed logical to compare the increases in optical density due to *the same number of ion pairs formed*, per unity of surface of the source. However, not knowing the mechanism of the fundamental law governing the formation of the colour, it was impossible for us to solve the second difficulty.

([16]) R. D. Evans: *Phys. Rev.*, **45**, 24 (1934).

Applying the formulae calculated by Evans assumed valid for solids, we find that, for the same number of α emerging per cm² of the source, the number of ions formed by a source of Rn + RaA + RaC′ is exactly double the number of ions formed by an infinitely thick source source containing the Th and U families in equilibrium. This value has been calculated assuming a ratio of Th/U = 3.4, but it varies little with change in the ratio.

If Δd_n is the increase in coloration corresponding to a dose of α_n per cm², the increase in coloration Δd_a due to a dose $\alpha_a/2$ must be compared to it, in order to account for the difference in ionization.

Table IV shows the comparisons of ionization doses necessary to obtain the same colour densities, both natural and artificial, for some haloes in granites of known age.

We considered interesting the comparison between the maximum values

TABLE IV. – *Natural and experimental irradiation doses necessary to obtain like increases in optical density in various biotites of granite.*

Δd	Elba Island and Vosges		Kalule	
	nat. dose α_n/cm²	exp. dose $(\alpha_a/2)$/cm²	nat. dose α_n/cm²	exp. dose $(\alpha_a/2)$/cm²
0.2	$3.5 \cdot 10^{14}$	$7 \cdot 10^{14}$	—	—
0.3	$8 \cdot 10^{14}$	$1.2 \cdot 10^{14}$	—	—
0.4	$1.3 \cdot 10^{15}$	$1.8 \cdot 10^{14}$	—	—
0.5	$1.8 \cdot 10^{15}$	$2 \cdot 10^{14}$	$3 \cdot 10^{14}$	$8 \cdot 10^{13}$
0.6	$2 \cdot 10^{15}$	$3 \cdot 10^{14}$	$4 \cdot 10^{14}$	$9 \cdot 10^{13}$
0.8	$3 \cdot 10^{15}$	$5 \cdot 10^{14}$	$7 \cdot 10^{14}$	$1.4 \cdot 10^{14}$
1	$5 \cdot 10^{15}$	$7 \cdot 10^{14}$	$8 \cdot 10^{14}$	$1.8 \cdot 10^{14}$

α_n = number of α per cm² emitted by the inclusion of the halo.
α_a = number of α per cm² emitted by the radon source.

of density obtained by experimental irradiation and the maximum densities as found in the saturated regions of haloes.

These saturated regions are easily recognized in the photo-measured profile of the halo insofar as the optical density remains constant with reference to distance from the inclusion. Table V shows the result of such a comparison. On examining Tables IV and V the following conclusions may be drawn:

1) In order to obtain the same increase in coloration, the experimental ionization dose required is less than the natural dose. In other words, for the same ionization or the same total energy loss, we have $\Delta d_a > \Delta d_n$. This result is to be expected, taking into account the previous consideration.

TABLE V. – *Comparison between the maximum densities of various granites obtained by experimental irradiation and the saturated haloes.*

Granite	Δd_{max} natural	Δd_{max} extrapolated experimental
Kalule	1.75	2.6
Vire	1.9	2.1
Chausey	1.8	2.1
La Bresse	1.45	1.4
St. Amarin	1.4	1.4
S.te Marie	1.1	1.0
Lausitz	1.8	2.1
Baveno	2	1.9

2) The maximum density values for any single biotite, whether obtained artificially, or measured on a saturated halo, are very close. It thus appears that, although the increase in density achieved by experimental irradiation is obtained more rapidly than in the case of the haloes, the same value of saturation is nevertheless achieved in both cases.

3) The ratio of artificial ionization dose to natural ionization dose required in order to obtain the same coloration, is of the same order for all the biotites and lies between $\frac{1}{4}$ et $\frac{1}{7}$. This difference in doses is too large to be accounted for solely by the mechanism of saturation of the coloration and the repartition of the ionization. This more rapid increase in coloration could be explained by the formation of less stable colour centers, which disappear in the course of time. The heat treatment of irradiated biotites would indicate the existence of such stability differences in the colours centers.

As a preliminary trial, we heated, for four days at 300 °C, two biotites from the same sample, one containing a halo, the other having been experimentally irradiated to saturation of the coloration. Absolutely no fading of the colour took place in either case.

4) The comparison made in Table IV also indicates correspondence between the sensitivities of a biotite to experimental and natural irradiations. The biotite of Kalule granite, which is more rapidly coloured artificially than the biotites of the Vosges or Elba-groups, is also that biotite which requires the smallest – dose for an equal increase in density of the haloes.

We have seen in our preceding article, that the haloes of the biotite of Kalule show an age of more than 3 000 million years (M.A.) basing ourselves on the simplified hypothesis that the sensitivity of this biotite was the same as the mean sensitivity of the other biotite of the granites investigated. This age was misleading as the Kibarian Age (1 000 M.A.) of this Kalule granite

2667

is well established. In the light of the results given here, this anomaly is resolved due to the exceptionally large sensitivity of this biotite.

On the other hand, the other results appear to be coherent within the experimental limits of the method and correspond well with biotites possessing analogous sensitivities.

7. – Influence on age measurements.

The method we proposed in order to measure the age of the haloes, was based on two hypotheses.

1) The stability of the halo coloration with respect to time.

2) An identical sensitivity for all the biotites.

We have nothing to add to the comments already made about the first hypothesis, in our previous publications.

The experimental irradiations carried out, show that the second hypothesis is too simple, and in certain cases, completely erroneous. It thus appears certain that age measurements cannot be based on this hypothesis, as we have done in our preceding work, and as was done by HAYASE ([13]).

We cannot, as yet, completely account for the sensitivity differences of the biotites, using the results obtained by the experimental irradiations. It is necessary to be more completely informed about the mechanism of the formation of the coloration, and either prove that the effect obtained as a result of irradiations corresponds with that of the haloes, or establish a constant correlation between these two effects.

It, however, seems possible to replace the hypothesis of an identical sensitivity by a more practical one which goes as follows—*two biotites presenting the same sensitivity curve to experimental irradiation, also have comparable sensitivities for the formation of haloes*—the method thus evolved would permit the measurement of the relative ages of the two biotites showing similar behaviour under experimental irradiation. Examples of the application of this method to the age of granitic and metamorphosic rocks will be published shortly ([17]).

8. – Conclusions.

We have reported, in this work, the α doses necessary for the formation of pleochroic haloes in biotites of various granites.

([17]) S. DEUTSCH: *Experientia*, à paraître (1957).

We have only studied those haloes resulting from the action of α-particles emitted by the uranium and thorium families in equilibrium, emitted in thick layers from inclusions which are large compared to the path of the α. The primary apparition of the halo takes place after 10^{14} α have been emitted per square centimeter (cm^2) of the inclusion, saturation starts after about $5 \cdot 10^{15}$ α/cm^2 and the inversion phenomenon commences at about $5 \cdot 10^{17}$ α/cm^2.

We have experimentally irradiated biotites of these same granites, using Rn +RaA +RaC′ as an α source, the alpha particles being completely absorbed in the biotite. The various biotites showed widely varying sensitivities in the α irradiations, the density increase for a similar dose varying by a factor as high as 5.

The evolution of the coloration approximates a law of the form

$$\Delta d = \Delta d_{\max} (1 - \exp [- \varrho \alpha]) ,$$

ϱ, $\Delta d_{\max}$ being two specific parameters and α the total dose of α per cm^2.

The coloration first appears after a dose of $2 \cdot 10^{13}$ α/cm^2, in agreement with the earliest results obtained by JOLY and RUTHERFORD on the biotites of pegmatite.

Saturation necessitates doses of from $7 \cdot 10^{14}$ α/cm^2 to $10 \cdot 10^{14}$ α/cm^2, and the inversion of the coloration has not taken place at $1.5 \cdot 10^{15}$ α/cm^2. All these doses appear to be weaker than those required to produce comparable effects in the case of the haloes.

It is, however, impossible to compare these doses directly with those received by the haloes, because of differences in the energy spectra of the α and because of geometrical differences in the irradiation conditions.

If, instead of comparing the doses in numbers of α, they were compared as numbers of ions formed, the increase in coloration would still take place more rapidly when experimentally irradiated than in the case of the haloes. This difference is still unexplained but could be due to variations in the geometrical conditions of emission, or possibly to the formation of supplementary and less stable colour centers, during a short but intense irradiation.

The maximum increases in optical density corresponding to the saturation of the coloration are much the same in the haloes and in the irradiated biotites.

A comparison between haloes and irradiated biotites indicates at least a qualitative correspondence between the sensitivities of a biotite to experimental and to natural radiations.

As regards measures of age, it is not yet possible to utilize this work on artificial coloration to determine the absolute age of the haloes. For relative determinations, the sensitivity differences must be taken into account. A suggested method would be to compare amongst themselves those biotites which

have the same sensitivity to experimental irradiation, assuming of course, that this similitude of sensitivity is valid in the formation of the haloes.

* * *

Our thanks are due to Miss J. STORMS and Mr. JANS for their invaluable help.

RIASSUNTO (*)

Abbiamo dato in questo lavoro le dosi di α necessarie alla formazione degli aloni pleiocroici nelle biotiti di differenti graniti. Abbiamo studiato soltanto gli aloni risultanti dall'azione delle α della famiglia dell'Uranio e del Torio in equilibrio, emesse in strato spesso da inclusioni grandi rispetto al percorso delle α. L'inizio della comparsa dell'alone si ha per 10^{14} α emesse per cm^2 dell'inclusione, la saturazione per circa $5 \cdot 10^{15}$ α/cm^2, l'inizio dell'inversione per $5 \cdot 10^{17}$ α/cm^2. Le biotiti degli stessi graniti sono state irradiate sperimentalmente con una sorgente di Rn + RaA + RaC', con completo assorbimento delle α nella biotite. Le diverse biotiti presentano sensibilità assai differenti alle irradiazioni delle α, potendo l'accrescimento di densità per una stessa zona variare di un fattore 5. L'evoluzione del colore segue approssimativamente una legge della forma

$$\Delta d_{\max} = \Delta d(1 - \exp[-\varrho\alpha]) ,$$

ϱ e $\Delta d_{\max}$ sono due parametri specifici e α la dose d'α per cm^2. L'inizio della colorazione appare per una dose di $2 \cdot 10^{13}$ α/cm^2 in accordo coi vecchi risultati di Joly e Rutherford su biotiti pegmatitiche. La saturazione richiede dosi da 7 a $10 \cdot 10^{14}$ α/cm^2 e l'inversione della colorazione non si manifesta ancora per dosi di $1.5 \cdot 10^{15}$ α/cm^2. Queste dosi appaiono più deboli di quelle necessarie a produrre gli stessi effetti negli aloni. Non è tuttavia possibile confrontare direttamente queste dosi con quelle date per gli aloni, date le differenze nello spettro di energia delle α e nelle condizioni geometriche d'irradiazione. Se anzichè confrontare le dosi in numero d'α le si confrontano in *numero di ioni formati* l'accrescimento della colorazione risulta più rapido nell'irradiazione sperimentale che negli aloni. I massimi accrescimenti di densità ottica che corrispondono alla saturazione della colorazione sono circa uguali negli aloni e nelle biotiti irradiate sperimentalmente. Il confronto degli aloni con le biotiti irradiate mostra che esiste una corrispondenza almeno qualitativa tra le sensibilità d'una biotite alle irradiazioni sperimentali e alle naturali. Per la datazione non è ancora possibile utilizzare queste esperienze di colorazione artificiale per una determinazione assoluta per mezzo degli aloni. Per le determinazioni relative bisogna tener conto delle differenze di sensibilità. Si propone un metodo consistente nel confrontare fra di loro delle biotiti dotate della stessa sensibilità all'irradiazione sperimentale, supponendo che questa similitudine di sensibilità sussista anche per la formazione degli aloni.

(*) *Traduzione a cura della Redazione.*

Théorie statistique du comptage de particules alpha émises par des désintégrations successives d'éléments radioactifs.

M. Huybrechts

Institut Interuniversitaire des Sciences Nucléaires - Centre de Bruxelles

(ricevuto il 6 Giugno 1957)

Résumé. — La distribution du nombre de particules α enregistrées dans un intervalle de temps t_0 par un compteur surmontant une source radioactive d'épaisseur quelconque est étudiée dans le cas général où la source contient des éléments radioactifs subissant des désintégrations successives. Le calcul des cumulants permet de montrer que la distribution est asymptotiquement gaussienne. Une méthode de calcul des probabilités conditionnelles de comptage des α émis par des désintégrations successives est développée dans l'Appendice. Les résultats sont appliqués aux familles de l'Uranium et du Thorium en équilibre, pour un intervalle de temps t_0 de 30 jours.

1. – Introduction.

Le nombre de particules α émises pendant un intervalle de temps t_0 par des éléments radioactifs à vies moyennes longues par rapport à t_0 et ne subissant que des désintégrations α simples est distribué suivant une loi de Poisson.

Il n'en est pas de même lorsque les éléments radioactifs subissent des désintégrations successives donnant naissance à plusieurs particules α.

L'attention a été attirée sur ce fait par Adams [1], qui a montré que la distribution du nombre d'α émis pendant un intervalle de temps de 5 minutes par la famille du Thorium en équilibre radioactif s'écartait notablement d'une loi de Poisson.

[1] N. I. Adams jr.: *Phys. Rev.*, **44**, 651 (1933).

2671

Les raisonnements de ADAMS ne s'appliquent cependant qu'au cas où aucun élément de la famille n'a une vie moyenne du même ordre de grandeur que l'intervalle de temps t_0.

Plus récemment, LINDEMAN [2] a généralisé les raisonnements de ADAMS, pour un intervalle de temps quelconque, ce qui lui a permis de calculer la distribution du nombre d'α émis par la famille du Thorium en équilibre radioactif pendant un intervalle de temps de 1 minute.

Nous considérons ici le cas général d'une source contenant des éléments radioactifs en filiation, l'équilibre radioactif n'étant pas nécessairement atteint.

Comme le nombre d'α émis n'est en général pas directement accessible à la mesure, nous étudions la distribution du nombre d'α enregistrés par un compteur surmontant la source.

Cette distribution, de forme compliquée, est difficilement utilisable lorsque le nombre moyen d'α comptés est grand. Par contre ses cumulants s'expriment par des relations simples en fonction des nombres moyens de groupes d'α associés émis et des probabilités conditionnelles de comptage. Ceci nous permet de montrer que la distribution du nombre d'α comptés est asymptotiquement gaussienne, Le cas particulier où la source est en équilibre radioactif est considéré à la Sect. 6.

La Sect. 8 est consacrée à l'estimation du nombre moyen d'α comptés, par la méthode des intervalles de confiance.

Une méthode de calcul des probabilités conditionnelles de comptage est développée dans l'Appendice, pour une source d'épaisseur quelconque avec ou sans écrans. Des expressions simples permettent de calculer aisément l'espérance mathématique et la variance du nombre d'α comptés.

Les résultats sont appliqués aux familles de l'Uranium et du Thorium en équilibre radioactif pour un intervalle de temps de 30 jours, ce qui est un temps d'exposition usuel pour la mesure d'activités faibles à l'aide d'émulsions nucléaires.

2. – Nous supposons que la source radioactive contient les éléments en filiation E_1, E_2, ..., E_f. Nous prenons comme origine du temps le début de l'intervalle t_0 et nous supposons qu'à un moment antérieur déterminé $t = -t_1$, seul l'élément E_1 était présent. Les descendants de E_1, que la source contient au temps $t = 0$, proviennent donc exclusivement de désintégrations d'atomes de E_1 présents au temps $t = -t_1$.

Si nous désignons par $N_i(t)$ le nombre d'atomes de l'élément E_i présents au temps t, on a donc

$$N_i(-t_1) = 0\,, \qquad \text{pour } i > 1.$$

[2] H. LINDEMAN: *Physica*, **21**, 589 (1955).

Les nombres d'atomes des éléments E_i présents au temps $t = 0$ sont des variables aléatoires dont les valeurs moyennes sont données par les relations de Bateman [3] qui peuvent s'écrire, en désignant par $\langle N_i(t)\rangle = E\{N_i(t)\}$ la valeur moyenne (ou espérance mathématique) de $N_i(t)$,

$$\langle N_i(0)\rangle = N_1(-t_1)\cdot P_{1,i-1}(t_1) \qquad (i = 1, 2, ..., f), \tag{2.1}$$

$P_{1,i-1}(t)$ désignant la probabilité d'obtenir *exactement* $(i-1)$ désintégrations successives d'un atome de E_1, présent au temps $t = -t_1$, dans l'intervalle de temps $(-t_1, 0)$, c'est-à-dire la probabilité de la transformation d'un atome de E_1 en un atome de E_i non désintégré au début de l'intervalle t_0.

On a

$$P_{1,i-1}(t_1) = \begin{cases} \displaystyle\sum_{j=1}^{i} \lambda_j \exp[-\lambda_j t_1] \prod_{\substack{l=1 \\ (l\neq j)}}^{i} \frac{\lambda_l}{\lambda_l - \lambda_j}, & \text{pour } i = 2, \ldots f \\ \exp[-\lambda_1 t_1], & \text{pour } i = 1. \end{cases} \tag{2.2}$$

La distribution conjointe des variables aléatoires $N_i(0)$ est, dans le cas général, donnée par une loi multinomiale.

Lorsque l'on a $N_1(-t_1) \gg 1$ et $P_{1,i-1}(t_1) \ll 1$ pour $i = 2, 3, ..., f$, on a $N_1(0) \cong N_1(-t_1)$ et la distribution conjointe de $N_2(0)$, $N_3(0)$ ... $N_f(0)$ peut être assimilée à un produit de lois de Poisson de paramètres $\langle N_2(0)\rangle$, $\langle N_3(0)\rangle$, ..., $\langle N_f(0)\rangle$ (pour $N_i(0) \ll N_1(-t_1)$, $i = 2, 3, ..., f$).

3. – Désignons par $P^{(\alpha)}_{i,k}(t_0)$ la probabilité d'émission de k particules α, dans l'intervalle de temps t_0, par des désintégrations successives d'un atome de l'élément E_i présent au début de t_0.

Considérons la suite des désintégrations successives de E_i. Si s et s' sont les nombres de désintégrations des plus petits groupes de désintégrations successives de E_i comportant respectivement k et $k+1$ alpha, on a

$$P^{(\alpha)}_{i,k}(t_0) = \mathcal{P}_{i,s}(t_0) - \mathcal{P}_{i,s'}(t_0) \qquad (s' \geqslant s+1), \tag{3.1}$$

$\mathcal{P}_{i,s}(t_0)$ désignant la probabilité d'obtenir *au moins* s désintégration (α ou β) successives d'un atome de E_i dans l'intervalle t_0.

On a

$$\mathcal{P}_{i,s}(t_0) = 1 - \sum_{j=i}^{i+s-1} C_{i,s,j} \exp[-\lambda_j t_0],$$

---

[3] H. Bateman: *Proc. Cambridge Phil. Soc.*, **15**, 423 (1910).

avec

$$C_{i,s,j} = \begin{cases} \prod_{\substack{l=i \\ (l \neq j)}}^{i+s-1} \frac{\lambda_l}{\lambda_l - \lambda_j}, & \text{pour } s = 2, 3, \ldots \\ 1, & \text{pour } s = 1. \end{cases} \tag{3.2}$$

Si plusieurs suites de désintégrations successives de E_i sont possibles, on les considérera séparément en tenant compte des probabilités des embranchements.

La probabilité pour qu'un atome de E_i soit formé à partir d'un atome de E_1 présent au temps $t = -t_1$ et subsiste au début de l'intervalle t_0 pour donner naissance, dans cet intervalle, à un groupe de k particules α est donc

$$P_{1,i-1}(t_1)\, P^{(\alpha)}_{i,k}(t_0)\,. \tag{3.3}$$

Par conséquent, le nombre moyen de groupes de k particules α émis dans l'intervalle t_0 par l'élément E_i est

$$\begin{cases} \theta_{i,k} = N_1(-t_1) P_{1,i-1}(t_1) P^{(\alpha)}_{i,k}(t_0) \\ \qquad = \langle N_i(0) \rangle P^{(\alpha)}_{i,k}(t_0)\,. \end{cases} \tag{3.4}$$

En sommant sur tous les éléments E_i, on obtient le nombre moyen de groupes de k particules α émis par toute la source dans l'intervalle t_0:

$$\theta_k = \sum_{i=1}^{f} \theta_{i,k}\,. \tag{3.5}$$

4. – Nous supposons que la source radioactive présente deux faces planes parallèles, la face supérieure étant surmontée d'un compteur de particules α. Nous admettons que tout α traversant la surface de séparation avec un parcours résiduel dans l'air supérieur à ϱ cm est enregistré par le compteur. Nous supposons de plus que la surface de la source est suffisamment grande pour que l'on puisse négliger la correction des bords.

Si nous mesurons les profondeurs dans la source radioactive à partir du plan de séparation et si nous les exprimons, ainsi que les parcours, en cm d'air, la probabilité conditionnelle de comptage d'une particule α de parcours R émise à la profondeur z est:

$$p = \begin{cases} \frac{1}{2}\left(1 - \frac{z}{R'}\right), & \text{pour } z < R', \\ 0, & \text{pour } z \geqslant R', \end{cases} \tag{4.1}$$

où $R' = R - \varrho$ est appelé le parcours effectif de l'α.

La probabilité complémentaire est

$$\overline{p} = \begin{cases} \frac{1}{2}\left(1 + \frac{z}{R'}\right), & \text{pour } z < R', \\ 1, & \text{pour } z \geqslant R'. \end{cases} \tag{4.2}$$

Divisons la source, parallèlement à la surface, en couches minces d'épaisseur Δz faible par rapport aux parcours effectifs, de telle façon que l'on puisse admettre que les probabilités conditionnelles de comptage des α restent constantes à l'intérieur de chaque couche.

Considérons un groupe de k particules α émis par des désintégrations successives d'un atome de l'élément E_i se trouvant à la profondeur z et désignons par $p(l\,|\,i,k;\,z)$ la probabilité conditionnelle de comptage de l particules α quelconques de ce groupe.

La probabilité pour qu'un atome de E_i soit formé à partir d'un atome de E_1 se trouvant à la profondeur z et subsiste au début de l'intervalle t_0 pour donner naissance, dans cet intervalle, à k particules α dont l seront comptées est donc

$$P_{1,i-1}(t_1)\,P^{(\alpha)}_{i,k}(t)\,p(l\,|\,i,\,k;\,z)\,. \tag{4.3}$$

D'autre part, si E est l'épaisseur de la source radioactive exprimée également en cm d'air, $(\Delta z/E)N_1(-t_1)$ est le nombre moyen d'atomes de E_1 que la couche mince z, $z+\Delta z$ contenait au temps $t = -t_1$.

Par conséquent, le nombre moyen de groupes de l particules α comptées provenant de groupes de k particules α émis par désintégrations successives des atomes de E_i de la couche z, $z+\Delta z$ sera

$$\frac{\Delta z}{E}\,N_1(-t_1)P_{1,i-1}(t_1)P^{(\alpha)}_{i,k}(t_0)p(l\,|\,i,\,k;\,z)\,. \tag{4.4}$$

En sommant sur les indices i et k, on obtient le nombre moyen de groupes de l particules α comptées provenant de la couche mince z, $z+\Delta z$,

$$\mu_l(z;\,\Delta z) = \frac{\Delta z}{E}\,N_1(-t_1)p_l(t_1,\,t_0;\,z)\,, \tag{4.5}$$

avec

$$p_l(t_1,\,t_0;\,z) = \sum_{i=1}^{f}\sum_{k=1}^{r} P_{1,i-1}(t_1)\,P^{(\alpha)}_{i,k}(t_0)\,p(l\,|\,i,\,k;\,z)\,, \tag{4.6}$$

si les groupes d'α émis par les éléments de la source dans l'intervalle t_0 comportent au plus r particules α.

Nous considérons ici uniquement le cas où l'on a $(\Delta z/E)\cdot N_1(-t_1) \gg 1$ et $p_l(t_1, t_0; z) \ll 1$ pour $l \neq 0$.

Comme $p(l|i, k; z)$ peut être de l'ordre de l'unité, il faut que, pour chaque élément E_i, le nombre moyen d'atomes présents au début de l'intervalle t_0 soit faible par rapport au nombre d'atomes de E_1 présents au temps $t = -t_1$ ou que la probabilité de désintégration α k-uple d'un atome dans l'intervalle t_0 soit faible, pour $k = 1, 2, ..., r$. Ceci est réalisé en particulier lorsque l'on a $t_1 \ll \lambda_1^{-1}$, ce qui entraine $N_1(0) \cong N_1(-t_1)$ et $\langle N_i(0)\rangle \ll N_1(-t_1)$ pour $i = 2, 3, ..., f$, et $t_0 \ll \lambda_1^{-1}$ ce qui entraine $P_{1,k}^{(\alpha)}(t_0) \ll 1$ pour $k = 1, 2, ..., r$.

On peut admettre alors que le nombre de groupes de l particules α comptées provenant de la couche mince z, $z \vdash \Delta z$, $n_l(z; \Delta z)$, est distribué suivant une loi de Poisson de paramètre $\mu_l(z; \Delta z)$, pour $n_l(z; \Delta z) \ll (\Delta z/E)\cdot N_1(-t_1)$.

En vertu de la propriété d'additivité de la loi de Poisson (Cramer [4] (16.5)), la distribution de n_l, nombre de groupes de l particules α comptées pour toute la source radioactive est également une loi de Poisson, dont le paramètre μ_l s'obtient en sommant $\mu_l(z; \Delta z)$ sur toutes les couches minces.

En remplaçant la somme par une intégrale, on obtient

$$\mu_l = N_1(-t_1) P_l(t_1, t_0; E)\,, \tag{4.7}$$

avec

$$P_l(t_1, t_0; E) = \sum_{i=1}^{f} \sum_{k=1}^{r} P_{1,i-1}(t_1) P_{i,k}^{(\alpha)}(t_0) P(l|i, k; E) \tag{4.8}$$

et

$$P(l|i, k; E) = \frac{1}{E} \int_0^E p(l|i, k; z)\, \mathrm{d}z\,. \tag{4.9}$$

En utilisant les égalités (2.1) et (3.4), on trouve

$$\mu_l = \sum_{i=1}^{f} \sum_{k=1}^{r} \langle N_i(0)\rangle P_{i,k}^{(\alpha)}(t_0) P(l|i, k; E) = \sum_{i=1}^{f} \sum_{k=1}^{r} \theta_{i,k} P(l|i, k; E)\,. \tag{4.10}$$

$P(l|i, k; E)$ est la probabilité conditionnelle de comptage de l particules α quelconques d'un groupe de k particules α émis par des désintégrations successives d'un atome de l'élément E_i choisi au hasard dans la source.

---

[4] H. Cramer: *Mathematical Methods of Statistics* (Princeton, 1946).

Les probabilités $P(l|i, k; E)$ sont calculées dans l'Appendice en fonction des parcours effectifs des α et de l'épaisseur de la source. On remarquera que $P(l|i, k; E)$, donné par l'expression (A.1.10), est une fonction homogène de degré 0. On trouverait donc les mêmes résultats en choisissant un milieu de référence autre que l'air pour exprimer les parcours effectifs et l'épaisseur de la source.

Source épaisses. – Lorsque l'épaisseur E de la source est supérieure ou égale au plus grand parcours effectif R'_{Max} de la source, on voit aisément que toutes les probabilités $P(l|i, k; E)$ sont, pour $l \neq 0$, inversement proportionnelles à E. Comme les $\theta_{i,k}$ sont proportionnels aux nombres moyens d'atomes contenus dans la source, c'est-à-dire, pour une concentration donnée, à l'épaisseur E, les nombres moyens de groupes de l particules α associées μ_l sont indépendants de E pour $l \neq 0$ et $E \geqslant R'_{\text{Max}}$. On peut donc effectuer les calculs pour une valeur quelconque de E supérieure ou égale au plus grand parcours effectif de la source. On prendra de préférence $E = R'_{\text{Max}}$, ce qui simplifie le calcul des probabilités conditionnelles de comptage.

5. – Distribution du nombre d'alpha comptés.

Lorsque les conditions de la Sect. 4 sont remplies, on peut admettre que les variables aléatoires $n_1, n_2, \ldots, n_l, \ldots, n_r$ sont indépendantes et que leur distribution conjointe est un produit de lois de Poisson

$$p(n_1, n_2, \ldots n_l, \ldots n_r) = \prod_{l=1}^{r} \exp[-\mu_l] \frac{\mu_l^{n_l}}{n_l!}. \tag{5.1}$$

La distribution du nombre d'α comptés, $n = \sum_{l=1}^{r} l n_l$, s'obtient en sommant (5.1) sur toutes les valeurs de $n_1, n_2, \ldots, n_r$ telles que $\sum_{l=1}^{r} l n_l = n$. On a donc

$$p(n) = \sum_{n_1} \ldots \sum_{n_l} \ldots \sum_{n_r} \prod_{l=1}^{r} \exp[-\mu_l] \frac{\mu_l^{n_l}}{n_l!}, \tag{5.2}$$

avec $\sum_{l=1}^{r} l n_l = n$.

Cette distribution est difficilement calculable, surtout pour de grandes valeurs de n.

Considérons sa fonction caractéristique

$$\Phi(u) = E\{\exp[iun]\} = \prod_{l=1}^{r} \exp[-\mu_l(\exp[ilu - 1]]. \tag{5.3}$$

On en déduit aisément les cumulants (ou semi-invariants) de n, définis comme les coefficients du développement en série de MacLaurin du logarithme de la fonction caractéristique (CRAMER (15.10)).

On trouve, pour le cumulant d'ordre ν,

$$\Gamma_\nu = \sum_{l=1}^{r} l^\nu \mu_l = \sum_{i=1}^{f} \sum_{k=1}^{r} \theta_{i,k} \sum_{l=1}^{k} l^\nu P(l \mid i, k; E) . \tag{5.4}$$

Des relations simples (CRAMER (15.10)) permettent d'en déduire les moments de n. En particulier, l'espérance mathématique

$$\mu = E\{n\} = \Gamma_1 = \sum_{l=1}^{r} l\mu_l \tag{5.5}$$

et la variance

$$\sigma^2 = \sigma^2\{n\} = \Gamma_2 = \sum_{l=1}^{r} l^2 \mu_l . \tag{5.6}$$

On voit, d'après les égalités (4.7) et (5.4), que tous les cumulants de n sont proportionnels à $N_1(-t_1)$. On peut donc les exprimer en fonction de $\mu = \Gamma_1$, sous la forme

$$\Gamma_\nu = \mu S_\nu ,$$

avec

$$S_\nu = \sum_{l=1}^{r} l^\nu c_l \qquad \text{et} \qquad c_l = \frac{\mu_l}{\mu} = \frac{P_l(t_1, t_0; E)}{\sum_{l=1}^{r} l P_l(t_1, t_0; E)} . \tag{5.7}$$

où S_ν et c_l sont indépendants de $N_1(-t_1)$.

On a évidemment

$$S_1 = 1 .$$

Effectuons le changement de variable aléatoire

$$x = \frac{n - \mu}{\sigma} , \tag{5.8}$$

et considérons x comme une variable aléatoire continue.

Les cumulants de x sont

$$(5.9)\qquad \begin{cases} \varkappa_1 = E\{x\} = 0\,, \\ \varkappa_2 = \sigma^2\{x\} = 1\,, \\ \varkappa_\nu = \dfrac{\Gamma_\nu}{\Gamma_2^{\nu/2}} = \mu^{1-\nu/2}\dfrac{S_\nu}{S_2^{\nu/2}}\,. \end{cases}$$

Lorsque μ tend vers l'infini, les coefficients c_l restant constants, les cumulants de x d'ordre supérieur à 2 tendent vers 0 comme $\mu^{1-\nu/2}$.

La densité de probabilité de x tend donc vers la gaussienne

$$(5.10)\qquad \varphi(x) = \frac{1}{\sqrt{2\pi}} \exp\left[-\frac{x^2}{2}\right],$$

et la distribution asymptotique de n est donnée par

$$(5.11)\qquad g(n) = \frac{1}{\sigma}\,\varphi\left(\frac{n-\mu}{\sigma}\right).$$

Lorsque μ n'est pas suffisamment grand pour que l'on puisse se limiter à l'approximation gaussienne, on peut utiliser le développement en série d'Edgeworth (Cramer (17.7)).

$$(5.12)\qquad f(x) = \varphi(x) - \frac{1}{3!}\varkappa_3\varphi^{(3)}(x) + \frac{1}{4!}\varkappa_4\varphi^{(4)}(x) + \frac{10}{6!}\varkappa_3^2\varphi^{(6)}(x) - \\ - \frac{1}{5!}\varkappa_5\varphi^{(5)}(x) - \frac{35}{7!}\varkappa_3\varkappa_4\varphi^{(7)}(x) - \frac{280}{9!}\varkappa_3^2\varphi^{(9)}(x) + \ldots,$$

avec

$$\varphi^{(\nu)}(x) = \frac{\mathrm{d}^\nu}{\mathrm{d}x^\nu}\varphi(x) = (-1)^\nu H_\nu(x)\varphi(x)\,,$$

$H_\nu(x)$ étant le polynome d'Hermite d'ordre ν. (Cramer (12.6)).

6. – Source en équilibre radioactif.

La source est en équilibre radioactif au début de l'intervalle t_0, lorsque la vie moyenne de l'élément E_1 et le temps t_1 qui s'est écoulé depuis le moment où seul l'élément E_1 était présent sont grands par rapport aux vies moyennes des descendants de E_1.

On a donc

$$\left.\begin{aligned} \lambda_1^{-1} &\gg \lambda_i^{-1} \quad (6.1) \\ t_1 &\gg \lambda_i^{-1} \quad (6.2) \end{aligned}\right\} \text{ pour } i > 1$$

ce qui entraine

$$\begin{aligned} \langle N_i(0)\rangle &\cong \frac{\lambda_1}{\lambda_i} N_1(-t_1) \exp\left[-\lambda_1 t_1\right], \quad (6.3) \\ &= \frac{\lambda_1}{\lambda_i} \langle N_1(0)\rangle, \\ &= a\lambda_i^{-1}. \end{aligned}$$

où $a = \lambda_1 \langle N_1(0)\rangle$ est l'activité de E_1, c'est-à-dire le nombre moyen de désintégrations de l'élément E_1 par seconde, au début de l'intervalle de temps t_0.

D'après les relations (6.1) et (6.3), on a

$$\langle N_i(0)\rangle \ll N_1(-t_1) \qquad \text{pour } i > 1.$$

Il suffit donc, pour que les conditions de la Sect. **4** soient remplies, que l'on ait $t_0 \ll \lambda_1^{-1}$, ce qui entraine $P_{1,k}^{(\alpha)}(t_0) \ll 1$.

Lorsque t_1 est très grand par rapport a λ_1^{-1}, on a $\langle N_1(0)\rangle \ll N_1(-t_1)$, et la condition $t_0 \ll \lambda_1^{-1}$ est superflue.

Dans le cas de l'équilibre radioactif, les relations de la Sect. **4** se simplifient notablement. En particulier, la relation (4.7) devient

$$\mu_l = a t_0 B_l, \quad (6.4)$$

avec

$$B_l = \sum_{i=1}^{r} \sum_{k=1}^{r} b_{i,k}(t_0) P(l \mid i, k; E)$$

et

$$b_{i,k}(t_0) = \frac{1}{\lambda_i t_0} P_{i,k}^{(\alpha)}(t_0). \quad (6.5)$$

Il est intéressant de remarquer que $b_{i,k}(t_0)$ est indépendant de t_0 pour $t_0 \ll \lambda_i^{-1}$.

On a également

$$\Gamma_\nu = a t_0 \sum_{l=1}^{r} l^\nu B_l \quad (6.6)$$

et, en particulier,

$$\mu = \Gamma_1 = at_0 \sum_{l=1}^{r} lB_l \,, \tag{6.7}$$

et

$$\sigma^2 = \Gamma_2 = \mu S_2 = at_0 \sum_{l=1}^{r} l^2 B_l \,. \tag{6.8}$$

7. – Cas particuliers.

7·1. *Distribution du nombre d'α émis.* – La distribution du nombre d'α émis dans l'intervalle de temps t_0 s'obtient en posant

$$P(l\,|\,i, k; E) = \delta_{l,k} = \begin{cases} 1 & \text{pour } l = k \\ 0 & \text{pour } l \neq k. \end{cases}$$

On obtient alors

$$\mu_l = \theta_l \tag{7.1}$$

et

$$\Gamma_\nu = \sum_{k=1}^{r} k^\nu \theta_k \,. \tag{7.2}$$

7·2. *Distribution du nombre d'α comptés en source mince.* – Lorsque l'épaisseur de la source est faible par rapport aux parcours effectifs, on peut admettre que la probabilité de comptage de chaque α émis est égale à $\frac{1}{2}$.

On a alors

$$P(l\,|\,i, k; E) = \frac{1}{2^k}\binom{k}{l} = \frac{1}{2^k}\frac{k!}{l!\,(k-l)!} \,. \tag{7.3}$$

On en déduit aisément les cumulants d'ordre 1 et 2, en remarquant que

$$\frac{1}{2^k}\sum_{l=1}^{k} l\binom{k}{l} = \frac{k}{2}, \tag{7.4}$$

et

$$\frac{1}{2^k}\sum_{l=1}^{k} l^2\binom{k}{l} = \frac{k(k+1)}{4} \,. \tag{7.5}$$

On trouve

$$\mu = \tfrac{1}{2} \sum_{k=1}^{r} k\theta_k \tag{7.6}$$

et

$$\sigma^2 = \tfrac{1}{4} \sum_{k=1}^{r} k(k+1)\theta_k \,. \tag{7.7}$$

Si nous désignons par $n^{(e)}$ le nombre d'α émis, on peut écrire les relations suivantes entre les espérances mathématiques et les variances des nombre d'α émis et comptés en source mince

$$E\{n\} = \tfrac{1}{2} E\{n^{(e)}\} \tag{7.8}$$

et

$$\sigma^2\{n\} = \tfrac{1}{4}\left(\sigma^2\{n^{(e)}\} + E\{n^{(e)}\}\right) . \tag{7.9}$$

8. – Estimation du nombre moyen d'alpha comptés dans l'intervalle de temps t_0.

Considérons m comptages indépendants effectués soit sur m sources identiques, soit sur la même source avec des intervalles de comptages suffisamment espacés pour que la corrélation entre comptages successifs soit négligeable. Dans ce dernier cas, il faut évidemment que l'évolution de la source radioactive soit suffisamment lente pour que l'on puisse admettre qu'elle est restée identique pendant toute la durée des comptages.

Nous nous limitons au cas où la distribution de la moyenne des nombres d'α comptés, $\bar{n} = (1/m) \sum_{i=1}^{m} n_i$ est pratiquement gaussienne. Ceci suppose que m est suffisamment grand, lorsque la distribution de n s'écarte notablement d'une gaussienne.

L'espérance mathématique et la variance de $\bar{n}$ sont

$$E\{\bar{n}\} = \mu \tag{8.1}$$

et

$$\sigma^2\{\bar{n}\} = \frac{1}{m}\sigma^2 = \mu \frac{S_2}{m} . \tag{8.2}$$

On en déduit la probabilité d'un écart de $\bar{n}$ inférieur à $a\sqrt{\mu(S_2/m)}$

$$P\left(\mu - a\sqrt{\mu \frac{S_2}{m}} < \bar{n} < \mu + a\sqrt{\mu \frac{S_2}{m}}\right) = 1 - \varepsilon \,, \tag{8.3}$$

avec

$$\varepsilon = 0.05 \quad \text{pour} \quad a = 1.96$$
$$= 0.01 \quad » \quad = 2.58$$
$$= 0.005 \quad » \quad = 2.81$$
$$= 0.001 \quad » \quad = 3.29\,.$$

Nous supposons que les probabilités $P_{1,i-1}(t_1)$, $P^{(\alpha)}_{i,k}(t_0)$ et $P(l\,|\,i, k; E)$ sont connues. S_2 est donc également connu.

On en déduit aisément un intervalle de confiance de niveau ε pour μ (voir CRAMER (34.2))

On a en effet

$$P\big(c_1(\bar{n}; \varepsilon) < \mu < c_2(\bar{n}; \varepsilon)\big) = 1 - \varepsilon\,, \tag{8.4}$$

avec

$$c_1(\bar{n}; \varepsilon) = \bar{n} + \frac{a^2 S_2}{2m} - a\sqrt{\frac{S_2}{m}}\sqrt{\bar{n} + \frac{a^2 S_2}{4m}}\,, \tag{8.5}$$

at

$$c_2(\bar{n}; \varepsilon) = \bar{n} + \frac{a^2 S_2}{2m} + a\sqrt{\frac{S_2}{m}}\sqrt{\bar{n} + \frac{a^2 S_2}{4m}}\,. \tag{8.6}$$

Pour $a^2(S_2/m) \ll \bar{n}$, on a

$$c_1(\bar{n}; \varepsilon) \cong \bar{n} - a\sqrt{\frac{S_2}{m}}\sqrt{\bar{n}} \tag{8.7}$$

et

$$c_2(\bar{n}; \varepsilon) \cong \bar{n} + a\sqrt{\frac{S_2}{m}}\sqrt{\bar{n}}\,. \tag{8.8}$$

$P\big(c_1(\bar{n}; \varepsilon) < \mu < c_2(\bar{n}; \varepsilon)\big)$ est la probabilité pour que la variable aléatoire $\bar{n}$ prenne une valeur telle que $c_1(\bar{n}; \varepsilon)$ et $c_2(\bar{n}; \varepsilon)$ soient respectivement inférieur et supérieur à μ.

Par conséquent, si l'on convient d'admettre dans chaque cas que μ est compris entre les valeurs de $c_1(\bar{n}; \varepsilon)$ et $c_2(\bar{n}; \varepsilon)$ trouvées expérimentalement, on a une probabilité $1 - \varepsilon$ d'émettre un jugement correct.

Si l'on adopte toujours la même règle, la proportion d'erreurs sera donc, à la longue, voisine de ε.

Il importe de remarquer que μ étant un paramètre inconnu et non une variable aléatoire, $P\big(c_1(\bar{n}; \varepsilon) < \mu < c_2(\bar{n}; \varepsilon)\big)$ ne peut être interprété comme la probabilité pour que μ soit compris entre les valeurs de $c_1(\bar{n}; \varepsilon)$ et de $c_2(\bar{n}; \varepsilon)$ trouvées expérimentalement.

9. – Application aux familles de l'Uranium et du Thorium en équilibre radioactif, pour un intervalle de temps t_0 de 30 jours.

Le Tableau I donne les probabilités conditionnelles de comptage $P(l\,|\,i, k; E)$ pour une source sans écran dont l'épaisseur est égale au plus grand parcours effectif de la famille ($E = R'_{max}$).

TABLEAU I. – *Probabilités conditionnelles de comptage $P(l\,|\,i, k; E)$ pour une source d'épaisseur $E = R'_{max}$:*

l	Famille de l'Uranium		Famille du Thorium			
	G (6, 4)	G (7, 3)	G (4, 5)	G' (4, 5)	G (5, 4)	G' (5, 4)
0	0.572 625	0.597 814	0.629 460	0.546 050	0.649 895	0.564 070
1	0.254 205	0.274 902	0.170 357	0.234 040	0.189 197	0.254 881
2	0.121 524	0.106 195	0.117 124	0.129 716	0.112 042	0.126 551
3	0.044 301	0.021 089	0.060 921	0.066 193	0.041 885	0.046 726
4	0.007 346	0	0.019 376	0.021 001	0.006 979	0.007 772
5	0	0	0.002 760	0.003 000	0	0
	$E = R'_{max} = 6.42$ cm			$E = R'_{max}$ 7.38 cm		

On suppose que toutes les particules α traversant la surface de séparation entre la source et le compteur avec un parcours résiduel dans l'air supérieur à $\varrho = 0.5$ cm sont enregistrées.

Nous avons utilisé les parcours donnés par FEATHER [5] pour la famille du Thorium ainsi que pour les éléments U_1, U_2, Io et RaF. Pour les autres éléments de la famille de l'Uranium, nous avons pris les parcours donnés par I. CURIE [6].

Les groupes $G(i, k)$ considérés sont constitués par les α émis par les désintégrations suivantes:

1) Famille de l'Uranium:

G(6, 4) : $\mathrm{Ra} \xrightarrow{\alpha} \mathrm{Rn} \xrightarrow{\alpha} \mathrm{RaA} \xrightarrow{\alpha} \mathrm{RaC'} \xrightarrow{\alpha} \mathrm{RaD}$

G(7, 3) : $\mathrm{Rn} \xrightarrow{\alpha} \mathrm{RaA} \xrightarrow{\alpha} \mathrm{RaC'} \xrightarrow{\alpha} \mathrm{RaD}$

---

[5] N. FEATHER: *Nucleonics*, **5**, 22 (1949).
[6] I. CURIE: *Radioéléments naturels* (Paris, 1946).

2) Famille du Thorium

G(5, 4) : $\mathrm{ThX} \xrightarrow{\alpha} \mathrm{Tn} \xrightarrow{\alpha} \mathrm{ThA} \xrightarrow{\alpha} (\mathrm{ThB} \xrightarrow{\beta}) \mathrm{ThC} \xrightarrow{\alpha} \mathrm{ThC''}$

G'(5, 4): $\mathrm{ThX} \xrightarrow{\alpha} \mathrm{Tn} \xrightarrow{\alpha} \mathrm{ThA} \xrightarrow{\alpha} (\mathrm{ThB} \xrightarrow{\beta} \mathrm{ThC} \xrightarrow{\beta}) \mathrm{ThC'} \xrightarrow{\alpha} \mathrm{ThD}$

G(4, 5) : $\mathrm{RdTh} \xrightarrow{\alpha} \mathrm{ThX} \xrightarrow{\alpha} \mathrm{Tn} \xrightarrow{\alpha} \mathrm{ThA} \xrightarrow{\alpha} (\mathrm{ThB} \xrightarrow{\beta}) \mathrm{ThC} \xrightarrow{\alpha} \mathrm{ThC''}$

G'(4, 5): $\mathrm{RdTh} \xrightarrow{\alpha} \mathrm{ThX} \xrightarrow{\alpha} \mathrm{Tn} \xrightarrow{\alpha} \mathrm{ThA} \xrightarrow{\alpha} (\mathrm{ThB} \xrightarrow{\beta} \mathrm{ThC} \xrightarrow{\beta}) \mathrm{ThC'} \xrightarrow{\alpha} \mathrm{ThD}$.

Pour le rapport des nombres de désintégrations α et β du ThC, nous avons pris la valeur 0.366/0.634 donnée par Lazar, Senftle et Farley (7).

Les probabilités conditionnelles de comptage de particules α émises par des désintégrations simples se calculent aisément par la formule $P(1\,|\,i, 1; E) = R'/4E$ (voir Appendice, Sect. 3).

Les Tableaux II et III donnent les valeurs numériques des coefficients B_l, ainsi que des expressions $\sum_{l=1}^{r} lB_l$, $\sum_{l=1}^{r} l^2 B_l$ et $S_2 = \sigma^2/\mu$ calculées pour les nombres d'α émis et pour les nombres d'α comptés en source mince et en source épaisse.

Les probabilités conditionnelles de comptage en source épaisse étant calculées pour une source d'épaisseur égale au plus grand parcours effectif de la

Tableau II. – *Famille de l'Uranium.*

	Famille complète en équilibre			Radium en équilibre avec ses descendants à vie moyenne plus courte (Ra → RaC')		
	Nombre d'α émis	Nombre d'α comptés en source		Nombre d'α émis	Nombre d'α comptés en source	
		mince	épaisse		mince	épaisse
B_1	4.183 16	2.364 48	0.684 639	0.183 16	0.364 48	0.388 339
B_2	0	0.375 00	0.118 718	0	0.375 00	0.118 718
B_3	0.183 17	0.227 11	0.040 050	0.183 17	0.227 11	0.040 050
B_4	0.81 684	0.051 05	0.006 000	0.816 84	0.051 05	0.006 000
$\sum_{l=1}^{r} lB_l$	8	4	1.066 225	4	2	0.639 585
$\sum_{l=1}^{r} l^2 B_l$	18.901 1	6.725 3	1.615 96	14.901 1	4.725 3	1.189 32
S_2	1.537	1.297	1.231	1.930	1.535	1.364

(7) N. H. Lazar, F. E. Senftle and T. Farley: *Oak Ridge Nat. Laboratory*, 1975, 43 (1956).

famille R'_{max}, il faut, pour obtenir μ_l, multiplier B_l par at_0, où a est l'activité de l'élément E_1 *pour une source d'épaisseur* $E = R'_{max}$.

TABLEAU III. – *Famille du Thorium.*

	Famille complète en équilibre			RdTh en équilibre avec ses descendants		
	Nombre d'α émis	Nombre d'α comptés en source		Nombre d'α émis	Nombre d'α comptés en source	
		mince	épaisse		mince	épaisse
B_1	1.170 18	0.756 31	0.298 887	0.170 18	0.256 31	0.231 472
B_2	0	0.320 74	0.123 368	0	0.320 74	0.123 368
B_3	0	0.298 94	0.060 347	0	0.298 94	0.060 347
B_4	0.174 47	0.138 56	0.017 977	0.174 47	0.138 56	0.017 977
B_5	0.817 02	0.025 53	0.002 379	0.817 02	0.025 53	0.002 379
$\sum_{l=1}^{r} lB_l$	5.953	2.976 6	0.810 469	4.953	2.476 6	0.743 054
$\sum_{l=1}^{r} l^2B_l$	23.217	7.585 05	1.682 599	22.217	7.085 05	1.615 184
S_2	1.975	1.595	1.441	2.118	1.691	1.474

Pour les éléments à vie moyenne courte par rapport à t_0, il n'a pas été tenu compte des atomes présents au début de t_0, leur nombre étant négligeable par rapport aux nombres d'atomes formés pendant t_0.

Rappelons que l'on a les relations

(6.4) $$\mu_l = at_0 B_l$$

(6.7) $$\mu = at_0 \sum_{l=1}^{r} lB_l$$

et

(6.8) $$\sigma^2 = \mu S_2 = at_0 \sum_{l=1}^{r} l^2 B_l .$$

* * *

Je remercie vivement MM. les Professeurs J. GÉHÉNIAU et R. CONSAEL ainsi que MM. D. HIRSCHBERG et E. PICCIOTTO pour de nombreuses suggestions et de précieux conseils, MM. les Professeurs P. GILLIS et J. TEGHEM pour l'intérêt qu'ils ont porté à ce travail et M.lle J. STORMS pour son aide dans le calcul des valeurs numériques.

APPENDICE

Calcul des probabilités conditionnelles de comptage $P(l\,|\,i,\,k;\,E)$.

1. – Considérons une désintégration α k-uple d'un atome de l'élément E_i et désignons par $G(i,\,k)$ le groupe des k particules α émises. Faisons abstraction de l'ordre de filiation qui n'importe pas pour le calcul des probabilités $P(l\,|\,i,\,k;\,E)$ et classons les α du groupe $G(i,\,k)$ par ordre de parcours décroissants, en les affectant d'un indice p variant de 1 à k. Si R_p indique le parcours de l'α_p, on a donc $R_1 > R_2 > \ldots > R_k$.

Désignons par $G_k(i,\,k) = (\alpha_1,\,\alpha_2,\,\ldots\,\alpha_p,\,\ldots\,\alpha_k)$ le groupe $G(i,\,k)$ ainsi ordonné et par $G_m(i,\,k)$ le groupe formé par les m premiers α de $G_k(i,\,k)$.

Supposons d'abord, pour la facilité des calculs, que l'épaisseur de la source radioactive est supérieure ou égale à tous les parcours effectifs des α du groupe $G(i,\,k)$ $(E \geqslant R_1')$.

Pour l'intégration de $p(l\,|\,i,\,k;\,z)$ nous distinguerons alors les régions suivantes:

$0 \leqslant z < R_k'$	Tous les α de $G(i,\,k)$ peuvent être comptés
$R_{m+1}' \leqslant z < R_m''$	Seuls les α de $G_m(i,\,k)$ peuvent être comptés
$R_2'' \leqslant z < R_1'$	Seul α_1 peut être compté
$R_1'' \leqslant z \leqslant E$	Aucun α de $G(i,\,k)$ ne peut être compté.

Calculons $p(l\,|\,i,\,k;\,z)$ dans la région $R_{m+1}' \leqslant z < R_m'$. Comme dans cette région, seuls les α du groupe $G_m(i,\,k)$ peuvent être comptés, on aura $p(l\,|\,i,\,k;\,z)=0$ pour $l > m$.

Désignons par H_l un groupe de l α extrait de $G_m(i,\,k)$, l'ordre des α dans le groupe H_l n'important pas, et par $p(H_l\,|\,G_m(i,\,k);\,z)$ la probabilité conditionnelle de compter tous les α du groupe H_l lorsque le groupe $G(i,\,k)$ est émis à la profondeur z avec $R_{m+1}' \leqslant z < R_m''$.

On voit aisément que l'on peut écrire, d'après (4.1) et (4.2),

$$p(H_l\,|\,G_m(i,\,k);\,z) = \frac{1}{2^m}\prod_{p=1}^{m}\left(1 + z\frac{\varepsilon_p(H_l)}{R_p''}\right). \tag{A.1.1}$$

avec

$$\varepsilon_p(H_l) = \begin{cases} -1 \text{ lorsque le groupe } H_l \text{ contient l'alpha } \alpha_p, \\ +1 \text{ lorsque le groupe } H_l \text{ ne contient pas l'alpha } \alpha_p. \end{cases}$$

En développant (A.1.1) d'après les puissances de z, on trouve

$$p(H_l\,|\,G_m(i,\,k);\,z) = \frac{1}{2^m}\left[1 + z\sum_{p=1}^{m}\frac{\varepsilon_p(H_l)}{R_p'} + z^2\sum_{p=1}^{m}\sum_{q=p+1}^{m}\frac{\varepsilon_p(H_l)\varepsilon_q(H_l)}{R_p'R_q'} + \right. \tag{A.1.2}$$

$$\left. + \ldots + z^m\frac{\varepsilon_1(H_l)\ldots\varepsilon_m(H_l)}{R_1'\ldots R_m'}\right].$$

La probabilité conditionnelle $p(l \mid i, k; z)$ s'obtiendra en sommant (A.1.2) sur tous les groupes H_l que l'on peut extraire de $G_m(i, k)$.

Effectuons les sommes terme à terme et posons

$$\text{(A.1.3)}\qquad \begin{cases} A_{l,m,0} = \binom{m}{l} = \begin{cases} \dfrac{m!}{l!\,(m-l)!}, & \text{pour } l = 0, 1, \ldots m, \\ 0, & \text{pour } l > m,\ l < 0 \text{ ou } m < 0, \end{cases} \\ A_{l,m,1} = \sum\limits_{H_l} \varepsilon_p(H_l), \\ A_{l,m,2} = \sum\limits_{H_l} \varepsilon_p(H_l)\varepsilon_q(H_l), \qquad (q > p), \\ \ldots\ldots\ldots\ldots \\ A_{0,m,j} = 1, \qquad (m, j = 0, 1, \ldots k), \\ A_{l,m,j} = 0. \qquad \text{pour } l > m \text{ ou } j > m. \end{cases}$$

Les coefficients $A_{l,m,j}$ sont des nombres entiers positifs, négatifs ou nuls dépendant seulement des indices l, m et j.

Tableau IV. – *Coefficients* $A_{l,m,j}$.

	$l=1$					$l=2$				$l=3$			$l=4$		$l=5$
$m=$	1	2	3	4	5	2	3	4	5	3	4	5	4	5	5
$j=0$	+1	+2	+3	+4	+5	+1	+3	+6	+10	+1	+4	+10	+1	+5	+1
1	−1	0	+1	+2	+3	−1	−1	0	+ 2	−1	−2	− 2	−1	−3	−1
2	0	−2	−1	0	+1	+1	−1	−2	− 2	+1	0	− 2	+1	+1	+1
3	0	0	−3	−2	−1	0	+3	0	− 2	−1	+2	+ 2	−1	+1	−1
4	0	0	0	−4	−3	0	0	+6	+ 2	0	−4	+ 2	+1	−3	+1
5	0	0	0	0	−5	0	0	0	+10	0	0	−10	0	+5	−1

$A_{0,m,j} = +1$ pour $j \leqslant m$

$A_{l,m,j} = 0$ pour $j > m$ ou $l > m$

Considérons d'abord $A_{l,m,1}$ et divisons la somme en deux parties étendues respectivement à tous les groupes H_l contenant α_p et à ceux ne contenant pas α_p.

Les groupes H_l contenant α_p s'obtiennent en ajoutant α_p aux groupes obtenus en choisissant $(l-1)\alpha$ parmi les $(m-1)\alpha$ autres que α_p du groupe $G_m(i, k)$. De même, les groupes H_l ne contenant pas α_p s'obtiennent en choisissant $l\,\alpha$ parmi les $(m-1)\,\alpha$ autres que α_p du groupe $G_m(i, k)$. Parmi les $\binom{m}{l}$ groupes H_l, il y en a donc $\binom{m-1}{l-1}$ qui contiennent α_p et $\binom{m-1}{l}$ qui ne contiennent pas α_p.

D'après la définition de $\varepsilon_p(H_l)$, on a donc

$$\text{(A.1.4)}\qquad A_{l,m,1} = \binom{m-1}{l} - \binom{m-1}{l-1}.$$

On obtient de même la formule de récurrence générale, valable pour $l, j = 1, 2, \ldots m$

$$A_{l,m,j} = A_{l,m-1,j-1} - A_{l-1,m-1,j-1} \,. \tag{A.1.5}$$

On en déduit:

$$A_{l,m,j} = \sum_{i=0}^{j} (-1)^i \binom{j}{i} \binom{m-j}{l-i} \,. \tag{A.1.6}$$

En introduisant les coefficients $A_{l,m,j}$ dans (A.1.2) et en remarquant qu'ils ne dépendent pas des indices $p, q, \ldots$, on peut écrire

$$p(l\,|\,i, k; z) = \frac{1}{2^m} \sum_{j=0}^{m} A_{l,m,j} B^{i,k}_{m,j} z^j \,, \tag{A.1.7}$$

avec

$$\left\{ \begin{array}{l} B^{i,k}_{m,0} = 1 \,, \\ B^{i,k}_{m,1} = \displaystyle\sum_{p=1}^{m} \frac{1}{R'_p} \,, \\ B^{i,k}_{m,2} = \displaystyle\sum_{p=1}^{m} \sum_{q=p+1}^{m} \frac{1}{R'_p R'_q} \,. \\ \ldots\ldots\ldots \\ B^{i,k}_{m,m} = \dfrac{1}{R'_1, R'_2 \ldots R'_m} \,, \\ B^{i,k}_{m,j} = 0 \,, \qquad \text{pour } j > m, \end{array} \right. \tag{A.1.8}$$

et

$$B^{i,k}_{m,j} = B^{i,k}_{m-1,j} + \frac{1}{R'_m} B^{i,k}_{m-1,j-1} \,. \qquad (m, j = 0, 1, \ldots k). \tag{A.1.9}$$

En intégrant (A.1.7) par rapport à z de $z = R'_{m+1}$ à $z = R'_m$ et en sommant sur toutes les régions d'intégration, on obtient finalement, en posant $R'_0 = E$ et $R'_{k+1} = 0$,

$$P(l\,|\,i, k; E) = \frac{1}{E} \sum_{m=0}^{k} \sum_{j=0}^{k} A_{l,m,j} B^{i,k}_{m,j} C^{i,k}_{m,j} \,, \tag{A.1.10}$$

avec

$$C^{i,k}_{m,j} = \frac{R'^{j+1}_m - R'^{j+1}_{m+1}}{2^m (j+1)} \,. \tag{A.1.11}$$

En sommant sur l, on obtient les relations

$$\sum_{l=0}^{k} p(l\,|\,i, k; z) = 1 \,, \tag{A.1.12}$$

et, en intégrant par rapport à z de $z = R'_{m+1}$ à $z = R'_m$,

$$\sum_{l=0}^{k} \sum_{j=0}^{k} A_{l,m,j} B^{i,k}_{m,j} C^{i,k}_{m,j} = R'_m - R'_{m+1} \,. \qquad (m = 1, 2, \ldots k). \tag{A.1.13}$$

Ces relations permettent une vérification aisée des calculs numériques.

On a également

$$\sum_{l=0}^{k} P(l\,|\,i,\,k;\,E) = 1\,. \tag{A.1.14}$$

2. – Considérons maintenant le cas où certains α du groupe $G(i,\,k)$ ont des parcours effectifs supérieurs à l'épaisseur de la source E.

Désignons par a l'indice du plus petit parcours effectif supérieur à E. On a donc $R'_1 > \ldots R'_a > E \geqslant R'_{a+1} \ldots > R'_k$.

Les probabilités $P(l\,|\,i,\,k;\,E)$ sont encore données par l'expression (A.1.10) si l'on pose $C^{i,k}_{m,j} = 0$ pour $m < a$ et si l'on remplace R'_a par E dans $C^{i,k}_{a,j}$.

Lorsque tous les parcours effectifs des α du groupe $G(i,\,k)$ sont supérieurs à E, on trouve

$$P(l\,|\,i,\,k;\,E) = \frac{1}{2^k} \sum_{j=0}^{k} A_{l,k,j} B^{i,k}_{k,j} \frac{E^j}{j+1}\,. \tag{A.2.1}$$

3. *Sources avec écrans.* – L'expression (A.1.10) reste valable également lorsque des écrans sont interposés entre la source radioactive et le compteur.

En effet, si les écrans ont un pouvoir d'arrêt total équivalent à celui de E' cm d'air, tout se passe comme si la source radioactive avait une épaisseur totale de $E + E'$, une couche superficielle d'épaisseur E' ne contenant pas d'éléments radioactifs. Il faudra donc intégrer $p(l\,|\,i,\,k;\,z)$ de E' à $E + E'$.

Si b et c sont respectivement les indices des plus petits parcours effectifs supérieurs à $E + E'$ et à E',

$$R'_1 > \ldots > R'_b > E + E' \geqslant R'_{b+1} > \ldots > R'_c > E' \geqslant R'_{c+1} > \ldots > R'_k\,,$$

on posera $C^{i,k}_{m,j} = 0$ pour $m < b$ et $m > c$ et on remplacera R'_b par $E + E'$ dans $C^{i,k}_{b,j}$ et R'_{c+1} par E' dans $C^{i,k}_{c,j}$.

Cas particulier: $k = 1$. Lorsque le groupe $G(i,\,k)$ se réduit à un seul α de parcours effectif R', on retrouve les expressions calculées par G. D. Finney et R. D. Evans [8].

$$a)\ \text{lorsque } E + E' \geqslant R', \quad P(1\,|\,i,\,1;\,E) = \frac{1}{4E} \cdot \frac{(R' - E')^2}{R'}\,, \tag{A.3.1}$$

$$b)\ \text{lorsque } E + E' < R', \quad P(1\,|\,i,\,1;\,E) = \frac{1}{4} \cdot \frac{2(R' - E') - E}{R'}\,. \tag{A.3.2}$$

4. *Calcul des cumulants de n.* – On peut calculer directement les cumulants de n, sans connaître les probabilités conditionnelles de comptage $P(l\,|\,i,\,k;\,E)$. En effet, on peut écrire

$$\sum_{l=1}^{k} l^\nu P(l\,|\,i,\,k;\,E) = \frac{1}{E} \sum_{m=0}^{k} \sum_{j=0}^{k} B^{i,k}_{m,j} C^{i,k}_{m,j} \Delta^{(\nu)}_{m,j}\,, \tag{A.4.1}$$

[8] G. D. Finney and R. D. Evans: *Phys. Rev.*, **48**, 503 (1935).

avec

$$\Delta^{(\nu)}_{m,j} = \sum_{l=1}^{k} l^{\nu} A_{l,m,j} \,. \tag{A.4.2}$$

Pour $\nu = 1$ et $\nu = 2$, on trouve

$$\Delta^{(1)}_{m,1} = (-1)^{j} \binom{m-j}{1-j} 2^{m-1}, \tag{A.4.3}$$

et

$$\Delta^{(2)}_{m,j} = (-1)^{j} \binom{m+1-j}{2-j} 2^{m-1}. \tag{A.4.5}$$

On a donc $\Delta^{(1)}_{m,j} = 0$ pour $j > 1$ et $\Delta^{(2)}_{m,j} = 0$ pour $j > 2$.

Dans le cas où aucun écran n'est interposé entre la source et le compteur et où l'épaisseur de la source est supérieure ou égale à tous les parcours effectifs des α du groupe $G(i, k)$, on trouve

$$\sum_{l=1}^{k} lP(l \,|\, i, k; E) = \frac{1}{4E} \sum_{m=1}^{k} R'_m \,, \tag{A.4.6}$$

$$\sum_{l=1}^{k} l^2 P(l \,|\, i, k; E) = \frac{1}{4E} \left[\sum_{m=1}^{k} m R'_m - \frac{1}{3} \sum_{m=2}^{k} R'^2_m \sum_{p=1}^{m-1} \frac{1}{R'_p} \right]. \tag{A.4.7}$$

Ces expressions permettent de calculer aisément l'espérance mathématique et la variance du nombre d'α comptés.

RIASSUNTO (*)

La distribuzione del numero di particelle α registrate nell'intervallo di tempo t_0 da un contatore sovrapposto a una sorgente radioattiva di spessore qualunque è stata studiata nel caso generale in cui la sorgente contiene elementi radioattivi che subiscono disintegrazioni successive. Il calcolo della accumulazione permette di dimostrare che la distribuzione è asintoticamente gaussiana. Nell'appendice è sviluppato un metodo di calcolo delle probabilità condizionate di conteggio delle α emesse per disintegrazioni successive. I risultati si applicano alle famiglie dell'Uranio e del Torio in equilibrio per un intervallo di tempo t_0 di 30 giorni.

(*) *Traduzione a cura della Redazione.*

IL NUOVO CIMENTO Vol. VI, N. 4 1° Ottobre 1957

Phenomenological Consideration on the Hyperfragments.

Y. Poc Kwon, J. Ôba (*) and T. Gotô (+)

Department of Physics, Osaka University - Osaka, Japan

(ricevuto il 13 Giugno 1957)

Summary. — On the basis of a simple model, the binding energy of Λ^0 in hyperfragments is calculated and the nature of Λ^0-nucleon force is discussed. On the same basis the Z-spectrum of hyperfragments produced in nuclear emulsions is also considered.

The first example of a hyperfragment was found by Danysz and Pniewski [1]. Later on, a great number of cases were found experimentally and systematic searches for hyperfragments were carried out especially by Fry *et al.* [2] and M. Blau [3]. Theoretical considerations on hyperfragments have also been given by many authors [4]. Most of authors considered the binding energy of a Λ^0 particle in nuclei and discussed the nature of the force between

---

(*) Now at Departments of Physics, Rikkyô University, Tokyo.

(+) Now at Department of Physics, Faculty of Engineering, Nihon University, Tokyo.

(1) M. Danysz and J. Pniewski: *Phil. Mag.*, **44**, 348 (1953).

(2) W. F. Fry, J. Schneps and M. S. Swami: *Phys. Rev.*, **101**, 1526 (1956).

(3) M. Blau: *Phys. Rev.*, **102**, 495 (1956).

(4) K. Nishijima: *Progr. Theor. Phys.*, **14**, 527 (1955); S. Iwao: *Progr. Theor. Phys.*, **13**, 111 (1955); R. N. Dalitz: *Phys. Rev.*, **99**, 1475 (1955); J. T. Jones and J. K. Knipp: *Nuovo Cimento*, **2**, 857 (1955); R. Gatto: *Nuovo Cimento*, **1**, 372 (1955); **2**, 373 (1955).

a Λ^0 and nucleons. However, as experimental data of Λ^0 binding energies are not enough accurate and some of them are uncertain, the conclusions of the theoretical consideration are not quite reliable.

In this note, we will investigate the Λ^0-binding energies based on a simple model and discuss the nature of the force between a Λ^0-particle and a nucleon. We will also consider the problem of the relative frequency of hyperfragments produced in high energy stars.

1. – Experimental summary of Λ^0-binding energies and the assumptions.

Although a considerable number of data of Λ^0-binding energies in hyperfragments has been reported, they are as yet not so accurate that we can obtain the knowledge of the detailed structure of hyperfragments. Only a few cases of heavy hyperfragments are completely analyzed. Λ^0-binding energies of light hyperfragments are obtained in many cases and they are consistent one another within the experimental errors. We summarize the experimental data, which we have adopted, in Table I.

We obtain the values listed in Table I using the decay Q-values of each event and the decay scheme $\Lambda^0 \to p + \pi^- + (36.9 \pm 0.2)$ MeV.

The Q-values of ${}^3H_\Lambda$-, ${}^4H_\Lambda$-, ${}^4He_\Lambda$- and ${}^5He_\Lambda$-decay are the weighted mean with the reciprocal of errors.

It is presumed from experiment that the Λ^0-binding energy in a hyperfragment differs essentially from the separation energy of the last neutron in a nucleus. Contrary to the complex variation of the separation energy of the last neutron, the Λ^0-binding energy increases gradually with mass number A ([5]). This may be explained qualitatively as follows. The main part of variation of the separation energy of the last neutrons is given by the variation of the difference of the symmetry effects of the nucleus (N, Z) and of the nucleus $(N, Z-1)$ or $(N-1, Z)$. The symmetry effect is caused by the Pauli principle, and since the Pauli-principle does not apply to the Λ^0-particle bound in a nucleus we can expect that a Λ^0-particle in a nucleus is always in the lowest energy state.

From the experimental facts, let us take the following simple model:

1) As the Λ^0-binding energy in ${}^3H_\Lambda$ is very small, it may be assumed that the force between a Λ^0-particle and a nucleon is weaker than that of the nucleon-nucleon and that the distortion of states of nucleons caused by the presence of a Λ^0 is very small. Thus we assume the potential of a Λ^0-particle in

([5]) T. Tati and H. Tati: *Nuovo Cimento*, **3**, 1136 (1956).

TABLE I. – *The Λ^0-binding energies data for various events* (*).

Hyper-fragment	Total number of events	Weighted mean binding energy (MeV)	
$^3H_\Lambda$	14	0.4 ± 0.3	
$^4H_\Lambda$	9	2.1 ± 0.3	
$^4He_\Lambda$	8	2.2 ± 0.4	
$^5He_\Lambda$	3	2.0 ± 0.5	
$^6Li_\Lambda$	1	5.5 ± 3.5	
$^7Li_\Lambda$	1	4.4 ± 0.9	
$^7Be_\Lambda$	2	5.5 ± 16	5.9 ± 8
$^8Be_\Lambda$	2	0 ± 5	3.7 ± 3
$^9Be_\Lambda$	2	6.5 ± 0.6	-0.2 ± 5
$^{11}C_\Lambda$	1	13 ± 6	
$^{14}N_\Lambda$	1	0 ± 11	
$^{16}O_\Lambda$	1	19.6 ± 14	

(*) $^3H_\Lambda$ H. YAGODA: *Phys. Rev.*, **98**, 153 (1953); O. SKIEGGESTAD *et al.*: *Nuovo Cimento*, **3**, 652 (1956); D. M. HASKIN *et al.*: *Phys. Rev.*, **102**, 244 (1956); A. BONETTI *et al.*: *Nuovo Cimento*, **11**, 210 (1954); A. DEBENEDETTI *et al.*: *Nuovo Cimento*, **12**, 466 (1954); R. LEVI-SETT: *Nuovo Cimento*, **2**, 263 (1955); G. CASTAGNOLI *et al.*: *Nuovo Cimento*, **2**, 550 (1955); M. SCHEIN *et al.*: *Nuovo Cimento*, **3**, 131 (1956); W. F. FRY *et al.*: *Phys. Rev.*, **101**, 1526 (1956).

$^4H_\Lambda$ O. HAUGERUD and S. O. SPRENSEN: *Phys. Rev.*, **99**, 1046 (1955); J. HORNBOSTEL and E. O. SALANT: *Phys. Rev.*, **102**, 502 (1956); M. W. FRIEDLANDER *et al.*: *Nuovo Cimento*, **2**, 663 (1955); M. SCHEIN *et al.*: *Phys. Rev.*, **100**, 1455 (1955); PH. RLSELET *et al.*: *Nuovo Cimento*, **3**, 505 (1956); W. F. FRY *et al.*: *Phys. Rev.*, **101**, 1526 (1956); J. CRUSSARD: *6th Rochester Conf.* (1956).

$^4He_\Lambda$ J. D. SORREL *et al.*: *Phys. Rev.*, **100**, 1484 (1955); N. SEEMAN *et al.*: *Phys. Rev.*, **100**, 1481 (1955); J. E. NAUGLE *et al.*: *Phys. Rev.*, **96**, 1383 (1954); R. HILL *et al.*: *Bull. Am. Phys. Soc.*, **29**, 60 (1954); A. SCLHEIN *et al.*: *Phil. Mag.*, **45**, 1284 (1954); W. F. FRY *et al.*: *Phys. Rev.*, **99**, 1561 (1955); **101**, 1526 (1956); F. GILBERT *et al.*: *Phys. Rev.*, **103**, 248 (1956).

$^5He_\Lambda$ W. F. FRY *et al.*: *Phys. Rev.*, **101**, 1526 (1956); J. CRUSSARD: *6th Rochester Conf.* (1956); P. H. FOWLER *et al.*: *Nuovo Cimento*, **4**, 158 (1956).

$^6Li_\Lambda$ M. BLAU: *Phys. Rev.*, **102**, 495 (1956).

$^7Li_\Lambda$ F. GILBERT *et al.*: *Phys. Rev.*, **103**, 248 (1956).

$^7Be_\Lambda$ W. F. FRY *et al.*: *Phys. Rev.*, **99**, 1561 (1955); C. CASTAGNOLI *et al.*: *Nuovo Cimento*, **2**, 550 (1955).

$^8Be_\Lambda$ M. BLAU: *Phys. Rev.*, **102**, 495 (1956); W. F. FRY *et al.*: **99**, 1561 (1956).

$^9Be_\Lambda$ W. F. FRY *et al.*: *Phys. Rev.*, **101**, 1526 (1956); M. BLAU: *Phys. Rev.*, **102**, 445 (1956).

$^{11}C_\Lambda$ W. F. FRY *et al.*: *Phys. Rev.*, **99**, 1561 (1955).

$^{14}N_\Lambda$ P. S. FREIER *et al.*: *Phys. Rev.*, **94**, 677 (1954).

$^{16}O_\Lambda$ M. BLAU: *Phys. Rev.*, **102**, 495 (1956).

a nucleus to be given by a Hartree type field, i.e.

$$\bar{V}(\boldsymbol{r}) = A\int \varrho(\boldsymbol{r}')V_{N\Lambda}(|\boldsymbol{r}-\boldsymbol{r}'|)\,\mathrm{d}\boldsymbol{r}' ,$$

where $V_{N\Lambda}(\boldsymbol{r})$ is the potential between a Λ^0 and a nucleon;
$\varrho(\boldsymbol{r})$ is the nucleon density of the nucleus;
A is the mass number of the nucleus.

2) For simplicity, we take only a central force, between a Λ^0 and a nucleon, i.e.

$$V_{N\Lambda}(\boldsymbol{r}) = g^2\frac{\exp[-\mu r]}{r} , \qquad \mu = \frac{c}{\hbar}\sqrt{m_\theta^2 - (m_\Lambda - m_N)^2} ,$$

where m_θ, m_Λ and m_N are masses of a θ-meson, a Λ^0-particle and a nucleon respectively.

This assumption is based on the meson theoretical consideration that the Λ^0-nucleon force is caused by the exchange of quanta of heavy mesons. If we follow this consideration honestly, we must take the exchange force between a Λ^0 and a nucleon. However, as we will see later on, the exchange effect is not important. We do not also consider the spin dependence of the Λ^0-nucleon force.

3) For the heavy nuclei ($A \geqslant 5$) we assume that the nucleon density distributes uniformly within the radius $R = 1.2\cdot A^{\frac{1}{3}}\cdot 10^{-13}$ cm of a sphere. For the light nuclei we will discuss particularly in a later section.

2. – Calculation of potential and binding energies of the Λ^0-particles and discussion of results.

Being based on the assumptions stated in the preceeding section, we calculate the binding energies of the Λ^0-particle by making use of the variational method where a trial function is $\psi_\Lambda \propto \exp[-\beta r]$.

For heavy hyperfragments, a Hartree type potential $\bar{V}(r)$ is as follows:

$$\bar{V}(r) = -V_0\left[1-(1+\alpha)\frac{\sinh\xi}{\xi}\exp[-\alpha]\right] \quad \text{for } \xi<\alpha ,\ \varrho_0 = \text{const}$$

$$-V_0\left[(\alpha\cosh\alpha - \sinh\alpha)\frac{\exp[-\xi]}{\xi}\right] \quad \text{for } \xi>\alpha ,\ \varrho_0 = 0$$

$$\alpha = \mu R , \qquad \xi = \mu r , \qquad V_0 = 4\pi\varrho_0 g^2/\mu^2 .$$

There is only one adjustable parameter, i.e. the depth of the potential V_0 which is normalized by adjusting the binding energy of the Λ^0-particle in $^9Be_\Lambda$ to be equal to 6.5 MeV. As the result of this normalization, the coupling constant $g^2/\hbar c$ becomes 0.45. Binding energies of the Λ^0 particle in various nuclei are shown in Fig. 1. The results obtained by making use of the square well potential are also added in Fig. 1 (by the broken line).

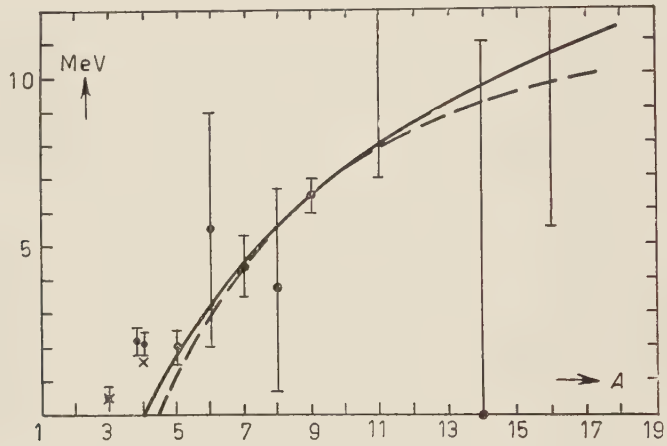

Fig. 1. – Λ^0-binding energies.

– – – square well potential. —— Hartree potential with straight cut density. x Hartree potential with exponential density.

Now we will consider the results in detail. As may be seen in Fig. 1, the results of our simple considerations agree with the tendency of experimental facts when mass number A is 5 or more. This may be not so much dependent on the form of the nucleon density owing to the following reason. Although the nucleon density, as is well known, decreases exponentially near $R = r_0 A^{\frac{1}{3}}$ instead of having a sharp boundary, the effect of this tail of the nucleon density may be so small that it can be neglected unless the greater part of the wave function of the Λ^0-particle spreads out of a nucleus. As a matter of fact, when the binding energy of the Λ^0 becomes 5 MeV or more the wave function of Λ^0 is almost inside the nucleus.

Contrary to the heavy hyperfragments, the situation in the case of light hyperfragments is quite different. Let us consider $^3H_\Lambda$ as an example. Because of the small binding energy of Λ^0 in $^3H_\Lambda$, one expects that the wave function almost spreads out of nuclear matter and then it is not justified to take a sharp boundary of the nucleon density. Diffuseness of the nuclear matter will be effective. In this case, therefore, we take the nucleon

density to be given by

$$\varrho(r) \propto \exp\left[-r/R\right],$$

where $R = 2.2 \cdot 10^{-13}$ cm which is the size of a deuteron. By using this nucleon density, we obtain the binding energy of Λ^0 in ${}^3H_\Lambda$ to be equal to 0.43 MeV. In the cases of ${}^4H_\Lambda$ and ${}^4He_\Lambda$, we take the same exponential type of nuclear density where R is taken to be $R_t = 2.26 \cdot 10^{-13}$ cm and obtain that the binding energy of Λ^0 is 1.6 MeV.

In the case of ${}^5He_\Lambda$, though the effect of the tail of the nucleon density may se considered to be large, we suppose that the tail of ${}^4He$ is comparatively hort due to the stability of ${}^4He$ and then this effect will be not so large.

In the case of the exchange force, we have to take $\varrho(r_i, r_\Lambda)$ for the nucleon density, the following quantity:

$$\varrho(r_i, r_\Lambda) = \int \mathrm{d}^3 r_1 \ldots \mathrm{d}^3 r_{i-1}\, \mathrm{d}^3 r_{i+1} \ldots \mathrm{d}^3 r_A\, \psi^*(r_1 \ldots r_{i-1} r_i r_{i+1} \ldots r_A)\, \psi(r_1 \ldots r_{i-1} r_\Lambda r_{i+1} \ldots r_A) .$$

In order to obtain the order of magnitude of the adjustable parameter, we uppose t hat

$$\varrho = \text{const} \qquad r < R,$$

$$= 0 \qquad r > R.$$

Taking the binding energy of Λ^0 in ${}^9Be_\Lambda$ to be equal to 6.5 MeV, we obtain $g^2/\hbar c = 0.5$ which is nearly equal to that of the non-exchange central force. Thus, it is expected that the exchange effect has not great influence on the binding energy of Λ^0.

From the value $g^2/\hbar c = 0.45$, we see that the well depth parameter of the potential between a Λ^0 and a nucleon is 0.56 and hence the bound state of a Λ^0 and a nucleon does not exist.

From the above discussion on a simple model we can understand the variation of binding energies of Λ^0 with the mass number A and it is far too hasty to draw a decisive conclusion on the nature of the Λ^0-nucleon force from binding energies of Λ^0 in hyperfragments.

3. – The relative frequency of hyperfragments in nuclear emulsion.

Finally, we will consider the mechanism of the production of hyperfragments in the high energy nuclear collision. While a Λ^0-particle produced in a nucleus travels inside the nucleus, it loses its kinetic energy and falls into such

a state that it does not run out of the nucleus by itself. Therefore, the low energy Λ^0-particle captured by a nuclear fragment must be cast out as a hyperfragment. Assuming the mechanism of the production of hyperfragments to be as stated above, we compare the relative frequency of hyperfragments with that of nuclear fragments ([6]). The matrix element for the Λ^0 traveling inside the nucleus to get in the bound state of a hyperfragment with mass number A is

$$M_A \propto \int \psi_\Lambda^{*f} V_A \psi_\Lambda^i \, \mathrm{d}^3 r_\Lambda \,,$$

$$= \int \psi_\Lambda^{*f} V_A \frac{\exp\left[i \boldsymbol{p}_\Lambda \boldsymbol{x}_\Lambda\right]}{\sqrt{v}} \, \mathrm{d}^3 r_\Lambda \,,$$

where ψ_Λ^i is the wave function of the initial state of Λ^0 and approximated by plane wave with the normalization volume v which is the volume of the nucleus, ψ_Λ^f is the final state wave function and V_A is the potential of a nuclear fragment which acts on the Λ^0-particle. The energy of Λ^0 inside the nucleus

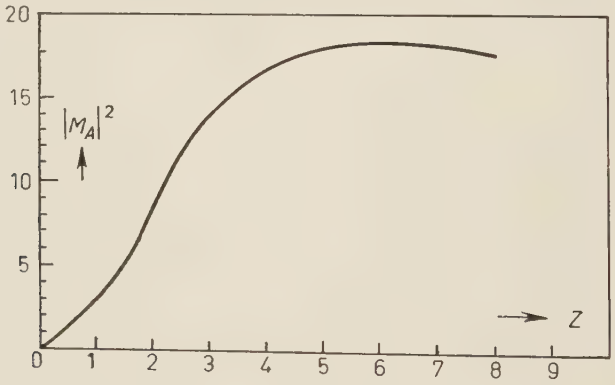

Fig. 2.

is assumed to be 20 MeV. Then making use of the square well potential which gives the correct tendency of binding energies of Λ^0, we obtain the matrix elements and shows their square in Fig. 2. Then multiplying these by the relative frequency of nuclear fragments, we get the relative frequency of observed hyperfragments which is shown in Fig. 3.

([6]) D. H. PARKINS: *Proc. Roy. Soc. London*, A **203**, 399 (1950); see also *Kosmische Strahlung*, ed. by HEISENBERG, p. 192.

Comparing the calculated results with the experimental charge distribution of hyperfragments, we recognize abnormal features at $Z = 2$, 4 and 1. Since we did not treat reasonably at $Z = 1$, the objects of our consideration are the cases at $Z=2$ and 4. In these cases, the observed frequency of hyperfragments is comparatively small against that of nuclear fragments. This may be related with the mechanism of the emission of α-particles and ^{8}Be. For instance, if most part of α-particles is directly knocked out by an incident particle as stated by BERNARDINI ([7]), these α-particles are emitted outside the nucleus before the Λ^0 completely loses its energy so that there is almost no chance of the formation of hyperfragments.

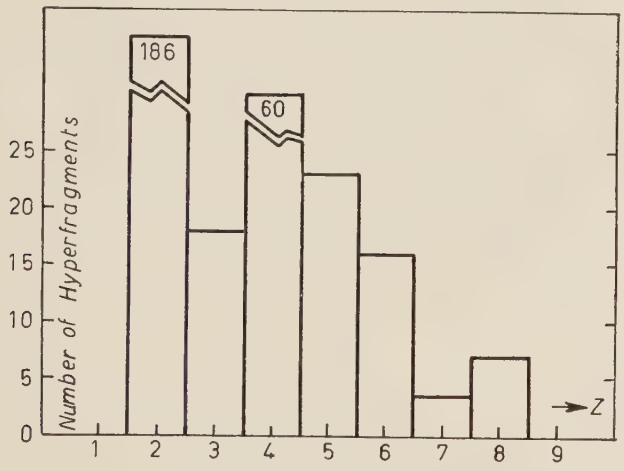

Fig. 3.

In this note we examined the features of hyperfragments on a simple model and roughly speaking it seems that most of the features are understandable with our simple assumptions. Experimental facts are not so copious and accurate that the decisive conclusions of Λ^0-nuclear interactions may be reliable. Hence our simple model is one of the possibilities and to study the nature of Λ^0-nuclear interactions one needs to investigate the slowing down process of Λ^0 in nuclei ([8]) which is related to high energy Λ^0-nuclear interaction beside the low energy phenomena treated in this note.

([7]) G. BERNARDINI: *Kosmische Strahlung*, ed. by HEISENBERG, p. 182.
([8]) JASTRAW treated this problem. R. JASTRAW: *Phys. Rev.*, **97**, 181 (1955).

* * *

Authors wish to thank Mr. R. NAKASIMA for his kind discussions especially on nuclear phenomena.

RIASSUNTO (*)

Sulla base di un modello semplice, si calcola l'energia di legame del Λ^0 negli iperframmenti e si discute la natura della forza Λ^0-nucleone. Sulla stessa base si considera lo spettro Z degli iperframmenti prodotti in emulsione nucleare.

(*) *Traduzione a cura della Redazione.*

On the Analysis of the Cosmic Ray Jets.

H. Huzita (*)

Istituto di Fisica dell'Università - Padova
Istituto Nazionale di Fisica Nucleare - Sezione di Padova

(ricevuto il 14 Giugno 1957)

Summary. — A new method for analysing cosmic ray jets is presented which is independent of the angular fluctuations of secondary particles for each event. Two events are analysed by this method and discussed.

1. – Introduction.

So far many cosmic ray jets found in photographic emulsions have been analyzed by using the number of shower particles and their angular distribution (e.g. median angle and other similar methods) (1). In such a procedure it is very difficult to exclude those events that are not nucleon-nucleon interactions: also the estimation of the primary energy is sensitive to the fluctuation in the angular distribution. Even if events are selected which have a small number of evaporation particles, it is very difficult and dangerous, as has clearly been shown by W. Heitler and C. H. Terraux (2), to select nucleon-nucleon interactions. This is because it is possible that at very high energies all secondary particles are collimated in a narrow cone and interact only with a small number of nucleons along their path, and subsequently give little excitation energy to the residual nucleus. To observe the phenomena of meson production more precisely it is desirable to know the energies of the primary and

(*) On leave of absence from St. Paul's University, Tokyo.

(1) C. C. Dilworth and S. J. Goldsack: *Nuovo Cimento*, **10**, 1261 (1953).

(2) C. Castagnoli, G. Cortini, C. Franzinetti, A. Manfredini and D. Moreno: *Nuovo Cimento*, **10**, 1539 (1953); W. Heitler and C. H. Terraux: *Proc. Phys. Soc.*, A **66**, 929 (1953).

secondary particles. Although it is nearly impossible to measure the primary energy directly in emulsion, it is possible to measure the energies of the secondary particles. In this paper a possible method of analysis by using the energies and angles of secondary particles with respect to the primary direction is presented and applied to two examples.

2. – Method.

When a high energy nucleon collides with another nucleon and π-mesons are produced, a meson, which has an energy E_c in the center-of-mass system of these two nucleons and an angle θ_c with respect to the primary particle, has an energy E_l in the laboratory system given by the equation:

$$E_l = \gamma_c(p_c\beta c \cos\theta_c + E_c) , \tag{1}$$

where β is the velocity of the nucleons in the center-of-mass system and γ_c is $1/\sqrt{1-\beta^2}$ (see Fig. 1).

In the energy range which we are considering, the velocity of the meson in the center-of-mass system is nearly equal to βc, and so the energy is given by the approximation

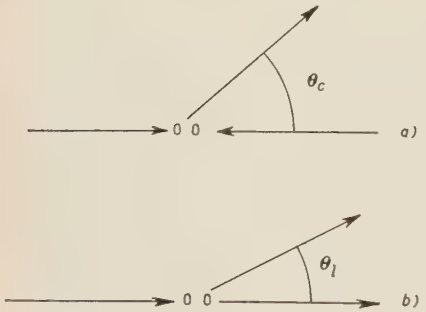

Fig. 1. – *a*) Center of mass System; *b*) Laboratory System.

$$p_c\beta c = E_c \tag{2}$$

and therefore we obtain

$$E_l = \gamma_c E_c(1 + \cos\theta_c) . \tag{3}$$

Using the relation between θ_c and θ_l,

$$\gamma_c \operatorname{tg}\theta_l = \operatorname{tg}\frac{\theta_c}{2} , \tag{4}$$

we have that

$$E_l = \frac{2\gamma_c E_c}{1 + \gamma_c^2 \operatorname{tg}^2\theta_l} ; \tag{5}$$

on rewriting, one obtains

$$\frac{1}{E_l} = \frac{1}{2\gamma_c E_c} + \frac{\gamma_c}{2E_c}\operatorname{tg}^2\theta_l . \tag{6}$$

When E_c is constant for all the mesons, then if we plot experimental results for a single event in the diagram of $(1/E_l) - \operatorname{tg}^2\theta_l$ all points must appear along one line (see Fig. 2). From the slope of this line and the point where

it crosses the $1/E_l$ — axis, we get the value $\gamma_c/2E_c$ and $1/2\gamma_c E_c$ respectively, which give γ_c and E_c independently. However E_c is not constant for all of the secondary mesons, but if the fluctuations are not too large the experimental points will be diffused along the line. Of course if these fluctuations are large such a line is not easy to find.

It may be difficult to determine this line from the experimental points systematically because, owing to the fact that one axis has an inverse dimension of energy the errors are not symmetrically distributed. However, the values γ_c and E_c are not too sensitive to the position and the inclination of this line and furthermore we do not hope to determine the energies with great precision. Once the line has been found it is easy to deduce the inelasticity coefficient k, which is

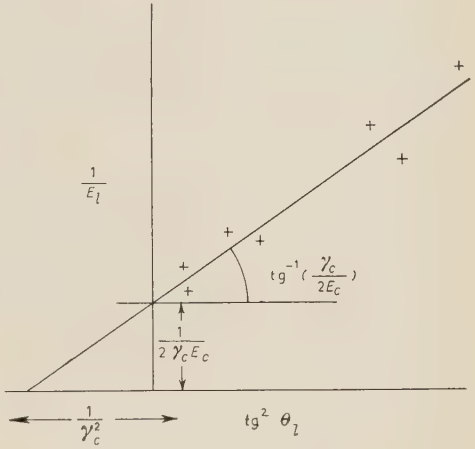

Fig. 2. – Schematic diagram of the $(1/E_l)$ — — $\mathrm{tg}^2\,\theta_l$ plot. + = expected esperimental points.

$$k = \frac{1.5\, n\, E_c}{2(\gamma_c - 1)Mc^2}, \tag{7}$$

where M is mass of the nucleon, n_s is the number of shower particles and c is the velocity of light. We assume that the numbers of π^+, π^0 and π^- are equal.

This method would appear to have certain advantages over previous methods of analysis in the following points:

1) An angular distribution has not been assumed, so the quantity γ_c does not depend on the fluctuations of such a distribution.

2) Even without a knowledge of the energies of all the secondary particles, the above analysis is possible. This fact therefore, would make it easier to collect examples. We can also avoid the necessity of measuring the energies of the particles which make very small angles with respect to the incident particle, and which therefore have very high energies and are consequently quite often impossible to measure by the scattering method.

3) It is possible to gain some information about the secondary interactions in the same nucleus.

4) Even if the energy spectrum is wide, the inelasticity coefficient will still be well determined, because in such cases the parameter E_c shows the

average energy of the secondary particles in the center-of-mass system. Therefore the inelasticity coefficient so obtained will probably be more reliable than that obtained from the limiting angle ([3]).

3. – Examples.

Good examples of high energy interactions are very rare because of the small number of events suitable for the energy measurement and also because of the difficulties of the energy measurements themselves. We consider the following examples:

1) *The event of Hopper, Biswas and Darby* ([4]). – In this case the energies of many secondary tracks have been measured. Fig. 3 and 4 show the results of the $(1/E_l) - \mathrm{tg}^2\,\theta_l$ plot. The collimation along the line is fairly good. We get $\gamma_c \sim 46$, $E_c \sim 0.3$ and $k \sim 0.03$. In the original paper the authors found $\gamma_c \sim 23$ and $k \sim 0.1$ which they obtained by putting the sum of the longitudinal momenta equal to zero.

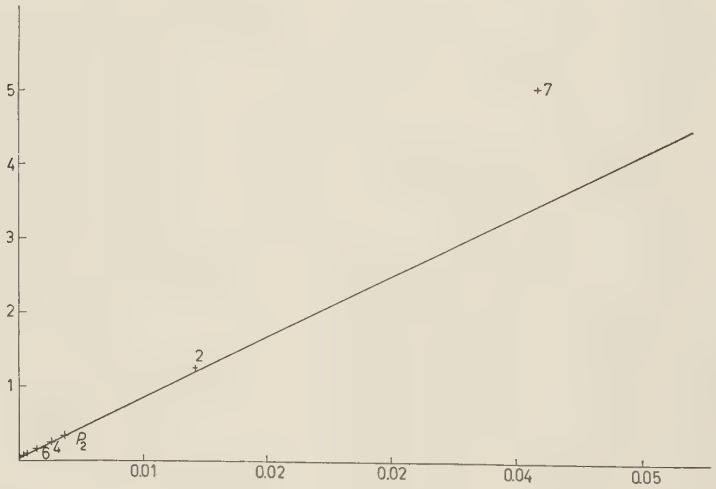

Fig. 3. – The event of Hopper, Biswas and Darby.

The angular distribution and the energy distribution in the center-of-mass system are shown in Fig. 5 and 6. The shaded part is that of the neutral mesons. The energy distribution is not well determined because the energies

([3]) G. Bertolino and G. Pescetti: *Nuovo Cimento*, **12**, 632 (1954).
([4]) V. D. Hopper, S. Biswas and J. F. Darby: *Phys. Rev.*, **84**, 457 (1951).

are rather low and the assumptions which are involved in formula (3) are not necessarily valid. However it is possible to know the shape of the energy distribution.

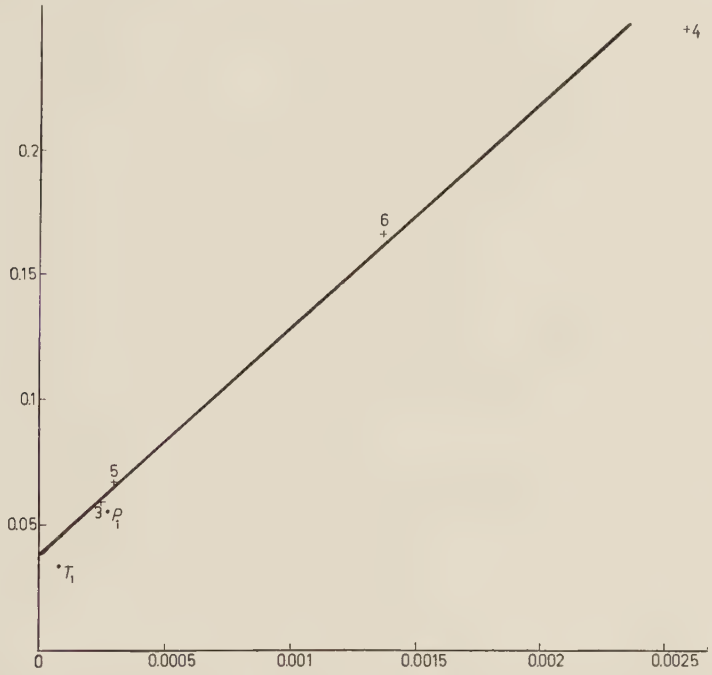

Fig. 4. – The event of Hopper, Biswas and Darby. Large scale representation of the curve for small values of θ_l.

2) *The event of the Turin Group* (5). – Recently a good example was found and measured by the Turin group. The results are shown in Fig. 7 and 8. It seems from the diagram that there are two groups of particles, in other words, two or more interactions have occured in the same nucleus. Of course it is possible to interpret the event as the result of one interaction with a wide energy distribution, but in this case there must exist a strong correlation between angle and energies; that is, higher energy particles are ejected at larger angles and the lower energy particles at smaller angles with respect to the primary; for if we draw one line in this diagram (for example, line C in Fig. 7), then in the part of the smaller angles nearly all the points must be above this line while in the part of the larger angles all the points must be under this line.

(5) A. Debenedetti, C. M. Garelli, L. Tallone and M. Vigone: *Nuovo Cimento*, **4**, 1142 (1956).

We have drawn lines A and B in Fig. 7 and 8 to correspond to the first and second interactions respectively. Near the intersection point of these lines, it is impossible to decide whether the particles should be identified with line A or line B: also there are two particles which have not been measured, and for a further two particles only a lower limit to their energies could be obtained. Such tracks are treated here in both interactions (we will call this group (AB) later): this has not influenced the factors γ_c and E_c, but only the angular distribution and inelasticity coefficient.

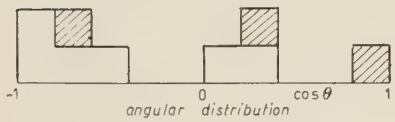

Fig. 5. – Angular distribution of the event of Hopper, Biswas and Darby.

Fig. 6. – Energy distribution of the event Hopper, Biswas and Darby.

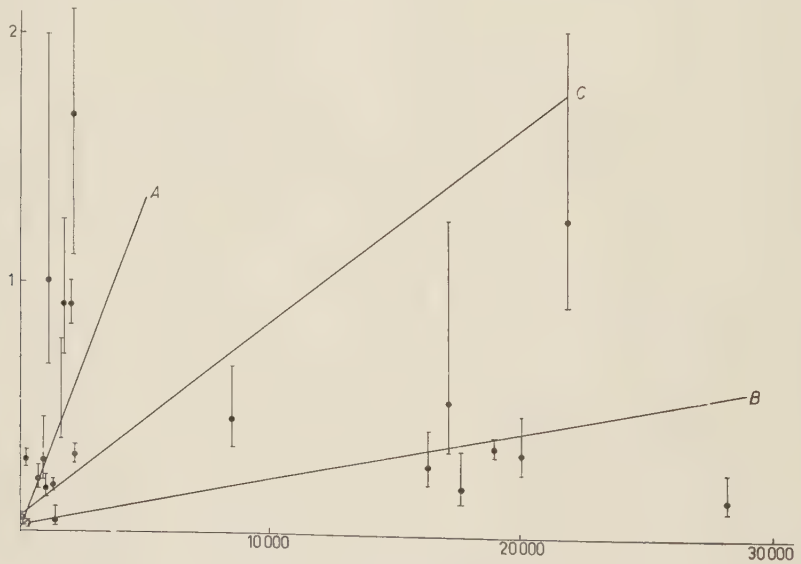

Fig. 7. – The Turin event.

The first interaction. – From the line A we get $\gamma_c \sim 195$, $E_c \sim 0.4$, and and $k \sim 0.04$ with group (AB), and $k \sim 0.03$ without group (AB). The angular and energy distributions are shown in Fig. 9 and 10. The shaded part

is due to the group (AB). The angular distribution shows a strong asymmetry; without the group (AB) it is all backwards. We will discuss this phenomena later.

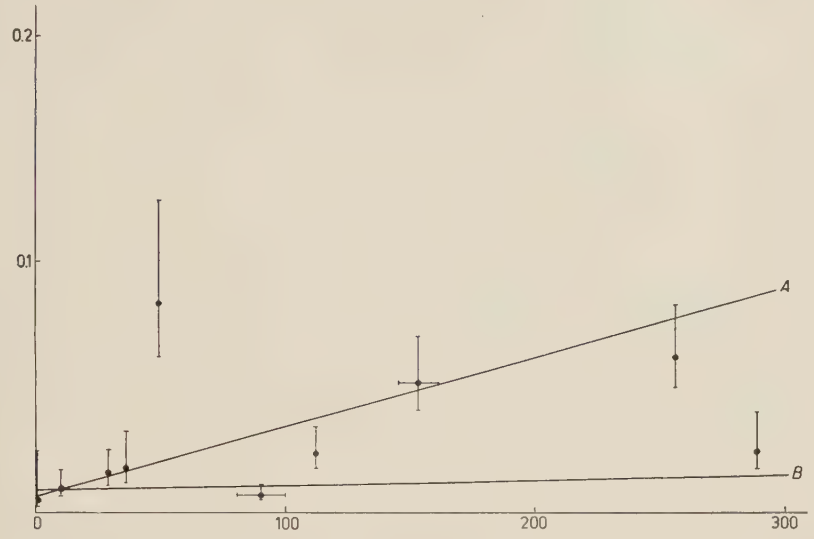

Fig. 8. – The Turin event. Large scale representation of the curve for small values of θ_l.

The second interaction. – From the line B we get $\gamma_c \sim 46$, $E_c \sim 1$ and $k \sim 0.4$ with group (AB), and $k \sim 0.2$ without group (AB). The angular and energy distributions are shown in Fig. 11 and 12. In Fig. 11 the shaded part is due to the group (AB). If the shaded part is included, the angular

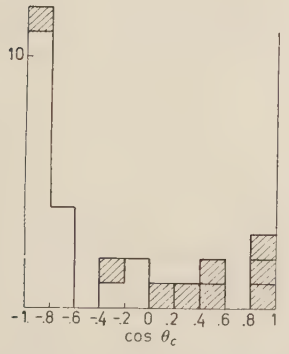

Fig. 9. – The angular distribution of the first interaction (Turin event).

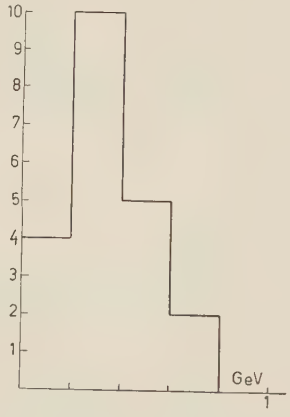

Fig. 10. – Energy distribution of the first interaction (Turin event).

distribution is completely symmetrical. The larger part of the group (AB) therefore would belong to the second interaction. The angular distribution of both the first and second interactions are consistent with a $\cos^2\theta_c$ distribution. DEBENEDETTI *et al.* have analyzed this event as one interaction and obtained $\gamma_c \sim 40 \div 50$. The angular distribution obtained by these authors is similar to the distribution obtained by the method proposed in this paper.

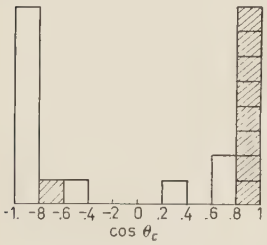

Fig. 11. – The angular distribution of the second interaction (Turin event).

Since the energy of the first interaction is large and the inelasticity coefficient is small, the E_c of the secondary interaction must be larger if the nucleons of the first interaction interact successively and produce the mesons. However the E_c in the secondary interaction is too small: therefore we must consider the following; after the first interaction, the nucleon which had not lost a large amount of energy, escaped without further interaction in the nucleus (perhaps track number 1). The mesons which are ejected forwards in the center-of-mass system in the first interaction will reach the nucleons in front of their motion, with which they may eventually interact, earlier than the mesons ejected backwards. Only the former could contribute to the meson production in the secondary interaction. The angular distribution of the first interaction and the E_c of the secondary interaction are consistent with this interpretation.

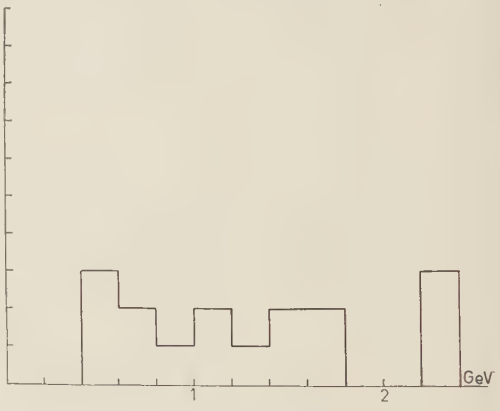

Fig. 12. – Energy distribution of the second interaction (Turin event).

4. – Conclusions.

From only two examples it is very difficult to compare the observations with theories and to decide between them. However we may consider the following points:

1) The energy spectrum of mesons in the center-of-mass system is not wide even in the energy range 10^{13} eV. Therefore the method described here may be suitable in the future for the analysis of good examples. Transverse

momenta are not large. This fact is common to the theory of Heisenberg and Landau (6).

2) The inelasticity coefficient is rather low. The theory of Heisenberg, and of Lewis *et al.* (7), deduces a small inelasticity, but in the theory of Fermi (8), and Landau this parameter does not appear but must be added *ad hoc.*

3) Angular distributions are sometimes isotropic (HBD) and sometimes have a sharp maximum in the forward and backward direction (Turin).

* * *

The author wishes to acknowledge many valuable discussions with Prof. W. F. Fry and Dr. M. Baldo-Ceolin, and the kind encouragement of Prof. N. Dallaporta. He also would like to express his thanks to Prof. S. Nakagawa and the members of the emulsion group of Rikkyo (St. Paul's) University. He also wishes to thank the Italian Government for a scholarship.

(6) W. Heisenberg: *Zeits. f. Phys.*, **124**, 628 (1948); **126**, 569 (1949); L. D. Landau: *Izv. Acad. Nauk*, **17**, 51 (1953).

(7) H. W. Lewis, J. R. Oppenheimer and S. A. Wouthuysen: *Phys. Rev.*, **73**, 127 (1948).

(8) E. Fermi: *Prog. Theor. Phys.*, **5**, 570 (1953).

RIASSUNTO

Si presenta un nuovo metodo, independente dalle fluttuazioni angolari delle particelle secondarie nei singoli eventi, per analizzare i getti dei raggi cosmici. Con questo metodo vengono analizzati e discussi due eventi.

On Polarization Effects in Coulomb Electron Scattering.

G. Passatore

Istituto di Fisica dell'Università - Genova
Istituto Nazionale di Fisica Nucleare - Sezione Aggregata di Genova

(ricevuto il 14 Giugno 1957)

Summary. — Polarization effects in Coulomb electron scattering are considered by using Stokes parameters technique. As four real parameters completely describe the intensity and the polarization of a beam, the transition probability is expressed by a T-matrix which operates on them and the general relation expressing the T-matrix in terms of the S-scattering matrix is then deduced. The T-matrix connecting the Stokes parameters of the scattered beam with those of the incident one is obtained in Born's first approximation. As is well known, in this approximation there are no polarizing effects, but it becomes easy to discuss explicitly the spin direction dependence on the scattering angle. The T-matrix expression for a general spherical field is then obtained without using Born approximation, and some general features, and in particular the polarizing effect, are discussed.

1. – Introduction.

Polarization effects in Coulomb scattering of an electron beam have been for the first time considered in detail by Mott ([1,2]), who particularly discussed asymmetry effects in double scattering experiments. Later Tolhoek and De Groot ([3]) have discussed the same effects by using density matrices to describe the beams of particles and by introducing « orientation coefficients » for the spins.

([1]) N. F. Mott: *Proc. Roy. Soc.*, A **124**, 425 (1929).
([2]) N. F. Mott: *Proc. Roy. Soc.*, A **135**, 429 (1932).
([3]) M. A. Tolhoek and S. R. De Groot: *Physica*, **17**, 1 (1951).

A treatment substantially equivalent to the latter, can be effected by using Stokes parameters technique, as worked out by FANO ([4,5]), which has already been used in other cases with particular success.

The parameters, introduced by STOKES ([6,7]) to describe beams of polarized light, are directly observable quantities which have very significant formal properties. The state of polarization can be described by four quantities: the intensity I and three more quantities forming a vector $\mathcal{P}$ in the space of polarization states; the modulus P of this vector, divided by intensity I, represents the degree of polarization and its direction can be linked up with the possible orientations of filters which characterize a definite polarization state.

The particularly significant formal properties mentioned above are recognized by forming a four-row and one-column matrix $\begin{pmatrix} I \\ \boldsymbol{P} \end{pmatrix}$ with the Stokes parameters I, P_1, P_2, P_3.

Let us now consider the beam undergoing an interaction: the Stokes parameters $\begin{pmatrix} I \\ \boldsymbol{P} \end{pmatrix}$ of the beam after the interaction are linearly related to those of the incident beam and therefore it is possible to determine a 4×4 T-matrix which will symbolically represent the interaction:

$$\begin{pmatrix} I' \\ \boldsymbol{P}' \end{pmatrix} = T_1 \begin{pmatrix} I \\ \boldsymbol{P} \end{pmatrix}. \tag{1}$$

If the beam undergoes successive interactions T_1, T_2, ..., it is possible to obtain the complete description of the final beam state by simply determining the matrix product $\ldots T_2 T_1$.

For this reason the knowledge of the T-matrix proves to be of interest for the elementary interactions which a beam of particles can undergo.

The T-matrix has been determined by PERRIN ([8]) for merely classic interactions for beams of light. FANO ([4,9]) has subsequently determined the same matrix in the case of the Compton effect. In this work we determine the T-matrix in the case of Coulomb electron scattering. In Sect. 2 we deduce the general relation between the scattering S-matrix and the T-matrix, in Sect. 3 we specify the frames of reference, and in Sect. 4 the T-matrix will be determined by describing the scattering in Born's first approximation. As

---

([4]) U. FANO: *Journ. Opt. Soc. Am.*, **39**, 859 (1949).
([5]) U. FANO: *Phys. Rev.*, **93**, 121 (1954).
([6]) C. G. STOKES: *Trans. Camb. Phil. Soc.*, **9**, 399 (1852).
([7]) M. S. WALKER: *Am. Journ. Phys.*, **22**, 170 (1954).
([8]) F. PERRIN: *Journ. Chem. Phys.*, **10**, 415 (1952).
([9]) W. H. MCMASTER: *Am. Journ. Phys.*, **22**, 351 (1954).

is well known, in such an approximation we have no polarizing effects, that is, the modulus of the vector $\boldsymbol{P}$ is not altered. However it is easy to discuss the electron spin variation with the scattering angle. In this way we determine, as a function of the energy, the scattering angle at which the longitudinal polarization is transformed into the transversal one.

In Sect. 5 the same T-matrix is deduced for the scattering in a central field without using Born approximation. We may then discuss the polarizing effect of Coulomb scattering and consider polarization effects in the double scattering.

Finally in the Appendix we shall show how the results of Sect. 4 are contained in those of Sect. 5.

2. – Relation between T-matrix and S scattering matrix.

In a scattering process the transition probability is expressed, as is known, by:

$$w_{FI} = |(\psi_F S \psi_I)|^2 , \tag{2}$$

where S is the scattering matrix, ψ_I the wave function for the initial state, ψ_F the one for the final state. We refer only to the case when the functions ψ_I and ψ_F describe a beam of photons or of particles with spin $\frac{1}{2}$.

As far as polarization is concerned, the states ψ_I and ψ_F can be described by density matrices ϱ_{ij} and τ_{hk}, each referring to two orthogonal basic states, which we denote as u_1, u_2 for ψ_I and v_1, v_2 for ψ_F respectively. Relation (2) can now be written as:

$$w_{FI} = \sum_{hk} \tau^*_{hk} \sum_{ij} S_{hi} S^*_{jk} \varrho_{ij} , \qquad (h, k, i, j = 1, 2), \tag{3}$$

where

$$S_{hi} = (v_h S u_i) . \tag{4}$$

The asterisk denotes hermitian conjugate.

S_{hi} is the element of the S-matrix for the transition between the states whose polarization is described by u_i and v_h respectively. The 2×2 matrix S_{hi} is of course a submatrix (in respect to polarization states only) of the complete scattering S-matrix, which therefore will depend also on the other observables specifying the initial and final states.

The relation (2) expresses the transition probability by means of an operator (S-matrix) which operates on amplitudes. The intensity and type of polarization of a beam are specified by the density matrix elements, i.e. by four quantities quadratic in the amplitudes and linearly independent. The

question then arises how to express the transition probability, rather than by the S-matrix, by some T-matrix which operates on four general forms quadratic in the amplitudes. It is therefore interesting to know how to construct the T-matrix if the S-matrix, which describes the interaction, is given.

Let U_α and V_β ($\alpha, \beta = 0 \div 3$) be four quadratic forms of the amplitudes, for ψ_I and ψ_F respectively, obtained from the elements of the density matrices by general unitary transformations:

$$U_\alpha = \sum_{i,j=1,2} \varepsilon_{\alpha,ij} \varrho_{ij} , \tag{5a}$$

$$V_\beta = \sum_{h,k=1,2} \eta_{\beta,hk} \tau_{hk} . \tag{5b}$$

It follows immediately that the relation (3) becomes:

$$w_{FI} = \sum_{hk} \sum_{\beta} \eta_{\beta,hk} V_\beta^* \sum_{ij} S_{hi} S_{jk}^* \sum_{\alpha} \varepsilon_{ij,\alpha}^* U_\alpha \tag{6a}$$

$$= \sum_{\beta} V_\beta^* \sum_{\alpha} [\sum_{hk} \eta_{\beta,hk} (\sum_{ij} S_{hi} S_{jk}^* \varepsilon_{ij,\alpha}^*)] U_\alpha \tag{6b}$$

$$= \sum_{\beta} V_\beta^* W_\beta \tag{6c}$$

after putting

$$W_\beta = \sum_{\alpha} T_{\beta\alpha} U_\alpha \tag{7}$$

$$T_{\beta\alpha} = \sum_{hk} \eta_{\beta,hk} \sum_{ij} S_{hi} S_{jk}^* \varepsilon_{ij,\alpha}^* . \tag{8}$$

In order to make more evident the meaning of the quantities W_β we observe that if ϱ' is the density matrix which describes the polarization of the scattered beam, whose wave function is $S\psi_I$, it follows from the (6a):

$$\varrho'_{hk} = \sum_{\alpha} \sum_{ij} S_{hi} S_{jk}^* \varepsilon_{ij,\alpha}^* U_\alpha \tag{9}$$

because, as is known, the transition probability w_{FI} can be expressed as the trace of the $\tau\varrho'$ product.

Therefore equation (7) can be written in the following way

$$W_\beta = \sum_{hk} \eta_{\beta,hk} \varrho'_{hk} . \tag{10}$$

If we now compare equation (10) with equation (5a) we see that the quantities W_β have for the scattered beam the same meaning as the quantities V_β for the final state here considered. Let us observe now that the hermitian character of the density matrix assures that the intensity and the type of polarization of a beam can be described by four real quantities. It is easy

to see that if we assume the first of these to be proportional to the intensity I and if the transformation (5) is unitary, the four quantities coincide, except for the factor $1/\sqrt{2}$, with the Stokes parameters in a generic frame of reference. As a consequence of a certain choice of the coefficients $\varepsilon_{\alpha,ij}$ the quantities U_α assume the simple expressions:

$$(11) \qquad \begin{cases} U_0 = (1/\sqrt{2})(\varrho_{11} + \varrho_{22}) , & U_1 = (1/\sqrt{2})(\varrho_{11} - \varrho_{22}) , \\ U_2 = (1/\sqrt{2})(\varrho_{12} + \varrho_{21}) , & U = (i/\sqrt{2})(\varrho_{12} - \varrho_{21}) , \end{cases}$$

where the factor $1/\sqrt{2}$ is a consequence of the unitary character of the transformation (5).

Generally, an arbitrary choice of the coefficients $\varepsilon_{\alpha,ij}$ in equation (5) is equivalent to a rotation of the axes to which the components U_1, U_2, U_3 of the vector $\boldsymbol{U}$ are related. We shall denote by 1, Q_1, Q_2, Q_3 the four quantities $\sqrt{2}\,V_\beta$, which assume the meaning of the Stokes parameters of the final state ψ_F. The first of these quantities has been put equal to one, as it follows from the normalization of the wave function ψ_F. Further, we denote by I, P_1, P_2, P_3 the quantities $\sqrt{2}\,U_\alpha$ (the Stokes parameters of the incident beam). Then the $T\begin{pmatrix} I \\ \boldsymbol{P} \end{pmatrix}$ quantities assume the meaning of the Stokes parameters of the scattered beam and equation (6) must be written as follows:

$$(12) \qquad I_{\boldsymbol{Q}} = \frac{1}{2}(1\boldsymbol{Q})T\begin{pmatrix} I \\ \boldsymbol{P} \end{pmatrix} ,$$

where we have introduced the intensity $I_{\boldsymbol{Q}}$ instead of the transition probability, the intensity of incident beam not having been normalized to one. If we divide by the incident flux Iv (where v is the speed of the incident particles) we obtain from equation (12) the differential cross-section depending on the initial and final polarization:

$$(13) \qquad \frac{\mathrm{d}\sigma}{\mathrm{d}\Omega} = \frac{1}{2Iv}(1\boldsymbol{Q})T\begin{pmatrix} I \\ \boldsymbol{P} \end{pmatrix} .$$

3. – Stokes parameters for the incident and the scattered beams.

Let us consider now the Coulomb electron scattering. Let the incident direction be along the polar axis of a system of co-ordinates, and θ and φ the polar angles of the scattering direction. We take as the basic polarization states those of longitudinal polarization represented by the spinors u_i $(i = 1,2)$ and v_h $(h = 1,2)$ for the incident and scattered beams respectively. The ex-

pression of these spinors is easily obtained: it is well known that the spinor:

$$N\begin{pmatrix} -Acp_z/(E+\mu) - Bc(p_x - ip_y)/(E+\mu) \\ -Ac(p_x + ip_y)/(E+\mu) + Bcp_z/(E+\mu) \\ A \\ B \end{pmatrix}, \qquad N = [(E+\mu)/2E]^{\frac{1}{2}} \qquad \mu = mc^2$$

represents an electron with positive energy, momentum $\boldsymbol{p}$ and spin in the direction with polar angles χ, ω given by:

$$B/A = \operatorname{tg}(\chi/2)\exp[i\omega] .$$

For direction of the spin we understand, following DARWIN ([10]), the direction of the spin axis in the rest system of the electron.

We now relate the meaning of the Stokes parameters to the directions of propagation and to the scattering plane as specified below (see also Fig. 1).

i) Stokes parameters for the incident beam (with momentum $\boldsymbol{p}_0$):

P_1: difference between the intensities corresponding to spin up and down in the direction $\boldsymbol{a}_1 = \boldsymbol{p}_0/|\boldsymbol{p}_0|$.

P_2, P_3: the same as P_1 with respect to the directions $\boldsymbol{a}_2 = \boldsymbol{a}_3 \wedge \boldsymbol{a}_1$, $\boldsymbol{a}_3 = (\boldsymbol{p}_0 \wedge \boldsymbol{p})/|\boldsymbol{p}_0 \wedge \boldsymbol{p}|$ respectively.

ii) Stokes parameters for the final state (with momentum $\boldsymbol{p}$):

Q_1: difference between the intensities corresponding to spin up and down in the direction $\boldsymbol{b}_1 = \boldsymbol{p}/|\boldsymbol{p}|$.

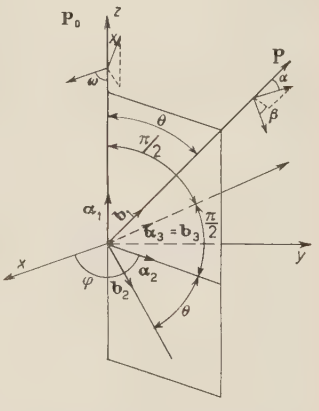

Fig. 1. – Geometrical relationship of the frames of reference used in the text.

Q_2, Q_3: the same as Q_1 with respect to the directions $\boldsymbol{b}_2 = \boldsymbol{b}_3 \wedge \boldsymbol{b}_1$, $\boldsymbol{b}_3 = \boldsymbol{a}_3$ respectively.

Of course, the Stokes parameters P_1', P_2', P_3' of the scattered beam have the same meaning.

It follows that P_1 and Q_1 describe the longitudinal polarization; P_2 and Q_2 the transversal one, in the scattering plane; P_3 and Q_3 the transversal one, perpendicular to the scattering plane. With these choices, between Stokes

([10]) C. G. DARWIN: *Proc. Roy. Soc.*, A **120**, 628 (1928).

parameters and polarization directions the following relations hold:

$$(14) \qquad P_1 = P\cos\chi\,, \qquad P_2 = P\sin\chi\cos(\omega-\varphi)\,, \qquad P_3 = P\sin\chi\sin(\omega-\varphi),$$

$$(15) \qquad P_1' = P'\cos\alpha\,, \qquad P_2' = P'\sin\alpha\cos\beta\,, \qquad P_3' = P'\sin\alpha\sin\beta\,,$$

where χ and ω are the polar angles which define the polarization direction of the incident beam in the system of reference where the scattering direction is specified by the polar angles θ and φ; α and β are the polar angles which define the polarization direction of the scattered beam with respect to the scattering direction as polar axis and to the scattering plane $\boldsymbol{b}_1\boldsymbol{b}_2$ as polar plane; P and P' are the polarization degrees of the incident and scattered beams multiplied by the respective intensities.

Furthermore, as a consequence of the choice made for the basic states and the Stokes parameters, the relations (5) are in this case:

$$(16a) \quad I = \varrho_{11}+\varrho_{22}\,, \quad P_1 = \varrho_{11}-\varrho_{22}\,, \quad P_2 = \varrho_{12}e^{i\varphi}+\varrho_{21}e^{-i\varphi}\,, \quad P_3 = i(\varrho_{12}e^{i\varphi}-\varrho_{21}e^{-i\varphi})$$

$$(16b) \quad 1 = \tau_{11}+\tau_{22}\,, \quad Q_1 = \tau_{11}+\tau_{22}\,, \quad Q_2 = \tau_{12}+\tau_{21}\,, \qquad Q_3 = i(\tau_{12}-\tau_{21})\,.$$

For the following development it is convenient to introduce the ratios of the quantities P_i, P_i' to the respective intensities I and I':

$$(17) \qquad p_i = \frac{P_i}{I}\,, \qquad p_i' = \frac{P_i'}{I'} \qquad (i=1,2,3).$$

Following the nomenclature of Tolhoek and De Groot [3] these ratios are the orientation coefficients for the incident and the scattered beams.

4. – Deduction of the T-matrix in the first Born approximation.

The first Born approximation for elastic Coulomb scattering gives for the S-matrix (4) the following expression [11]:

$$(18) \qquad S_{hi} = M(v_h u_i)\,,$$

where

$$(19) \qquad M = (2\pi/\hbar)\varrho(E)[4\pi\hbar^2e^2Z/|\boldsymbol{p}-\boldsymbol{p}_0|^2]^2$$

$$(20) \qquad \varrho(E) = pcE/(2\pi\hbar c)^3 \quad \text{(density of final states)}$$

u_i $(i=1,2)$ and v_h $(h=1,2)$ are the basic spinors for the incident and scattered beams. From (8), (18), (16), after some obvious calculations one obtains

[11] Cf. for example: W. Heitler: *The Quantum Theory of Radiation* (Oxford), 3rd ed., p. 241.

the T-matrix:

$$(21)\quad T=MN^4\begin{pmatrix} 1+F^2+2F\cos\theta & 0 & 0 & 0 \\ 0 & 2F+(1+F^2)\cos\theta & (1-F^2)\sin\theta & 0 \\ 0 & -(1-F^2)\sin\theta & 2F+(1+F^2)\cos\theta & 0 \\ 0 & 0 & 0 & 1+F^2+2F\cos\theta \end{pmatrix}$$

where

$$(22)\qquad F=(E-\mu)/(E+\mu)\,.$$

A brief discussion of these results is the following.

If the beam is unpolarized, the cross-section averaged over the initial and summed over the final polarization states becomes:

$$\frac{\mathrm{d}\sigma}{\mathrm{d}\Omega}=\frac{1}{2Iv}[(1100)+(1-100)]T\begin{pmatrix} I \\ 0 \\ 0 \\ 0 \end{pmatrix}=\frac{1}{2}\left[\frac{r_0^2Z^2}{(1-\cos\theta)^2}\,\frac{\mu^2}{c^2p^2}\left(1+\cos\theta+\frac{2\mu^2}{c^2p^2}\right)\right],$$

where

$$v=pc^2/E\,.$$

So we obtain the well known Mott formula [11].

The orientation coefficients (17) of the scattered beam are:

$$(23a)\qquad p_1'=\frac{2F+(1+F^2)\cos\theta p_1+(1-F^2)\sin\theta p_2}{1+F^2+2F\cos\theta}$$

$$(23b)\qquad p_2'=\frac{-(1-F^2)\sin\theta p_1+[2F+(1+F^2)\cos\theta]p_2}{1+F^2+2F\cos\theta}\,,$$

$$(23c)\qquad p_3'=p_3\,.$$

From these it follows:

$$\sum_{i=1}^{3}p_i^2=\sum_{i=1}^{3}p_i'^2$$

that is, the polarization degree is not affected by the scattering in this approximation. The relations (23) show also that, in this approximation, the polarization normal to the scattering plane is not affected, while the one in the scattering plane is in general affected.

We suppose now the incident beam totally polarized. As a consequence of (14) and (15), the relations (23) become:

$$(24a)\qquad \cos\alpha=\frac{[2F+(1+F^2)\cos\theta]\cos\chi+(1-F^2)\sin\theta\sin\chi\cos(\omega-\varphi)}{1+F^2+2F\cos\theta}\,,$$

$$(24b) \qquad \sin\alpha\cos\beta = \frac{-(1-F^2)\sin\theta\cos\chi + [2F+(1+F^2)\cos\theta]\sin\chi\cos(\omega-\varphi)}{1+F^2+2F\cos\theta},$$

$$(24c) \qquad \sin\alpha\sin\beta = \sin\chi\sin(\omega-\varphi).$$

For example, if the electron spin is parallel to the momentum, from (24) it follows:

$$\cos\alpha = \frac{2F+(1+F^2)\cos\theta}{1+F^2+2F\cos\theta} \qquad \beta = \pi.$$

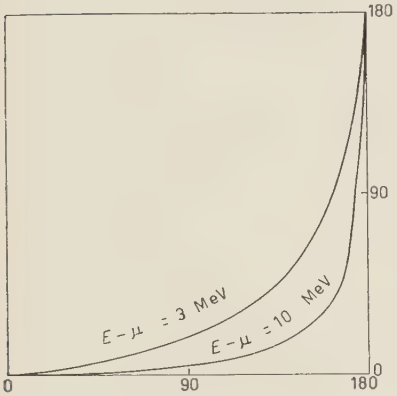

Fig. 2. – Angle between the spin and the momentum of the scattered electron against the scattering angle for the spin of the incoming electron parallel to the momentum.

From here it follows that the spin direction remains in the scattering plane and it is in any case contained in the angle between the incidence and the scattering directions (Fig. 2). With increasing scattering angle, the spin deviates from the scattering direction, and at the scattering angle given by:

$$(25) \qquad \cos\theta = (\mu^2 - E^2)/(\mu^2 + E^2)$$

the longitudinal polarization is transformed into the transversal one. This angle is nearly $\pi/2$ at low energy ($E \sim \mu$) and increases rapidly with increasing energy.

If the spin of the incident electron is in the scattering plane, it follows from (24) that it remains in this plane. This result is peculiar to this approximation, and it is closely related to the absence of any polarizing effect, as we shall show later.

3. – Expression of the T-matrix in the general case.

Now we consider the general case of a spherical potential decreasing with the distance more rapidly than $1/r$, or also the case of the Coulomb potential.

The components ψ_j of the spinor describing the scattered beam asymptotically have been determined by DARWIN ([12]) and, omitting the radial depen-

([12]) C. G. DARWIN: *Proc. Roy. Soc.*, A **118**, 654 (1928).

dence, this spinor can be written as:

$$(26)\qquad \begin{pmatrix}\psi_1\\ \psi_2\\ \psi_3\\ \psi_4\end{pmatrix} =$$

$$= N\begin{pmatrix} f(\theta)\cos\theta + g(\theta)\sin\theta & [-f(\theta)\sin\theta + g(\theta)\cos\theta]e^{-i\varphi} & 0 & 0\\ [f(\theta)\sin\theta - g(\theta)\cos\theta]\,e^{i\varphi} & f(\theta)\cos\theta + g(\theta)\sin\theta & 0 & 0\\ 0 & 0 & f(\theta) & -g(\theta)\,e^{-i\varphi}\\ 0 & 0 & g(\theta)\,e^{i\varphi} & f(\theta)\end{pmatrix}\begin{pmatrix} -F^{\frac{1}{2}}A\\ F^{\frac{1}{2}}B\\ A\\ B\end{pmatrix}$$

where $f(\theta)$ and $g(\theta)$ are the functions introduced by DARWIN multiplied by the square root of the velocity (pc^2/E); the spinor on the right hand side represents the incident beam, and the constants A and B specify its spin in the usual manner.

From equation (26) and equation (27), assuming always as basic states those of longitudinal polarization, one obtains the elements of the matrix (4):

$$(27)\quad S_{hi} = \begin{pmatrix} f(\theta)\cos(\theta/2) + g(\theta)\sin(\theta/2) & [-g(\theta)\cos(\theta/2) + f(\theta)\sin(\theta/2)]\,e^{-i\varphi}\\ g(\theta)\cos(\theta/2) - f(\theta)\sin(\theta/2) & [g(\theta)\sin(\theta/2) + f(\theta)\cos(\theta/2)]\,e^{i\psi}\end{pmatrix}$$

From (8), (16), (27) we can deduce the T-matrix:

$$(28)\qquad T = (|f(\theta)|^2 + |g(\theta)|^2)\cdot$$

$$\cdot\begin{pmatrix} 1 & 0 & 0 & \nu(\theta)\\ 0 & \lambda(\theta)\cos\theta + \mu(\theta)\sin\theta & \lambda(\theta)\sin\theta - \mu(\theta)\cos\theta & 0\\ 0 & -\lambda(\theta)\sin\theta + \mu(\theta)\cos\theta & \lambda(\theta)\cos\theta + \mu(\theta)\sin\theta & 0\\ \nu(\theta) & 0 & 0 & 1\end{pmatrix}$$

where

$$(29)\qquad \begin{cases} \lambda(\vartheta) = (|f|^2 - |g|^2)/(|f|^2 + |g|^2)\,,\\ \mu(\theta) = (fg^* + f^*g)/(|f|^2 + |g|^2)\,,\\ \nu(\theta) = i(fg^* - f^*g)/(|f|^2 + |g|^2)\,.\end{cases}$$

The orientation coefficients of the scattered beam are:

$$(30a)\qquad p_1' = (1 + \nu p_3)^{-1}[(\ \ \lambda\cos\theta + \mu\sin\theta)p_1 + (\lambda\sin\theta - \mu\cos\theta)p_2]\,,$$

$$(30b)\qquad p_2' = (1 + \nu p_3)^{-1}[(-\lambda\sin\theta + \mu\cos\theta)p_1 + (\lambda\cos\theta + \mu\sin\theta)p_2]\,,$$

$$(30c)\qquad p_3' = (1 + \nu p_3)^{-1}(\nu + p_3)\,.$$

The polarization degree $p' = P'/I'$ of the scattered beam can be expressed as a function of the polarization degree $p = P/I$ of the incident beam and its orientation coefficient relative to the normal to the scattering plane:

$$p' = (1 + \nu p_3)^{-1}[p^2 + \nu^2(1 - p^2 + p_3^2) + 2\nu p_3]^{\frac{1}{2}} . \tag{31}$$

A brief discussion will be as follows:

1) the intensity of the scattered beam, summed over the polarization states is:

$$I'(\theta, \varphi) = I[|f|^2 + |g|^2](1 + \nu p_3) . \tag{32}$$

As $p_3 = p \sin \chi \sin(\omega - \varphi)$, equation (32) shows the well-known azimuthal variation of the intensity. Of course, the azimuthal effect is present only if the incident beam has a transversal polarization degree.

2) If the incident beam is unpolarized, the scattered one has a polarization degree:

$$p' = \nu(\theta) . \tag{33}$$

In this case the polarization direction is normal to the scattering plane, as it follows from $p_1' = p_2' = 0$, $p_3' = \nu(\theta)$. The polarizing effect of the scattering from a central field has been shown firstly by MOTT ([1,2]). The result concerning the polarization direction agrees with that recently reported by TOLHOEK ([13,14]).

3) If the incident beam is polarized in the scattering plane, the scattered beam is polarized out of the plane. As a consequence of the interaction the spin leaves the scattering plane. Indeed, from $p_3 = 0$, it follows that $p_3' = \nu(\theta) \neq 0$. As we have seen in the Coulomb case this result cannot be obtained in Born's first approximation.

4) This rotation of the spin out of the scattering plane accounts for the polarizing effect in the scattering of an unpolarized beam. An unpolarized beam can be described as an incoherent superposition of two beams polarized in opposite directions and with the same intensity. We choose these beams as polarized in the scattering plane. Denoting by a bar any quantity which, before or after scattering, refers to one polarization state of the incident beam

---

([13]) H. A. TOLHOEK: *Rev. Mod. Phys.*, **28**, 277 (1956).
([14]) L. WOLFENSTEIN: *Phys. Rev.*, **75**, 1664 (1949).

and by two bars those referring to the other one, we have:

$$\begin{pmatrix} \bar{p}_1 \\ \bar{p}_2 \end{pmatrix} = -\begin{pmatrix} \bar{\bar{p}}_1 \\ \bar{\bar{p}}_2 \end{pmatrix} \quad \bar{p}_3 = \bar{\bar{p}}_3 = 0 , \quad \begin{pmatrix} \bar{p}_1' \\ \bar{p}_2' \end{pmatrix} = -\begin{pmatrix} \bar{\bar{p}}_1' \\ \bar{\bar{p}}_2' \end{pmatrix} \quad \bar{p}_3' = \bar{\bar{p}}_3' = \nu(\theta) .$$

From this, one deduces that if the first beam gives a scattered beam with spin of polar angles α and β, the second gives a scattered beam with spin of polar angles $\pi - \alpha$, $\pi - \beta$. As α and $\pi - \alpha$ can be anomalies of opposite directions, β and $\pi - \beta$ are not azimuths of opposite directions. It follows that the partial polarization of the scattered beam comes out from the fact that spin goes out from the scattering plane, so that opposite spins in the incident beam are no longer opposite in the scattered one.

Of course, if the spin were left in the scattering plane ($\beta = 0$), to the opposite spins in the incident beam would correspond again opposite spins in the scattered one and so the polarizing effect would be absent.

5) If the incident beam is totally polarized normally to the scattering plane, its polarization is not affected by the scattering. Indeed, from $p_1 = p_2 = 0$, $p_3 = 1$, it follows that $p_1' = p_2' = 0$, $p_3' = 1$. This result has been already obtained in a different way by TOLHOEK and DE GROOT [3].

6) If the incident beam is partially polarized, the polarization degree of the scattered beam depends on the scattering angle; for each value of θ, there is an azimuthal dependence of the polarization degree. In order to discuss this dependence in detail it is necessary to have an explicit knowledge of the function $\nu(\theta)$ which depends on the particular kind of spherical potential.

7) If the incident beam is longitudinally polarized, the scattered one is no longer polarized longitudinally. Longitudinal polarization is changed into the transversal one at the scattering angle θ which satisfies the equation:

$$\text{tg}\, \theta = -\lambda(\theta)/\mu(\theta) . \tag{34}$$

In order to discuss in detail the transformation of longitudinal polarization into the transversal one, it is necessary to have the explicit knowledge of the functions $\lambda(\theta)$ and $\mu(\theta)$, which depend on the particular kind of spherical potential.

8) In the case of double scattering, the T-matrix which connects the Stokes parameters of the scattered beam with those of the incident one is given by $T(\theta_2) R(\varphi) T(\theta_1)$, where $R(\varphi)$ is the matrix which describes the rotation of the angle φ around the first scattering direction. θ_1 and θ_2 are the angles of the first and second scattering and φ is the angle between the two scatte ing

planes. Besides recovering the well known results concerning the azimuthal dependence of the intensity ([1,2]), it becomes, in principle, possible to obtain the angular dependence of the degree of polarization for the scattered beam in the general case of whatever polarization of the incident beam. A detailed discussion of this dependence requires first of all the explicit knowledge of the functions λ, μ and ν.

In any case that would be difficult on account of the complicated form of the matrix $T(\theta_2)\,R(\varphi)\,T(\theta_1)$. In the Coulomb case, however, numerical calculations could be made by using the results obtained by McKinley and Feshbach ([15]) and more recently by Curr ([16]).

* * *

The author wishes to express his gratitude to Professor A. Borsellino for suggesting this work and for his constant encouragement and helpful discussions.

Appendix

Comparison between the general results and those obtained in Born's first approximation for the Coulomb case.

In the Coulomb case it is easy to compare the results obtained in Sect. 5 with those obtained in Born's first approximation.

The results of Born's first approximation are again obtained by assuming for the functions $f(\theta)$ and $g(\theta)$ their first order approximations in a power series of the fine structure constant. These approximations for $f(\theta)$ and $g(\theta)$ functions are ([15-17]):

$$(35)\qquad \begin{cases} f(\theta) = (1/2)[\alpha Zc/k][(1-\beta^2)^{\frac{1}{2}} + \cot^2(\theta/2)] \\ g(\theta) = (1/2)[\alpha Zc/k]\cot(\theta/2)[1-(1-\beta^2)^{\frac{1}{2}}] \end{cases}$$

where

$$k^2 = (1/\hbar^2)(E^2/c^2 - m^2c^2)\,, \qquad \alpha = 1/137\,, \qquad \beta = v/c\,.$$

([15]) W. A. McKinley and H. Feshbach: *Phys. Rev.*, **74**, 1759 (1948).

([16]) M. R. Curr: *Proc. Phys. Soc.*, A **68**, 156 (1955).

([17]) N. F. Mott and H. S. W. Massey: *The Theory of Atomic Collisions* (Oxford), 2nd ed., p. 80.

It is not difficult to see that the matrix elements (21) deduced in Born's first approximation are obtained by substituting equations (35) in the matrix elements (28).

RIASSUNTO

Usando la tecnica dei parametri di Stokes si considerano gli effetti di polarizzazione nello scattering coulombiano di elettroni. Poichè quattro parametri reali descrivono completamente l'intensità e la polarizzazione di un fascio, la probabilità di transizione viene espressa mediante una matrice T che opera su di essi e viene inoltre dedotta la relazione generale che esprime la matrice T mediante la matrice di scattering S. Viene ottenuta la matrice T che collega i parametri di Stokes del fascio diffuso a quelli del fascio incidente in prima approssimazione di Born. Come è ben noto, in questa approssimazione non si hanno effetti polarizzanti, ma risulta facile discutere esplicitamente la dipendenza della direzione dello spin dall'angolo di scattering. Viene quindi ottenuta, senza usare l'approssimazione di Born, l'espressione generale della matrice T per un campo centrale e vengono discusse alcune caratteristiche generali, in particolare l'effetto polarizzante.

On the Strong Interactions.

J. C. Polkinghorne

Tait Institute, University of Edinburgh, Scotland

(ricevuto il 19 Giugno 1957)

Summary. — A previous four-dimensional isotopic formalism is rediscussed in the light of suggestions by Gell-Mann and Schwinger concerning the types of strong interactions. A form for the medium-strong K-meson interactions is investigated.

1. – Introduction.

Gell-Mann [1] and Schwinger [2] have recently drawn attention to evidence that the interaction of baryons and K-mesons may be characterized by a weaker coupling constant than that for the interaction of baryons and π-mesons. This suggests that the strong interactions of the original Gell-Mann and Pais [3] classification may consist of two groups:

(i) the medium-strong (MS), involving K-mesons,

(ii) the very strong (VS), involving π-mesons.

According to the currently accepted principle that the stronger the interaction the more extensive its symmetry properties one might expect that the MS interactions would be symmetrical under rotations in the ordinary three-dimensional isotopic space and that the VS interactions would possess further symmetries. One way of introducing these additional symmetries would be to consider a four-dimensional isotopic space.

---

[1] M. Gell-Mann: *Phys. Rev.*, **106**, 1296 (1957) and *Proceedings of the 7th Rochester Conference* (1957).

[2] J. Schwinger: *Proceedings of the 7th Rochester Conference* (1957).

[3] M. Gell-Mann and A. Pais: *Proceedings of the International Physics Conference. Glasgow* (1954).

SALAM and the author (4) have proposed a classification scheme that uses a four-dimensional Euclidean isotopic space. The nucleons together with the cascade particles form the $(\frac{1}{2}, \frac{1}{2})$ representation of the rotation group in (4); the Σ-particles form the (1, 0) representation; and the Λ (0, 0) representation. The π-mesons form the (1, 0) representation for bosons and the K-mesons the $(\frac{1}{2}, \frac{1}{2})$ representation. One aesthetic feature of this scheme is that the charge of a particle is given by the simple expression

$$Q = I_{12} = \mu_3 + \tau_3 \,. \tag{1}$$

μ_3 and τ_3 are components of the generators of the two three-dimensional rotation groups associated in the usual way (5) with the four-dimensional rotation group. A difficulty in the scheme as originally formulated arose from the difference in mass between the nucleons ($\mu_3 = \frac{1}{2}$ doublet) and the cascade particles ($\mu_3 = -\frac{1}{2}$ doublet). It is now natural to suppose that this difference arises from the MS interactions. Accordingly we postulate the following symmetry requirements:

(i) *MS interactions.* Symmetrical under τ-rotations only. They conserve τ_3, μ_3, $|\tau|$.

(ii) *VS interactions.* Symmetrical under the full four-dimensional rotation group. They conserve τ_3, μ_3, $|\tau|$, $|\mu|$.

We shall be concerned in this note to investigate some of the consequences of this assumption. GELL-MANN (1) and SCHWINGER (2) have also considered essentially four-dimensional formalisms. They differ from us, however, in their grouping of the particles.

It may be remarked that in the original paper by SALAM and the author (1) an attempt was made to separate the τ-meson and treat it as the (0, 1) representation. This has not proved in accord with nature. However, it is possible that charged particles corresponding to this representation have been seen (6). They would be doubly strange and so we should expect them to decay according to the schemes

$$\omega^{\pm} \to \mathrm{K}^{\pm} + \pi^0 \,, \tag{2}$$

$$\omega^{+} \to \mathrm{K}^{0} + \pi^{+} \,, \tag{3}$$

$$\omega^{-} \to \overline{\mathrm{K}}^{0} + \pi^{-} \,, \tag{4}$$

(4) A. SALAM and J. C. POLKINGHORNE: *Nuovo Cimento*, **2**, 685 (1955).

(5) H. WEYL: *Theory of Classical Groups* (Princeton, 1939).

(6) Y. EISBERG: *Phys. Rev.*, **96**, 541 (1954); W. F. FRY, J. SCHNEPS and M. S. SWAMI: *Phys. Rev.*, **97**, 1189 (1955); *Nuovo Cimento*, **2**, 346 (1955).

provided they were sufficiently massive. The masses of ω^+ and ω^- would have to be equal if the triplet where self-charge conjugate. The particle ω^0 would, of course, be highly unstable.

2. – VS interactions.

The nucleon-cascade quartet forms the $(\frac{1}{2}, \frac{1}{2})$ or vector representation. The vector N_α has components (*)

$$(5) \qquad \begin{cases} N_1 = \dfrac{N^+ - \Xi^-}{\sqrt{2}}\,, \\ N_2 = \dfrac{N^+ + \Xi^-}{\sqrt{2}i}\,, \\ N_3 = \dfrac{-N^0 - \Xi^0}{\sqrt{2}}\,, \\ N_4 = \dfrac{N^0 - \Xi^0}{\sqrt{2}i}\,. \end{cases}$$

The Σ triplet forms the (1,0) or self-dual antisymmetric tensor representation given by

$$(6) \qquad \begin{cases} \Sigma_{12} = \Sigma_{34} = \Sigma^0, \\ \Sigma_{23} = \Sigma_{14} = \dfrac{\Sigma^+ + \Sigma^-}{\sqrt{2}}\,, \\ \Sigma_{31} = \Sigma_{24} = \dfrac{\Sigma^+ - \Sigma^-}{\sqrt{2}i}\,. \end{cases}$$

The Λ is the (0, 0) or scalar representation. The π-triplet is another (1, 0) representation. The VS interactions are to be invariant in ([4]) and so are given by

$$(7) \qquad g_1 \bar{N}_\alpha N_\beta \pi_{\alpha\beta} + g_2 \bar{\Sigma}_{\alpha\beta} \Sigma_{\beta\gamma} \pi_{\gamma\alpha} + g_3 [\bar{\Sigma}_{\alpha\beta} \Lambda \pi_{\alpha\beta} + \text{h. c.}]\,.$$

Lorentz-space factors such as γ_5 have been omitted. In terms of the three-dimensional notation this may be written as

$$(8) \qquad \begin{cases} + ig_1 [N \boldsymbol{\tau} N \cdot \boldsymbol{\pi} + \bar{\Xi} \boldsymbol{\tau} \Xi \cdot \boldsymbol{\pi}] \\ + 4ig_2 \bar{\boldsymbol{\Sigma}} \Lambda \boldsymbol{\Sigma} \cdot \boldsymbol{\pi} + 4ig_3 [\boldsymbol{\Sigma} \Lambda \cdot \boldsymbol{\pi} + \text{h. c.}]\,. \end{cases}$$

(*) The normalization is arbitrary and is chosen for convenience.

The four-dimensional theory therefore reduces the VS coupling constants from four (7) to three. A similar result has been given by D'Espagnat, Prentki and Salam (8) using Van der Waerden spinors. If

$$g_2 = -g_3 \tag{9}$$

the Σ and Λ may be associated together in

$$\Sigma'_{\alpha\beta} = \Sigma_{\alpha\beta} + \Lambda\delta_{\alpha\beta}\,, \tag{10}$$

and (7) may be written

$$g_1 \bar{N}_\alpha N_\beta \pi_{\alpha\beta} + g_2 \bar{\Sigma}'_{\alpha\beta} \Sigma'_{\beta\gamma} \pi'_{\gamma\alpha}\,. \tag{11}$$

There is, however, no compelling reason for expecting (9) to hold as Σ' is a reducible representation of the rotation group.

3. – MS interactions.

The K-mesons form a $(\frac{1}{2}, \frac{1}{2})$ representation. Their interactions with baryons that are invariant under rotations in (4) may be written

$$if_1 \bar{N}_\alpha \Sigma_{\alpha\beta} K_\beta + if_2 N_\alpha \Lambda K_\alpha + \text{h. c.} \tag{12}$$

In terms of three-dimensional notation this may be written (*)

$$-f_1[\bar{N}\boldsymbol{\tau}\cdot\boldsymbol{\Sigma}K + \bar{\Xi}\boldsymbol{\tau}\cdot\boldsymbol{\Sigma}\bar{K}] - f_2[\bar{N}\Lambda K + \bar{\Xi}\Lambda\bar{K}] + \text{h. c.} \tag{13}$$

Under the assumption of Sect. **1** we are also concerned with interactions which do not conserve $|\mu|$. The simplest way of constructing an interaction with

$$\Delta|\mu| = 1 \tag{14}$$

is to introduce a « spurion » corresponding to $|\mu| = 1$ and zero electric charge, i.e. the $\mu_3 = 0$ member of the (0, 1) representation. This « spurion » should

---

(7) A. Salam: *Nuclear Physics*, **2**, 176 (1956).

(8) B. d'Espagnat, J. Prentki and A. Salam: *Nuclear Physics*, **3**, 446 (1957).

(*) The interaction (13) differs in form from similar interactions written by Salam (7). This is because we use the isotopic doublet K not K^*.

be represented by the anti-self-dual antisymmetric numerical tensor

$$A_{\alpha\beta}=\begin{bmatrix} 0 & 1 & 0 & 0 \\ -1 & 0 & 0 & 0 \\ 0 & 0 & 0 & -1 \\ 0 & 0 & 1 & 0 \end{bmatrix}. \tag{15}$$

The desired interaction is then given by

$$if_1'\bar{N}_\alpha A_{\alpha\beta}\Sigma_{\beta\gamma}K_\gamma + if_2'\bar{N}_\alpha A_{\alpha\beta}\Lambda K_\beta + \text{h. c.} \tag{16}$$

In three-dimensional notation this becomes

$$-f_1'[\bar{N}\boldsymbol{\tau}\cdot\boldsymbol{\Sigma}K - \bar{\Xi}\boldsymbol{\tau}\cdot\boldsymbol{\Sigma}\bar{K}] - f_2'[\bar{N}\Lambda K - \bar{\Xi}\Lambda\bar{K}] + \text{h. c.}\,. \tag{17}$$

The interactions (13) and (17) differ in the relative sign of the nucleon and cascade interactions. Since self-energies depend upon the square of the coupling constant the interaction (16) will not give a mass difference between the nucleons and cascade particles. To obtain this we must take a linear combination of (12) and (16). We therefore conclude that the MS interactions have the rule

$$\Delta|\mu| = 0,\ 1\ ; \tag{18}$$

and that this is equivalent to an arbitrary combination of the three-dimensional interactions.

* * *

I wish to thank Professor A. Salam and Dr. J. C. Taylor for an interesting discussion.

RIASSUNTO (*)

Al lume di suggerimenti di Gell-Mann e Schwinger si ridiscute un precedente formalismo isotopico quadridimensionale riguardante i tipi di interazione forte. Si esamina una forma per le integrazioni medio-forti dei mesoni K.

(*) *Traduzione a cura della Redazione.*

The Differential and Directional Positive Excess of Mesons at Sea Level.

U. Fasoli, I. Modena, E. Pohl (*) and J. Pohl-Rüling

Istituto di Fisica dell'Università - Padova
Istituto Nazionale di Fisica Nucleare - Sezione di Padova

(ricevuto il 22 Giugno 1957)

Summary. — Results are given of a period of observation of the intensity of positive and negative μ-mesons arriving at zenithal angles of 15°, 30°, 45° and 60°. The interpretation of the experimental data which is given here indicates that the E-W symmetry is due solely to the horizontal component of the Earth's magnetic field, which introduces a difference in the path length in the atmosphere for the mesons of different sign. Particular consideration is given to the fact that the exponent γ which appears in the meson energy spectrum is dependent on the zenithal angle.

1. – Introduction.

As a continuation of the measurements on the positive excess of μ-mesons carried out in this laboratory over a period of years ([1-4]), we present the results obtained with an apparatus suitable for the measurement of the directional excess: this has variable zenithal and azimuthal angles and has been in operation since 1954. The apparatus is appreciably different from the type which

(*) Now at the Abteilung für Radiologie und Isotopenforschung, Physiologisches Institut der Universität Innsbruck, Innsbruck, Austria.

([1]) E. Beretta, I. Filosofo and B. Sommacal: *Nuovo Cimento*, **9**, 317 (1952).

([2]) E. Beretta, I Filosofo, B. Sommacal and G. Puppi: *Nuovo Cimento*, **10**, 1354 (1953).

([3]) I. Filosofo, E. Pohl and J. Pohl-Rüling: *Nuovo Cimento*, **12**, 809 (1954).

([4]) U. Fasoli, C. Maroni, I. Modena, E. Pohl and J. Pohl-Rüling: *Nuovo Cimento*, **5**, 473 (1957).

was first used by us for this purpose [2] and is essentially equal to that used for our first series of measurements and in the vertical direction [3].

The iron yoke and windings of the magnet, together with the counter trays and electronic circuits are mounted as a single unit which may be rotated about vertical and horizontal axes, thus allowing the apparatus to be oriented in any direction over a complete hemisphere. To obtain a more clearly defined acceptance angle we have used shorter counters than in previous work: those in current use have effective dimensions of 4.9 cm $\times$40 cm. Each of the 8 triple coincidence channels has half angles of 4°25′ and 17°37′ respectively in the direction of the diameter and length of the counters.

As has already been described in earlier works [2,3] the selection between the positive and negative particles is total in this apparatus, except for the triple coincidences provoked by showers. These events, however, are excluded by anti-coincidences whose efficiency has been shown to be excellent by an examination of the background rate. This has been measured without the magnetic field and with the second counter tray displaced in such a way that events would certainly be eliminated which were due to scattering, since in the absence of a magnetic field these would result in an increase in the number of spurious counts. The contribution of scattering to our measurements has been exhaustively discussed in a previous work [2].

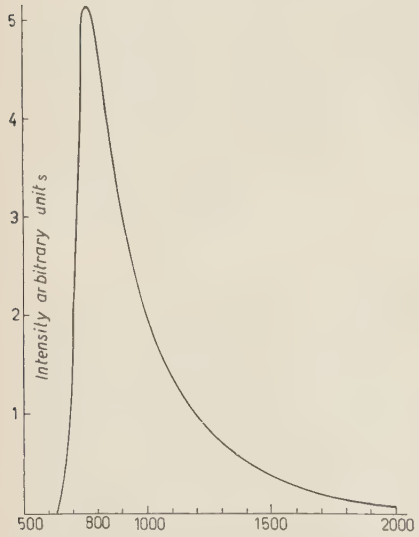

Fig. 1. The acceptance curve of the apparatus.

The meson energy band selected by the magnetic discriminator (the iron nuclei have a thickness of 50 cm and the intensity of the field is 13000 gauss) does not differ very much from that of our first apparatus [2,4] and has a maximum at 0.75 GeV. Taking into account the spectrum of the mesons, the acceptance curves of the apparatus may be obtained (Fig. 1).

To avoid possible anomalies due to the geometry of the counters, the magnetic field has been reversed every 24 hours, and the apparatus has been maintained in the same direction for two consecutive days. While the zenith angle has been kept constant for a long period, the apparatus has been rotated every two days to the four geomagnetic directions N-E-S-W successively. Further, every eight days the axis of the apparatus was turned to the azimuthal angle symmetrical to the vertical to avoid anomalies in the geometry of the apparatus.

2. – Experimental data.

As a check for the apparatus, and as a useful comparison with the other apparatus [4] we have carried out a period of counting in the vertical direction both at the beginning and at the end of the experiments care was taken to orient the counters alternatively N-S and E-W.

The data which are given in Table I yield a value of the positive excess which is in excellent agreement with all our preceeding measurements.

TABLE I. – *Vertical measurements.*

Direction of counter axes	$\frac{\mu^+}{\text{hour}}$	$\frac{\mu^-}{\text{hour}}$	$\frac{\mu^+ + \mu^-}{\text{hour}}$	$\frac{\mu^+}{\mu^-}$	Excess $\frac{2(\mu^+ - \mu^-)}{\mu^+ + \mu^-} \cdot 100$
N – S	36.69 ± 0.21	30.04 ± 0.19	66.73 ± 0.40	1.22 ± 0.03	19.93 ± 0.86
E – W	37.60 ± 0.23	30.97 ± 0.20	68.67 ± 0.43	1.22 ± 0.03	19.62 ± 0.90
mean	37.20 ± 0.16	30.52 ± 0.14	67.72 ± 0.30	1.22 ± 0.02	19.80 ± 0.62
contemporary measurements with other apparatus	—	—	—	—	20.04 ± 0.20

The periods during which the measurements with various zenith angles φ have been carried out, are given in Table II.

TABLE II.

	Period	Effective number of days
15°	30.1 – 1. 3.1956	70
30°	16.8 – 1.12.1955	100
45°	25.1 – 1. 8.1955	169
60°	21.4 – 17.12.1956	141

The experimental data are given in Table III.

TABLE III.

Azimuth ϑ	$\frac{\mu^+}{\text{hour}}$	$\frac{\mu^-}{\text{hour}}$	$\frac{\mu^+ + \mu^-}{\text{hour}}$	$\frac{\mu^+}{\mu^-}$	Excess $= 2\frac{\mu^+ - \mu^-}{\mu^+ + \mu^-} 100$	Zenith φ
N	33.74 ± 0.30	28.25 ± 0.27	61.99 + 0.57	1.19 ± 0.04	17.52 ± 1.28	
E	33.14 »	28.86 »	62.00 »	1.15 »	13.82 ± 1.27	
S	33.93 »	28.12 »	62.05 »	1.21 »	18.72 ± 1.26	15°
W	35.07 »	27.88 »	62.95 »	1.26 »	22.86 ± 1.29	
mean values:	33.97 ± 0.15	28.28 ± 0.14	62.25 ± 0.29	1.20 ± 0.02	18.23 ± 0.64	
N	24.16 ± 0.44	20.18 ± 0.36	44.34 ± 0.86	1.20 ± 0.04	17.94 ± 1.23	
E	22.99 »	20.54 »	43.53 »	1.12 »	11.26 ± 1.27	
S	24.00 »	20.12 »	44.12 »	1.19 »	17.56 ± 1.25	30°
W	25.72 »	19.40 »	45.12 »	1.33 »	27.98 ± 1.27	
mean values:	24.22 ± 0.22	20.06 ± 0.18	44.28 ± 0.40	1.21 ± 0.02	18.68 ± 0.64	
N	13.28 ± 0.26	11.10 ± 0.22	24.38 ± 0.48	1.20 ± 0.04	17.90 ± 1.31	
E	12.41 »	11.94 »	24.35 »	1.04 »	3.91 ± 1.35	
S	13.34 »	10.89 »	24.23 »	1.23 »	20.24 ± 1.35	45°
W	14.74 »	10.33 »	25.07 »	1.43 »	35.20 ± 1.35	
mean values:	13.44 ± 0.13	11.07 ± 0.11	24.51 ± 0.24	1.22 ± 0.02	19.31 ± 0.67	
E	3.94 ± 0.05	4.53 ± 0.05	8.47 ± 0.10	0.87 ± 0.02	−13.90 ≃ 1.70	
W	5.71 ± 0.06	3.39 ± 0.05	9.10 ± 0.11	1.68 »	51.20 ± 1.68	60°
mean values:	4.83 ± 0.04	3.96 ± 0.04	8.79 ± 0.07	1.28 ± 0.02	18.65 ± 1.20	

3. – Interpretation of the experimental data.

To interpret the motion of a meson, we may consider the magnetic field of the earth as divided into its vertical and horizontal components.

The horizontal component is normal to the E-W plane, i.e. to the plane passing through the vertical at the observation point; and through the E-W line. Let us suppose that the telescope is pointed in a certain direction in the E-W plane with a zenith angle ϑ; the mesons which arrive from that direction have been acted upon by both components of the earth's magnetic field, but while the vertical component acts in the same way on the mesons of either

sign, the horizontal component leads to a disymmetry such that the path of one type of meson is longer than that of the other by a certain distance Δt, (see Fig. 2).

Suppose now that we turn the telescope about the vertical (maintaining the angle ϑ constant), then the component of the earth's field in the observation plane will not lead to a dissimmetry in the paths of the mesons, but the normal component will do so: this will be $H_0 \cdot \sin \varphi$, where H_0 is the horizontal component and φ is the azimuthal angle of the plane of observation.

The increase in the path length with respect to the path which would have been followed had the earth's field not been present is sufficiently small to allow us to simplify the problem by assuming that the motion of the mesons occurs in the plane of observation under the influence of only the horizontal component of the earth's field. We therefore do not consider the effect of the vertical component which is the same for both types of meson.

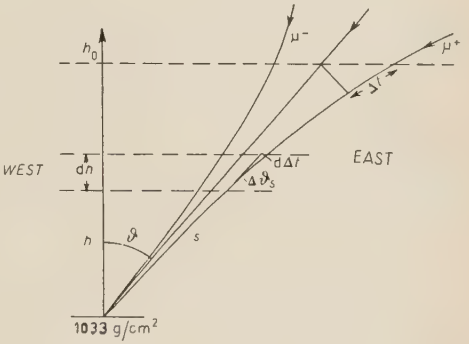

Fig. 2. – Meson trajectories in the East-West plane.

We may now calculate the change in path length introduced by the horizontal component in the E-W plane. For this purpose we introduce the following notation:

h = height of the atmosphere above the observation point in g/cm²;

s = length of the arc of the trajectory of the mesons, in g/cm²;

ϑ = zenith angle of the observations;

r = radius of curvature of the trajectory at one of its points;

P = momentum of the mesons in MeV/c;

Δt = path increase in g/cm²;

$\mathrm{d}\Delta t$ = elementary path increase in g/cm²;

$\Delta\vartheta$ = deflection angle of the trajectory from the direction of observation;

$\varrho(s)$ = density of the air at the point S.

From Fig. 2 one obtains

$$(1) \qquad \mathrm{d}\Delta t = \frac{\mathrm{d}h}{\cos\,(\vartheta + \Delta\vartheta_s)} - \frac{\mathrm{d}h}{\cos\vartheta} = \mathrm{d}h\left(\frac{1}{\cos\,(\vartheta + \Delta\vartheta_s)}\right) - \frac{1}{\cos\vartheta}\,.$$

Expading in series the expression in brackets and taking only the first term it becomes

$$\mathrm{d}\Delta t = \mathrm{d}h\,\Delta\vartheta_s \frac{\sin\vartheta}{\cos^2\vartheta} = \frac{\mathrm{tg}\,\vartheta}{\cos\vartheta}\,\mathrm{d}h\,\Delta\vartheta_s\,,$$

thus

$$\Delta t = \frac{\mathrm{tg}\,\vartheta}{\cos\vartheta}\int_0^{h_0}\mathrm{d}h\,\Delta\vartheta_s\,. \tag{1'}$$

We will now derive the expression for the function $\Delta\vartheta_s$. As is well known

$$\mathrm{d}\vartheta_s = \frac{\mathrm{d}s}{\varrho(s)}\cdot\frac{1}{r}$$

and since

$$r = \frac{P}{300\cdot10^{-3}H_0}\,, \qquad d\vartheta = \frac{300\cdot10^{-3}H_0}{P}\,\frac{\mathrm{d}s}{\varrho(s)}\,. \tag{2}$$

It will now be convenient to express $\mathrm{d}\vartheta_s$ as a function of range (R) and therefore we make use of Olbert's function ([5]),

$$\frac{\mu c}{P} = \frac{a}{b+R} - K\,, \tag{3}$$

where μ = mass of the meson: $a = 53.5$ g/cm^2

$b = 56$ g/cm^2 and $K = 2.07\cdot10^{-3}$.

Combining (3) with (2) one has

$$\mathrm{d}\vartheta_s = \frac{300\cdot10^{-6}\cdot H_0}{\mu c}\left(\frac{a}{b+R} - K\right)\frac{1}{\varrho(s)}\,\mathrm{d}s\,,$$

thus

$$\Delta\vartheta_s = \int_0^s \mathrm{d}\vartheta_s = c\int_0^s\left(\frac{a}{b+R+s'} - K\right)\frac{\mathrm{d}s'}{\varrho(s')}\,, \tag{4}$$

where

$$c = \frac{300\cdot10^{-6}\cdot H_0}{\mu c}$$

(R now represents the residual range).

([5]) S. OLBERT: *Phys. Rev.*, **92**, 454 (1953).

Introducing expression (4) in (1′) we get

$$\Delta t = c\,\frac{\operatorname{tg}\vartheta}{\cos\vartheta}\int_0^{h_0} \mathrm{d}h \int_0^{s}\left(\frac{a}{b+R+s'}-K\right)\frac{\mathrm{d}s'}{\varrho(s')}\,. \tag{5}$$

To evaluate the integral (4) we may integrate along the straight line of observation, without serious errors: one then obtains

$$\Delta\vartheta_h = \int_0^{h}\left(\frac{a}{b+R+(h/\cos\vartheta)}-K\right)\frac{1}{\varrho(h/\cos\vartheta)}\,\frac{\mathrm{d}h}{\cos\vartheta}\,. \tag{4′}$$

Note that $\varrho(h/\cos\vartheta)=\varrho(h)$, and that, due to the significance attributed by us to h, the pressure at the point $h/\cos\vartheta$ of the rectilinear trajectory is given by

$$p(h) = 1033 - h = p_0 - h\,,$$

where $p_0 = 1033$ = pressure at sea-level.

Making use of the hypsometric formula, we obtain for $\varrho(h)$ the expression

$$\varrho(h) = \frac{p(h)}{Z_0}$$

(Z_0 = reduced height of the atmosphere, which we have taken as 8 km). Finally, with this substitution (4′) becomes with $(b+R)\cos\vartheta = B$

$$\Delta\vartheta_h = \int_0^{h}\left(\frac{a}{B+h}-\frac{K}{\cos\vartheta}\right)\frac{\mathrm{d}h}{(P_0-h)/Z_0)} = \tag{4″}$$

$$= Z_0\left[\int_0^{h}\frac{a}{B+h}\,\frac{\mathrm{d}h}{p_0-h} - \frac{K}{\cos\vartheta}\int_0^{h}\frac{\mathrm{d}h}{p_0-h}\right].$$

This integral may easily be calculated and one obtains

$$\Delta\vartheta_h = \frac{aZ_0}{p_0+B}\left(\ln\frac{B+h}{B}-\ln\frac{p_0-h}{p_0}\right)+\frac{KZ_0}{\cos\vartheta}\ln\frac{p_0-h}{p_0}\,. \tag{6}$$

Substituting in (5) one finally gets

$$\Delta t = c\,\frac{\operatorname{tg}\vartheta}{\cos\vartheta}\int_0^{h_0}\mathrm{d}h\left[\frac{aZ_0}{p_0+B}\left(\ln\frac{B+h}{B}-\ln\frac{p_0-h}{p_0}\right)+\frac{KZ_0}{\cos\vartheta}\ln\frac{p_0-h}{p_0}\right], \tag{7}$$

which on integrating becomes

$$(7') \qquad \Delta t = c\,\frac{\operatorname{tg}\vartheta}{\cos\vartheta}\,Z_0\left\{\frac{a}{p_0+B}\,(B+h_0)\left(\ln\frac{B+h_0}{B}-1\right)+\right.$$

$$\left.+\,(p_0-h_0)\left(\ln\frac{p_0-h_0}{p_0}-1\right)\left(\frac{a}{p_0-B}\;\frac{K}{-\cos\vartheta}\right)-\left[-B\,\frac{a}{p_0+B}-p_0\left(\frac{a}{p_0+B}\;\frac{K}{-\cos\vartheta_0}\right)\right.\right.$$

It may easily be confirmed that the term $(p_0 - h_0)(\ln(p - h_0/p_0) - 1)$ tends to zero as $h_0 \to p_0$ and so the integral is convergent at the point $h_0 = p_0$.

With the formula which has been obtained, we have calculated the path difference for the mesons for various energies and for various inclinations, assuming that they were produced at the limits of the atmosphere ($h_0 = p_0$). The values are given in Table IV.

TABLE IV.

Zenith angle	0.7 GeV	0.75 GeV	0.9 GeV	1.0 GeV	1.2 GeV	1.5 GeV	2.0 GeV
15°	8.24	7.9	7.3	6.8	6.14	5.4	4.43
30°	22.4	21.6	19.8	18.6	16.8	14.64	12.4
45°	52	50	46.2	43.7	40.1	35	32.4

From (1) and from Fig. 2 one sees at once that Δt as calculated by us for the positive mesons is equal to Δt for the negatives. In the eastward direction Δt is positive for the μ^+-mesons and negative for the μ^--mesons, while the reverse is true in the westward direction.

If we attribute the asymmetry found experimentally for the positive and negative mesons at various azimuthal angles to the path increases which have been calculated theoretically, we must admit that for every zenith inclination ϑ the following type of expression must be valid

$$(8) \qquad \mu_{\vartheta\varphi} = \mu_{\vartheta_0}[1 - a_\vartheta \sin(\varphi + \alpha)]\,,$$

(μ_{ϑ_0} = intensity for $\varphi = 0$, is the azimuth of the observation plane with zero at North and increasing towards East). In fact, as we have already observed, the various Δt are proportional to $H_0 \sin\varphi$, and so since the absorbed mesons are proportional to Δt, they will also be proportional to $\sin\varphi$. We have used the method of least mean squares to try to adapt this formula to our expemental data, both for the mesons of the two signs and for the total intensity (positive mesons plus negative mesons).

The values of a_ϑ and α are given in Table V.

TABLE V.

	a_ϑ	α	a_ϑ	α	a_ϑ	α
Inclination	Total		positive mesons		negative mesons	
15°	0.00765	3°40′	0.0285±0,00658	5°40′	−0.0176±0.0073	7°30′
30°	0.0181	6°30′	0.0564±0.0126	− 3°20′	−0.0285±0.0127	3°
45°	0.0150	−11°40′	0.0867±0.0141	1°30′	−0.0734±0.0149	7°30′

With these values the hourly counting rates for positive and negative mesons have been calculated in terms of the angles ϑ and φ. In Fig. 3 are given the curves calculated from the experimental data. As can be seen, the experimental data are well represented by equation (8).

We must now see if it is really possible to interpret the behaviour of the cosmic radiation at various zenithal and azimuthal angles in a satisfactory way, making use of the hypothesis which we have put forward regarding the path difference for the mesons of the two signs introduced by the horizontal component of the earth's field.

For this purpose we will start from the supposition that the hypotheses used by us in a preceeding work (4) (*) are valid for any direc-

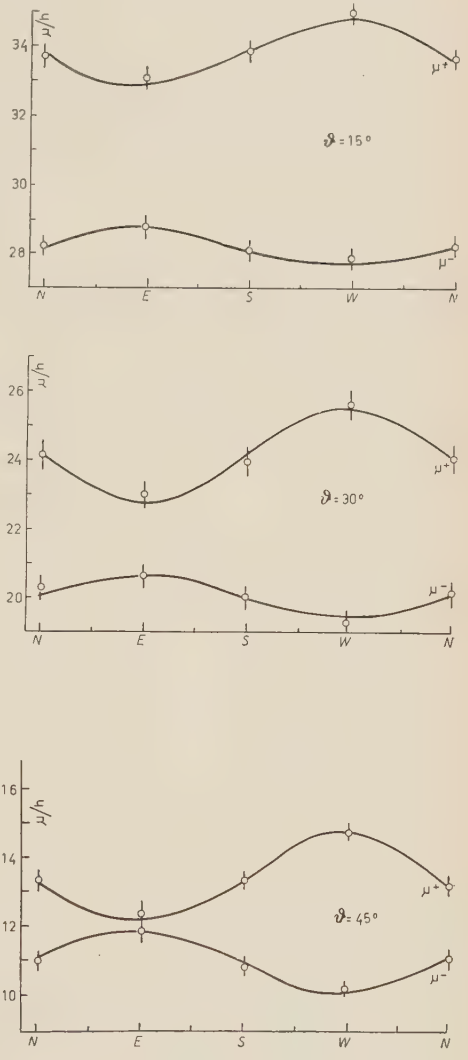

Fig. 3. – Hourly counting rates for positive and negative mesons in function of the zenithal and azimuthal angles (ϑ and φ): the circles represent the experimental points, the errors being the statistical errors: the curves are calculated by means of expression (8).

(*) The assumptions which have been made are the following:

1) The primary nucleonic component is absorbed exponentially in the atmo-

tion of observation. In this way we can apply the formula for the spectrum (already used by us in this earlier work) to represent separately the mesons of different sign. It will however be necessary to make a comparison with the experimental data in order to determine what values of the exponent γ for the spectrum for the various azimuthal angles are required to give agreement with the observations.

The formula predicted for the inclination ϑ becomes

$$\mu_{\vartheta}^{\pm} = \frac{1}{2}\frac{\gamma A}{K^{\gamma}}\frac{B}{B+K\eta}\left\{\pm\frac{\delta}{2}\frac{\Lambda}{R}\left[\frac{\Lambda\varepsilon}{\eta t}\right]^{b/\eta}+\left[\frac{R\varepsilon}{\eta t}\right]^{b/\eta}\right\}\int\frac{1}{\eta^{\gamma+1}}\,. \tag{9}$$

We have taken $\delta =$ excess at production $= 0.30$.

Taking into account the path length in the direction inclined towards East and of the increase introduced by the magnetic field, one then has

$$\eta = +\frac{\beta t}{\cos\vartheta}\pm\beta\,\Delta t\,.$$

We may now expand in series the factor $1/\eta^{\gamma+1}$ in (9) and introducing the azimuth φ we have

$$\mu_{\vartheta}^{\pm} = \frac{1}{2}\frac{\gamma A}{K^{\gamma}}\frac{B}{B+K\eta}\left\{\mp\frac{\delta}{2}\frac{\Lambda}{R}\left[\frac{\Lambda\varepsilon}{\eta t}\right]^{b/\eta}+\left[\frac{R\varepsilon}{\eta t}\right]^{b/\eta}\right\}\cdot \tag{9'}$$

$$\cdot\frac{1}{(\varepsilon+(\beta t/\cos\vartheta)\,)^{\gamma+1}}\left[1\mp(\gamma+1)\frac{\varepsilon\,\Delta t}{\varepsilon+(\beta t/\cos\vartheta)}\sin\varphi\right].$$

If we now wish to interpret the experimental results we must integrate (9') over the acceptance curve (Fig. 1) of the apparatus. Indicating with $f(\varepsilon)$ the analytical expression of this curve we then have

$$\mu_{\vartheta}^{\pm} = \int_{0.63}^{2}\frac{1}{2}\frac{\gamma A}{K^{\gamma}}\frac{B}{B+K\eta}\left\{\pm\frac{\delta}{2}\frac{\Lambda}{R}\left[\frac{\Lambda\varepsilon}{\eta t}\right]^{b/\eta}+\left[\frac{R\varepsilon}{\eta t}\right]^{b/\eta}\right\}\cdot \tag{10}$$

$$\cdot\frac{1}{(\varepsilon+(\beta t/\cos\vartheta)\,)^{\gamma+1}}\left[1\mp(\gamma+1)\frac{\beta\,\Delta t}{\varepsilon+(\beta t/\cos\vartheta)}\sin\varphi\right]f(\varepsilon)\,\mathrm{d}\varepsilon\,.$$

sphere with an absorption length equal to the mean free path for inelastic collisions ($\Lambda = 80$ g/cm^2).

2) The total nucleonic component (primary + secondary) is absorbed exponentially in the atmosphere with an absorption length $R = 125$ g/cm^2.

3) The cross-section for pion production depends only on the E-W ratio of the energies of the emitted pion and of the struck nucleus (the hypothesis is necessary to allow us to affirm that the mesonic secondary component conserves the spectrum of the primary flux).

We have used expression (10) and the experimental data for the total intensity μ_ϑ at various inclinations in the N-S plane for determining the value of γ. This parameter is found to vary with the zenithal angle; a qualitative justification of this fact will be given later.

The values found are given in Table VII.

We have made use of these values to calculate the counting rates of the positive and negative mesons and the total towards E and W; these are given in Table VI. They are in good agreement with the experimental data (Table III).

Table VI.

Azimuth	$\frac{\mu^+}{\text{hour}}$	$\frac{\mu^-}{\text{hour}}$	$\frac{\mu^+ + \mu^-}{\text{hour}}$	Zenith
90° = E	33.6	29.1	62.7	15°
270° = W	34.7	28.7	63.4	
90° = E	22.8	20.86	43.4	30°
270° = W	25.0	19.35	44.9	
90° = E	12.3	1 .99	24.55	45°
270° = W	14.4	10.69	24.64	

We again observe that by means of the mean value theorem (10) may be written

$$\mu_\vartheta^\pm = \left[1 \pm (\gamma+1)\frac{\beta\overline{\Delta t}}{\varepsilon + (\beta t/\cos\vartheta)}\sin\varphi\right]\int_{0.63}^{2}\frac{1}{2}\frac{\gamma A}{K^\gamma}\frac{B}{B+K\eta}\cdot$$

$$\cdot\left\{\pm\frac{\delta}{2}\frac{A}{R}\left[\frac{A\varepsilon}{\eta t}\right]^{b/\eta} + \left[\frac{R\varepsilon}{\eta t}\right]^{b/\eta}\right\}\frac{1}{(\varepsilon + (\beta t/\cos\vartheta))^{\gamma+1}} f(\varepsilon)\,\mathrm{d}(\varepsilon)\,,$$

where the term with the bar indicates a suitable mean value.

On comparison with (8) it must follow that

$$(11)\qquad (\gamma+1)\frac{\beta\overline{\Delta t}}{\varepsilon + (\Delta t/\cos\vartheta)} = a_\vartheta\,.$$

Introducing into (11) the values of Δt calculated for the direction ϑ and for an energy of 0.70 GeV corresponding to the peak of the curve in Fig. 1, we find for $\gamma+1$ the values given in Table VII.

TABLE VII.

	Calculated with the values of total intensity in the N-S plane	Calculated with (11)	Calculated with (13)	Calculated with the spectrum
15°	2.45 ± 0.49	$3{,}6 \pm 1.18$	2.28	2.47
30°	2.67 ± 0.45	2.83 ± 0.83	2.92	2.55
45°	2.91 ± 0.31	2.84 ± 0.72	2.91	2.86

One sees that for 45° and 30° the values of $\gamma+1$ agree with the mean of $\gamma+1$ obtained from (9′) for the mesons of both signs. The agreement is not good at 15° but is always within the errors.

4. – The exponent γ.

A fact which must now be considered is that γ has different values according to the various inclinations (in particular it increases with an increase in the angle ϑ, i.e. with an increase in the energy of the primary particle).

This fact may be considered as being due to a displacement of the meson spectrum for different zenithal angles.

An indication in this sense may be obtained from the following considerations. Suppose that the spectrum in the direction ϑ is of the form

$$I_\vartheta = \frac{A\gamma}{\eta^{\gamma+1}} = \frac{A\gamma}{(\varepsilon + (\beta t/\cos\vartheta))^{\gamma+1}} = \frac{A\gamma \cos^{\gamma+1}\vartheta}{(\varepsilon\cos\vartheta + \beta t)^{\gamma+1}}$$

$$\text{and} \qquad \frac{I_\vartheta}{I_0} = \left(\frac{\varepsilon + \beta t}{\varepsilon\cos\vartheta + \beta t}\right)^{\gamma+1} \cos^{\gamma+1}\vartheta \approx \cos^{\gamma+1}\vartheta \,.$$

On the other hand if we express the dependence of the intensity of the mesons by $\cos^n\vartheta$, where n is a number to be determined, one then has

$$I_\vartheta = I_0 \cos^n\vartheta \,, \tag{12}$$

where I_0 is the intensity in the vertical direction, and $f(\varepsilon)$ is again the acceptance function of the apparatus.

One obtains from (12)

$$\mu_\vartheta = I_0 \int f(\varepsilon)\cos^n\vartheta \,\mathrm{d}\varepsilon = I_0 \,\overline{\cos^n\vartheta} \int f(\varepsilon)\,\mathrm{d}\varepsilon = \mu_0 \,\overline{\cos^n\vartheta} \,.$$

From our calculations it results that the mean direction at which our

apparatus is sensitive coincides with the direction of observation and so $\overline{\cos\vartheta} = \cos\vartheta$. If $\int f(\varepsilon)\,\mathrm{d}\varepsilon$ is the constant of the apparatus.

Thus

$$n = \ln \frac{\mu_\vartheta}{\mu_0} \frac{1}{\ln \cos\vartheta} \approx \gamma + 1 \,. \tag{13}$$

This gives the values for n from which it results that, at least qualitatively, the values of $\gamma+1$ vary with the inclination.

The values are given in Table VII.

A further confirmation, with numerical data in better agreement with those found by us, is directly forthcoming from the production spectrum of π-mesons. We have derived the parameter γ for the values of the production energy at the various inclinations, obtaining the results which, together with those calculated in the foregoing manner, are given in Table VII.

5. – Conclusions.

Within the precision allowed by the statistical errors, all these considerations lead to the conclusion that the asymmetry in the E-W plane which is shown by the mesons at various zenithal angles, can largely be attributed to the horizontal component of the Earth's magnetic field.

It is to be remembered that the data have been interpreted by assuming a positive excess at production of 30%.

* * *

The authors are indebted to Prof. G. Puppi for his help and encouragement during the supervision of this work. Thanks are due to Mr. Salmaso who carried out the calculations.

RIASSUNTO

Sono esaminati i risultati di un periodo d'osservazioni sull'intensità dei mesoni μ^+ e μ^- ad inclinazioni zenitali di 15°, 30°, 45°, 60°. L'interpretazione qui data dei risultati sperimentali indica che l'asimmetria E-W è dovuta solamente alla componente orizzontale del campo magnetico terrestre che introduce una differenza di cammino nell'atmosfera per i mesoni dei due segni. Una particolare discussione è fatta sull'esponente γ che compare nello spettro d'energia dei mesoni e che risulta variabile con l'angolo zenitale.

Inelastic Scattering of 150 MeV Negative Pions by Carbon and Lead (*+).

R. H. Miller

The Enrico Fermi Institute for Nuclear Studies
The University of Chicago - Chicago, Ill.

(ricevuto il 1° Luglio 1957)

Summary. — Energy sensitive counters of the Čerenkov or scintillation type were used in conjunction with a pulse height analyzer to measure the energy spectrum of 150 MeV negative pions scattered from carbon or lead at various angles. Most of the pions scattered into the backward hemisphere had an energy less than 40 MeV. This is in contrast to the result of a Monte Carlo calculation based on a simple Fermi gas model, in which most of the pions scattered backwards have energies above 60 MeV. The measurements indicate that the absorption of pions by carbon is about that predicted by the Monte Carlo calculation, while the absorption by lead is about $\frac{1}{4}$ that expected.

1. – Introduction.

Although the scattering of pions with protons has been studied rather extensively (1), the experimental information on the scattering with complex

(*) Research supported by a joint program of the Office of Naval Research and the U.S. Atomic Energy Commission.

(+) Based on a thesis submitted to the Faculty of the Department of Physics, the University of Chicago, in partial fulfilment of the requirements for the Ph.D. degree.

(1) H. L. Anderson: *Proceedings of the Sixth Annual Rochester Conference* (New York, 1956), p. I-20.

nuclei is still very meagre ([2-4]). Considerable interest attaches to the extent to which simple models are capable of giving a good description of the processes involved ([5,6]). In these models the scattering is constructed from the pion-nucleon interactions, which are assumed not to be appreciably modified within nuclei, while the absorption is supposed due to the process $\pi^- + D = N + N$ ([7]). The knowledge of these fundamental processes is now sufficient so that definite predictions may be obtained from the models. The present series of experiments was undertaken to improve in accuracy and detail the knowledge of the interaction of pions with complex nuclei. This paper deals with the energy and angular distribution of 150 MeV negative pions observed to be inelastically scattered from carbon or lead. Negative pions were used because of the greater flux available. The energy was chosen as near the 180 MeV pion-nucleon scattering resonance as was consistent with high counting rates. This has the effect of maximizing the inelastic processes since the cross-section for the individual pion-nucleon scattering is a maximum here while the real part of its amplitude in the forward direction is small. Thus there should be little elastic contribution to the total scattering other than diffraction and Coulomb scattering. The results are compared with Monte Carlo calculations kindly carried out for this purpose by METROPOLIS *et al.* ([8]) on a simple Fermi gas model. A paper by T. FUJII ([9]) will describe the observations of the elastic scattering and make the comparison with a simple optical model using potentials calculated by WATSON *et al.* ([5]) from the knowledge of the fundamental scattering and absorption processes. It will be shown that while these models have a certain utility in giving the general characteristics of the interaction, they fail to give correctly most of the detailed behavior observed in these experiments.

([2]) A. E. IGNATENKO: *Proceedings of the CERN Symposium* (CERN Organization for Nuclear Research, Geneva, 1956), Vol. **2**, p. 313. A review of Russian work.

([3]) H. BYFIELD, J. KESSLER and L. LEDERMAN: *Phys. Rev.*, **86**, 17 (1952); J. KESSLER and L. LEDERMAN: *Phys. Rev.*, **94**, 689 (1954).

([4]) P. ISAACS, A. SACHS and J. STEINBERGER: *Phys. Rev.*, **85**, 718 (1952); A. PEVSNER, J. RAINWATER, R. E. WILLIAMS and S. J. LINDENBAUM: *Phys. Rev.*, **100**, 1419 (1955); R. E. WILLIAMS, J. RAINWATER and A. PEVSNER: *Phys. Rev.*, **101**, 412 (1956); R. E. WILLIAMS, W. F. BAKER and J. RAINWATER: *Phys. Rev.*, **104**, 1695 (1956); W. F. BAKER, J. RAINWATER and E. R. WILLIAMS: *Bull. Am. Phys. Soc.*, **2**, 6 (1957).

([5]) R. M. FRANK, J. L. GAMMEL and K. M. WATSON: *Phys. Rev.*, **101**, 891 (1956).

([6]) M. H. JOHNSON: *Phys. Rev.*, **83**, 510 (1951).

([7]) K. A. BRUECKNER, R. SERBER and K. M. WATSON: *Phys. Rev.*, **84**, 258 (1951).

([8]) R. BIVINS, N. METROPOLIS, M. STORM, A. TURKEVICH, J. M. MILLER and G. FRIEDLANDER: *Bull. Am. Phys. Soc.*, **2**, 63 (1957).

([9]) T. FUJII: to be published. The writer is indebted to Mr. FUJII for the use of his results before publication.

2743

2. – Energy sensiti e detectors.

A Čerenkov counter was used as an energy sensitive counter (ESC) by pulse height analyzing its output ([10]). If the entire range over which a pion can produce Čerenkov light be within the radiator of the counter, more light is produced with increasing energy because of the longer path as well as because of the increased radiation from the greater velocity. Because the Čerenkov counter counts only charged particles whose velocity is greater than the velocity of light in the radiator material, it rejects nucleonic background. When used with a pulse height analyzer, the Čerenkov counter has the additional advantage of simultaneously recording events over the entire part of the energy spectrum for which Čerenkov light is produced. The disadvantages of the Čerenkov counter include small light output, causing a noise problem; a pulse height spectrum that is not simply related to the energy spectrum; and instrumental complexity. In spite of these difficulties, energy resolution on the order of ± 7 MeV was obtained over the energy range of $115 \div 150$ MeV in these experiments. A Čerenkov counter of this type is limited at low energies where little or no Čerenkov light is produced, and loses its energy sensitivity at high energies because the range over which a pion can produce Čerenkov light becomes longer than the radiator.

In the energy range below the Čerenkov threshold, a scintillation counter was used by pulse height analyzing its output. Energy resolution of $\pm 15 \div 20$ MeV was obtained. The scintillator does not share the ability of the Čerenkov counter to discriminate pions over nucleonic background, but since the light output is much larger the noise problem is not severe. When used with negative pions, the scintillator light output varies widely from pion to pion because charged star products following pion capture after the pions come to rest contribute to the total light output. For this reason the scintillator should be much easier to use with positive pions, for which this type of capture does not occur. Both the Čerenkov and scintillation counters have high counting efficiencies.

In contrast, the type of detector used by RAINWATER *et al.* ([4]) uses two scintillation counters with sufficient absorber between them to accept only pions with energy near that of the incident beam. This method has the advantage of simplicity, but straggling limits the accuracy of energy determination, and absorption and scattering in the absorber limit the counting efficiency. RAINWATER *et al.* ([4]) report energy resolution of $\pm 15 \div 20$ MeV for 80 MeV

([10]) J. R. WINCKLER, E. N. MITCHELL, K. A. ANDERSON and L. PETERSON: *Phys. Rev.*, **98**, 1411 (1955).

pions. The energy resolution of a detector of this type must be limited to obtain a satisfactory counting efficiency. At higher energies, poorer energy resolution is expected because of the additional range straggling. By using a third counter in anticoincidence behind the second counter, this method can be extended to energies below that of elastic scattering. A modification of the method using two counters with absorber between them is the method which demands a coincidence with the muon from decay of a pion brought to rest in the second counter ([11]). This method is not applicable to the counting of negative pions because of capture processes. An alternative possibility would be a magnetic spectrometer. It has the advantage of measuring the differential energy spectrum directly, both for elastic and inelastic scattering. The use of an existing magnet was considered which was estimated to have an energy resolution of $\pm$ 8 MeV at 150 MeV with a solid angle of 0.014 steradian. This solid angle is much smaller than that obtainable with counters, and would require much more intense pion beams to compete with the Čerenkov and scintillation counters with a pulse height analyzer. In principle the magnetic spectrometer affords the best energy resolution for studying elastic scattering with high angular definition, but it is not as well suited to the measurements of energy spectra for the inelastic scattering. The magnetic spectrometer and absorber counter methods might be extended to measure an entire energy spectrum simultaneously, but the instrumentation required is as complex as that for the pulse height analysis (PHA) method.

In these experiments the PHA method was used. The number of counts in a PHA channel represents an integral over energy of the unknown energy spectrum multiplied by the probability that a pion of given energy will produce a pulse in that channel. It is necessary to unfold the PHA's to give the required energy spectrum. Because of the width of the probability function, poor statistical use is made of the counts in the determination of energy spectra. The probability function, or calibration, is determined by making a PHA of the ESC output with monoenergetic beams at each of several different energies. The calibration includes the effects of straggling and absorption of the pions, statistics of the photoelectrons, and charged star products in the scintillator.

The ESC's had tapered sensitive elements to improve the light collection by internal reflection. The amount of taper was determined by the area of target illumination and the distance from the target at which the counter was to be operated. A pair of scintillation counters was mounted with the ESC to define the solid angle and to produce a gating pulse for the pulse height analyzer. For the Čerenkov ESC's, the radiators were made as long as the

([11]) See, for example, W. Imhof: *University of California Radiation Laboratory Report UCRL-3833* (1956).

range over which a 150 MeV pion can produce Čerenkov light. Measurements at various angles were made by moving the ESC.

At forward angles, the tapered lucite counter, which had a cast lucite Čerenkov radiator 18 inches long tapering from 2 inches to 5 inches, was used. A 5 inch DuMont photomultiplier (Type 6364) was fitted to the larger end. This counter was operated 24 inches from the target and had a solid angle of 0.0055 steradian with an angular half width of 3°.

For scattering beyond 45° a larger counter, which had an angular half width of 11° and a solid angle of 0.12 steradian when operated 14 inches away from the target, was used (Fig. 1). The sensitive element of this counter was

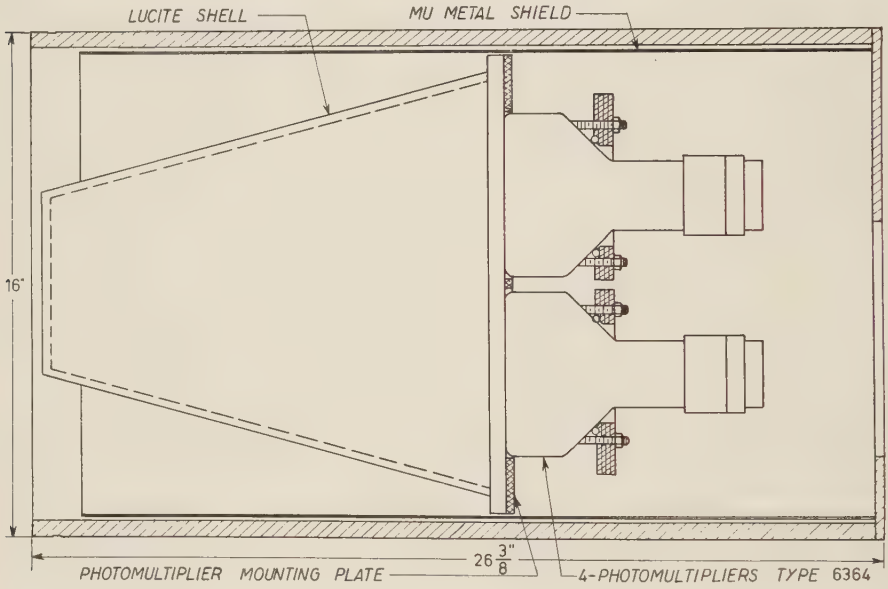

Fig. 1. – Large liquid counter.

17 liters of liquid contained in a lucite shell 14 inches long and tapering from $5\frac{7}{8}$ to $13\frac{5}{8}$ inches. The larger end was fitted with four DuMont 5 inch photomultipliers. For use as a Čerenkov counter, the shell was filled with a mixture of distilled water and 10 mg/l of light shifter, DuPont coompund MDD 3169 ([12]). For use as a scintillator, the shell was filled with a mixture of phenylcyclohexane with 3 g/l of PBD ([13]). This counter is referred to hereafter as the « liquid Čerenkov » or the « scintillator » according to its filling.

([12]) E. Heiberg and J. Marshall: *Rev. Sci. Instr.*, **27**, 618 (1956).

([13]) F. N. Hayes, D. G. Ott, V. N. Kerr and B. S. Rogers: *Nucleonics*, **13**, No. 12, 38 (1955); F. N. Hayes, D. G. Ott and V. N. Kerr: *Nucleonics*, **14**, No. 1, 42 (1956).

3. – Experimental arrangement.

The meson beam produced by the cyclotron was brought through a strong focus lens and the rotary shield to the experimental area, where it was deflected by a wedge magnet to select a beam of (150 ± 6) MeV negative pions ([14]) (Fig. 2). The pion beam had an intensity of $5 \cdot 10^5$ per minute time

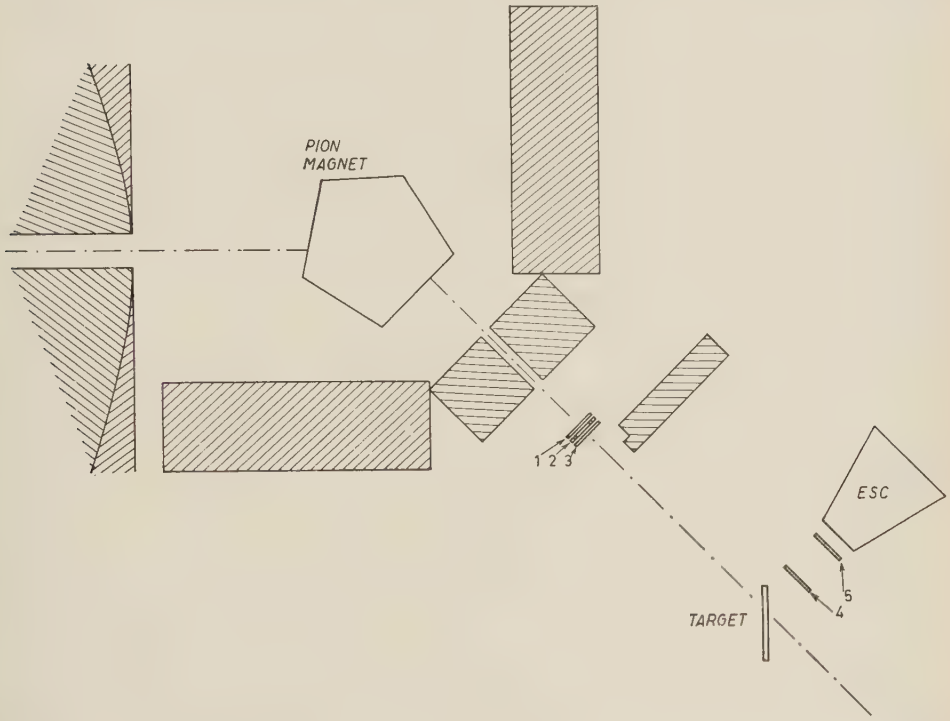

Fig. 2. – Experimental arrangement. The sandwich of beam monitoring counters is 1, 2 and 3. ESC is the energy sensitive counter. The gating counters mounted with the ESC are 4 and 5. Shielding is shaded.

average with a duty factor of 180. Muons and electrons contaminated the beam by (8 ± 1) percent. The beam was circular in profile with a radial dependence which was roughly Gaussian with a $1/e$ radius of 1 inch and angular spreads of $+1°$ vertically and horizontally. The incident pions were estimated to have an rms energy spread of 3 MeV. Lower energy beams for the calibration of the energy sensitive counters were obtained from the 150 MeV beam by

([14]) S. Warshaw and S. C. Wright: to be published.

the use of absorbers. For this purpose, the absorbers were placed between the cyclotron and the wedge magnet, so that the magnet would remove muons from the incident beam and would reduce the energy broadening by range straggling in the absorber.

The incident beam was monitored by a sandwich of three scintillation counters, one of which used spots of scintillator to cover about 1/12 of the beam area to reduce the counting rate to allow reliable scaling. The partial counter was not included in the multiple coincidences for gating purposes. The coincidence circuits used where similar to those described by ANDERSON *et al.* ([15]) as modified by DAVIDON and FRANK ([16]).

Pulses from the energy sensitive counters (ESC's) were stretched at the counters, then amplified in linear amplifiers and sent to a 100 channel pulse height analyzer ([17]). This pulse height analyzer will accept pulses approximately 400 microseconds apart, so will accept only one pulse per cyclotron beam burst. It has a quoted stability of 0.1 percent. The circuits used in the pulse height analyzer are of standard design and need pulses of about 1 microsecond length, and amplified to about a 100 volt peak level. The pulse height analyzer can be gated to accept pulses in coincidence with other counters. The analyzer was gated by a fast quadruple coincidence ($\sim 2 \cdot 10^{-8}$ s) of two counters in the beam monitoring sandwich and the two gating counters mounted with the ESC's. The quadruple counts were recorded, as were the quintuples resulting from a fast coincidence of the quadruples with a clipped output of the ESC. The quadruples count records the sum of the elastic and inelastic scattering.

The angles at which each ESC was used and the average counting rates with the various targets are given in Table I. The counting rates refer to the quintuples count which differs slightly from the total count in the pulse height analyzer because of accidental counts in the analyzer and different threshold levels for the analyzer and the quintuples coincidence circuits. Each time an ESC was set up at an angle, pulse height analysis (PHA) runs were made with the carbon and lead targets, and a PHA run was made with no target. The target-in target-out difference was attributed to scattering from the target. Each time the angle was changed, the ESC was returned to the in-line position to check drifts in the PHA calibration before setting up a new angle. All angular measurements were repeated to check the consistency of the data. The various angles were set up to $\pm 1°$. To estimate the accidentals in the PHA, the PHA of the ungated singles of the liquid ESC with the cyclotron

---

([15]) H. L. ANDERSON, M. GLICKSMAN and R. L. MARTIN: *Proceedings of the National Electronics Conference*, **9**, 483 (1953).

([16]) W. DAVIDON and R. FRANK: *Rev. Sci. Instr.*, **27**, 15 (1956).

([17]) Model PA-3; Pacific Electro-Nuclear Company, Culver City, California.

TABLE I. – *Counting rates (counts per minute, time average).*

Counter angle		Target				
(Note (1))	(deg)	1 in. C	½ in. C	¼ in. Pb	⅛ in. Pb	None
T. L.	18.5	146	91	252	115	27
T. L.	24	97	58	76	37	12
T. L.	31	56	28	29	15	4.3
T. L.	36.5	28	15	14	6.3	2.2
T. L.	44	13	6.4	6.9	3.6	0.75
Ck.	45	230	127	100	41	4.3
Ck.	60	46	24	42	—	0.34
Ck.	75	30	20	20	7.5	0.25
Ck.	90	41	22	24	—	0.35
Ck.	115	33	11	10	5.1	0.34
Ck.	138	22	11	8.7	5.3	0.22
Sc.	45	266	—	113	—	6.9
Sc.	90	185	—	67	—	1.3
Sc.	138	200	—	100	—	2.5

(1) T. L. = Tapered lucite counter; Ck. = Liquid Čerenkov counter; Sc. = Liquid scintillation counter.

beam on was run at each angle. Checks on the voltages of the photomultipliers and on the gain of the amplifier system through the pulse height analyzer were run each time an angle setup was made.

A transmission measurement was made to determine the attenuation cross-sections for both carbon and lead. The mean half angle subtended by the transmission counter at the target was 25°. The integrated elastic cross-section was subtracted from the attenuation cross-section to determine the total cross-section for inelastic processes. By subtracting the integrated cross-section determined from the quadruples counts from the attenuation cross-section, the sum of the absorption and charge exchange cross-sections was determined.

4. – Pulse height analyses.

Typical calibration curves for the liquid Čerenkov counter are shown in Fig. 3. The experimental points of a typical run are shown compared to one of the curves. The errors shown are due to counting statistics alone. The broad peak is interpreted as the distribution of pulse heights arising from the statistics on the photoelectrons and straggling at the end of the range over

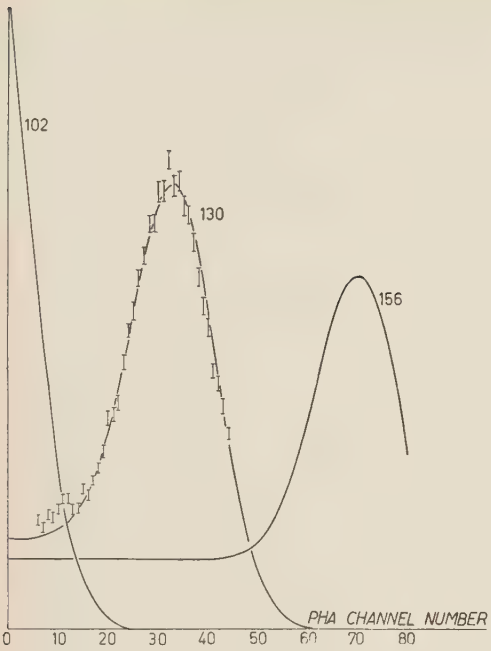

Fig. 3. – Smoothed calibrations for liquid Čerenkov energy sensitive counter. Number of counts per channel vs. channel of the pulse height analysis, for 3 different monoenergetic pion beams at 102, 130, and 156 MeV. An experimental calibration at 130 MeV is shown for comparison.

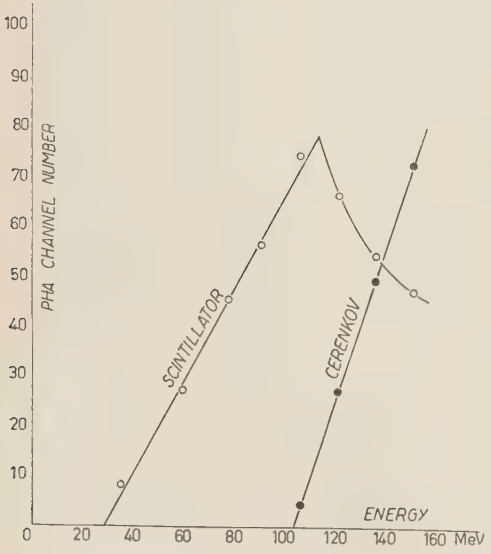

Fig. 4. – Channel of the pulse height analysis in which the peak of the calibrations appears for various energies of monoenergetic calibration beams, for the scintillation counter and liquid Čerenkov counter.

which the pions can produce Čerenkov light. A long tail extending toward the smaller pulses is presumed to arise from the nuclear encounters of some of the pions before they reach the end of the Čerenkov range. From the width of the peak, it is inferred that 100 to 200 photoelectrons are collected for a pulse at 150 MeV. About 270 photoelectrons were expected assuming 0.1 probability per quantum to produce a photoelectron and 0.5 light collection efficiency. The channel of the pulse height analysis (PHA) in which the peak appears is very nearly a linear function of the energy (Fig. 4). The shape of the PHA's at various energies is very similar if expressed as a function of the channel relative to the peak. The Čerenkov counter is assumed to produce a pulse for every pion which enters it, so its efficiency at any given energy is the probability that the pulse falls within the range of the PHA. The gating counters mounted with the energy sensitive counters (ESC's) served to assure that most of the pions would not escape through the side walls of the counter; this was borne out in the off center beam tests of the counters. The contri-

bution of muons to the calibration curve is a separate peak of larger pulses which has been removed from Fig. 3. The calibration curves for the two Čerenkov counters are quite similar, so only those for the liquid Čerenkov are shown.

For energies at which a pion stops within the scintillator (less than 107 MeV), the calibration curves from the energy sensitive liquid scintillator are quite similar to those of the Čerenkov, except for a shoulder on the large pulse side of the peak (Fig. 5). This shoulder is interpreted as arising from charged star products from pion capture in the scintillator material. The scintillator calibrations are not much narrower than those of the Čerenkov in spite of the greater light collection, because of straggling and the energy width of the calibrating beams. For these energies, the channel of the PHA in which the peak appears is very nearly a linear function of the energy (Fig. 4). The curve does not extend to the origin because a pion must have sufficient energy to traverse the gating counters and the front wall of the liquid counter before it can reach the scintillator fluid, and because of the threshold operation in the pulse height analyzer. A break in the curve of the channel of the peak as a function of energy appears at higher energies, where a pion can travel all the way through the scintillator. The amount of light produced then decreases with increasing energy, because of the smaller ionization of the more energetic particles. The characteristic shoulder on the large pulse side of the peak diminishes with increasing energy because the capture and resultant star formation are reduced. This shoulder is not noticeable at 150 MeV. Because the energy analysis cannot separate the contributions of energies above and below the knee, the contribution of the energies above the knee must be subtracted. For this purpose, data from the Čerenkov counter runs were used in conjunction with the calibrations run on the scintillator at these higher energies.

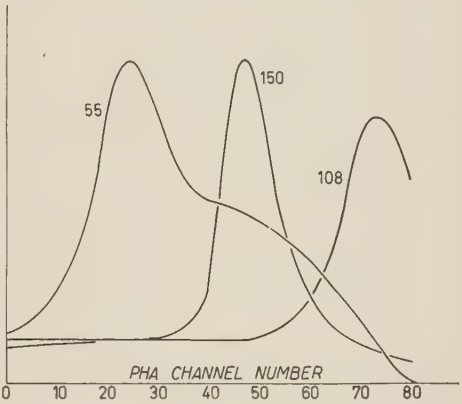

Fig. 5. – Calibrations for liquid scintillation energy sensitive counter for 3 different monoenergetic pion beams at 55, 150, and 108 MeV. At 150 MeV, pions travel all the way through the scintillating material without stopping.

Both of these energy sensitive counters had a drift in the channel in which the peak of the calibration appeared at a given energy. The drift was probably a gain drift in the photomultipliers. For the purposes of this experiment, the effect was corrected by taking frequent calibration runs and recording the position of the peaks at any given time. This record made it possible to deter-

mine the energy belonging to any particular channel of the PHA to within $1 \div 2$ MeV at any time during the runs.

Fig. 6 shows typical PHA's which had to be energy analyzed to give the plots of cross-sections as a function of energy. The actual PHA is not a smooth curve as shown, but consists of a point at each channel number with random variations due to counting statistics in each. The curves shown were drawn through the middle of the spread of these points. Most of the sharp rise toward the low end of the PHA for carbon at 90° in the Čerenkov counter is due to accidental counts. An energy analysis of these accidentals was made by subjecting a PHA of ungated singles in the pulse height analyzer to the same energy analyzing process as was used on the angular data. Ninety percent of the ungated singles from the liquid Čerenkov counter appeared in the energy analysis at around 102 MeV, the lowest energy tabulated. Because of the large fraction of accidental counts present, the lowest energy values from the liquid Čerenkov counter beyond 60° are not regarded as reliable.

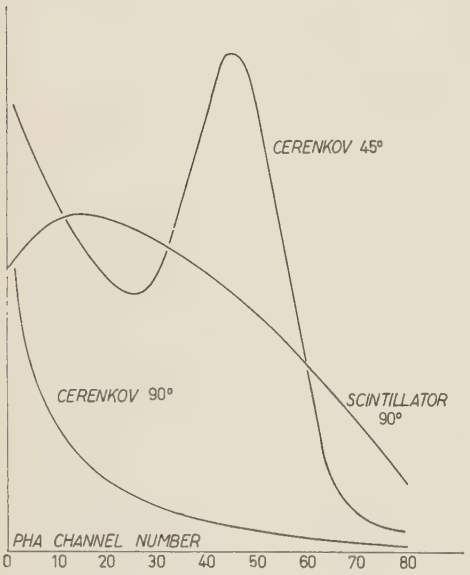

Fig. 6. – Pulse height analyses run with a carbon target at 45° and 90° with the liquid Čerenkov counter, and at 90° with the liquid scintillation counter.

5. – Energy analysis process.

The results which are required of the energy sensitive counter (ESC) are the number of events occurring at some energy E. The energy analysis (EA) process described takes a pulse height analysis (PHA) run at a given angle with a given target and converts it into an energy spectrum at that angle. The least squares method used cannot produce a continuous spectrum, but gives a histogram of the number of events, a_j, associated with each of several energies, E_j.

The ESC sees a « true » number of counts, m_ν (in the statistical sense), in channel ν of the PHA. The actual number of counts in channel ν, M_ν, approximates to m_ν, and is assumed to differ only because of the finite sampling. M_ν is accordingly Poisson distributed about m_ν, and the limit in which M_ν can be treated as normally distributed is considered. If necessary, channels of the PHA are grouped to assure that M_ν can be treated as normally

distributed. Averaging over the energy dependences of the cross-sections as smeared out by the energy changes of a pion within the target and considering only single encounters, m_ν is given by:

$$m_\nu = \int \mathrm{d}E\, K_\nu(E) \int_{\text{Target}} \mathrm{d}V\, N(\boldsymbol{x})\, I(\boldsymbol{x}) \int_{\text{Counter}} \mathrm{d}A\, \frac{\cos\delta}{r^2}\, \frac{\mathrm{d}^2\sigma}{\mathrm{d}\Omega\,\mathrm{d}E} = \int \mathrm{d}E\, K_\nu(E)\, q(E)\,,$$

where E is the energy at which the pion leaves the target, $N(\boldsymbol{x})$ is the number of scattering centers per cm³ in the target at position $\boldsymbol{x}$, $I(\boldsymbol{x})$ is the number of pions per cm² at position $\boldsymbol{x}$ integrated over the time of the run, $\boldsymbol{r}$ is the vector from the volume element $\mathrm{d}V$ at $\boldsymbol{x}$ in the target to the element of area $\mathrm{d}A$ on the counter, $\cos\delta$ is the cosine of the angle formed by $\boldsymbol{r}$ and the normal to $\mathrm{d}A$, $K_\nu(E)$ is the probability that a pion of energy E will produce a pulse in channel ν of the pulse height analyzer, and $\mathrm{d}^2\sigma/\mathrm{d}\Omega\,\mathrm{d}E$ is the cross-section sought. There is a similar equation for each channel of the PHA, so the problem is to find a solution, $\mathrm{d}^2\sigma/\mathrm{d}\Omega\,\mathrm{d}E$, which is consistent with a large number of equations. The volume and area integrations reduce in lowest order to

$$q(E) = A(\theta)\, T_{123}\, \frac{\mathrm{d}^2\sigma}{\mathrm{d}\Omega\,\mathrm{d}E}\,,$$

where $A(\theta)$ is the coefficient resulting from the evaluation of the integral and T_{123} is the corrected number of monitor counts. $A(\theta)$ includes the corrections arising from turning the target to half the angle of the counter and other corrections listed in detail in Sect. 6.

To calibrate the counter, $q(E)$ is replaced by a spectrum which is non-zero only in some small region near E_j

$$m_\nu \approx K_\nu(E_j)\, q(E)\, \Delta E\,; \qquad K_\nu(E_j) \approx \frac{M_\nu}{q(E)\,\Delta E} = A_{\nu j}\,.$$

The use of different energies E_j results in a (non-square) matrix $A_{\nu j}$ which approximates to the set of continuous functions $K_\nu(E)$. The $A_{\nu j}$ are referred to as calibrations. Each ESC has its own set of calibrations.

For the measurements runs, an approximate solution can be obtained in the form

$$m_\nu \approx \sum_j A_{\nu j}\, q(E_j)\, \Delta E_j = \sum_j A_{\nu j}\, a_j\,.$$

The reduction to this form is immediate if the energy spectra of the $A_{\nu j}$ and the a_j are regarded as histograms with the blocks of the histogram centered at (equidistant) energies E_j. If the energy spectrum of the $A_{\nu j}$ and the a_j be regarded as « trapezoidal » (linear interpolations between the values at E_j),

there exists a non-singular linear transformation of the amplitudes which satisfies the above equation. The histogram approximation and the trapezoidal approximation thus contain equal amounts of information, so the simpler histogram approximation is used.

The actual number of counts in a channel of the pulse height analyzer, M_ν, is not exactly equal to the « true » number m_ν, so a statistical method of reduction must be used. The method used in reducing the raw data is similar to the « modified χ^2-minimum method » ([18]). The essential features of this method are the reduction of the statistical variables to mean zero and unit standard deviation, and the subsequent solution of the problem by a least-squares method. Accordingly a function

$$\chi^2 = \sum_\nu \frac{(M_\nu - m_\nu)^2}{\Delta_\nu^2} ,$$

is formed. It is assumed in this form of writing that the various channels of the PHA are independent. The Δ_ν^2 are the variances of the counts in channel ν of the PHA. Differentiating χ^2 by a_j, it is found that the solution to the problem can be written in the form

$$a_j = \sum_k (G^{-1})_{jk} C_k$$

$$C = \sum_\nu \frac{M_\nu}{\Delta_\nu^2} A_{\nu k} ;$$

$$G_{jk} = G_{kj} = \sum_\nu \frac{A_{\nu j} A_{\nu k}}{\Delta_\nu^2} .$$

The amplitudes a_j can thus be found by inverting the matrix G. The a_j so found are correlated random variables whose means are the values given and whose moment matrix is G^{-1} ([19]). This method is the same as the maximum likelihood method usually used in reducing experimental data in the limit where the data are normally distributed instead of Poisson distributed.

The measured number of counts in channel ν of the pulse height analyzer, M_ν, was taken as the difference of the target-in and target-out counts in channel ν; $M_\nu = D_\nu - B_\nu$. Δ_ν^2 was estimated as $D_\nu + B_\nu$. This estimate of Δ_ν^2 from the measured value rather than from the calculated estimate is an approximation in the method that is valid when the data are normally distributed. The approximation has the consequence that Δ_ν^2 is not dependent on the a_j and thus makes no contribution to the differentiation by a_j. This makes

([18]) H. Cramér: *Mathematical Methods of Statistics* (Princeton, 1951), Sect. 30.3.
([19]) F. Solmitz: *Notes of the Least Squares and Maximum Likelihood Methods* (unpublished).

the algebraic process linear and is the feature that makes the method similar to the « modified χ^2-minimum method ». Measurement errors in the $A_{\nu j}$ are not included in estimating Δ_ν^2.

The value of χ^2 can be obtained by observing that

$$\chi^2 = \sum_\nu \frac{M_\nu^2}{\Delta_\nu^2} - \sum_j a_j C_j .$$

This provides a check on the calculations.

The problem must be completely redone for each target and angle because the matrix G is different for each set of data.

This problem has been coded for the AVIDAC electronic computer at the Argonne National Laboratory. The AVIDAC was given the $A_{\nu j}$, the D_ν, and B_ν; it then calculated the matrix G, inverted G, checked the inversion, calculated C_j and evaluated a_j and $\sum_\nu M_\nu^2/\Delta_\nu^2$ from which the χ^2 estimates were made.

The errors quoted on a_j from the energy analysis are the square roots of the diagonal elements of the moment matrix and have the following meaning: If one of the elements a_j be changed by the amount indicated, *and* the corresponding changes induced by the correlations be made in the remaining elements, the value of χ^2 will be increased by one. Any other combination of changes in the elements of a_j will cause more rapid changes in χ^2.

In some cases, the pulse height analysis had other components added to the count in channel ν. Examples arose with 1) accidental counts in the Čerenkov counter; 2) protons in the scattered pion beams counted by the scintillator; 3) electrons from converted γ-rays from the decay in the target of charge exchange π^0's; and 4) the scintillator where the higher energies produced PHA's which could not be analyzed directly because of their similarity to the lower energy components. The subtraction process described here was used to obtain the corrected EA's in these cases. In each case the argument is formally the same, so it is given for the case of the scintillator subtractions only. The integral over energy is broken into two parts, above and below the knee of the channel of the peak vs. energy curve (Fig. 4). Each integral can then be replaced by a sum as before, with the result

$$m_\nu = \sum_j A_{\nu j} a_j + \sum_k P_{\nu k} p_k ,$$

where the P's and p's mean the same thing as the A's and a's, but refer to energies above 107 MeV. The p_k are known amplitudes determined from the Čerenkov energy analysis of the same target at the same angle. Let $P_{\nu k}$ be represented as

$$P_{\nu k} = \sum_j A_{\nu j} S_{jk} ,$$

by an EA process identical to that used for the a_j previously, so

$$m_\nu = \sum_j A_{\nu j}(a_j + \sum_k S_{jk} p_k) .$$

There are now correlations between the various channels of the PHA which are induced by the determination of the subtraction amplitudes. The form for the problem is

$$\chi^2 = \sum_{\mu,\nu} H_{\mu\nu}[M_\mu - m_\mu][M_\nu - m_\nu] ,$$

where $(H^{-1})_{\mu\nu} = \Delta_\nu^2 \delta_{\mu\nu} + \Gamma_{\mu\nu}$ is the moment matrix of $[M_\mu - m_\mu]$; Δ_ν^2 is the (diagonal) moment matrix of the measured values, M_ν; $\Gamma_{\mu\nu} = \sum_{j,k} P_{\mu j} P_{\nu k} \Delta p_j \Delta p_k$; and $\Delta p_j \Delta p_k$ is given by the moment matrix of the energy analysis of Čerenkov data which yields the p_k. By direct evaluation some of the larger elements of $\Gamma_{\mu\nu}$ were 1-2; while some of the smaller off-diagonal elements ran down to 0.1 or less. All elements evaluated were positive. Since the Δ_ν^2 were around 200 for these same places, the $\Gamma_{\mu\nu}$ were ignored by comparison. The weighting for the various channels is thus that given directly by the measurements, so the same EA routine can be used whether or not the subtractions are present. The subtraction is then done in the EA, energy-by-energy. For the application to the scintillator subtraction process, the Čerenkov data must be multiplied by the ratio of the energy intervals between the energies of the scintillator EA to those of the Čerenkov EA.

In the actual EA, smoothed calibrations were used. It was found that the calibrations could be expressed as a function of the channel relative to the channel of the peak for the energy in question

$$A_{\nu j} = N_j F(\nu - \nu_j) ,$$

where N_j is a normalizing coefficient, ν is the (variable) channel of the PHA, and ν_j denotes the channel in which the peak of the pulse height distribution appears at energy E_j. For the function $F(\nu - \nu_j)$ a form suggested by the experimental calibrations was used. Thus, for the liquid Čerenkov counter, $F(\nu - \nu_j)$ was a Gaussian of 10-channel half width above and below ν_j with a constant number $\frac{1}{5}$ of the peak value added to all channels $\nu < \nu_j$. For the scintillator, $F(\nu - \nu_j)$ was tabulated from a curve obtained by smoothing the averages of calibrations for 5 different energies. A χ^2-test applied to the scintillator calibrations thus obtained indicated that on the average $F(\nu - \nu_j)$ differed from the measured values by 2 standard deviations; one standard deviation is the expected value if $F(\nu - \nu_j)$ describes the situation perfectly. This method of forming the calibrations was not used on the tapered lucite

counter where the experimental calibrations (apart from a normalization dependent upon the energy) were used directly.

6. – Calculations.

In all, some 85 energy analysis (EA) calculations were run for the three counters at the various angles with the various targets. The separate runs with the same angle, target, and energy sensitive counter (ESC) were combined where possible. In each case a plot of the 5-channel sums of the pulse height analysis (PHA) was made to verify the agreement of the broad features of the PHA before making the combination. The entire PHA for a target and angle was grouped in 5-channel sums if the raw data had fewer than 10 counts in each of several channels. Grouping was done in this way to avoid giving more weight to one part of the pulse height spectrum than to another. All the tapered lucite data were grouped into 5-channel sums because the calibrations did not seem to justify the retention of the full number of channels. Eighty channels of PHA data were retained, thus all EA's had either 80 or 16 input channels.

The nature of the PHA's to be reduced is shown in Fig. 6. Some typical EA's and moment matrices as printed out by the computer before the subtractions were made are given in Tables II to IV. These EA's are scaled to represent the actual number of pions in the various energies. The correlations, given by the off-diagonal elements of the moment matrix divided by the square

TABLE II. – *Matrix and vector for Čerenkov energy analysis for carbon target at* 90°. $\chi^2 = 67$. (Expectation is 74).

Energy	155	145	134	124	114	103
Vector	387	270	858	1468	1821	8633
Matrix	5611	— 4109	1660	— 1342	583	— 1098
		8061	— 5189	2825	— 2102	2496
			9184	— 7038	4684	— 6299
				13990	— 12283	15326
					26537	— 41041
						121119

root of the product of the two diagonal elements each connects, are quite large. Thus for calculations of derived quantities involving more than one energy, the error estimates may be quite different from those shown on the plots.

The number of energies into which the PHA can be energy analyzed is a

TABLE III. – *Matrix and vector for scintillator energy analysis into 6 energies for carbon target and 90°.* $\chi^2 = 115$.

Energy	109	95	77	61	44	28
Vector	18	2446	2758	249	5304	6031
Matrix	61730	−45410	−13740	7073	23477	−24405
		84565	−35694	−10185	−1206	13314
			96097	−50835	−17259	22574
				101275	−51486	2918
					134643	−93780
						103883

TABLE IV. – *Matrix and vector for scintillator energy analysis into 5 energies for carbon target at 90°.* $\chi^2 = 145$.

Energy	110	90	69	49	28
Vector	280	3368	2931	5334	7293
Matrix	49765	−35779	−10344	26757	−19368
		71554	−35980	−16390	23200
			76860	−43605	8653
				94912	−63014
					71448

compromise between trying to get as many energies as possible and troubles in the calculation arising from difficulty in inverting the matrices. This feature of the practical calculation places a limit on the energy resolution obtainable from the ESC's in addition to those limitations inherent in the counter itself. The matrices from full 80 channel calculations were easier to invert than those from the calculations with the 5-channel sums. There seems to be no simple criterion to determine the number of energies into which the data may be analyzed.

Neither the energy spread of the calibrating beam nor the energy broadening of the elastically scattered pions by straggling and by different path lengths through the target had any systematic effect on the energy analysis. They contributed to the uncertainty in the energy determination without affecting the amplitudes.

In the calculations of cross-section, corrections were applied for certain systematic effects. These corrections were included in the factor $A(\theta)$ of Sect. 5. A geometrical correction was applied for the different number of effective scatterers as the target was turned to bisect the angle between the beam and

the ESC. The pion decay in flight between the target and the ESC was about 4 percent for the higher energy pions. The correction for the attenuation of the incident beam in the target varied from 2 to 5 percent with the target and angle. About 2 percent of the pions going to the ESC were scattered out or absorbed in the first counter of the gating pair mounted with the ESC and did not contribute to the quadruples count. An additional 3 percent were scattered out or absorbed before entering the ESC. The muon and electron contamination of the beam was around 8 percent, while the contribution to the total count of muons Coulomb scattered by the target was less than 1 percent at all angles. The geometrical corrections for the finite size of the counter used by ANDERSON *et al.* [20] could not be applied here because it is not possible to make the assumptions about smoothness of the cross sections which can be made in the case of scattering by hydrogen. The magnitude of these corrections was estimated and found to be largest for the elastic scattering, where it was around 5 percent. The large counter size may account for the possible loss of some features of the elastic scattering, such as diffraction minima, but it was not expected to obscure the general features of the inelastic scattering.

Plural inelastic scatterings do not appear within the experimental accuracy. With lead at angles less than 30°, corrections for multiple Coulomb scattering were made by the method of MARTIN [21].

Corrections which must be applied through the use of the subtraction process described in Sect. 5 include those for spurious counts in the ESC's caused by nucleons and γ-rays from absorptions or charge exchange events. A proton must have energy near 70 MeV to record in the counter. The cross-section for production of a proton of $E > 70$ MeV by a 150 MeV negative pion is about 1/20 geometrical and is somewhat forward peaked [22-24]. Estimates of the energy spectrum of these protons indicated that almost all proton pulses in the scintillator would appear in the lowest energy of the EA. The protons made a contribution to the measured differential cross-sections at 90° of about 1 mb/sr for carbon and 10 mb/sr for lead. A correction for this was applied to the cross-sections from the quadruples counts and to the lowest energy of the scintillator EA. The neutron counts were negligible. The expected PHA of electrons from the conversion of π^0 γ-rays would energy analyze

---

[20] H. L. ANDERSON, W. DAVIDON, M. GLICKSMAN and U. E. KRUSE: *Phys. Rev.*, **100**, 279 (1955).

[21] R. L. MARTIN: *Phys. Rev.*, **87**, 1052 (1952).

[22] G. BERNARDINI, E. T. BOOTH, L. LEDERMAN and J. TINLOT: *Phys. Rev.*, **82**, 105 (1951); G. BERNARDINI, E. T. BOOTH and L. LEDERMAN: *Phys. Rev.*, **83**, 1075 (1951); G. BERNARDINI and F. LEVY: *Phys. Rev.*, **84**, 610 (1951).

[23] A. H. MORRISH: *Phys. Rev.*, **90**, 674 (1953); *Phil. Mag.*, **45**, 47 (1954).

[24] A. TURKEVICH: Private communication.

into a distribution peaking at the top energy of the Čerenkov counter. In the scintillator, the electrons would contribute to some of the lower energies. In lead the correction for the γ-rays of π^0 decay was about 5 mb/sr and in carbon the correction was negligible. These corrections, estimated from the high-energy parts of the energy analysis at backward angles, are in agreement with the corrections expected from the charge exchange cross-sections reported by LEDERMAN *et al.* [3].

Because the histogram approximation has been used in the energy analysis, the ordinates of the plots of energy dependent cross-sections are the height of a histogram block which extends 5 MeV above and below the point plotted. Where a curve is drawn through the plotted points, this curve is the locus of the top center of a histogram block.

The errors shown in the plots of energy dependent cross-sections are determined from the diagonal elements of the moment matrices and the error estimates of the coefficients for the reduction of the EA's to energy dependent cross-sections. Errors in the coefficients affect all energies in the same way and are properly represented by a moment matrix. The final moment matrix is the sum of the two. The energy dependent cross-sections in the $120 \div 150$ MeV range of the Čerenkov are correlated to those in the $60 \div 100$ MeV range of the scintillator at a given angle because of the subtraction. The values in the 60 : 100 MeV range at 45° are quite uncertain because of the large elastic scattering at this angle.

There is a negative region in the EA's of the scintillator data at 138° for both carbon and lead which probably results from a faster decrease of count with increasing PHA channel number that can be constructed with the calibrations. The best fit is obtained from the available calibrations with a large value at low energies and a negative value at higher energies to bring the counts down rapidly with increasing channel number. The experimental calibrations at very low energies ($\sim$10 MeV) had this type of rapid drop-off of count with increasing PHA channel number. A negative region thus implies that most of the pions counted were at an energy even lower than the lowest energy of the EA.

Elastic cross-sections have been determined where possible as the area under the elastic peak. Where a peak is not clear, an upper limit can be set on the amount of elastic scattering. This limit is usually quite small. In carbon at 138°, the elastic cross-section is less than about 0.5 mb/sr, while for lead at the same angle the elastic cross-section is less than about 2 mb/sr.

The cross-sections determined from the quadruples counts are not reliable at extreme forward angles ($\cos\theta \gtrsim 0.9$) because of the decay of part of the incident pion beam between the deflecting magnet and the target, which produces muons at a slight angle to the beam that can multiple scatter into the counters at forward angles. The Čerenkov counter did not respond to these

muons because of their low energy. The muon energy is low because those muons which contribute are those at the extreme angles, which come off slightly backwards to the pion motion, so have velocity less than the pion velocity and energy around 100 MeV. Order-of-magnitude estimates indicate that 10 percent of the quadruples counts at 18.5° in lead were multiply scattered muons. These muons do not affect the calculation of the absorption plus charge exchange cross-section determined by subtraction of the integrated quadruples cross-section from the attenuation cross-section, because the muons were counted by the transmission counter used in the determination of the attenuation cross-section.

7. – Monte Carlo calculations.

Quasi-elastic scattering, in which the scattering of pions by complex nuclei is described as the result of incoherent scattering by individual nucleons, can be calculated by the Monte Carlo method ([6-8-25]). Monte Carlo calculations were run on the MANIAC electronic computer at the Los Alamos Scientific Laboratory for comparison with the present experimental results, using the calculation coded by METROPOLIS *et al.* ([8]). In this calculation, the cascade developed by a pion moving through a Fermi gas of nucleons is followed in a three dimensional geometry. The pion interacts with nucleons according to the observed cross-sections for pions and free nucleons. Energy and momentum are conserved at each interaction. The Pauli principle is taken into account by requiring that the energy of the recoil nucleon be above the Fermi energy for any allowed collision. Pion absorption takes place on two nucleons. For a pion which is not absorbed, the charge, energy, and direction of the pion as it leaves the nucleus are tabulated. A large number of incident pions is followed and the tabulations predict the energy and angular distributions of the inelastically scattered pions, the amount of charge exchange scattering (and double charge exchange, which happens only rarely) and true absorption. Most of the elastic scattering is diffraction scattering or Coulomb scattering and does not appear in the Monte Carlo calculation. Elastically scattered pions which are described by the Monte Carlo calculation appear as transparencies, and emerge from the nucleus undeflected and with unchanged energy. METROPOLIS *et al.* have compared the nucleon cascades with photographic emulsion data with satisfactory agreement indicated ([8]).

In the calculations run for comparison with the present experiment, the nucleonic cascades were ignored. The cross-sections used for the pion-nucleon scattering were $\sigma(\pi^- \mathrm{P}) = (5.3 + 3.5\eta^2 + 3.2\eta^4)$ mb and $\sigma(\pi^- \mathrm{N}) = (3 + 8.75\eta^2 +$

([25]) A. MINGUZZI, G. PUPPI and A. RANZI: *Nuovo Cimento*, **11**, 697 (1954).

$+10.75\eta^4)$ mb, where η is the pion momentum in the laboratory in μc units. The angular distribution of the scattering was taken of the form $a+b\cos\theta+$

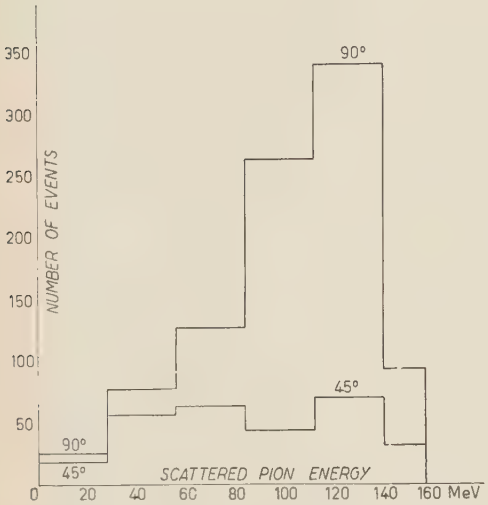

Fig. 7. – Monte Carlo calculation. Energy spectrum of negative pions scattered at 45° and at 90°. The energy of a pion scattered by a free nucleon is 137 MeV at 45° and 102 MeV at 90°.

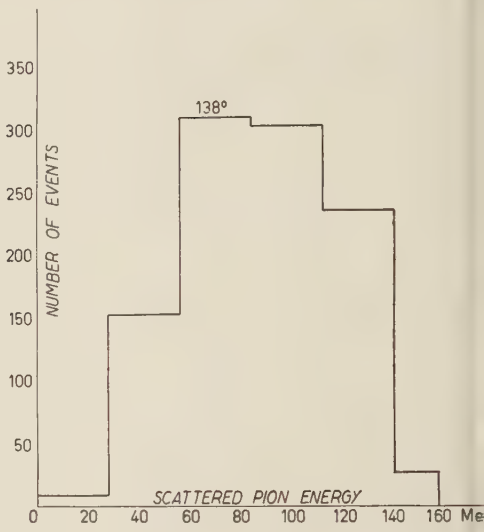

Fig. 8. – Monte Carlo calculation. Energy spectrum of pions scattered at 138°. The energy of a pion scattered by a free nucleon is 77 MeV.

$+c\cos^2\theta$, with the coefficients a, b and c parameterized to give an energy dependence in accord with the available experimental data for each of the types of elementary interaction. The nuclear radius, $r = r_0 A^{\frac{1}{3}}$, was based on $r_0 = 1.569 \cdot 10^{-13}$ cm, and the Fermi energy was taken as 23.8 MeV for both protons and neutrons in carbon. The deaths were estimated by assigning an ab-

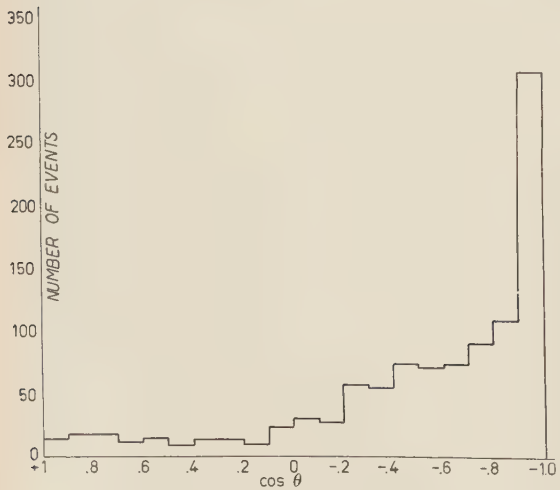

Fig. 9. – Monte Carlo calculation. Angular distribution of scattering in which a 157 MeV incident pion is scattered inelastically with final energy in the range 56÷84 MeV.

sorption cross-section to π^- P collisions according to the arguments of BRUECKNER *et al.* (7). This is expressed in the relation $\sigma_A = \Gamma\sigma_D$, where Γ is a constant determined from experiments at low energy to be about 4, and σ_D is the cross-section for the absorption of pions by the reaction $\pi^- + D = N + N$. The energy dependence of σ_A is assumed to be the same as that of σ_D. The absorption cross-section used was $(18/\eta)(0.14+\eta^2)$ mb (5). The calculations are not completely appropriate for carbon because a Fermi gas description of the nucleons is not accurate and because carbon has a small number of nucleons to treat by this type of statistical method.

The results of the calculations for carbon, which refer to 11390 incident 157 MeV negative pions and to 4200 inelastically scattered negative pions, are summarized in Figs. 7, 8 and 9. The results for lead are the same to within the statistical accuracy to which the calculations were carried.

Figs. 7 and 8 give the energy spectrum in an angular interval which corresponds to the width of the large liquid counter at 45°, 90° and at 138°. The scattering at 45° is depressed because of the Pauli principle. The scattered pions of the Monte Carlo calculation are broadly peaked about the energy of a pion scattered at the same laboratory angle by a free nucleon. The peaking at this energy indicates that most of the scattering proceeded by a single pion-nucleon encounter. The broadening of the peak is a consequence of the Fermi energy of the nucleons in the nucleus. A different momentum distribution would alter the shape of the peak but would not change the energy of the peak very much. The predominance of single encounters is probably a consequence of the Pauli principle (6) and of the smaller pion-nucleon cross-sections at lower energy (1).

The angular distribution of the scattering in the energy interval $56 \div 84$ MeV is shown in Fig. 9. The scattering is preferentially backward. Scattering in this energy interval is typical of that at most energies.

8. – Results.

The energy dependent differential cross-sections, $d^2\sigma/d\Omega\, dE$, for scattering from carbon at several angles are shown in Figs. 10, 11, 12 and 13. Fig. 10, which gives the data at 18.5°, is typical of the scattering from carbon at forward angles as measured with the tapered lucite counter. In Fig. 10, the energies on the half thickness target points are corrected for the difference in ionization losses between the full thickness and half thickness targets. The elastic scattering forms a distinct peak whose width is indicative of the counter resolution. The low sub-peak at 100 MeV shown in Fig. 10 persists through all angles to 45°, but its ratio to the elastic scattering changes by a factor four. Thus, it is unlikely that the lower energy peak is due to some instrumental

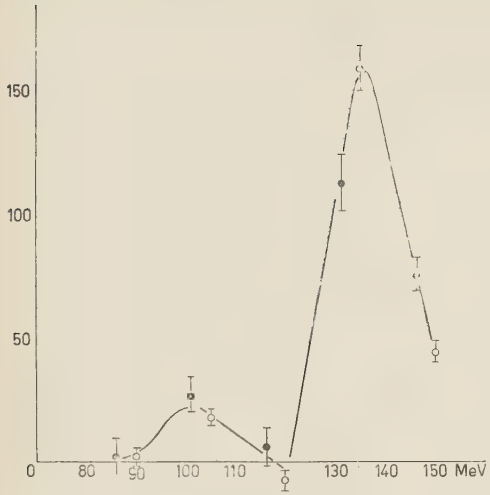

Fig. 10. – Energy analysis of scattering from carbon at 18.5° as measured on the tapered lucite counter. Ordinates in (mb/sr) 10 MeV. Open circles are full thickness target points; closed circles are half thickness target points. Elastic energy is 138 MeV.

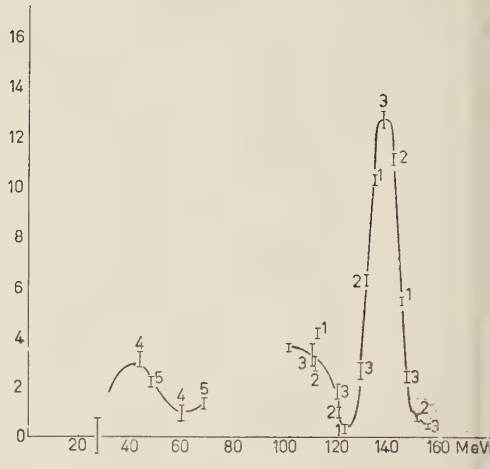

Fig. 11. – Energy analysis of scattering from carbon at 45°, as measured with the liquid Čerenkov and liquid scintillation counters. Points numbered 1, 2 and 3 are different sets of data run with the liquid Čerenkov counter. Points numbered 4 and 5 are the scintillator data analyzed into 6 and 5 energies respectively. The ordinate is (mb/sr)·10 MeV.

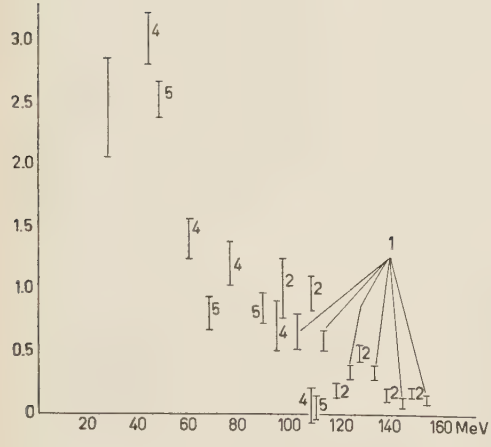

Fig. 12. – Energy analysis of scattering from carbon at 90° as measured with the liquid Čerenkov and liquid scintillation counters. Ordinates and points as in Fig. 11, except points numbered 2 are half thickness target points.

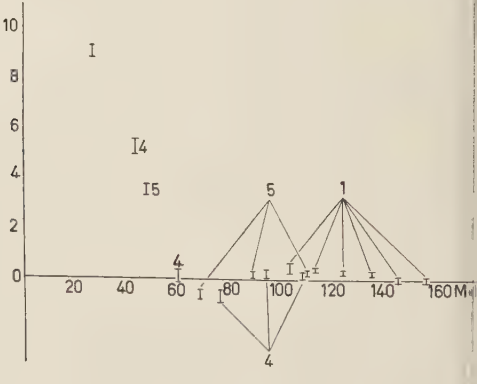

Fig. 13. – Energy analysis of scattering from carbon at 138°. Ordinates and points as in Fig. 12.

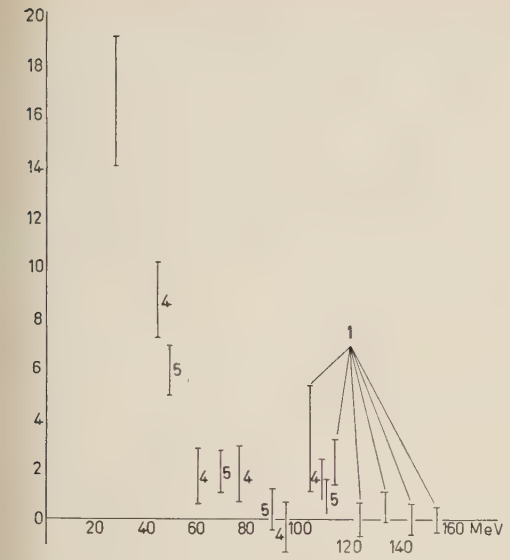

Fig. 14. – Energy analysis of scattering from lead at 90°. Description as in Fig. 11.

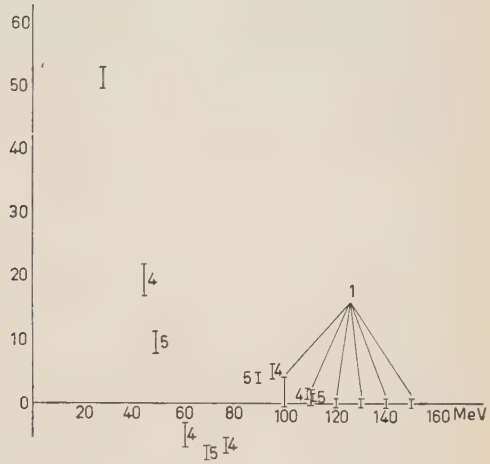

Fig. 15. – Energy analysis of scattering from lead at 138°. Description as in Fig. 11.

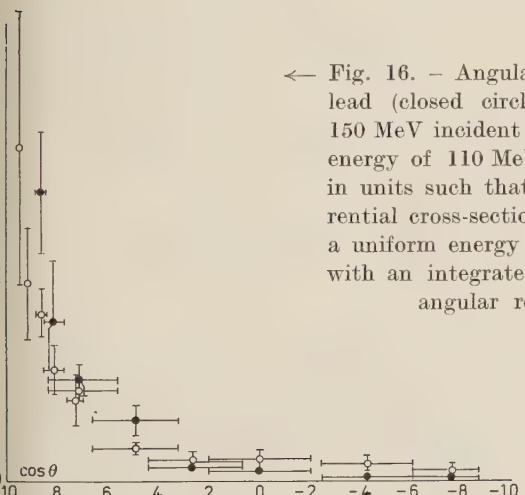

← Fig. 16. – Angular distribution of inelastic scattering from lead (closed circles) and carbon (open circles) in which a 150 MeV incident pion is scattered inelastically with a final energy of 110 MeV. The ordinate, $d^2\sigma/d\Omega\,dE$, is expressed in units such that a value of 1 is the energy dependent differential cross-section of an isotropic angular distribution and a uniform energy distribution from 0 to the full elastic energy with an integrated cross-section equal to the geometric. The angular resolution of the counter is shown.

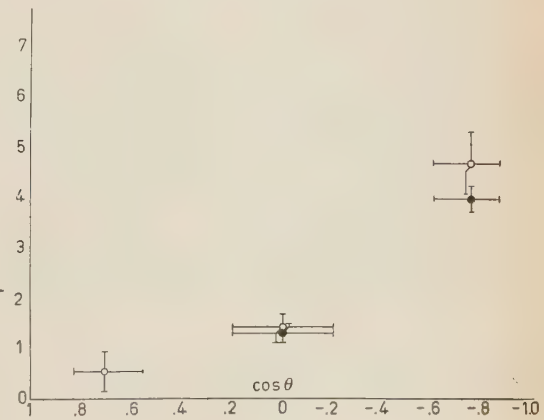

→ Fig. 17. – Angular distribution of inelastic scattering from lead and carbon in which a 150 MeV incident pion is scattered inelastically with final energy of 30 MeV. Description as in Fig. 16.

difficulty or a property of the calculation. No multiple scattering effects are noticeable at 18.5° for carbon. Figs. 11, 12 and 13 combine the scintillator data with the liquid Čerenkov counter data to extend the energy analysis down to 30 MeV. The form of the Čerenkov data has the same features as in Fig. 10, but there is a rapid decrease of the elastic scattering with increasing angle, until at 90° and beyond, no elastic scattering is observed above the instrumental background.

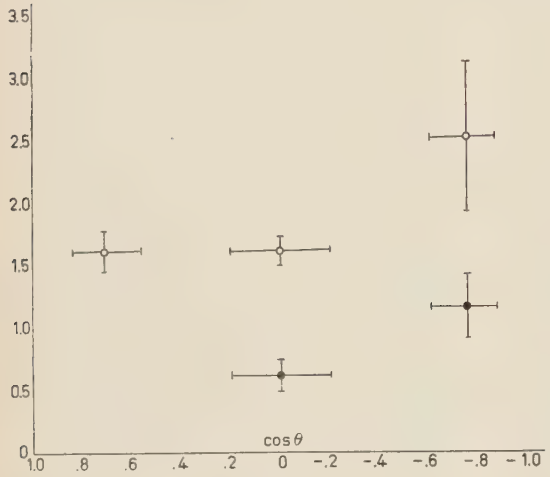

Fig. 18.

The energy dependent differential cross-sections, $d^2\sigma/d\Omega\, dE$, for scattering from lead at 90° and 138° are shown in Figs. 14 and 15. No elastic scattering is observed above the instrumental background.

There is some inelastic scattering in the energy range of the Čerenkov counters at forward angles (Fig. 16) and considerable very low energy scattering in the backwards directions (Figs. 17 and 18). The measured energy spectrum of the pions inelastically scattered from carbon (Figs. 11, 12 and 13) may be compared with the predictions of the Monte Carlo calculations (Figs. 7 and 8), which refer to the same scattering angles. The measured energy of the pions inelastically scattered backwards is about 40 MeV below that predicted by the Monte Carlo calculations. It is interesting to note that the inelastic forward scattering detected by the Čerenkov counters lies about 40 MeV below the energy of a pion scattered from a free nucleon, which is about the same interval by which the backward inelastic scattering is below the pion nucleon scattering at those angles. The general features of the strongly inelastic scattering are the same in carbon and lead, although the inelastic scattering from lead seems to be at a slightly lower energy. This energy difference is probably due to the Coulomb field. Thus it is likely that the inelastic scattering described here is a property of most complex nuclei.

It has been noted in connection with previous experiments ([2,3,26]) that the energy of inelastically scattered pions was considerably below the energy of

([26]) M. Blau and M. Caulton: *Phys. Rev.*, **96**, 150 (1954).

a pion scattered by a free nucleon, which led to the suggestion that the pion may have experienced more than one collision in the nucleus. This experiment indicates that the inelastically scattered pions emerging from nuclei have even lower energy than has been previously reported. However, the Monte Carlo calculations at 150 MeV indicate that events in which the pion suffers more than one collision before leaving the nucleus are improbable. The experimental disagreement with the predictions of the quasi elastic scattering model as

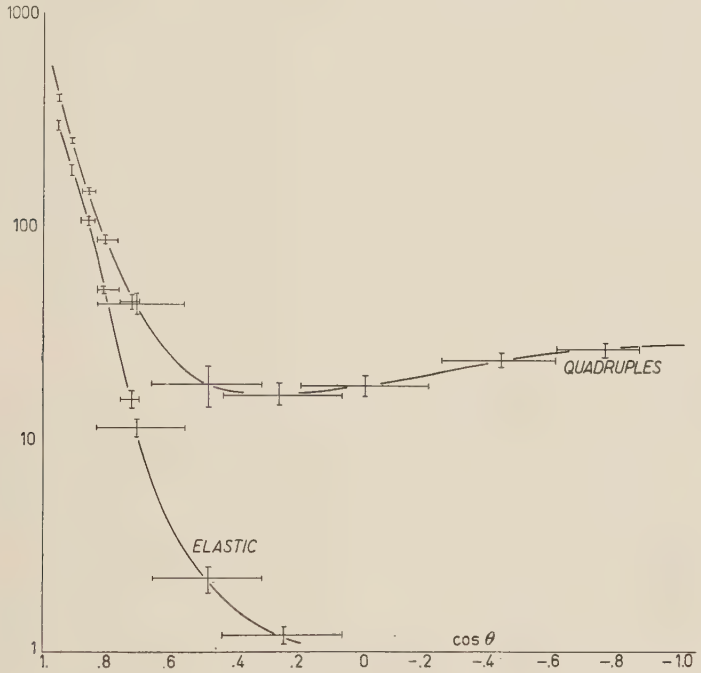

Fig. 19.

worked out in the Monte Carlo calculations is in contrast to the results of the inelastic scattering of protons and electrons ([27,28]) in which the energy of the inelastically scattered particles can be explained by the quasi elastic scattering model. The Monte Carlo calculation does not include many body forces or a potential, either of which may have a significant effect on the scattering. Because of the short mean free path for pions in nuclear matter at this energy, the conditions at the nuclear surface are expected to be important. These may differ from the average conditions within the nucleus which are used in the Monte Carlo calculation.

([27]) J. M. Wilcox and B. J. Moyer: *Phys. Rev.*, **99**, 875 (1955).
([28]) R. Hofstadter: *Rev. Mod. Phys.*, **28**, 214 (1956).

The quadruples cross-section includes the scattered pions at all energies above 15 MeV. The angular distribution of the quadruples cross-section (Fig. 19 and 20) shows a slight backward rise, a forward peak due to Coulomb and diffraction scattering, and a broad minimum in the $60° \div 90°$ region. The quadruples differential cross-sections agree favorably with the sum of the elastic and inelastic differential cross-sections as given by KESSLER and LEDERMAN [3] at 125 MeV, but are almost double the values given by the Russian

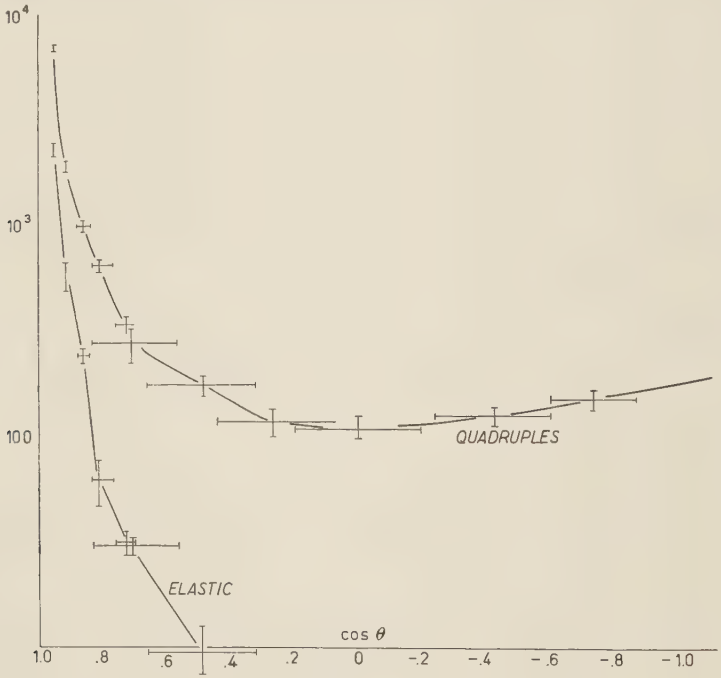

Fig. 20.

cloud chamber group [2]. The comparison with the Russian data thus indicates that the total scattering cross-section decreases by about a factor two between 150 and 240 MeV, in rough agreement with the cross-sections for pion-nucleon scattering. This feature is in rough agreement with the trends of transmission experiments at higher energies [2], and lends support to the quasi elastic scattering model.

The total cross-sections determined in this experiment are tabulated in Table V. The geometric cross-sections given use $\sigma_{ge} = \pi r_0^2 A^{\frac{2}{3}}$, with r_0 equal to a pion Compton wave length, and include the Coulomb correction for negative pions [29]. The errors listed are standard deviations.

[29] R. M. STERNHEIMER: *Phys. Rev.*, **101**, 384 (1956).

The quadruples cross-section given in Table V is the quadruples differential cross-section integrated over the solid angle outside the transmission counter. The difference between the attenuation and quadruples cross-sections represents absorption and charge exchange events to which the counters are not sensitive.

TABLE V. – *Total cross-sections (millibarns).*

Cross-sections	Target	
	Carbon	Lead
Geometric	329	2425
Attenuation	542 ± 28	2750 ± 150
Quadruples	350 ± 20	2370 ± 150
Absorption+Charge exchange	192 ± 34	380 ± 310
Charge exchange ([3])	20	100
Absorption	172 ± 35	280 ± 310
Absorption/geometric	0.52 ± 0.11	0.12 ± 0.13
Monte Carlo, deaths/events	0.42	0.54
Elastic	110 ± 30	263 ± 27
Inelastic processes	430 ± 42	2490 ± 160

The two effects cannot be separated in this experiments so the charge exchange cross-sections of KESSLER and LEDERMAN ([3]) have been subtracted to give the absorption cross-sections of Table V. The ratio of absorption to geometric cross-section is given for comparison with the ratio of deaths to total events from the Monte Carlo calculations on carbon and lead. The absorption in carbon is in fair agreement with the Monte Carlo, but in lead the Monte Carlo predicts four times the observed absorption. The absorption cross-section deduced for lead is small because the cross-section determined from the quadruples count is large. It is possible that the corrections for protons and γ-rays as estimated in Sect. 6 are satisfactory for carbon but inadequate for lead. It is a weakness in the experimental method that it does not allow for the independent determination of these corrections, which accordingly must be verified by comparison of the present results with the results of other experiments. The previously mentioned agreement with the sum of the elastic and inelastic differential cross-sections of KESSLER and LEDERMAN ([3]) for 125 MeV π^- on lead was taken as corroboration of the quadruples cross-section determined in this experiment. The small absorption deduced for lead relative to that predicted by the Monte Carlo calculation implies that the absorption probability assigned to a collision of a negative pion with a nuclear proton, without regard for factors such as nuclear size, is not an adequate description of the actual absorption process ([30]).

([30]) The values of the ratio $g=(\sigma_{ab})/(Z\sigma_D)$ obtained in this experiment are 2.5 ± 0.5 for carbon and 0.29 ± 0.32 for lead. The corresponding values from the Monte Carlo

The elastic cross-section given in Table V is the elastic differential cross-section integrated over the solid angle outside the transmission counter. The elastic cross-section is smaller than has been previously reported ([2,3]) probably because of the more stringent definition of elastic scattering used in this experiment. The difference between the attenuation and elastic cross-sections is the cross-section for inelastic processes, which is somewhat uncertain because of the forward inelastic scattering. The cross-section for inelastic processes in carbon is greater than geometric by $2\frac{1}{2}$ standard deviations. The cross-section for lead is essentially geometric. The observed cross-section for inelastic processes is larger than that calculated from the optical model with reasonable values of the real and imaginary parts of the optical potential ([5]) by a partial waves solution including the Coulomb field and using a square well whose radius is based on the pion Compton wave length ([9]). The application of the experimental results regarding the angular distribution of the elastic scattering and the measured large value of the cross-section for inelastic processes to the determination of optical model parameters is discussed by FUJII ([9]).

9. – Conclusions.

The inelastic scattering of negative pions is preponderantly backward and is characterized by great energy losses. The energy of inelastically scattered pions leaving a nucleus is considerably lower than predicted by the quasi elastic scattering model in a Monte Carlo calculation based on a simple Fermi gas model. This is in contrast to the experimental results regarding the scattering of protons and electrons, in which the quasi elastic scattering model gives correctly the energy of the inelastically scattered particles. Furthermore, the absorption of pions in lead is less than that predicted by the Monte Carlo calculation by a factor of four.

* * *

It is a pleasure to acknowledge the advice and assistance of Professor H. L. ANDERSON, who suggested this problem. Professors S. C. WRIGHT and

calculation are 1.94 and 1.18. These values combine with the corresponding values of. LEDERMAN *et al.* (ref. ([3])) for carbon at 62 MeV, $\Gamma \gtrsim 3.3$; and of TENNEY and TINLOT (*Phys. Rev.*, **92**, 974 (1953)) for beryllium, $\Gamma = 3.2^{+1.1}_{-0.8}$ at 39 MeV and $\Gamma = 5.6^{-2.1}_{-1.1}$ at 20 MeV to form a straight line through the origin when plotted against $1/kR$. The slope of this line, including values of g derived from the absorption cross-sections quoted by TRACY (*Phys. Rev.*, **91**, 960 (1953)) and by SAPHIR (*Phys. Rev.*, **104**, 535 (1956)) is $g=(7.4\pm0.6)/kR$ at a 20% level of confidence by a least squares fit. The pion wave number is k, and R is the nuclear radius.

A. TURKEVICH of the University of Chicago and Dr. W. C. DAVIDON of the Argonne National Laboratory assisted with many helpful discussions. The writer is grateful to Dr. DONALD FLANDERS and JEAN HALL of the Argonne National Laboratory for making the AVIDAC available for computing energy analyses. Drs. N. METROPOLIS, M. STORM and R. BIVINS of the Los Alamos Scientific Laboratory very kindly conducted the MANIAC calculations of several thousand events by the Monte Carlo method for carbon and lead targets. Mr. T. FUJII assisted in assembling the equipment, conducting the experiment, and the subsequent analysis of the data. Mr. J. FAINBERG was very helpful during the runs. The efforts of Mr. C. BORDEAUX and the cyclotron operating staff through several weeks of around-the-clock runs are gratefully acknowledged.

RIASSUNTO (*)

Si sono usati contatori di Čerenkov o a scintillazione sensibili all'energia collegati ad un analizzatore dell'altezza degli impulsi per misurare lo spettro d'energia di pioni negativi di 150 MeV dopo scattering a vari angoli su carbonio o piombo. La maggioranza dei pioni si trovò nell'emisfero posteriore con energia inferiore a 40 MeV. Ciò è in contrasto coi risultati di un Montecarlo basato su un semplice modello di un gas di Fermi in cui la maggioranza dei pioni diffusi all'indietro hanno energie superiori a 60 MeV. Le misure indicano che l'assorbimento dei pioni in carbonio corrisponde approssimativamente a quello predetto dal Montecarlo, mentre l'assorbimento in piombo è circa $\frac{1}{4}$ del previsto.

(*) *Traduzione a cura della Redazione.*

Non Conservation of Parity and the Universal Fermi Interaction (*).

J. Tiomno

Faculdade Nacional de Filosofia and Centro Brasileiro de Pesquisas Físicas Rio de Janeiro, D.F.

(ricevuto il 2 Luglio 1957)

Summary. — The possibility of the Universal Fermi Interaction is re-examined in face of the recent experimental results on non conservation of parity. It is shown that if we associate to the μ-meson and to the electron neutrinos of opposite spirality then we can regain the Universal Fermi interaction in the form $S+P+T$ in the usual β-decay ordering in opposition to the exclusion of the U.F.I. which results from the Yang-Lee theory. This interaction previously proposed by Caianiello and by the present author has the special feature of being symmetrical in the exchange of the two particles or of the two antiparticles. The predictions of this theory for μ^+ decay coincide with those of the Yang-Lee theory with the difference that the positron spin points forward instead of backward.

The recent suggestion of Lee and Yang [1] that parity might not be conserved in weak interactions has led to experimental work which has not only verified this conjecture both for β-decay [2] and for μ-decay [3] but also brought new information on the Fermi interactions. The fact that the experi-

---

(*) Work done under the auspices of the Conselho Nacional de Pesquísas.

(1) T. D. Lee and C. N. Yang: *Phys. Rev.*, **104**, 254 (1956).

(2) C. S. Wu, E. Ambler, R. W. Hayward, D. D. Hoppes and R. P. Hudson: *Phys. Rev.*, **105**, 1415 (1957).

(3) R. L. Garwin, L. M. Lederman and M. Weinrich: *Phys. Rev.*, **105**, 1415 (1957); J. I. Friedman and V. L. Telegdi: *Phys. Rev.*, **105**, 1681 (1957).

mental results are in very good agreement with the 2-component neutrino theory [4] has been interpreted as an indication of the validity of this theory. However the interaction which leads to the correct results for the μ-decay [5] is of the form $A+V$ in the charge exchange ordering $(\bar{\mu}^{+}\nu')(\bar{e}\nu)$ in contradistinction to the interaction

$$\alpha S T + T + \beta P \qquad (|\alpha| \sim 1;\ \beta \sim +1) \tag{1}$$

needed for β-decay [6] (usual ordering: $(\bar{P}N)(\bar{e}\nu)$). This might be an indication of the non-validity of the Universal Fermi Interaction. Indeed LEE and YANG [7] have proved on very general grounds that the experimental results definitively exclude the U.F.I. if we accept the following postulates:

1) conservation of the number of light particles;

2) validity of the two component theory with only one kind of neutrino (and of antineutrino).

The idea of the U.F.I. is however so appealing and simplifying that one should try to keep it even if one or both of these postulates should be discarded. FEYNMAN [8] has indeed pointed out a possibility of recovering the U.F.I. by the use of Majorana neutrinos and appropriate projection operators

$$P_{\pm} = \tfrac{1}{2}(1 \pm \gamma_5) \tag{2}$$

conveniently used so to reproduce the experimental results. In this case both postulates 1) and 2) are violated and unless the operators $P_{\pm}$ are used only for the light particles (Feynman choses to associate them to the charged particles) the tensor interaction is killed also for β-decay in disagreement with the experience.

We wish to point out another possibility which is not only more symmetrical but violates only postulate 2. This is done by assumming that there are two kinds of neutrinos ν_e and ν_μ of opposite spirality which are associated to the electron and μ^{-}-mesons in the same way as the neutron is associated to the

---

[4] T. D. LEE and C. N. YANG: *Phys. Rev.*, **105**, 1671 (1957); A. SALAM: *Nuovo Cimento*, **5**, 299 (1957); L. LANDAU: *Nucl. Phys.*, **3**, 127 (1957).

[5] T. D. LEE (private communication).

[6] H. M. MAHMOUD and E. J. KONOPINSKI: *Phys. Rev.*, **88**, 1266 (1952) (and references therein quoted).

[7] T. D. LEE: communication to the *Seventh International Conference on High Energy Nuclear Physics*, Rochester, April 1957.

[8] R. P. FEYNMAN: Communication to the *Rochester Conference*, April 1957.

proton. Thus we have the following pairs of « particles » (*):

$$(\mathrm{p}, \mathrm{n}); \quad (\mathrm{e}^+, \nu_e'); \quad (\mu^+, \nu_\mu') . \tag{3}$$

$$\mathrm{p}^- \nu_e = \nu_e ; \qquad \mathrm{p}^+ \nu_\mu = \nu_\mu . \tag{4}$$

The Universal Interaction should be written as a sum for all pairs of particles of interactions of the type

$$(\overline{\psi}^r_+ O \psi^r_0)(\overline{\psi}^s_0 O \psi^s_+) + \text{h. c.} \tag{5}$$

Also we take for the direct π-μ interaction:

$$\pi^+ \overline{\mu}^+ \nu_e' + \text{h. c.} \tag{6}$$

(and not $\pi^+ \overline{\mu}^+ \nu_\mu'$) which correspond to the fact that we have $\pi^+ \Sigma^+ \mathrm{n} + \text{h. c.}$ for Σ^+ decay (Σ^+ and n belonging to different pairs). Interaction (6) is the same as the one used by LEE and YANG and leads to μ^-'s with spin pointing back in the π-μ-decay.

Now we shall prove that if we take the interaction (5) as

$$S + P - T \tag{7}$$

(which correspond to $S + P + T$ in the β-decay ordering, being thus compatible with (1)) the same energy spectrum and angular distribution for μ-decay as with the Yang-Lee interaction results from the interaction:

$$(\overline{\nu}_\mu \mu^-)(\overline{\mathrm{e}} \nu_e) + \text{h. c.} \qquad (S + P - T) . \tag{8}$$

This equivalence can be easily shown if we use the ordering $(\overline{\nu}_e' \mu^-)(\overline{\mathrm{e}} \nu_\mu')$ for which (8) takes the form

$$(\overline{\nu}_e' \mu^-)(\overline{\mathrm{e}} \nu_\mu') , \qquad \text{(scalar).} \tag{9}$$

while the Yang-Lee interaction becomes

$$(\overline{\nu}_e' \mu^-)(\overline{\mathrm{e}} \nu_e') , \qquad \text{(scalar).} \tag{10}$$

It is clear from the comparison of (9) and (10) that if the polarization of the

(*) In (3), (4) we use primes for neutrino « particles » to conform with the usual notation of β-decay. For the present purpose it is not necessary to include the hyperon pairs.

electron is not measured no difference can be detected for the spectrum. Indeed the ϱ factor, angular and energy distribution will be the same ([9]) for (9) and (10) except that the electron will come out in (9) polarized oppositely to its velocity instead of in the same direction as in (10). Measurement of the polarization of the electron in μ-decay should decide between the two theories.

It should be mentioned that the U.F.I. (5), (7) has the special feature of being symmetrical in the exchange both of « particles » and of « antiparticles », on which grounds it has been proposed before ([10]).

Direct application of the U.F.I. (5), (7) to β-decay and to μ-capture are impaired by the fact that these interactions correspond to bare particles. For interactions with actual nucleons such as in β-decay and μ-capture emission and reabsorption of virtual π-mesons result in different renormalizations of the S, T and P coupling constants which become different ([11]). The difference between S and T couplings has been indeed observed in β-decay ([12]), and is in good agreement with the assumption of equal S, T couplings for bare nucleon interactions ([13]). However as it is not well known how large these differences are we shall quote a few results of our Universal Interaction which should be approximately valid if the renormalized couplings are not much different from the unrenormalized ones.

1) The λ factor proposed by MICHEL ([14]) is equal to 1.33 in reasonable agreement with the experimental value 1.16 ± 0.12 ([15]).

2) For β-decay interaction, which is here

$$(\bar{\mathrm{p}}\,\mathrm{n})(\bar{\mathrm{e}}\nu_{\mathrm{e}}) + \mathrm{h.\,c.} \qquad (S + P + T) \tag{11}$$

we obtain no angular (p, e) correlation.

3) The μ capture interaction which here is

$$(\bar{\mathrm{p}}\,\mathrm{n})(\bar{\mu}^{-}\nu_{\mu}) + \mathrm{h.\,c.} \qquad (S + P + T) \tag{12}$$

([9]) After this work was acomplished we received a pre-print of a paper by T. KINOSHITA and A. SIRLIN in which a class of interactions is shown to give the same results as in Yang-Lee theory for μ-decay. Our interaction (8) seems to be the only one of this class suitable for the Universal interaction. These results have been also obtained by E. M. FERREIRA (to be published in *An. Acad. Bras. Ci.*).

([10]) E. CAIANIELLO: *Nuovo Cimento*, **10**, 43 (1953); J. TIOMNO: *Nuovo Cimento*, **1**, 226 (1955). See also: E. J. KONOPINSKI and E. J. MAHMOUD: *Phys. Rev.*, **92**, 1045 (1953).

([11]) R. J. FINKELSTEIN and S. A. MOSZKOVSKY: *Phys. Rev.*, **95**, 1695 (1954).

([12]) R. GERHART: *Phys. Rev.*, **95**, 288 (1954).

([13]) S. S. GERSHTEIN and IA. B. ZEL'DOVICH: *Soviet Phys. J.E.T.P.*, **2**, 576 (1956).

([14]) L. MICHEL: *Progress in Cosmic Ray Physics* (Amsterdam, 1952).

([15]) L. MICHEL and A. WIGHTMAN: *Phys. Rev.*, **93**, 354 (1954).

leads to the fact that neutrons from μ-capture in Hydrogen will come out polarized in the direction of the polarization of μ^-.

4) Interaction (12) leads to the angular correlation of the neutrons in μ-capture in Hydrogen:

$$1 + \boldsymbol{n}\cdot\boldsymbol{p}_n/E_n\,, \tag{13}$$

where $\boldsymbol{n}$ is the polarization vector for μ^-, $\boldsymbol{p}_n$ and E_n being the momentum and energy of the neutron.

Conclusions 2)-4) are easily verified if the interactions are written in the ordering:

$$(\bar{n}\,p^-\mu^-)(\bar{\nu}_\mu P) \qquad \text{(scalar)}, \tag{14}$$

$$(\bar{n}\,p^+e)\ \ (\bar{\nu}_e P) \qquad \text{(scalar)}. \tag{15}$$

Finally it seems worthwhile to mention that in contradistinction to the Yang-Lee theory which can lead to the decay

$$\mu \to e + \gamma \tag{16}$$

the present theory gives vanishing probability for this process.

* * *

We are thankful to Professor L. Marquez for helpful discussions.

RIASSUNTO (*)

Al lume dei recenti risultati sperimentali sulla non conservazione della parità si riesamina la possibilità dell'interazione universale di Fermi. Si dimostra che associando al mesone μ e all'elettrone neutrini di spiralità opposta si può riottenere nella disposizione usuale del decadimento β l'interazione universale di Fermi nella forma $S+P+T$ in opposizione all'esclusione di tale interazione che risulta dalla teoria di Lee e Yang. Questa interazione precedentemente proposta da Caianiello e dallo scrivente ha la speciale caratteristica di essere simmetrica nello scambio di due particelle o di due antiparticelle. Le predizioni di questa teoria per il decadimento μ^- coincidono con quelle della teoria di Lee e Yang con la differenza che lo spin del positone è diretto in avanti anzichè indietro.

(*) *Traduzione a cura della Redazione.*

On the Phase Grating in Suspensions Crossed by Ultrasounds.

F. Porreca

Istituto di Fisica Sperimentale dell'Università - Napoli

(ricevuto il 22 Luglio 1957)

Summary (*). — After having experimentally measured the luminous intensity of the diffracted lines wich remain in certain substances after the action of ultrasonics, we have tried to ascertain the type of phase grating producing the effect, assuming the refraction index to obey some variation laws. Basing on these laws we have calculated the theoretical intensity distribution of the diffracted lines and found the experimental values to be in good agreement with the calculated ones assuming that after the action the ultrasounds in the liquid the variation law of the refraction index conserves a redressed sinusoidal semiwaves shape. The order of magnitude of the maximum variation of the index ($1.6 \cdot 10^{-6}$) which may be calculated in such conditions results to be in fair agreement with the one experimentally measured in a preceding experience.

(*) *Editor's translation.*

As is well known, recent experiments on the optical diffraction by a phase grating, produced in a suspension by the action of stationary ultrasonic waves, have allowed observation of the permanence of the even order diffracted lines, even when the high frequency vibrations have ceased. This is due to the establishment of a phase grating with $\lambda^*/2$ constant (λ^* being the ultrasonic wave length), due to the periodical change of the refraction index for the accumulation of suspended particles in the nodal planes by ultrasonic waves. The line intensity decreases with time, according to an exponential law [1].

Intensity distribution of the diffracted lines depends on the law of refraction index change along the phase lattice, which remains in the liquid after the cessation of the ultrasonics.

[1] F. Porreca: *Nuovo Cimento*, **4**, 679 (1956).

In this paper our aim is to see whether we can establish this variation law. We have therefore, first of all, experimentally determined the line distribution intensity, produced by such a phase lattice, and therefore without ultrasounds. The measuring is done immediately after the cessation of the ultrasonics (approximately $\frac{1}{2}$ s later) by photographing the spectrum, and by transforming the blackening of the photographic plate into intensity by well-known methods.

Intensity distribution, for a certain suspension, changes according to the concentration, duration, intensity and frequency of the ultrasonics; it further depends on the time interval between the stopping of the crystal oscillation and the measuring of the intensity. It is therefore necessary to put the piezoelectric quartz into oscillation, by means of an oscillator, which can provide constant output power in order to have a constant ultrasonic power; successive measuring must be done at even intervals, after the cessation of the high frequency vibrations, using trains of ultracustic waves of a constant duration.

This can be obtained by making use of an interrupting device of the oscillating circuit and a light pencil shutter, functioning so as to superpose successive blackenings of the photographic plate only in the moment in which the measuring of the various order intensity is required, until sufficient exposure is reached.

The shutter stops the light pencil as long as the ultrasonic perturbation acts, allowing, however, the passage of diffracted light during a very short time $\Delta t = 0.2$ s after the quartz has stopped to oscillate since the time $\Delta t = 0.5$ s. This shutter may consist of a very thin split with an adjustable amplitude. The split is placed on the edge of a wooden disk, rotating at a constant angular speed around an axis parallel to the optical axis of the system, and is set between a monochromatic Na-light source and the collimator to form the parallel light pencil, which crosses the substance under investigation. At each disk revolution, when the rotating split is set in a line with the fixed split of the collimator in the direction parallel to the optical axis, the light may strike the photographic plate, whilst no radiation can strike it during the remaining revolution period of the disk.

A metallic circular sector, whose length may be varied, and which creeps on a fixed contact, functioning as interrupter of the oscillating circuit, is fixed on the disk. The contact time indicates the duration of the ultrasonic perturbation. This time is 5 s and remains constant during the successive disk revolutions.

The revolution time is 60 s, and it is maintained much longer than the ultrasonic perturbation time and the diffracted line permanence, so that between the stopping and restoring of the ultrasonic perturbation (55 s) there may be a sufficiently long interval of time; in this interval, with the elimination of the slight convective motions due to the energy absorption which the medium

has accumulated during the ultrasonic perturbation, the initial homogeneous conditions of the liquid may be restored. At each revolution, with these experimental devices, one may be assured of finding the same initial experimental conditions.

Fig. 1 illustrates the synchronism of the experimental operations which we have described, showing the time distribution of the ultrasonic perturbation and that of the photographic plate blackening.

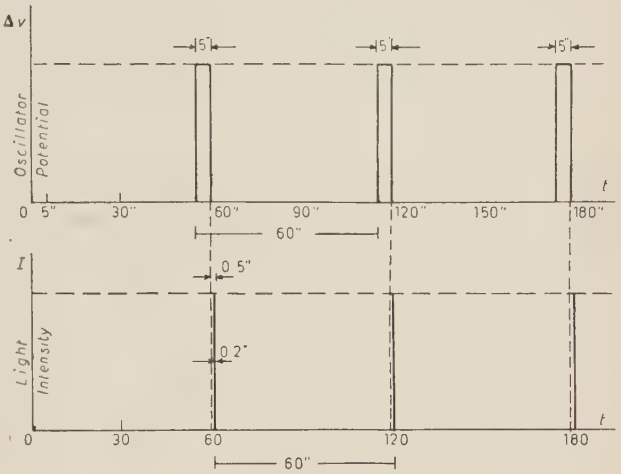

Fig. 1.

The total exposure time is 1 s and therefore the total duration of the experimental phases, required to obtain the photograph, is 5 minutes. For this reason the suspension concentration may be supposed to remain unchanged. The substance under investigation is contained in a vessel in whose lowest part is located the piezoelectric crystal, which oscillates on the 3-rd harmonic (1.8 MHz). One surface of the crystal is in direct contact with the liquid crossed by ultrasounds. In order to obtain the stationary waves, a reflecting brass plate, much thicker than the ultrasonic wave length λ^* is placed on the wall opposite the quartz. This plate may be subjected to micrometric displacements, thus changing its position with regard to the ultrasonic wave direction. Moreover its distance d from the quartz may be adjusted so that the established conditions may be satisfied to get stationary waves

$$d = r\,\frac{\lambda^*}{2} \qquad (r \text{ integer and positive}).$$

The diffraction effect, which is due to the ultrasonic modulation of the medium under investigation, is shown by the well-known optical arrangement (many times described), the only modification being to place the photographic plate in the spectrum plane. We examined a suspension of starch in water with a concentration 0.08 g/l. The line permanence time from the stopping of the ultrasonic perturbation is (12 ± 1) s, much long r than the 0.2 s in which the light passes at each revolution of the shutter disk. The distribu-

tion of the blackening corresponding to the diffracted lines is examined with a Moll microphotometer. The lines intensity values, which are observed immediately after the cessation of the oscillating circuit and obtained by averaging numerous experimental measurements, always in the same experimental conditions, are shown in Table I.

TABLE I.

Diffraction Order	I % experimental	I % theoretical	
		law 1	law 2
0	100	100	100
1	12 ± 2	12	12
2	4 ± 1	0.3	1.2
3	1.9 ± 1	0	0
4	1.2 ± 1	0	0

In order to determine the type of phase grating which produces this diffraction pattern, we have compared the experimental intensity behaviour with the theoretical one, computed by RAMAN and NATH in the case of ultracustic progressive ([2]) and stationary waves ([3]). They performed detailed research evaluating the light intensity distribution of the diffracted orders, in cases where phase lattices are produced by a refraction index change, according to the functions

$$\Delta\mu(x) = \Delta\mu \sin 2\pi(\nu^* t - x/\lambda^*) , \tag{1}$$

$$\Delta\mu(x) = \Delta\mu \sin 2\pi\nu^* t \sin 2\pi x/\lambda^* . \tag{2}$$

Intensity behaviour depends on the parameter $v = 2\pi\Delta\mu L/\lambda$, where $\Delta\mu$ is the maximum change of the refraction index, and L is the thickness of the modulated medium, measured in the direction of the incident light of wave length λ. When $\Delta\mu$ rises, the number of lines of the diffraction spectrum increases. Experimental results are in satisfactory agreement with the theoretical previsions: the phase lattices, which correspond to the variation laws (1) and (2) of the refraction index, are experimentally obtained in the case of the liquids crossed by ultracustic progressive and stationary waves. However,

([2]) C. V. RAMAN and N. S. NAGENDRA NATH: *Proc. Ind. Acad. Sci.*, **2**, 406 (1935).
([3]) C. V. RAMAN and N. S. NAGENDRA NATH: *Proc. Ind. Acad. Sci.*, **3**, 75 (1936).

none of these intensity distributions, even for different values of the parameter v, agree with the experimental values: in Table I are shown the theoretical values which are nearest to the experimental ones, calculated respectively in the cases (1) and (2) relative to the values $v = 0.6$ and $v = 0.9$, chosen to coincide with the relative intensity of the 1-st order which is 12% of the central line.

We may conclude that the agreement is unsatisfactory. We must therefore exclude the possibility that we are dealing with a lattice which is characterized by the variation laws (1) and (2) of the refraction index.

In an attempt to find a behaviour of the intensity which most agrees with the experimental distribution, we took as variation law of the refraction index other types of periodical functions.

a) We may assume that the ultrasonic standing waves distribution accumulates the suspended particles in the liquid in distinct groups at equal distance from each other, so that the refraction index varies according to the diagram *a*) of Fig. 2, corresponding to the Fourier expansion

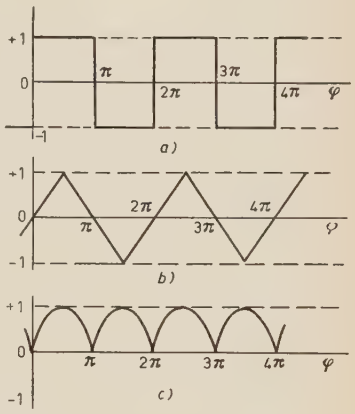

Fig. 2.

$$(3) \qquad \Delta\mu(x) = \Delta\mu \frac{4}{\pi} \sum_{0}^{\infty} \frac{\sin[(2K+1)2\pi x/\lambda^*]}{2K+1} .$$

b) The refraction index varies linearly, among the nodes and the antinodes according to a periodical law graphically shown in Fig. 2 *b*) and analytically expressed by the expansion

$$(4) \qquad \Delta\mu(x) = \frac{8}{\pi^2} \sum_{0}^{\infty} (-1)^k \frac{\sin[(2K+1)2\pi x/\lambda^*]}{(2K+1)^2} .$$

c) A periodical variation law, according to which the refraction index has an intermediate value between the foregoing ones, is represented by the diagram *c*) Fig. 2, with sinusoidal positive semi-waves and has the expansion

$$(5) \qquad \Delta\mu(x) = \Delta\mu \frac{2}{\pi}\left[1 - \sum_{1}^{\infty} \frac{2}{(2K+1)(2K-1)} (-1)^K \cos 2K \frac{2\pi x}{\lambda^*}\right] .$$

In agreement with RAMAN and NATH, the intensity calculation of the various diffracted orders of a parallel light pencil of width p, depends on the evaluation of the following integral:

$$(6) \qquad \int_{-p/2}^{p/2} \exp[2\pi i\, lx + \Delta\mu(x)L)/\lambda]\, \mathrm{d}x ,$$

which gives the amplitude of the luminous front in the point $B(x)$ of the plane on which the diffracted light falls (Fig. 3).

In the integrand function $lx = x\cos\varphi = AB$ represents the phase change which the wave undergoes in the predetermined direction, in comparison with the incident one.

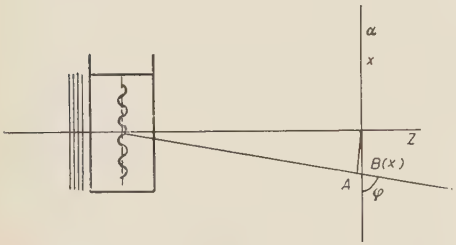

Fig. 3.

The evaluation of the diffraction integral (6), in the case where the refraction index variation $\Delta\mu(x)$ follows the equations (3), (4) and (5), is carried out more easily. As the series expansion integral is quickly convergent, it is sufficient to take into account only the first expansion terms in order to arrive at the intensity values of the diffracted fringes, with certainly less error than in the case of the experimental values. This fact was numerically verified to the value $r = 1.5$ of the parameter (*). The relative values for I, obtained according to (3) and (4) are not in agreement, for any value of v, with the experimental values of Table I.

On the other hand we found a satisfactory agreement on examination of the theoretical results which we obtained, assuming a periodical change of refraction index according to the expansion (5).

In this case, in fact, we come to the conclusion that the diffraction pattern is composed of so many light maxima as the following conditions:

$$ul \pm 2r\cdot 2b = 0\,, \qquad ul \pm (2r+1)2b = 0\,,$$

i.e.

$$ul \pm nb = 0\,,$$

where $u = 2\pi/\lambda$, $b = 2\pi/\lambda^*$, r is a positive integer number, including zero; hence the number n which expresses the order of the diffracted lines, is certainly an even number. With the expansion (5) we foresee only the even order fringes, as it is experimentally verified on observation of the diffraction pattern which remains after the stopping of the ultrasonic perturbation.

The resolving intensity formulas are given in Table II where J_K is the Bessel function of order K.

The experimental distribution in Table I of the line intensity is in satisfactory agreement with that calculated according to (5) for the value of the parameter $v = (0.85 \pm 5)\cdot 10^{-2}$ and shown in Table III.

(*) More details on the numerical calculations and the theoretical results in the case of the laws (3) and (4) will be the subject of another paper.

TABLE II.

Diffraction order	I
0	$\cos^2 v J_0^2(\frac{2}{3}v)$
2	$\sin^2 v J_1^2(\frac{2}{3}v)$
4	$\cos^2 v J_2^2(\frac{2}{3}v)$
6	$\sin^2 v J_3^2(\frac{2}{3}v)$
8	$\cos^2 v J_4^2(\frac{2}{3}v)$
10	$\sin^2 v J_5^2(\frac{2}{3}v)$
12	$\cos^2 v J_6^2(\frac{2}{3}v)$

TABLE III.

Diffraction order	I
0	100
1	12.8
2	3.2
3	1.2
4	0.7

From the parameter value which was obtained in this way, one may evaluate $\Delta\mu$, i.e. the maximum change of the refraction index; from $v = 2\pi\Delta\mu L/\lambda = 0.85$, as we can substitute for L the quartz diameter (5 cm) and $\lambda = 5\,890$ Å, we have

$$\Delta\mu = 1.6 \cdot 10^{-6} .$$

This result agrees with the experimental value, measured in a different way in a previous investigation [4], and this agreement confirms the results which

[4] A. CARRELLI and F. PORRECA: *Nuovo Cimento*, **10**, 1406 (1953).

we have obtained regarding nature and type of the phase lattice which is the subject of our paper.

* * *

The author is much indebted to Prof. Antonio Carrelli for his help and clever suggestions.

RIASSUNTO

Misurata sperimentalmente la distribuzione d'intensità luminosa delle righe diffratte, che rimangono in certe sostanze dopo l'azione degli ultrasuoni, si è tentato di conoscere il tipo di reticolo di fase che produce l'effetto, ammettendo alcune leggi di variazione dell'indice di rifrazione. In base ad esse si è calcolata la distribuzione teorica d'intensità delle righe diffratte e si è trovato un buon accordo tra i valori sperimentali e quelli calcolati nel caso in cui si supponga che dopo l'azione degli ultrasuoni nel liquido permanga una legge di variazione dell'indice di rifrazione a semionde sinusoidali raddrizzate. L'ordine di grandezza della variazione massima di indice ($1.6 \cdot 10^{-6}$) calcolabile in queste condizioni risulta in buon accordo con quello sperimentalmente misurato in un precedente lavoro.

Correlation of Gas Bubble Chamber Results with Glaser's Theory.

C. Henderson and G. Kalmus

Physics Department, University College London

(ricevuto il 24 Luglio 1957)

Summary. — The boundaries of the sensitive region of a methane-propane gas bubble chamber have been shown to approximate to lines of constant n, in the case of this chamber $n = 2$ and $n = 6$, where n is the parameter defined by Glaser's equation.

In a previous paper by a group at this College [1] it was shown that there is a well defined region in which a propane-methane gas bubble chamber is radiation sensitive.

It was decided to see how the boundaries of the sensitive region were related to lines of constant n, where n is defined by Glaser's equation [2]

$$P - p \geqslant \left| \frac{3}{2} \left(\frac{4\pi}{n^2 e^2} \right)^{\frac{1}{3}} \gamma^{\frac{4}{3}} \varepsilon^{\frac{1}{3}} \right| .$$

In this case P is the sum of the partial pressures of gas and saturated vapour at the operating temperature, p is the hydrostatic pressure whilst the chamber is sensitive, e the elementary charge, γ the surface tension, and ε the dielectric constant (which has been assumed to have a constant value of 1.6 esu). The value of p was found to be 160 lbs/sq.in., by means of a pressure transducer in the chamber.

---

[1] F. W. Bullock C. Dodd, C. Henderson, and G. Kalmus; *Nuovo Cimento*, **6**, 324 (1957).

[2] D. A. Glaser: *Suppl. Nuovo Cimento*, **11**, 361 (1954).

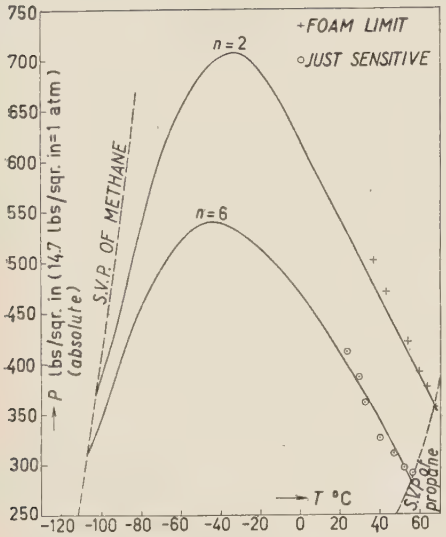

Fig. 1. – Full curves are lines of constant $n=2$ and $n=6$ as calculated from Weinaug and Katz, broken lines are *svp* curves of methane and propane, ⊙ and + are experimental points for onset of sensitivity and foam respectively.

As can be seen from the graph, the shape of the boundary lines as marked by the points + and ⊙ approximates very closely to the lines of constant n, the foam limit being close to $n = 2$, as would be expected on Glaser's theory, whilst $n \sim 6$ appears to mark the onset of sensitivity. The lines $n = 2$ and $n = 6$ have been plotted starting from the saturated vapour pressure curve of propane, and ending at that of methane. The necessary connection between P, γ and temperature was obtained from the paper of Weinaug and Katz ([3]) and derives partly from their own experiments and partly by extrapolation in which the values for pure methane, given by Katz and Saltman's ([4]) correlation were used as a guide.

Thus it would seem reasonable to suppose that in going from a pure propane to a pure methane chamber, the sensitive region will be approximately that between the lines $n = 2$ and $n = 6$ as shown, and that pure methane operates in the temperature range -103 °C to -106 °C.

([3]) C. F. Weinaug and D. L. Katz: *Ind. Eng. Chem.*, **35**, 239 (1943).
([4]) D. L. Katz and W. Saltman: *Ind. Eng. Chem.*, **31**, 91 (1939).

RIASSUNTO (*)

Si è dimostrato che i limiti della regione sensibile di una camera a bolle a metano-propano si approssimano alle linee di n costante; nel caso della camera oggetto del lavoro $n = 2$ e $n = 6$, n essendo il parametro definito dall'equazione di Glaser.

(*) *Traduzione a cura della Redazione.*

IL NUOVO CIMENTO Vol. VI, N. 4 1° Ottobre 1957

Potential Inelastic Scattering by Complex Nuclei.

A. Tomasini

Istituto di Fisica dell'Università - Bologna
Istituto Nazionale di Fisica Nucleare - Sezione di Bologna

(ricevuto il 29 Luglio 1957)

Summary. — We show that it exists an inelastic scattering of any type of particle by complex nuclei, due essentially to the perturbation produced by the incident particle on the overall potential experienced by the nucleons of the nucleus. A particle which enters a nucleus and goes out without being captured, determines an increase or a decrease of the overall potential, during the short time it is inside the nucleus; so that the nucleus can make a transition to an excited level. We show that the anomalous inelastic scattering of 23 MeV (and 18 MeV) protons by intermediate and heavy nuclei, should be due to such a type of excitation; all quantitative features of the process are well explained, and also the quantitative results are in agreement, in spite of the crude approximations made.

1. – Introduction.

A particle can be scattered inelastically by a complex nucleus in a number of ways: the particle can be captured giving rise to a compound nucleus, which in turn decays emitting the same particle with lower energy; or the particle can interact directly with one nucleon (or possibly with more nucleons) and leave the nucleus without being captured. The latter type of interaction can occur inside or outside the nucleus, i.e. the particle can enter effectively into the nucleus, or else it can remain outside and interact with the nucleons of the diffuse rim of the nucleus. Other types of inelastic scattering are due to Coulomb excitation and to the excitation of the surface oscillations of the nucleus.

We want to point out here that it exists an other type of inelastic scat-

2787

tering, due essentially to the perturbation on the overall potential experienced by the nucleons of the nucleus, produced by the particle which enters the nucleus. With such a type of interaction we can explain the anomalous inelastic scattering of 23 MeV protons by intermediate and heavy nuclei [1]: in the energy spectrum of 23 MeV protons inelastically scattered by nuclei with $Z > 40$ there is a well defined peak, with a loss of energy of about 2.5 MeV. The difficulties in explaining such a peak as due to the excitation of a single level by direct interaction, are in the regularity between even and odd elements and across closed shell; also an explaination in terms of collective motion is difficult.

2. – Perturbation of the potential.

It is well known [2] that the overall potential experienced by the nucleons in the nucleus is evaluable, at least in principle, with a self consistence method, once the reaction matrix G of the scattering between single nucleons is known. If the i-th and the j-th nucleons are in the states n_i and n_j the potential experienced by the i-th nucleon is

$$V = \sum_{j \neq i} (n_i n_j \,|\, G_{ij} \,|\, n_i n_j) \,. \tag{1}$$

Let us assume that the potential matrix $(\boldsymbol{r}' \,|\, V \,|\, \boldsymbol{r})$ is diagonal in space representation

$$(\boldsymbol{r}' \,|\, V \,|\, \boldsymbol{r}) = V(\boldsymbol{r})\, \delta(\boldsymbol{r}' - \boldsymbol{r}) \,.$$

We attribute to each state of single nucleon a well defined energy. These assumptions cannot invalidate the essential conclusions we will arrive at [3]. When an extra nucleon interacts with the nucleus, it gives rise to a « compound system », which is not necessarily a compound nucleus, but which signifies simply the nucleus and the extra nucleon in interaction. In the compound system we have a succession of elementary interactions between the extra nucleon and the nucleons of the nucleus; each of such interactions is evaluable with a G matrix. The non diagonal elements of G,

$$(n_0' n_i' \,|\, G_{0i} \,|\, n_0 n_i)$$

[1] B. L. Cohen: *Phys. Rev.*, **105**, 1549 (1957): B. L. Cohen and S. W. Mosko: *Phys. Rev.*, **106**, 995 (1957).

[2] The argument has been discussed extensively by: H. A. Bethe: *Phys. Rev.*, **103**, 1353 (1956). The symbols we will use are taken from this work.

[3] For the implications of these assumplions see ref. [2].

are responsible for the direct interactions of the normal type, since they change the state of the system. The diagonal elements represent elementary interactions in which the system remains in the initial state; however such interactions determine a perturbation on the overall potential. In fact now the potential experienced by the i-th nucleon is given by

$$V' = \sum_{j \neq i} (n_i n_j | G_{ij} | n_i n_j) + (n_0 n_i | G_{0i} | n_0 n_i) = V + V_i . \tag{2}$$

V_i is a perturbation potential between the extra nucleon and the i-th nucleon so that the nucleus, in the overall process of interaction between the extra nucleon and the nucleus, can make a transition into an excited state, although in each elementary interaction the extra nucleon never changes its state. (2) is correct if during the interaction the states of single nucleons are the same as before; clearly this is not strictly true, however it appears a reasonable approximation. The compound system lives a short time, if there is no formation of compound nucleus; in this case we can assume that during the interaction the nuclear volume does not change, and the number of interactions increases, i.e. that V_i is really a potential added to V. In other words during the interaction the nuclear density is increased, so that the potential is increased. If the extra particle has a repulsive interaction with the nucleons the potential is decreased, but the effect will be the same.

If $\boldsymbol{x}_0$ and $\boldsymbol{\xi}_i$ are the co-ordinates of the extra particle and of the i-th nucleon, in its simplest form V_i can be assumed sferically simmetric in $\boldsymbol{x}_0$ and $\boldsymbol{\xi}_i$:

$$V_i(\boldsymbol{x}_0, \boldsymbol{\xi}_i) = V_i f(r) f(r_i) ,$$

where $r = |\boldsymbol{x}_0|$, $r_i = |\boldsymbol{\xi}_i|$, and f is a function which gives the form of the potential. Let us assume for a moment that the non-diagonal elements of G are all zero; in such a case the nucleus is « transparent » for the normal types of inelastic interactions. Let us consider the elastic scattering of a nucleon by the nucleus; in Born approximation the matrix element for the process is given by:

$$H_{if} = \frac{1}{L^2} (\exp[i\boldsymbol{k}_0' \cdot \boldsymbol{x}_0] | f(r) | \exp[i\boldsymbol{k}_0 \cdot \boldsymbol{x}_0] (\sum_i V_i (\varphi_1^{(i)} \dots \varphi_A^{(i)} | f(r_i) | \varphi_1^{(i)} \dots \varphi_A^{(i)}) =$$

$$= \frac{1}{L^3} (\exp[i\boldsymbol{k}_0' \cdot \boldsymbol{x}_0] | f(r) | \exp[i\boldsymbol{k}_0 \cdot \boldsymbol{x}_0]) \sum_i V_i (\varphi_i^{(i)} | f(r_i) | \varphi_i^{(i)}) ,$$

where $\boldsymbol{k}_0$ and $\boldsymbol{k}_0'$ are the momenta of the incident and of the scattered nucleon, and $|\boldsymbol{k}_0'| = |\boldsymbol{k}_0|$; the index $(^i)$ stays for initial state and L^3 is an arbitrary normalization volume. We assume that every nucleon is in a well defined state.

So in Born approximation the real potential of an optical model is given by:

$$V_r = \sum_i V_i(\varphi_i^{(i)} | f(r_i) | \varphi_i^{(i)}) \,. \tag{3}$$

From (3) one obtains: $V_i > V_r/A$. In order to evaluate an order of magnitude of the integrals in (3) we assume for $f(r_i)$ a square well of radius R_0; if $\int_{r>R_0} |\varphi_i^{(i)}|^2 \mathrm{d}\tau_i \ll 1$, the integrals in (3) are very close to unity. The radial wave functions outside the nucleus are essentially of the type $\exp[-\beta_i r_i]/\beta_i r_i$, where $\beta_i = \sqrt{(2m_i B_i)}/\hbar^2$ and B_i is the binding energy of the i-th nucleon; one derives:

$$\int_{r>R_0} |\varphi_i^{(i)}|^2 \mathrm{d}\tau_i \cong \frac{4\pi}{\frac{4}{3}\pi R_0^3} \int_{R_0}^{\infty} \frac{\exp[-2\beta_i r_i]}{\beta_i^2} \mathrm{d}r_i = \frac{3}{2} \frac{\exp[-2\beta_i R_0]}{(\beta_i R_0)^3} \,,$$

which is very small also for states near the top of the energy distribution, if R_0 is large. Therefore for large nuclei we can assume: $V_i = V_r/A$.

In first approximation the matrix element of inelastic scattering due to V_i is:

$$H_{\mathrm{if}} = \frac{1}{L^3} (\exp[i\boldsymbol{k}_0' \cdot \boldsymbol{x}_0] | f(r) | \exp[i\boldsymbol{k}_0 \cdot \boldsymbol{x}_0]) \sum_i V_i(\varphi_1^{(f)} \dots \varphi_A^{(f)} | r(f_i) | \varphi_1^{(i)} \dots \varphi_A^{(i)}) \,, \tag{4}$$

($^{(f)}$ final state). H_{if} is different from zero only if all the nucleons but one, after the interaction, are in the initial state. Let us consider a transition in which the k-th nucleon jumps into an excited level; one obtains:

$$H_{\mathrm{if}} = \frac{1}{L^3} (\exp[i\boldsymbol{k}_0' \cdot \boldsymbol{x}_0] | f(r) | \exp[i\boldsymbol{k}_0 \cdot \boldsymbol{x}_0]) V_k(\varphi_k^{(f)} | f(r_k) | \varphi_k^{(i)}) . \tag{5}$$

The cross-section for the process is:

$$\sigma(\vartheta) \mathrm{d}\Omega = \frac{k_0'}{k_0} \left(\frac{m}{2\pi\hbar^2} \right)^2 L^6 | H_{\mathrm{if}} |^2 \mathrm{d}\Omega \,, \tag{6}$$

where m is the mass of the nucleons. H_{if} is different from zero only if the k-th nucleon in the final state has the same angular momentum and z projection of the angular momentum and of the spin, as in the initial state; therefore such an interaction excites only levels of the nucleus which have the same spin and the same parity as the ground state. If we take into account explicitly the spin functions of the extra nucleon, (5) and (6) do not change, since H_{if} is different from zero only if the spin has the same projection in the final as in the initial state; we cannot have spin flip of the scattered nucleon.

The angular distribution is given only by the function

$$(\exp[i\boldsymbol{k}_0'\cdot\boldsymbol{x}_0]\,|\,f(r)\,|\exp[i\boldsymbol{k}_0\cdot\boldsymbol{x}_0])$$

and it does not depend on the internal state of the nucleus.

3. – Anomalous inelastic scattering.

If the nucleus is heavy the excited levels are close to each other; therefore in order to explain the anomalous scattering of 23 MeV protons we assume that a group of levels is excited. We are interested in the differential cross-section in energy and angle; we have:

$$\sigma(E_0', \vartheta)\,\mathrm{d}E_0'\,\mathrm{d}\Omega = \frac{k_0'}{k_0}\left(\frac{m}{2\pi\hbar^2}\right)^2 L^6 \sum_i |H_{ii}|_i^2 \varrho_i\,\mathrm{d}E_0'\,\mathrm{d}\Omega\,, \tag{7}$$

where E_0' is the energy of the scattered particle and ϱ_i is the density of final states of the i-th nucleon. In order to obtain reasonable results we must take into account that the nucleus is far from being « transparent »; at this energy the nucleus is about completely « black », and it is transparent only near the surface. We remark that if only one of the elementary interactions experienced by the extra nucleon changes its state, the potential inelastic scattering is completely masked by direct interactions. We must take into account only nucleons which traverse the nucleus without changing its state; so we have limited the integrals in (6) at the rim of the nucleus; here we have taken a potential of the type:

$$f(r > R) = R\exp[\alpha R]\frac{\exp[-\alpha r]}{r}\,.$$

(7) now becomes:

$$\sigma_R(E_0', \vartheta)\,\mathrm{d}E_0'\,\mathrm{d}\Omega = \tag{8}$$

$$= \frac{k_0'}{k_0}\left(\frac{m}{2\pi\hbar^2}\right)^2 \frac{V_r^2}{A} R^2 \exp[2\alpha R]\,F(E_0', R, \vartheta) \sum_i \left|\int_R^\infty \varphi_i^{(f)*}\frac{\exp[-\alpha r_i]}{r_i}\varphi_i^{(i)}\,\mathrm{d}\tau_i\right|^2 \varrho_i\,\mathrm{d}E_0'\,\mathrm{d}\Omega\,,$$

where

$$F(E_0', R, \vartheta) = \left|\int_R^\infty \exp[i(\boldsymbol{k}_0 - \boldsymbol{k}_0')\cdot\boldsymbol{x}_0]\frac{\exp[-\alpha r]}{r}\,\mathrm{d}\tau\right|^2.$$

The angular distribution is given by $F(E_0', R, \vartheta)$, and it would be the same also if the peak at $-Q \cong 2.5$ MeV in the energy spectrum would be due to a single level and not to a group of levels; however in such a case the difficulties in explaining the regularities of the peak are the same as remarked before. We now assume that the energy spectrum is of the type required, and we will see how the angular distribution of the peak results. We have taken: $R = r_0 A^{\frac{1}{3}}$ with $r_0 = 1.14 \cdot 10^{-13}$ cm, which is a reasonable value, since R is not really the radius of the nucleus, but a shorter one; $\alpha = 0.9 \cdot 10^{-13}$ cm^{-1}, equal for every nucleus, which is in agreement with the values obtained in the experiments on nuclear radii ([4]) (however the value of α is not very critical). Fig. 1 shows the angular distribution of the peak at $-Q = 2.3$ MeV in Ag. Fig. 2 shows the position of the maxima of the angular distribution versus A;

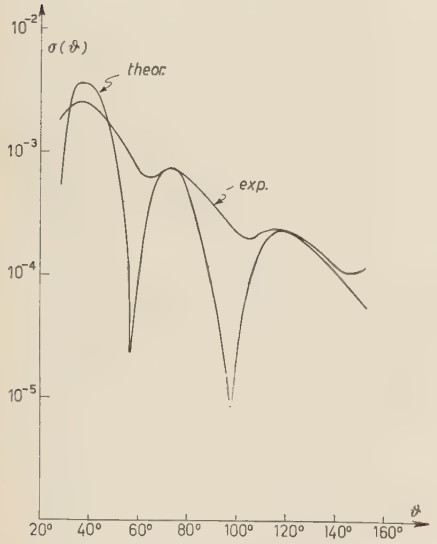

Fig. 1. – Differential cross-section of the peak at $-Q = 2.3$ MeV in Ag. The ordinates are in arbitrary units. The experimental curve is taken from reference ([1]).

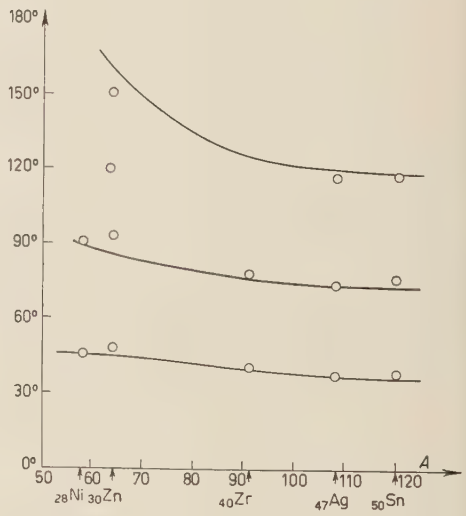

Fig. 2. – Maxima of the angular distributions of the peak at $-Q \simeq 2.5$ MeV versus A. The lines are evaluated; the circles are experimental ([1]).

two nuclei with $Z < 40$ are included, Zn ($-Q = 2.99$) and Ni ($-Q = 3.06$); however in such two lighter nuclei the peak could arise from the excitation of single levels with other types of interaction: in Zn there is an experimental maximum at 120° not foreseen, while in Ni the second maximum is higher

([4]) R. HOFSTADTER: *Rev. Mod. Phys.*, **28**, 214 (1956).

than the first one, and this result is not explained by the present model. In Zr a maximum at 130° could be masked, since the maxima are not very sharp, and $\sigma(\vartheta)$ is flat from 120° to 150°. Clearly such discrepancies could arise from the crudeness of the approximations made.

$F(E_0', R, \vartheta)$ is also an oscillating function of R; therefore one foresees that the peak at $-Q \cong 2.5$ MeV must disappear in nuclei with $\sim 150 < A < \sim 180$, it must reappear in nuclei with $A > \sim 180$, and it must disappear again in heavier nuclei. In fact in the experimental results the peak disappears in Ta an W, it reappears smooth in Pt and Au, it is very sharp in Pb and Bi, it is smoother in Th, and finally it disappears in U.

4. – Energy spectra and total cross-sections.

If we want to determine the energy spectrum of the inelastically scattered protons, we must assume a model for the nucleus, i.e. we must write the wave functions of the nucleons in the nucleus. The nucleons which are excited are near the surface of the nucleus, where the potential decreases sharply; therefore they have low kinetic energy, and we simply assume that initially they have zero energy; for the final state we take a plane wave.

Now we must take into account the pairing energy, which binds in a pair two nucleons on the same level; when a nucleon of a pair jumps into an excited level, an energy is necessary equal to the pairing energy in order to loose the pair, so that in the final state the nucleon will have an energy lower than that given to it by the extra nucleon. The pairing energy, for nuclei with mass close to each other, is quite independent of the type of nucleus; for instance in an odd nucleus the unpaired nucleon has no pairing energy, but its contribution is small in comparison with the contribution of the other nucleons. The nucleons near the surface of the nucleus have a great angular momentum, so that their pairing energy is large; it can be of the order of $1.5 \div 2$ MeV. Now (8) becomes:

$$\sigma_R(E_0', \vartheta)\,\mathrm{d}E_0'\,\mathrm{d}\Omega = \frac{24 m^3 V_T^2 R^3}{\pi \hbar^6 A}\,\frac{k_0'}{k_0}\,\frac{(y\sin x_0 + x_0\cos x_0)^2}{x_0^2(x_0^2+y^2)^2}\cdot \frac{(y\sin x + x\cos x)^2}{x(x^2+y^2)^2}\,\mathrm{d}E_0'\,\mathrm{d}\Omega\,, \tag{9}$$

where: $y = \alpha R$; $x_0 = R\sqrt{k_0^2 + k_0'^2 - 2k_0k_0'\cos\vartheta}$; $x = R(2m/\hbar^2)^{\frac{1}{2}}(E_0 - E_0' - E_p)^{\frac{1}{2}}$; E_0 is the energy of the incident nucleon and E_p is the pairing energy. Fig. 3 shows the energy spectra at 90° to the incident beam, for three nuclei. Besides the peak at $-Q \cong 2.5$ MeV, there is another maximum smoother and lower than the first one; this second maximum has been marked with an arrow in

Fig. 3. In the experimental results it appears such a small maximum overlapped to the smooth spectrum due to other types of interaction; probably this maximum is not due to fluctuations, since it appears in all the nuclei. It can look strange that good results are obtained with very rough approximations; however we point out that at least the sharp first peak is not very dependent on the form of the wave functions. In fact the overlapping of the initial and of the final wave functions diminishes quickly as far as the energy in the final state is very different from the energy in the initial state; the sharpness of the peak is obtained essentially neglecting the Pauli principle. If all the nucleons of the nucleus were interested in the process, the small energy losses should be strongly inhibited by the Pauli principle, since the nucleons which are at the bottom of the energy distribution in the initial state, cannot jump into the lowest excited levels; for instance if we consider a very large nucleus, i.e. if we assume that the wave functions of the nucleons are plane waves, the maximum in the energy spectrum would be at about $-Q = 10$ MeV. However near the surface of the nucleus there are nucleons which are near the top of the energy distribution, so that the Pauli principle is really ineffective in our case.

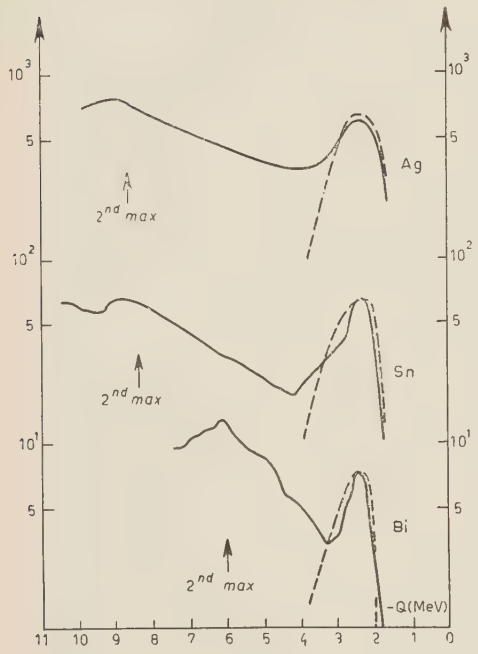

Fig. 3. – Energy spectra at 90° to the incident beam; full lines are experimental (1), broken lines are calculated; the arrows mark the position of the second calculated maximum. The ordinates are in arbitrary units.

The potential inelastic scattering could be responsible for the whole spectrum of $-Q < 4$ MeV; many nuclei show two peaks in this energy range: the first one at $-Q \cong 2.5$ MeV and the second one at $-Q \cong 3$ MeV; this splitting could be due to a difference in the pairing energy for protons and neutrons.

By integrating (9) we obtain the total cross-section; it results slowly decreasing as R increases. We have taken $V_r = 40$ MeV, which is the value one obtains from elastic scattering experiments (5). The integrated cross-

(5) See for instance: P. C. Gugelot: *Physica*, **22**, 1019 (1956).

section for $-Q < 4$ MeV varies from 20 mb for Zr to 16 mb for Te. If we take only the peak at $-Q \cong 2.5$ MeV the experimental values oscillate between ~ 10 mb and ~ 16 mb; while if we take the whole spectrum with $-Q < 4$ MeV, we have values oscillating between ~ 20 mb and ~ 24 mb.

If we neglect the variation of the nuclear transparency, the total cross-section is proportional to V_r^2/E_0; however the nuclear transparency varies with the energy. At $E_0 - 100$ MeV the cross-section is 12 mb, for a mean nucleus completely transparent, and taking plane waves as wave functions, while it is 2 mb for a nucleus transparent only near the surface.

5. – Conclusions.

The potential inelastic scattering seems to explain well the anomalous scattering of 23 MeV protons. We have completely neglected Coulomb effects: in mean nuclei the height of the Coulomb barrier is about one half the energy of the protons, so that one may expect that the main characteristics of the process do not change; however in the heaviest nuclei Coulomb effects could be very important. An effect of Coulomb forces should be a dispersion of the particles, so that minima and maxima in the angular distribution should become smoother and the agreement between experimental and theoretical results should improve.

In the energy spectrum of 18 MeV protons inelastically scattered by many nuclei ([6]) there is a peak with a loss of energy of about $2 \div 3$ MeV; this effect must be the same as for 23 MeV protons.

The potential inelastic scattering must appear also in the scattering of other particles, but the experimental results are not refined enough to make comparisons. For π-mesons the effect must be very small at energies lower than 15 MeV, since for these energies V_r is very small; the effect must appear at higher energies.

* * *

I wish to thank Prof. G. Puppi for discussions on the argument of this paper.

([6]) P. C. Gugelot: *Phys. Rev.*, **93**, 425 (1954).

RIASSUNTO

Si mostra che esiste uno scattering anelastico di ogni tipo di particella da parte di nuclei complessi, dovuto essenzialmente alla perturbazione causata dalla particella incidente sul potenziale globale sentito dai nucleoni nel nucleo. Una particella che entra in un nucleo ed esce senza essere catturata determina un aumento o una diminuzione del potenziale globale, durante il breve tempo in cui essa è dentro al nucleo: ne consegue che il nucleo può compiere una transizione in un livello eccitato. Si mostra che lo scattering anelastico anomalo dei protoni di 23 MeV (e di 18 MeV) deve essere dovuto ad un tale tipo di eccitazione; sono ben spiegate tutte le caratteristiche qualitative del processo, e, nonostante si siano usate approssimazioni molto grossolane, anche i risultati quantitativi concordano.

Urto nucleare elastico di positroni da 2 MeV in argon.

C. Giori e C. Succi

Istituto di Scienze Fisiche dell'Università - Milano
Istituto Nazionale di Fisica Nucleare - Sezione di Milano

(ricevuto il 18 Agosto 1957)

Riassunto. – La deflessione nucleare elastica a grande angolo in argon è stata studiata con una camera a diffusione. In circa 5475 m di traccia utilizzata si sono osservate 580 deflessioni con angolo proiettato maggiore od uguale a 20°; particolare cura è stata rivolta alla determinazione dello spettro vero d'energia delle tracce prese in considerazione. Il confronto tra i dati sperimentali e quelli teorici, ottenuto applicando il metodo della traccia proiettata ha messo in evidenza un buon accordo con la distribuzione angolare delle deflessioni prevista dalle teorie quantistiche.

1. – Introduzione.

Lo scattering nucleare elastico di elettroni e positroni è stato studiato sperimentalmente da molti autori impiegando come strumenti di rivelazione sia contatori sia camere di Wilson. A causa delle notevoli difficoltà connesse con la sperimentazione, i dati racolti con entrambe le tecniche sono piuttosto incerti, e nel caso di esperimenti eseguiti con camere di Wilson assolutamente insufficienti per poter trarre conclusioni definitive.

Avendo sperimentato l'efficacia della camera a diffusione in tale tipo di ricerca, ci è sembrato interessante impiegare questo strumento per studiare con statistica ampia ed in una regione di energia non eccessivamente bassa, lo scattering nucleare elastico dei positroni in gas.

La presente ricerca avente lo scopo di confrontare i dati che si ottengono sperimentalmente con quelli ricavabili mediante le formule di Rutherford [1]

[1] E. Rutherford: *Phil. Mag.*, **21**, 669 (1911).

e di MOTT (2) nell'approssimazione di MASSEY (3) e di MCKINLEY e FESHBACH (4), è stata eseguita impiegando come sorgente il ^{66}Ga che emette positroni di 4.14 MeV di energia massima.

2. – Considerazioni sulla raccolta dei dati.

La probabilità che un positrone dotato di velocità βc in un mezzo di numero atomico Z, contenente N nuclei per cm^3 venga deflesso in un cm di percorso di un angolo compreso tra θ e $\theta + d\theta$ è espressa dalla formula:

$$P(\theta, \beta)\, d\theta = N \left(\frac{Ze^2}{2m_0c^2}\right)^2 \frac{1-\beta^2}{\beta^4} F(\theta, \beta) 2\pi \sin\theta\, d\theta\,, \tag{1}$$

con

$$F(\theta, \beta) = \operatorname{cosec}^4 \frac{\theta}{2}, \tag{2}$$

secondo RUTHERFORD, e

$$F(\theta, \beta) = \operatorname{cosec}^4 \frac{\theta}{2} \cdot \left[1 - \beta^2 \sin^2 \frac{\theta}{2} - \frac{\pi Z \beta}{137} \sin \frac{\theta}{2} \left(1 - \sin \frac{\theta}{2}\right)\right], \tag{3}$$

secondo MOTT (nell'approssimazione di MCKINLEY e FESHBACH).

I risultati che si ricavano dalla (1), sia nell'espressione di Rutherford sia in quella di Mott, non sono direttamente confrontabili con quelli che si ricavano dall'esame dei fotogrammi che contengono le tracce dei positroni: si è perciò deciso di ricorrere al metodo della traccia proiettata (5-7), che, con l'aggiunta della condizione della lunghezza critica (8,9), oltre permettere di trasformare le (1) (2) e (3), in formule direttamente utilizzabili, rende superflua la ricostruzione stereoscopica di tutte le tracce e perciò più spedita l'esecuzione delle misure.

Il numero di deflessioni da aspettarsi tra 20° e 90°, in intervalli angolari di 10° gradi di ampiezza, per diversi valori dell'energia, calcolato trasformando con il metodo sopracitato le formule di Rutherford e Mott (nell'approssima-

(2) N. F. MOTT: *Proc. Roy. Soc.*, A **124**, 425 (1929).
(3) H. S. W. MASSEY: *Proc. Roy. Soc.*, A **181**, 14 (1942).
(4) W. A. MCKINLEY jr. e H. FESHBACH: *Phys. Rev.*, **74**, 1759 (1948).
(5) F. OPPENHEIMER: *Phys. Rev.*, **54**, 310 (1938).
(6) R. B. RANDELS, K. T. CHAO e H. R. CRANE: *Phys. Rev.*, **68**, 64 (1945).
(7) C. O'CEALLAIGH e M. D. MCCARTHAIGH: *Proc. Roy. Irish Acad.*, A **50**, 13 (1945).
(8) F. C. BARKER: *Journ. Scient. Instr.*, **25**, 65 (1948).
(9) C. O'CEALLAIGH: *Proc. Roy. Irish Acad.*, A **53**, 33 (1950).

zione di McKinley e Feshbach) è riportato nella tabella I. I dati sono stati normalizzati a 1000 m di traccia.

Nel presente lavoro la disposizione sperimentale ed il metodo di lettura dei fotogrammi sono praticamente gli stessi già usati da Lovati e Succi [10] nella misura dello scattering nucleare elastico di elettroni: qui particolari precauzioni sono state prese per evitare che i quanti gamma emessi dal ^{66}Ga investissero la camera riducendone la sensibilità.

I fotogrammi raccolti sono circa 24500 e contengono 38118 tracce di positroni aventi raggio di curvatura compreso tra 25 cm e 65 cm, ed una lunghezza complessiva di 7762 m; sono state conteggiate 580 deflessioni elastiche con angolo $N > 20°$, nelle quali la lunghezza della traccia prima e dopo l'evento era maggiore di 3 cm.

Tabella I. – *Numero di deflessioni da attendersi secondo le teorie di Rutherford e di Mott, per diversi intervalli angolari e diverse energie. Le cifre in carattere tondo si riferiscono ai dati della teoria di Rutherford, quelle in neretto ai dati di Mott.*

	20°-30°	30°-40°	40°-50°	50°-60°	60°-70°	70°-80°	80°-90°
1 MeV	235.3 **208.2**	73.2 **60.8**	30.3 **23.4**	15.0 **10.7**	8.47 **5.47**	5.25 **2.85**	3.51 **1.80**
1.5 MeV	121.2 **106.7**	37.7 **31.3**	15.6 **12.0**	7.76 **5.50**	4.36 **2.81**	2.70 **1.45**	1.80 **0.92**
2 MeV	77.4 **68.1**	24.1 **19.8**	10.0 **7.30**	4.96 **3.43**	2.79 **1.74**	1.72 **0.88**	1.15 **0.55**
2.5 MeV	51.0 **44.5**	15.8 **12.9**	6.58 **4.46**	3.26 **2.22**	1.83 **1.12**	1.13 **0.56**	0.76 **0.35**
3 MeV	38.1 **33.5**	11.8 **9.75**	4.91 **3.40**	2.43 **1.69**	1.37 **0.86**	0.85 **0.43**	0.56 **0.27**
3.5 MeV	28.3 **24.7**	9.3 **7.74**	3.89 **2.82**	1.93 **1.35**	1.08 **0.68**	0.67 **0.35**	0.45 **0.22**
4 MeV	23.2 **20.3**	7.2 **5.90**	3.00 **2.12**	1.48 **1.02**	0.83 **0.51**	0.51 **0.26**	0.34 **0.16**

Applicando il criterio della lunghezza critica di traccia e le correzioni necessarie per tenere conto della presenza del vapore dell'alcool in seno all'argon, la lunghezza utile di traccia è risultata di 5475 m; nessuna correzione è stata

[10] A. Lovati e C. Succi: *Nuovo Cimento*, **2**, 1224 (1955).

apportata al numero totale di deflessioni per tenere conto del contributo dei componenti dell'alcool perchè questa è risultata inferiore all'1%.

Per eseguire la presente ricerca sono stati impiegati in totale circa 6 millicurie di radiogallio fornito dalla Philips-Roxane di Amsterdam in quattro spedizioni per via aerea, ciascuna delle quali era sufficiente per circa 60 ore di lavoro.

3. – Determinazione dello spettro vero dei positroni conteggiati.

Per poter effettuare correttamente il confronto fra i dati raccolti sperimentalmente e quelli teorici è necessario conoscere lo spettro vero dei positroni, le cui tracce sono state utilizzate ai fini della misura; d'altra parte la curvatura vera delle particelle introdotte nella camera è alterata dallo scattering multiplo coulombiano e non è in generale facile risalire dallo spettro delle curvature misurate, allo spettro delle curvature vere.

Per ovviare a questa difficoltà un metodo corretto consiste: 1) nell'adottare una disposizione sperimentale che permetta di introdurre nella camera i positroni senza alterare lo spettro emesso dalla sorgente e, 2) nel valutare con buona approssimazione l'effetto dei tagli che si devono operare nello spettro delle tracce raccolte per escludere quelle che, essendo di energia troppo bassa o troppo alta, si presentano con curvatura mal rilevabile.

Lo spettro di positroni del ^{66}Ga, alterato per effetto dello scattering multiplo coulombiano prodotto dal gas della camera è stato ricavato procedendo nel modo seguente:

a) dallo spettro dei positroni emessi dal ^{66}Ga, ottenuto da Langer e Moffat ([11]) si è ricavato l'istogramma di Fig. 1, che dà il numero di tracce in funzione del loro raggio di curvatura vera prodotta dal campo magnetico in cui la camera è immersa;

b) facendo uso della formula di Williams ([12]), si è calcolato lo spettro di curvatura che deriva, per effetto dello scattering multiplo coulombiano, da ogni singolo elemento dell'istogramma precedente;

c) sommando gli spettri ottenuti si è ricavato lo spettro di curvatura dei positroni del ^{66}Ga quando attraversano il gas della camera.

La Fig. 2) illustra graficamente il procedimento seguito. Nella Fig. 3) questo spettro viene confrontato con l'istogramma che dà, per le tracce utilizzate

([11]) L. M. Langer e R. D. Moffat: *Phys. Rev.*, **80**, 651 (1950).
([12]) E. J. Williams: *Phys. Rev.*, **58**, 292 (1940).

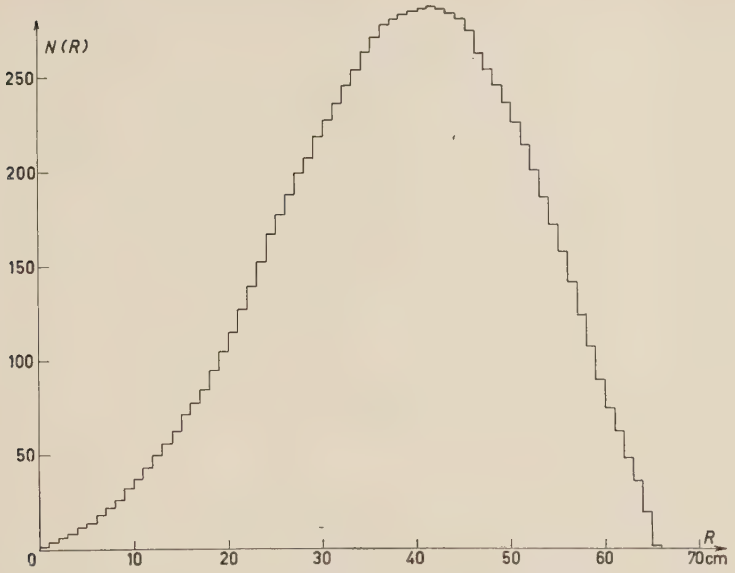

Fig. 1. – Numero di positroni emessi dal ^{66}Ga in funzione del raggio di curvatura in un campo magnetico di $B = 250$ gauss. Le ordinate sono in unità arbitrarie.

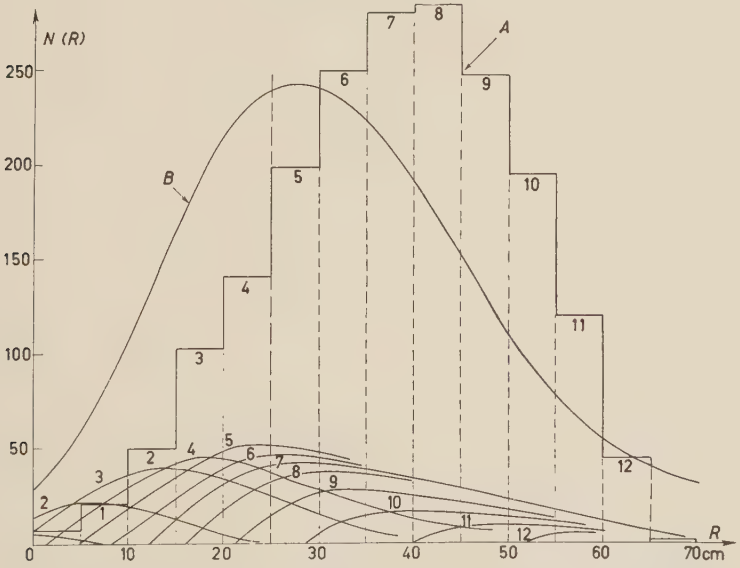

Fig. 2. – Determinazione dello spettro apparente dei positroni del ^{68}Ga. Curva A, istogramma vero (equivalente a quello di Fig. 1). Curve 1, 2, 3, ..., spettri apparenti derivati per effetto dello scattering multiplo dagli elementi 1, 2, 3, ... dell'istogramma A. Curva B, spettro delle curvature apparenti.

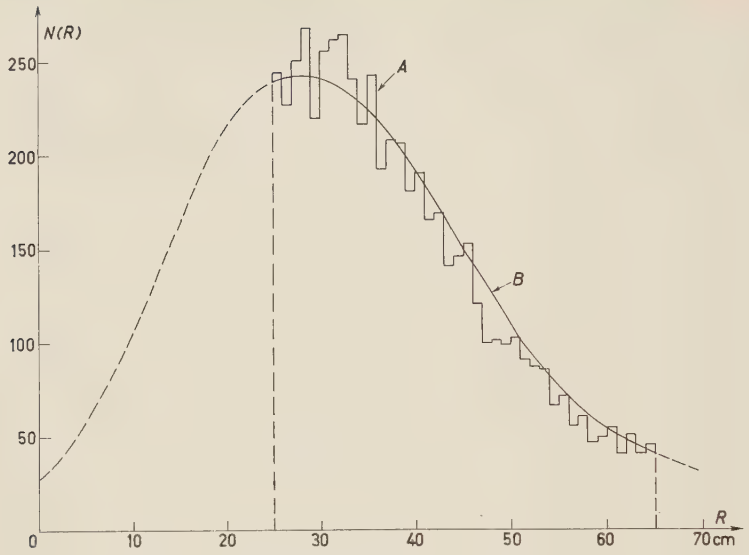

Fig. 3. – Confronto tra l'istogramma sperimentale delle curvature dei positroni conteggiati (curva A), e lo spettro delle curvature apparenti (curva B).

Fig. 4. – Istogramma delle curvature vere dei positroni conteggiati.

ai fini della presente misura, la loro distribuzione in funzione della curvatura misurata sui fotogrammi: come si può constatare l'accordo è soddisfacente.

Dal diagramma B di Fig. 2, è facile rilevare che in prossimità dei valori di $R = 25$ cm ed $R = 65$ cm dei raggi di curvatura, la dispersione dovuta allo scattering multiplo fa si che tracce aventi raggi veri compresi tra 25 cm

e 65 cm risultino, nello spettro disperso esterne a questo intervallo, mentre tracce aventi raggi veri, rispettivamente maggiori di 25 cm e minori di 65 cm, risultino interne.

Il procedimento ora schematizzato permette anche di determinare la composizione di ogni elemento dello spettro di curvatura apparente (Fig. 2, curva *B*) e perciò di valutare l'effetto dei tagli operati nello spettro delle tracce contenute nei fotogrammi. L'istogramma dei positroni le cui tracce sono state impiegate per eseguire le misure, è stato ricavato numericamente ed è mostrato in Fig. 4; l'energia media è risultata di 2.02 MeV.

4. – Risultati sperimentali e confronto con la teoria.

Per determinare correttamente il numero di deflessioni da aspettarsi secondo la teoria di Rutherford e di Mott, per la lunghezza totale di traccia utilizzata, è necessario conoscere, oltre l'andamento dell'istogramma delle curvature, anche la lunghezza delle tracce di ogni elemento dell'istogramma stesso.

Poichè nel nostro caso la lunghezza media delle tracce misurate varia con regolarità da 19 cm, per quelle di raggio 25 cm, a 22 cm, per quelle di raggio 65 cm, l'errore che si commette, assumendo come lunghezza di ogni traccia il valore medio della lunghezza media delle tracce di uguale curvatura, risulta assai piccolo.

Il numero totale di deflessioni da aspettarsi secondo RUTHERFORD e MOTT, in ogni intervallo angolare di 10° di ampiezza, per la lunghezza totale di traccia utilizzata è riportato nella Tabella II insieme ai risultati sperimentali.

TABELLA II.

	20°-30°	30°-40°	40°-50°	50°-60°	60°-70°	70°-80°	80°-90°	20°-90°
RUTHERFORD	392.94	123.95	51.39	24.61	14.36	8.88	5.92	622.05
MOTT	345.10	101.82	38.69	16.80	8.95	4.89	2.85	519.10
Sperimentali	397	109	41	15	9	6	3	580

Nella Tabella III, con i risultati delle precedenti esperienze eseguite con camere a nebbia e diffusori gassosi, sono riportati i valori dei rapporti R_R ed R_M, tra il numero totale di deflessioni osservate e quelle da aspettarsi secondo le teorie.

TABELLA III.

	Energia MeV	Elemento	Angolo di deflessioni	Lunghezza traccia m	Numero deflessioni	R_E	R_M
HOWATSON e ATKINSON [13]	0.7	A	20°-90°	163	65.5	0.79	0.92
CUSAK [14]	0.3	N	$\geqslant 20°$	146	114	—	0.63
ROY e GROVEN [15]	0.53-0.98	N	15°-85°	712	85	—	0.97
Presente lavoro	2.02	A	20°-90°	5475	580	0.93	1.12
»	2.02	A	30°-90°	5475	183	0.80	1.05
»	2.02	A	40°-90°	5475	74	0.70	1.02
»	2.02	A	50°-90°	5475	33	0.61	0.98

5. – Conclusioni.

Come si può rilevare dalla Tabella II, l'accordo tra i dati sperimentali e quelli previsti dalla teoria di Mott, se si eccettua l'intervallo angolare $20° \div 30°$, è soddisfacente.

Si può osservare che il numero di deflessioni relative a questo intervallo risulta sovrastimato perchè: 1) si riferisce a misure eseguite prevalentemente su tracce di bassa energia, e perciò maggiormente influenzate dallo scattering multiplo, e, 2) perchè l'osservatore, preoccupato di non omettere deflessioni di poco superiori di 20° finisce col conteggiarne anche molte di quelle inferiori.

Nella regione relativa alle deflessioni $\geqslant$ a 30°, il buon accordo con la teoria di Mott è confermato dalla costanza del rapporto R_M relativo ai vari intervalli angolari, cosicchè, pur non volendo sottolineare eccessivamente il fatto che il valore di R_M risulti tanto prossimo all'unità, si può ritenere che l'importanza dei termini che esprimono il contributo dello spin del positrone nella collisione nucleare elastica, sia sufficientemente dimostrata.

* * *

È nostro gradito dovere ringraziare il Prof. G. POLVANI ed il Prof. P. CALDIROLA per il vivo interesse mostrato alla presente ricerca.

Siamo vivamente grati al Dott. R. ATTARDO ed alla Dott. G. MARCAZZAN, ed ai Sig. G. GENNARO e B. NICOLAI per l'aiuto prestatoci durante l'esecuzione delle misure.

([13]) A. F. HOWATSON e J. R. ATKINSON: *Phil. Mag.*, **42**, 1136 (1951).
([14]) N. CUSAK: *Phil. Mag.*, **63**, 671 (1952).
([15]) R. R. ROY e L. GROVEN: *Phys. Rev.*, **87**, 619 (1952).

Sentiti ringraziamenti vogliamo pure rivolgere all'I.N.F.N., agli Amici dell'Istituto ed all'A.N.I.D.E.L. per gli aiuti finanziari accordatici.

SUMMARY

The nuclear elastic scattering of the positrons of energy about 2 MeV has been analysed by means of a diffusion cloud chamber. A total length of 7 762 m was measured in about 24 500 photographs. The total number of scatterings $\geqslant 20°$ is 580 with 183 deflections greater than 30°. The comparision between experimental and theoretical data obtained by applying the methode of the projected tracks, has put in evidence a good agreement with the angular distribution of scattering as predicted by the quantum theories.

Sugli impulsi prodotti dai raggi cosmici nei fotomoltiplicatori.

U. Amaldi jr.

Istituto di Fisica dell'Università - Roma (*)
Istituto Nazionale di Fisica Nucleare - Sezione di Roma

(ricevuto il 10 Giugno 1957)

Riassunto. — Gli impulsi prodotti in un fotomoltiplicatore (Dumont 6291) dalle particelle ionizzanti veloci della radiazione cosmica vengono studiati con un dispositivo di coincidenza, analizzandone la distribuzione in ampiezza in diverse condizioni sperimentali. Il contributo dell'effetto Čerenkov nel vetro della finestra viene messo nettamente in evidenza sfruttando le sue caratteristiche direzionali. L'ampiezza media di un impulso Čerenkov è di ~ 5 fotoelettroni. Viene valutato un limite superiore per l'eventuale contributo di un meccanismo di scintillazione e discusso un possibile contributo di estrazione diretta di elettroni dal fotocatodo e dai dinodi.

1. – Introduzione.

L'origine degli impulsi che si osservano all'uscita di un fotomoltiplicatore (FM) al buio è tutt'ora poco conosciuta. La distribuzione degli impulsi osservati non è interpretabile unicamente in termini delle fluttuazioni statistiche della emissione termoionica del catodo e della moltiplicazione secondaria sui dinodi: essa infatti risulta troppo ricca di impulsi grandi (corrispondenti, per esempio, a più di 5 elettroni in partenza dal catodo) [1].

Indirettamente connesso con la questione precedente è il fatto osservato da molti autori, che due fotomoltiplicatori affacciati e al buio presentano un numero di impulsi di coincidenza molto superiori a quello calcolabile per le coincidenze casuali [2-5]. Le interpretazioni che sono state finora avanzate

(*) Attualmente presso il Laboratorio di Fisica dell'Istituto Superiore di Sanità.
(1) I. Pelchowitch: *Rev. Scient. Instr.*, **26**, 470 (1955).
(2) F. N. Hayes, R. D. Hiebert e R. L. Scuch: *Science*, **116**, 140 (1952).
(3) B. N. Audric e J. V. P. Long: *Journ. Scient. Instr.*, **30**, 467 (1953).
(4) Y. Koechlin, I. Pelchowitch e A. Rogozinski: *Compt. Rend.*, **238**, 660 (1954).
(5) E. M. Baker e B. M. Tolbert: *Rev. Scient. Instr.*, **25**, 1218 (1954).

per quest'ultimo fenomeno sono: *a*) eccitazione di atomi dei dinodi, per effetto del bombardamento elettronico, con successiva emissione di luce raccolta dai catodi di entrambi i FM affacciati ([2]); *b*) scintillazioni prodotte nel vetro della finestra dei FM dalle particelle β emesse dal ^{40}K radioattivo contenuto nel vetro stesso ([3,4]); *c*) scintillazioni nel vetro della finestra di un FM prodotte dalle particelle dei raggi cosmici e viste da entrambi i FM ([5]).

In nessuno dei lavori citati è stata eseguita una analisi diretta dalla distribuzione in ampiezza degli impulsi di coincidenza; è chiara invece l'importanza di un simile studio sia per la identificazione dei diversi meccanismi, sia per la determinazione del loro contributo alla distribuzione degli impulsi singoli di un FM, e in particolare alla coda di impulsi grandi a cui si è accennato. In particolare, l'unico lavoro in cui viene preso in esame l'effetto dei raggi cosmici è quello di BAKER e TOLBERT ([5]); ma dai loro risultati, mancando una analisi dettagliata delle distribuzioni in ampiezza, si può soltanto dedurre una indicazione qualitativa sulla esistenza di questo effetto.

È sembrato perciò utile eseguire uno studio più accurato degli impulsi che vengono provocati in un FM attraversato da una particella ionizzante veloce della radiazione cosmica, avendo particolarmente in mente due distinti meccanismi di produzione di luce nel vetro della finestra del FM: *a*) effetto Čerenkov, *b*) scintillazione (con costante di tempo dell'ordine di 10^{-6} s o inferiore).

I risultati ottenuti (con un FM Dumont 6291) mettono in evidenza il contributo del meccanismo di emissione di luce Čerenkov, e suggeriscono la presenza di un contributo minore, ma non del tutto trascurabile, del meccanismo di scintillazione. I risultati relativi agli «impulsi Čerenkov» sono immediatamente estendibili a qualsiasi altro tipo di FM a catodo frontale, e, data la relativamente grande ampiezza media, possono risultare di notevole importanza nelle applicazioni dei FM in dispositivi di coincidenza.

2. – Dispositivo sperimentale.

Le particelle ionizzanti dei raggi cosmici incidenti sulla finestra del fotomoltiplicatore in esame (FM_1) vengono identificate mediante l'impulso che

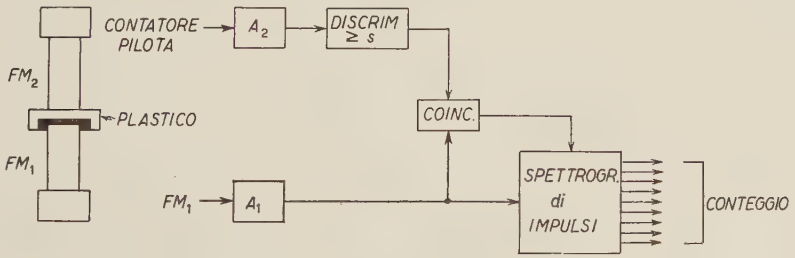

Fig. 1.

esse producono in un contatore (pilota) sovrapposto alla finestra stessa. Il contatore pilota è costituito da un disco di plastico fluorescente (spessore 5 cm) avvolto in un involucro di stagnola e dal fotomoltiplicatore FM_2, a contatto ottico col plastico (fig. 1). La finestra di FM_2 e il plastico fluorescente costituiscono così un largo telescopio per raggi cosmici, il cui asse è disposto

verticalmente. FM_1 è accuratamente protetto dalla luce proveniente dal contatore pilota, ed entrambi sono rinchiusi in una scatola a tenuta di luce. Una schermatura di Pb, dello spessore di almeno 5 cm da ogni lato, protegge il dispositivo dalla parte più molle della radiazione cosmica e dalla radioattività delle pareti del laboratorio.

Gli impulsi di FM_1 (costante di tempo di uscita $1.1 \cdot 10^{-6}$ s) convenientemente amplificati da A_1 (tempo di salita $7 \cdot 10^{-8}$ s) vengono analizzati in ampiezza mediante uno spettografo di impulsi (del tipo descritto da GATTI (6)) il cui funzionamento è comandato dalla coincidenza fra gli impulsi di FM_1 e quelli del contatore pilota. Il circuito di coincidenza ha un tempo risolutivo $2\tau = 2.4 \cdot 10^{-6}$ s.

Le misure sono state eseguite con diversi valori per la soglia S di accettazione degli impulsi del contatore pilota. Le distribuzioni degli impulsi FM_1 che saranno discusse nel seguito sono state ottenute con una soglia S_0 che garantiva un rendimento del contatore pilota prossimo al 100% per particelle al minimo di ionizzazione attraversanti il telescopio in direzione verticale, ma al tempo stesso escludeva la quasi totalità degli impulsi di ampiezza inferiore a $\frac{1}{3}$ della ampiezza media(*). Le distribuzioni ottenute con valori di S minori di S_0 sono (a parte un piccolo fattore di intensità) assai simili a quelle qui discusse, fino a valori di S pari a circa 1/10 S_0.

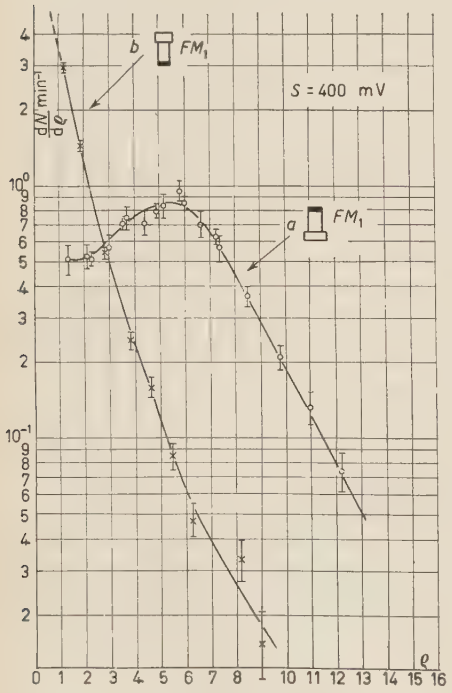

Fig. 2.

3. – Risultati sperimentali.

Le misure eseguite consistono nella determinazione delle distribuzioni differenziali in ampiezza degli impulsi di coincidenza di FM_1 in diverse condizioni sperimentali. Tali disposizioni sono state scelte avendo presente la direzionalità della luce prodotta per effetto Čerenkov in confronto con l'isotropia della luce di scintillazione, ed il fatto che il flusso dei raggi cosmici è concentrato attorno alla verticale rivolta verso il basso.

1) La superficie del vetro della finestra è resa completamente assorbente per la luce mediante applicazioni di un disco di velluto nero a contatto ottico con il vetro stesso.

a) FM_1 guarda verso l'alto (fig. 2, curva *a*)

b) FM_1 guarda verso il basso (fig. 2, curva *b*)

( ) E. GATTI: *Nuovo Cimento*, **11**, 153 (1954).

(*) La distribuzione differenziale in ampiezza degli impulsi di coincidenza del *contatore pilota* mostra un massimo molto pronunciato.

2) La superficie del vetro della finestra è resa riflettente mediante deposito di uno strato di argento.

a) FM_1 guarda verso l'alto fig. (3, curva *a*)

b) FM_1 guarda verso il basso (fig. 3, curva *b*).

Le ampiezze degli impulsi sono espresse in funzione del numero ϱ di elettroni in partenza dal catodo, determinato, a partire dalla ampiezza V all'uscita del fotomoltiplicatore, in base a misure dirette del guadagno G e della capacità C di uscita dal fotomoltiplicatore ($\varrho = VC/eG$ dove e è la carica dell'elettrone); l'errore massimo stimato su ϱ è del 3%. Gli errori sulle frequenze (che sono stati individualmente corrette dal contributo delle coincidenze casuali) rappresentano gli errori statistici di conteggio (standard deviation).

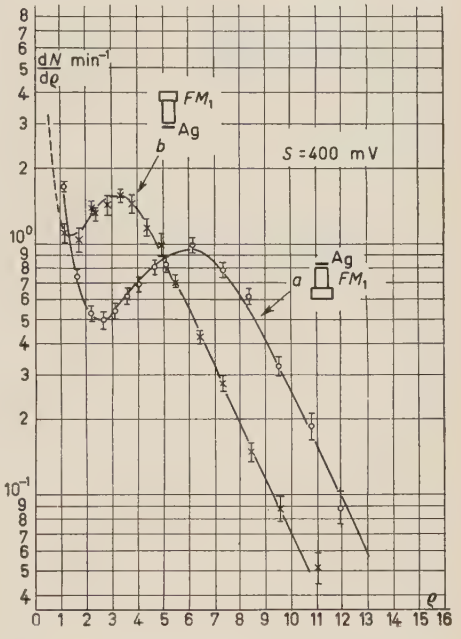

Fig. 3.

4. – Discussione.

Le distribuzioni ottenute si prestano a una immediata e semplice interpretazione. I massimi delle curve 2*a* e 3*a* sono dovuti alla luce di Čerenkov prodotta nel vetro in direzione della superficie fotosensibile dalle particelle ionizzanti veloci che attraversano la finestra. Il numero dei fotoelettroni corrispondente al massimo è in ottimo accordo con quello che si può calcolare dalla teoria dell'effetto Čerenkov, dalle caratteristiche del vetro della finestra e dal rendimento fotocatodico medio, per una particella relativistica verticale: 80 fotoni circa nei 3 mm di vetro d'indice di rifrazione 1,5, e quindi di 5 fotoelettroni con un rendimento fotocatodico del 6%.

Il massimo della curva *b* della fig. 3 è dovuto alla medesima luce di Čerenkov riflessa verso il fotocatodo dal deposito di argento; la distribuzione osservata è coerente con la 3*a* per un coefficiente di riflessione del 65%. Quest'ultimo è un valore ragionevole se si tien conto dello spettro di emissione Čerenkov, dalla curva di risposta del fotocatodo e del fatto che il deposito di argento realizzato non era molto spesso.

Nella disposizione corrispondente alla distribuzione *b* della fig. 2 la luce di Čerenkov è completamente assorbita dal disco di velluto nero applicato sulla finestra e il massimo scompare. Rimane tuttavia una distribuzione di impulsi di coincidenza, anche di ampiezza notevole, non attribuibile a coincidenze casuali. Ciò indica che, oltre l'effetto Čerenkov, esiste almeno un altro meccanismo attraverso il quale le particelle dei raggi cosmici possono produrre impulsi in un FM. Si può cercare di identificare questo meccanismo con una scin-

tillazione prodotta nel vetro delle stesse particelle responsabili della curva $2a$. Occorre allora tener conto del fatto che all'ampiezza degli impulsi della $2a$ contribuisce anche circa il 50% dei fotoni eventualmente emessi per scintillazione, mentre all'ampiezza degli impulsi della $3a$ contribuiscono, oltre alla luce di Čerenkov direttamente incidente sul deposito sensibile del fotocatodo: *a*) una frazione della luce di scintillazione maggiore che nel caso precedente, a causa della riflessione sulla superficie argentata (circa l'80% anzichè il 50%); *b*) quella frazione della luce di Čerenkov che, riflessa sulla superficie interna della finestra (su cui è depositato il fotocatodo), veniva completamente assorbita dal disco di velluto nero nel caso precedente, mentre ora può essere rinviata verso il catodo attraverso una nuova riflessione sulla superficie esterna argentata (o, eventualmente, più riflessioni successive).

Ci si attende, pertanto, una traslazione della curva $3a$ rispetto alla $2a$, dalla cui entità si potrebbe stimare, in linea di principio, il contributo relativo della luce di scintillazione e della luce Čerenkov. Una tale traslazione è effettivamente rilevabile dalle fig. 2 e 3. Tenendo conto delle osservazioni precedenti e di una possibile lieve variazione del guadagno del FM (le due distribuzioni sono state rilevate a distanze di circa due settimane l'una dall'altra) abbiamo valutato un limite superiore per il rapporto tra il numero totale dei fotoni emessi per scintillazione e il numero totale di fotoni emessi per effetto Čerenkov da una particella ionizzante dei raggi cosmici: esso risulta, per il FM impiegato, pari a circa 0,2.

Per chiarire l'origine degli impulsi della distribuzione $2b$ abbiamo eseguito la seguente misura ausiliaria. Dalla finestra di un FM Dumont 6364 non funzionante è stato ricavato un disco di vetro dello spessore di circa 5 mm che è stato sovrapposto, in contatto ottico, alla finestra di FM_1 e ricoperto col solito disco di velluto nero. La distribuzione degli impulsi di coincidenza di FM_1 ottenuti in queste condizioni e nella disposizione schematizzata in fig. 4 è rappresentata dalla curva $4a$, mentre la curva tratteggiata riproduce la $2b$. I punti sperimentali intorno a questa ultima curva rappresentano il risultato di una nuova misura, eseguita immediatamente dopo la determinazione della $4a$, nelle stesse condizioni in cui era stata ottenuta la $2a$; l'ottimo accordo delle due serie di misure dà affidamento circa la loro attendibilità. Il confronto tra le due distribuzioni $4a$ e $2b$ indica che, mentre un effetto di scintillazione del vetro è certamente presente, esso non è sufficiente a spiegare tutta l'ampiezza degli impulsi osservati (si noti che lo spessore del vetro, presumibilmente dello stesso tipo, è stato più che raddoppiato).

Un altro possibile meccanismo attraverso il quale i raggi cosmici possono produrre impulsi in un FM è l'estrazione diretta di elettroni dal fotocatodo e dai dinodi. Questo meccanismo potrebbe essere responsabile sia di parte della ampiezza degli impulsi della $2b$ e della $4a$ (principalmente per estrazione dal catodo) sia dell'andamento della $2a$ e della $3a$ per $\varrho < 2 \div 3$ (per estrazione dai dinodi da parte di particelle che attraversano il contatore pilota lateralmente e colpiscono i dinodi di FM_1 senza attraversare la finestra).

Per quel che riguarda le frequenze assolute, l'integrale della distribuzione di impulsi Čerenkov, calcolato con una ragionevole estrapolazione a zero del massimo della curva $2a$ dà circa 5.5 impulsi al minuto. Il numero di particelle che attraversano il telescopio è stato determinato direttamente sostituendo alla finestra di FM_1 un secondo, sottile contatore a scintillazione. Se ne può dedurre per FM_1 considerato come un contatore di Čerenkov con una

soglia equivalente a 3 elettroni dal catodo, un rendimento del 60% e un «anti-rendimento» (7) del 10%.

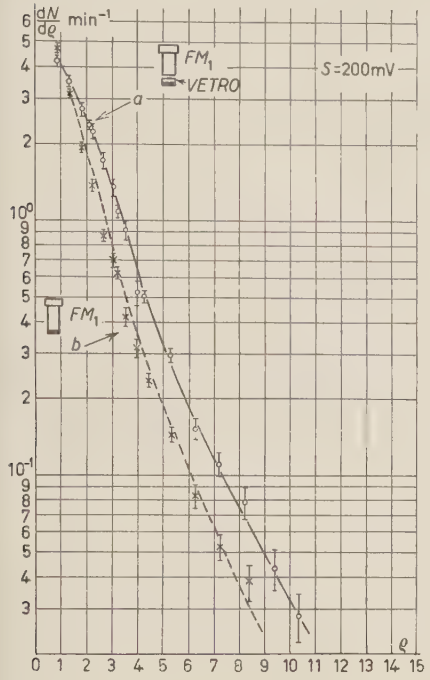

Fig. 4.

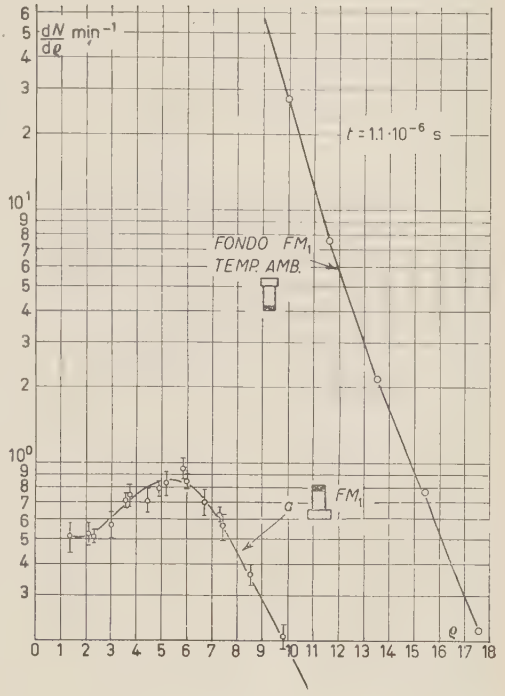

Fig. 5.

Il contributo dei raggi cosmici alla distribuzione degli impulsi singoli che si osservano all'uscita di un fotomoltiplicatore al buio risulta, dunque, nettamente identificabile ma quantitativamente assai piccolo. A titolo d'esempio, nella fig. 5 la distribuzione $2a$ è messa a confronto con la determinazione degli impulsi singoli dello stesso fotomoltiplicatore (a temperatura ambiente). Una discussione più precisa non ci sembra possibile sulla base dei risultati ottenuti, anche perchè la distribuzione degli impulsi singoli dipende criticamente dalla scelta della costante di tempo di uscita t del fotomoltiplicatore (al contrario delle distribuzioni degli impulsi di coincidenza). La curva di fig. 5 è stata ottenuta con $t=1.1\cdot10^{-6}$ s.

* * *

Vivamente ringrazio il prof. L. Mezzetti per avermi suggerito l'argomento del presente lavoro e per avermi continuamente assistito e guidato con critiche e discussioni durante tutto il suo svolgimento. Sono grato anche al prof. B. Ri-

(7) M. Mandò: *Nuovo Cimento*, **12**, 5 (1954).

SPOLI per avermi prestato lo spettrografo d'impulsi da lui costruito e messo a punto e per gli utili consigli.

SUMMARY

The pulses produced in a photomultiplier (Dumont 6291) by the traversal of the fast ionizing particles of the cosmic radiation has been studied by means of a coincidence arrangement, through careful analysis of the pulse height distributions obtained in various conditions. The contribution of the Čerenkov effect in the glass of the window has been clearly established through its directional properties. The average pulse height of a Čerenkov pulse is ~ 5 photoelectrons. An upper limit for the contribution of isotropic scintillation is evaluated, and the possible contribution of the mechanism of direct extraction of electrons from the photocathode and the dynodes is discussed.

Effacement des alpha dans les plaques Ilford C 2.

S. Deutsch (*) et E. Picciotto

Laboratoire de Physique Nulcéaire, Université Libre de Bruxelles

(ricevuto il 18 Luglio 1957)

Summary. — The fading of α-particle tracks in Ilford C 2 emulsions has been studied. After irradiation by an alpha source, the photographic plates were stored in air, at various temperatures for a period of four months. They were then compared with a standard plate which had been developed immediately after irradiation. Amongst the plates stored at — 35 °C no particle track fading was noticed, neither was a diminution in the number of tracks. Amongst those plates stored at 4 °C and at 15 °C, the grain density of the particle tracks had lessened and respective percentage losses of 38 % and 72 % in the number of tracks were noticed.

La technique de mesure des activités α la plus sensible est actuellement celle des émulsions nucléaires. La sensibilité de cette méthode est limitée par le phénomène d'effacement de l'image latente (fading) au cours du temps. Ce phénomène peut introduire des erreurs considérables lors de la mesure des activités faibles nécessitant des temps d'exposition de l'ordre de quelques semaines ou quelques mois.

Les influences de divers facteurs: température, humidité et nature de l'atmosphère ambiante, pH de la gélatine, sur le fading de divers types d'émulsions ont été étudiées par plusieurs auteurs [1].

Une température et une humidité basse, et l'absence d'oxygène diminuent l'effet du fading. La plupart des auteurs ont évalué cet effet en mesurant la variation de l'espacement ou du nombre de grains dans des traces de même énergie, après conservation de plaques irradiées pendant des temps croissants,

(*) Chercheur à l'Institut Interuniversitaire des Sciences Nucléaires.

(1) G. P. S. Occhialini, et C. F. Powell: *Nature*, **159**, 186 (1947); J. La Palme et P. Demers: *Phys. Rev.*, **72**, 536 (1947); H. Yagoda et N. Kaplan: *Phys. Rev.*, **71**, 910 (1947); G. Albouy et H. Faraggi: *Journ. Phys. et Rad.*, **10**, 105 (1949); E. Picciotto: *Compt. Rend.*, **228**, 247 (1949); G. Leide: *Ark. f. Fysik*, **11**, 329 (1956).

dans des conditions déterminées. Ce type d'estimation est justifié dans le cas de la mesure des grandeurs qui dépendent de la densité de grains.

Dans le cas de la mesure des radioactivités α d'échantillons solides, le pourcentage de perte d'α à l'observation doit être pris comme critère du fading. La seule étude dans ce sens a été faite par R. COPPENS [2]: il a utilisé, soit une source de pechblende pulvérisée, soit une source de polonium, mais ses expériences ne portent que sur des temps de conservation d'au maximum 12 jours, à divers degrés d'humidité, les températures variant de 14 à 50 °C. Dans ces conditions, il trouve un effacement déjà considérable en 12 jours, dans les émulsions Ilford C 2.

Dans le cadre de la mesure de l'activité α de météorites métalliques [3], on a étudié le fading des α dans des plaques Ilford C 2, conservées pendant 122 jours, non recouvertes, à l'air, en l'absence de dessèchant et à diverses températures.

Quatre plaques ont été exposées pendant 10 min à la même source de pechblende. La diffusion du radon hors de la source peut amener une faible fluctuation du nombre d'α émis pendant ce temps.

Une plaque témoin a été immédiatement développée pendant 15 min à 20° dans le révélateur suivant:

Amidol	0.88 g
Sulfite de sodium	1.8 g
Bromure de potassium à 10%	2 cm³
pour 100 cm³ d'eau.	

Ces conditions correspondent à un développement relativement poussé, comme le montre la Fig. 1.

Les autres plaques ont été conservées pendant 122 jours, dans les conditions indiquées au tableau ci-dessous, puis développées ensemble comme la plaque témoin.

Les Figs. 1, 2, 3, 4 montrent l'apparence des traces dans les diverses plaques. Les α de la plaque *A* sont identiques à ceux du témoin; par contre, les α des plaques *B* et *C* montrent des effets croissants de fading par la diminution de leur longueur et de leur densité de grains, qui rendent leur comptage incertain.

Les résultats des comptages des α encore identifiables de chacune des 4 plaques sont donnés dans le tableau suivant:

Plaques	$t°$ de conservation	Humidité relative en % de l'air ambiant	Nombre d'α	% des traces restantes
témoin	—	—	2 350	100
A	— 35°	0	2 450	~ 100
B	4°	50 %	1 450	62
C	15°	50 %	650	28

[2] R. COPPENS: *Compt. Rend.*, **227**, 61 (1948).

[3] S. DEUTSCH, F. HOUTERMANS et E. PICCIOTTO: *Nature* (1957) (à paraître).

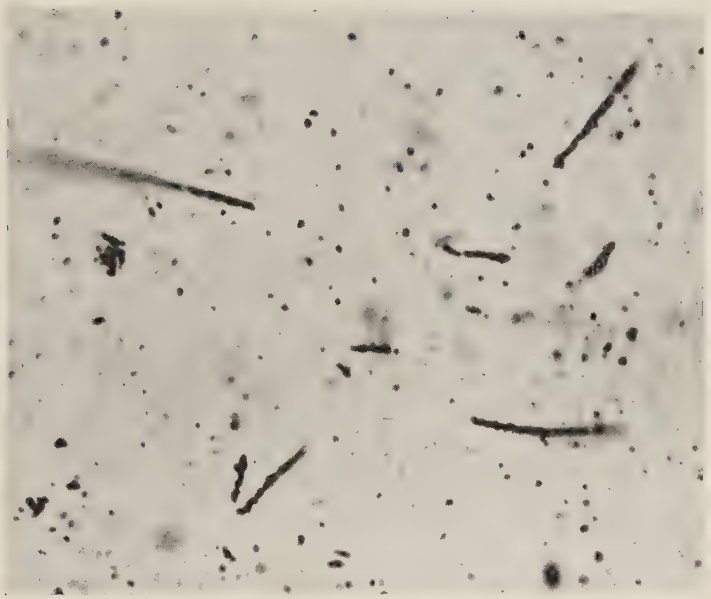

Fig. 1. – Alpha de la pechblende dans la plaque témoin Ilford C-2.

Fig. 2. – Alpha dans une plaque conservée à — 35 °C pendant 122 jours.

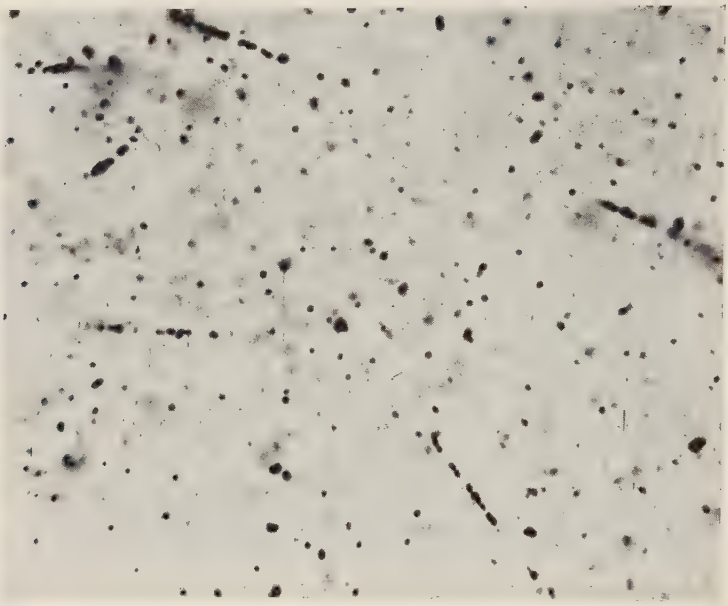

Fig. 3. – Alpha dans une plaque conservée à 4 °C pendant 122 jours.

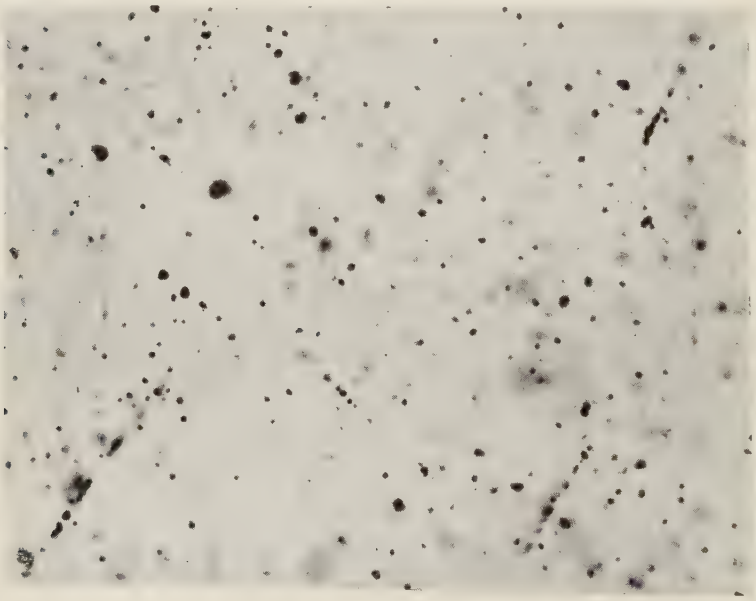

Fig. 4. – Alpha dans une plaque conservée à 15 °C pendant 122 jours.

Il faut remarquer que les conditions d'irradiation sont particulièrement sévères. Lors de la mesure d'activité α d'échantillons solides sur plaques photographiques (conservées dans les mêmes conditions), le pourcentage d'α perdu sera plus faible. En effet, les α d'un échantillon sont émis durant toute l'exposition, et ainsi soumis en moyenne, pendant un temps plus court, aux agents causant le fading. De plus, la plaque photographique est recouverte par l'échantillon, et ainsi, moins accessible à l'oxygène de l'air.

La conservation à 4° permet de compter encore 60% au moins des traces enregistrées, celle à 15° supprime plus de 70% des traces.

On voit qu'à — 35° C, les plaques Ilford C 2 peuvent être conservées au moins 4 mois sans trace d'effacement.

Ces conditions nous ont permis de mesurer des activités de l'ordre de $5 \cdot 10^{-7}$ $\alpha/cm^2 \cdot s$. La diminution de l'humidité de l'atmosphère ambiante ou la conservation des plaques en atmosphère inerte permettra sans doute, même à 4°, d'éviter le fading pendant des temps aussi longs.

RIASSUNTO (*)

Si è studiata l'evanescenza delle tracce di particelle α nelle emulsioni Ilford C2. Dopo irradiazione con una sorgente α, le lastre furono conservate in aria, a varie temperature, per un periodo di quattro mesi. Furono poi confrontate con una lastra campione sviluppata immediatamente dopo l'irradiazione. Nelle lastre conservate a — 35 °C non fu riscontrata alcuna evanescenza nè diminuzione del numero di tracce. Nelle lastre conservate a 4 °C e a 15 °C la densità di grani delle tracce delle particelle è diminuita e furono osservate delle diminuzioni percentuali del numero di tracce rispettivamente del 38% e del 72%.

(*) *Traduzione a cura della Redazione.*

Neutron Yield Functions for the Nucleonic Component of Cosmic Radiation.

R. R. Brown

Department of Physics, University of California - Berkeley, Cal.

(ricevuto il 26 Luglio 1957)

Summary. — In view of recent proposed changes of cosmic ray geomagnetic co-ordinates and primary spectra, calculations have been made to determine if the yield function for the nucleonic component of cosmic radiation introduced by Fonger is in need of revision. As a result of these calculations, a modified form of Fonger's yield function is proposed for calculations with the revised spectra and co-ordinate system. The implications of this modification for the spectra of solar flare radiation are considered.

1. – Introduction.

In analysing the results of investigations of the intensity of cosmic radiation obtained with local neutron production monitors [1], it has been found that intensity variations as functions of geomagnetic latitude λ, atmospheric depth x and time t may be described in terms of the incident primary spectra and a yield function, which gives the production rate of disintegration neutrons at an atmospheric depth x resulting from unit flux of primary radiation of atomic number Z and kinetic energy per nucleon E. In particular, for neutron monitors located deep in the atmosphere, the observed neutron intensity has been shown to be proportional to

$$I_v(\lambda, x, t) = \sum_Z \int_{E_Z(\lambda,t)}^{\infty} S_Z(E, x) j_Z(E, t)\, \mathrm{d}E\,, \tag{1}$$

[1] J. A. Simpson, W. H. Fonger and S. B. Treiman: *Phys. Rev.*, **90**, 934 (1953).

where I_v is the neutron intensity at λ, x and t resulting from vertically incident primary particles with differential energy spectra $j_z(E, t)$ and $E_z(\lambda, t)$ is the vertical cut-off energy per nucleon due to the geomagnetic field.

In applying this expression to problems, it is convenient to separate the yield function into a product of two functions ([2]), one which depends on the mass number A of primary particles of charge Z, the other which depends on the kinetic energy per nucleon E of the incident particles and the depth in the atmosphere x:

$$S_Z(E, x) = k_Z S(E, x) , \tag{2}$$

where $k_Z = A$. Physically, this assumes that the binding of nucleons in primary nuclei is unimportant at cosmic ray energies and that following the break-up of heavy nuclei high in the atmosphere, the individual nucleons proceed downward to produce effects deeper in the atmosphere. Thus, we have

$$I_v(\lambda, x, t) = \sum_Z k_Z \int_{E_Z(\lambda,t)}^{\infty} S(E, x) j_Z(E, t)\, dE . \tag{3}$$

Fonger ([2]), in studying the energy dependence of the 27-day intensity variations, introduced an empirical yield function of the following form:

$$\begin{cases} S(E, 680) = 0 , & E < E_0, \\ S(E, 680) = C \ln [(1 + E)/(1 + E_0)] , & E > E_0, \end{cases} \tag{4}$$

where $E_0 = 0.83$ GeV, E is the kinetic energy per nucleon of the primary particles and C is a constant. This function was obtained by fitting the latitude curve for neutron monitors ([3]) at 680 g/cm² atmospheric depth with Eq. (3). The primary differential spectra used in this calculation were those given by Kaplon *et al.* ([4]):

$$j_1(E) = \frac{4\,280}{(1 + E)^{2.07}} \text{ (protons)} ,$$

$$j_2(E) = \frac{540}{(1 + E)^{2.35}} \text{ (alphas)} ,$$

$$j_7(E) = \frac{27}{(1 + E)^{2.35}} \text{ (C, N, O)} ,$$

$$j_{12}(E) = \frac{11}{(1 + E)^{2.35}} \quad (Z \geqslant 10) ,$$

([2]) W. H. Fonger: *Phys. Rev.*, **91**, 351 (1953).

([3]) J. A. Simpson and W. C. Fagot: *Phys. Rev.*, **90**, 1068 (1953).

([4]) M. F. Kaplon, B. Peters, H. L. Reynolds and D. M. Ritson: *Phys. Rev.*, **85**, 295 (1952).

where the units are particles per m²-sr-s with kinetic energy per nucleon E. Since the yield function was proposed by FONGER, measurements of the location of the cosmic ray geomagnetic equator and the geomagnetic effects for α-particles and heavy nuclei have led to the conclusion that the conventional geomagnetic coordinate system, based on surface magnetic field measurements, is not the proper system to use in studying cosmic ray phenomena. Thus, from an analysis of cosmic ray data from two recent equatorial crossings, as well as earlier measurements, SIMPSON *et al.* [5] have proposed that the correct system of coordinates is obtained by shifting westward the inclined magnetic dipole of the earth by about $40 \div 45°$, the inclination of the dipole remaining essentially unchanged. This shift of the geomagnetic equator changes the coordinates of cosmic ray monitors over the earth and in so doing, partly explains the anomalous results from emulsion studies of α-particles and heavy nuclei.

Recently, SINGER [6] has made geomagnetic corrections to experimental data obtained earlier, as well as a detailed study of albedo contributions to balloon and rocket experiments. As a result, Singer proposes that there is a significant difference in the spectrum exponents for primary radiation, i.e. the velocity spectra of heavy primary particles are not identical, and suggests that the following spectra apply in the latitude sensitive region:

$$j_1(E) = \frac{4\,600}{E_t^{2.15}} \quad \text{(protons)},$$

$$j_2(E) = \frac{736}{E_t^{2.6}} \quad \text{(alphas)},$$

$$j_7(E) = \frac{80}{E_t^{3.0}} \quad \text{(C, N, O, F)},$$

$$j_{12}(E) = \frac{69}{E_t^{3.3}} \quad (Z \geqslant 10),$$

where the units are particles per m²-sr-s with total energy per nucleon E_t.

In view of these results, it is of interest to reexamine the fit of latitude curves derived using Fonger's yield function with experimental data. In addition, it is important to determine if a revision of the yield function is necessary since estimates of the spectra of direct and scattered flare radiation have been based on this function.

In the following sections the results of calculations are given which indicate, in view of the changes in geomagnetic coordinates and primary spectra, that the yield function is in need of revision. A modified form of Fonger's yield function is proposed and results of further calculations are given to show the improvement obtained with this new function. In addition, the implications of this modification for the spectra of solar flare radiation are considered.

---

[5] J. A. SIMPSON, K. B. FENTON, J. KATZMANN and D. C. ROSE: *Phys. Rev.*, **102**, 1648 (1956).

[6] S. F. SINGER: *Progress in Elementary Particles and Cosmic Ray Physics* (New York, 1957), vol. **4**.

2. – Calculations.

The neutron latitude curve at 680 g/cm^2 atmospheric depth reported by SIMPSON and FAGOT ([3]) was used in studying the fit of calculated latitude variations obtained with different trial functions. These data are given in Table I, where the different monitor counting rates are expressed relative to the Huancayo monitor. In addition, the geomagnetic coordinates and proton cut-off momenta for these stations (Huancayo, Mexico City, Sacramento Peak, Climax and Chicago), as calculated by PFOTZER ([7]) using both the conventional eccentric dipole and the westward shifted eccentric dipole models, are given in Table I.

TABLE I.

		Conventional eccentric dipole		Westward shifted eccentric dipole	
	Relative counting rate	Latitude	Cut-off (GeV/c)	Latitude	Cut-off (GeV/c)
Huancayo	1.00	— 1°	13.6 (*)	— 3.6°	13.8 (*)
Mexico City	1.52	29°	11.8 (*) 8.75 (+)	30.5°	10.4 (*) 8.4 (+)
Sac. Peak	2.08	42°	4.66 (+)	44.3°	4.16 (+)
Climax	2.46	48°	3.24 (+)	50.3°	2.70 (+)
Chicago	2.54	53°	2.23 (+)	53°	2.24 (+)

(*) Values related to the main cone.
(+) Values related to the Störmer cone.

In carrying out the calculations, the differential spectra proposed by SINGER and the yield function developed by FONGER were substituted in Eq. (3). The integrands in Eq. (3), weighted according to $k_z = A = 2Z$, are shown in Fig. 1; the cut-off energies for each station based on the conventional eccentric dipole system, as calculated from PFOTZER's paper ([7]), are indicated by vertical lines in Fig. 1. The integrations were carried out by graphical methods from the cut-off energies of the primary components at each station to an energy of 20 GeV/nucleon; beyond that energy, the integrations were obtained

([7]) G. PFOTZER: *Proceedings of the 1957 IUPAP Cosmic Ray Conference*, in *Suppl. Nuovo Cimento* (in press).

by a combination of graphical and analytical methods after suitable approximations were made in the integrands in Eq. (3). The contributions of the heavy primary particles beyond 20 GeV/nucleon were neglected.

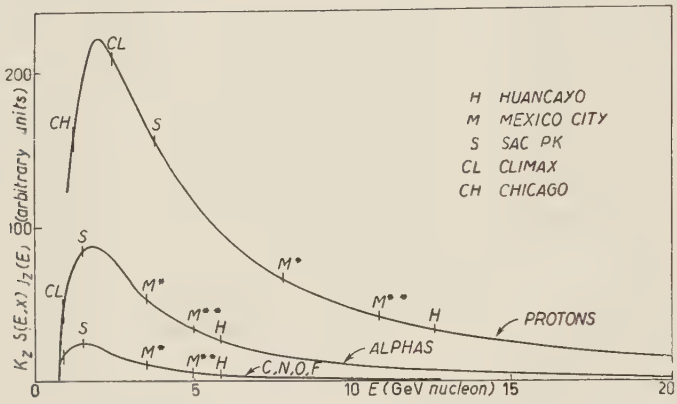

Fig. 1. - $k_z S(E, x) j_z(E)$ as a function of kinetic energy per nucleon for proton, α-particles and C, N, O, F, nuclei. Cut-off energies at each station are indicated by vertical lines and identified by appropriate symbols. (The curve for nuclei with $Z \geqslant 10$ has been omitted for the sake of clarity as it lies close to the C, N, O, F curve.)

There is some error introduced in carrying out the integrations for the proton and α-particle curves as the exponents in the primary spectra increase in magnitude at energies beyond the latitude sensitive region. Thus, the contributions of high energy protons and α-particles in Eq. (3) are overestimated; however, the error is about 3% for Huancayo and becomes smaller as stations at higher latitudes are considered. The error introduced by completely neglecting the high energy contributions of heavy nuclei is much smaller and of the opposite sign.

3. – Results.

The latitude variation derived, as outlined above, falls below the experimental curve for latitudes in the range $10° \div 35°$ and above the experimental curve in the range $40° \div 55°$. The calculations were repeated using the westward shifted dipole system. This resulted in bringing the calculated latitude variation into better agreement with the experimental curve for the lower latitude range; however, the fit of the calculated curve deteriorated at higher latitudes.

In view of these results, additional trial functions were used in the calculations. For the purpose of improving the fit of the calculated curve, trial functions were chosen in such a way as to reduce the contribution of low energy particles relative to that of particles of higher energy. The trial functions used differed from that due to Fonger by multiplicative factors and are given

below:

$$(7)\qquad \begin{cases} S'(E, 680) = 0\,, & E < E_0, \\ S'(E, 680) = C\left(\dfrac{E}{E + E_0}\right) \ln\left[(1 + E)/(1 + E_0)\right]\,, & E > E_0, \end{cases}$$

and

$$(8)\qquad \begin{cases} S''(E, 680) = 0\,, & E < E_0, \\ S''(E, 680) = C\left(\dfrac{E}{E + E_0}\right)^2 \ln\left[(1 + E)/(1 + E_0)\right]\,. & E > E_0, \end{cases}$$

The results obtained with these functions, as well as with Fonger's yield function, for both systems of coordinates are summarized in Table II.

TABLE II.

		Relative counting rates					
	Exp.	Conventional eccentric dipole			Westward shifted eccentric dipole		
Yield function	—	S	S'	S''	S	S'	S''
Huancayo (*)	1.00	1.00	1.00	1.00	1.00	1.00	1.00
Mexico City (*)	1.52	1.15	1.10	1.09	1.31	1.24	1.24
(+)	—	1.47	1.39	1.37	1.55	1.46	1.43
Sac. Peak (+)	2.08	2.22	2.04	1.92	2.36	2.18	2.04
Climax (+)	2.46	2.58	2.33	2.16	2.76	2.48	2.29
Chicago (+)	2.54	2.84	2.53	2.29	2.88	2.56	2.33

(*) Values related to the main cone.
(+) Values related to the Störmer cone.

4. – Discussion.

Inspection of Table II shows that the modified yield function S' gives the best over-all fit with the experimental latitude curve when combined with the westward shifted dipole and the revised primary spectra. In view of the modifications suggested by these calculations, it is of interest to consider the implications of this result for calculations of the spectra of flare radiation for the February 23, 1956 solar cosmic ray outburst.

In this connection, the calculation of the momentum spectrum of flare

radiation arriving directly in the 0400 local time impact zone from the sun depends on a comparison of the intensity increases at different latitudes due to particles of rather limited ranges of momenta. Thus, PFOTZER ([7]), by comparing the intensity increase at Stockholm due to protons with momenta in the range $2.3 \leqslant p \leqslant 3.1$ GeV/c with the intensity increase at Göttingen due to protons with momenta in the range $3.9 < p < 5.1$ GeV/c, finds a flare momentum spectrum with exponent $\gamma \simeq -3.6$. Replacing Fonger's yield function by the modified function S' results in an increase of the magnitude of γ of about 10% for the Stockholm-Göttingen calculation.

For the momentum spectrum of radiation scattered by interplanetary magnetic fields into regions outside the 0400 local time impact zone, PFOTZER ([7]) obtains an exponent $\gamma \approx -7$ by fitting the experimental data with a curve obtained by integrating Eq. (3) over a wide range of momenta. Replacing the yield function S by S' will result in increasing the magnitude of γ; however, the relative increase in the exponent should be greater in this case because of the wider range of momenta entering into this calculation.

* * *

The author is indebted to Dr. G. PFOTZER for providing copies of his manuscripts in advance of publication.

RIASSUNTO (*)

In vista di cambiamenti delle coordinate geomagnetiche e degli spettri primari dei raggi cosmici recentemente proposti si sono eseguiti calcoli per determinare se la funzione di rendimento per la componente nucleonica della radiazione cosmica introdotta da Fonger necessiti di una revisione. Come risultato di tali calcoli si propone una forma modificata della funzione di rendimento di Fonger da servire nei calcoli con gli spettri e i sistemi di coordinate modificati. Si prendono in considerazione le conseguenze di tale modificazione per gli spettri della radiazione dei flares solari.

(*) *Traduzione a cura della Redazione.*

Una nuova camera di Wilson di grandi dimensioni.

E. Fiorini. R. Giacconi (*) e C. Succi

Istituto di Scienze Fisiche dell'Università - Milano
Istituto Nazionale di Fisica Nucleare - Sezione di Milano

(ricevuto il 14 Agosto 1957)

Alla memoria di Antonino Mura

Riassunto. — Viene descritta una grande camera di Wilson avente un volume interno di oltre un metro cubo ed un volume illuminato di $120 \times 114 \times 50$ cm^3. La camera può contenere lastre di materiale fino ad un peso di alcune tonnellate; le sue caratteristiche sono tali che essa può venire impiegata sia nel campo della radiazione cosmica sia con grandi macchine acceleratrici. Le apparecchiature ausiliarie della camera sono state progettate in modo da consentire tanto il funzionamento normale quanto il funzionamento con surcompressione.

1. – Introduzione.

L'avvento delle grandi macchine acceleratrici, recentemente costruite in molti Stati, ha avuto l'effetto di ridurre notevolmente, nell'ambito delle energie raggiunte, l'importanza e lo sfruttamento dei raggi cosmici come sorgente di particelle ad alta energia. D'altra parte, poichè il limite massimo dell'energia raggiunta dalle particelle accelerate artificialmente non supera oggi i 10 GeV, i raggi cosmici costituiscono ancora l'unica sorgente utilizzabile per esperienze sulle interazioni di particelle con energia superiore.

Purtroppo, anche a quote di montagna, il flusso di queste particelle è estremamente basso così che, per raccogliere un numero sufficiente di eventi, si rendono necessarie apparecchiature estese e particolarmente efficienti.

Per poter estendere il campo delle ricerche già eseguite sulle interazioni nucleari ad alta energia, abbiamo costruito una camera di Wilson con dimensioni notevolmente superiori a quelle delle camere tradizionalmente impiegate.

(*) Dal 1° Settembre 1956 presso l'Istituto di Fisica dell'Università di Indiana, U.S.A.

La camera e le relative apparecchiature sono state progettate in modo che essa potesse venire impiegata sia nel campo della radiazione cosmica sia con grandi macchine acceleratrici.

Nella progettazione si è pertanto posta particolare attenzione ai problemi connessi con la semplicità delle strutture e dei comandi, la riduzione del tempo morto, la sicurezza di funzionamento e la possibilità di controllo a distanza.

La camera ha dimensioni d'ingombro $156 \times 156 \times 98$ cm^3, volume illuminato di $120 \times 114 \times 50$ cm^3 e può contenere fino a 25 lastre di materiale di un cm di spessore, per un peso massimo di 5 tonnellate.

2. – Struttura della camera.

La camera è stata realizzata con tre getti in Silumin, aventi uno spessore costante di 25 mm; le superfici interne sono state piallate e rettificate al decimo di millimetro presso le officine della Società Innocenti di Milano. I tre pezzi sono stati sottoposti, nel Laboratorio Prove Materiali del Politecnico di Milano, ad un accurato esame radiografico che non ha rivelato imperfezioni di rilievo.

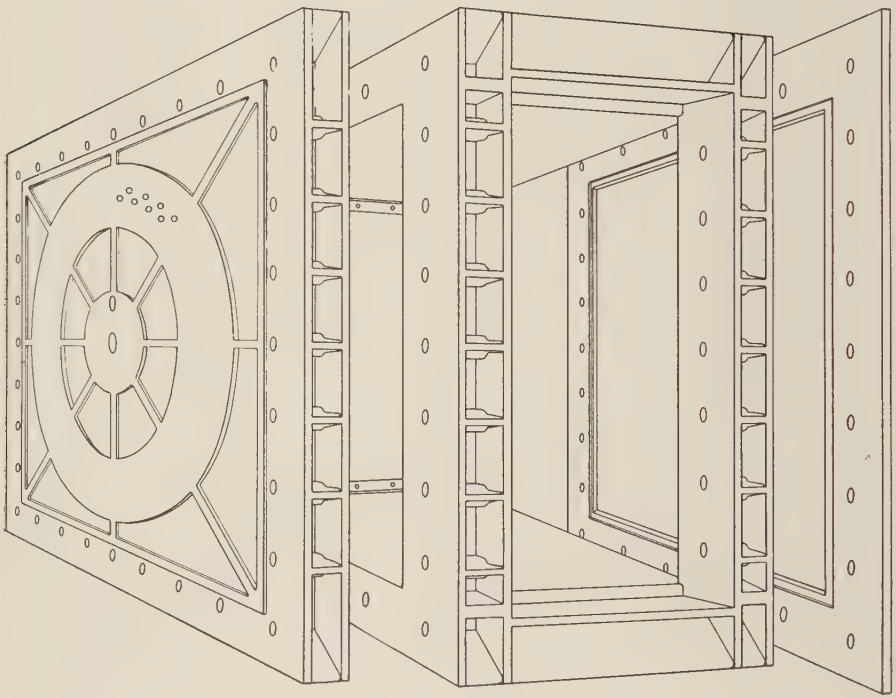

Fig. 1. – Assembramento delle tre parti della camera.

L'assembramento delle parti è mostrato nel disegno di Fig. 1; due fotografie della camera sono riportate nelle Fig. 2 e 3.

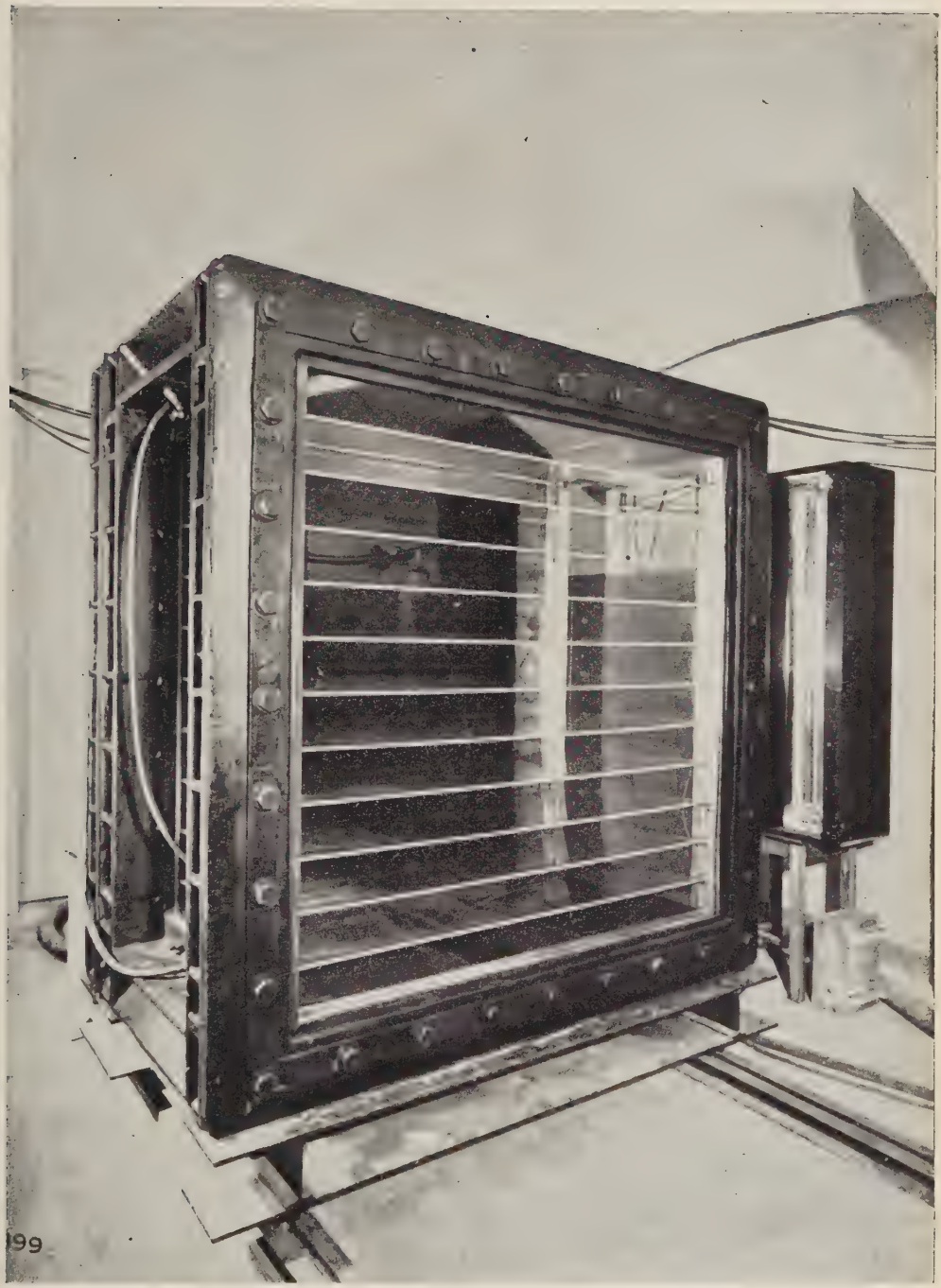

Fig. 2. – Vista anteriore della camera.

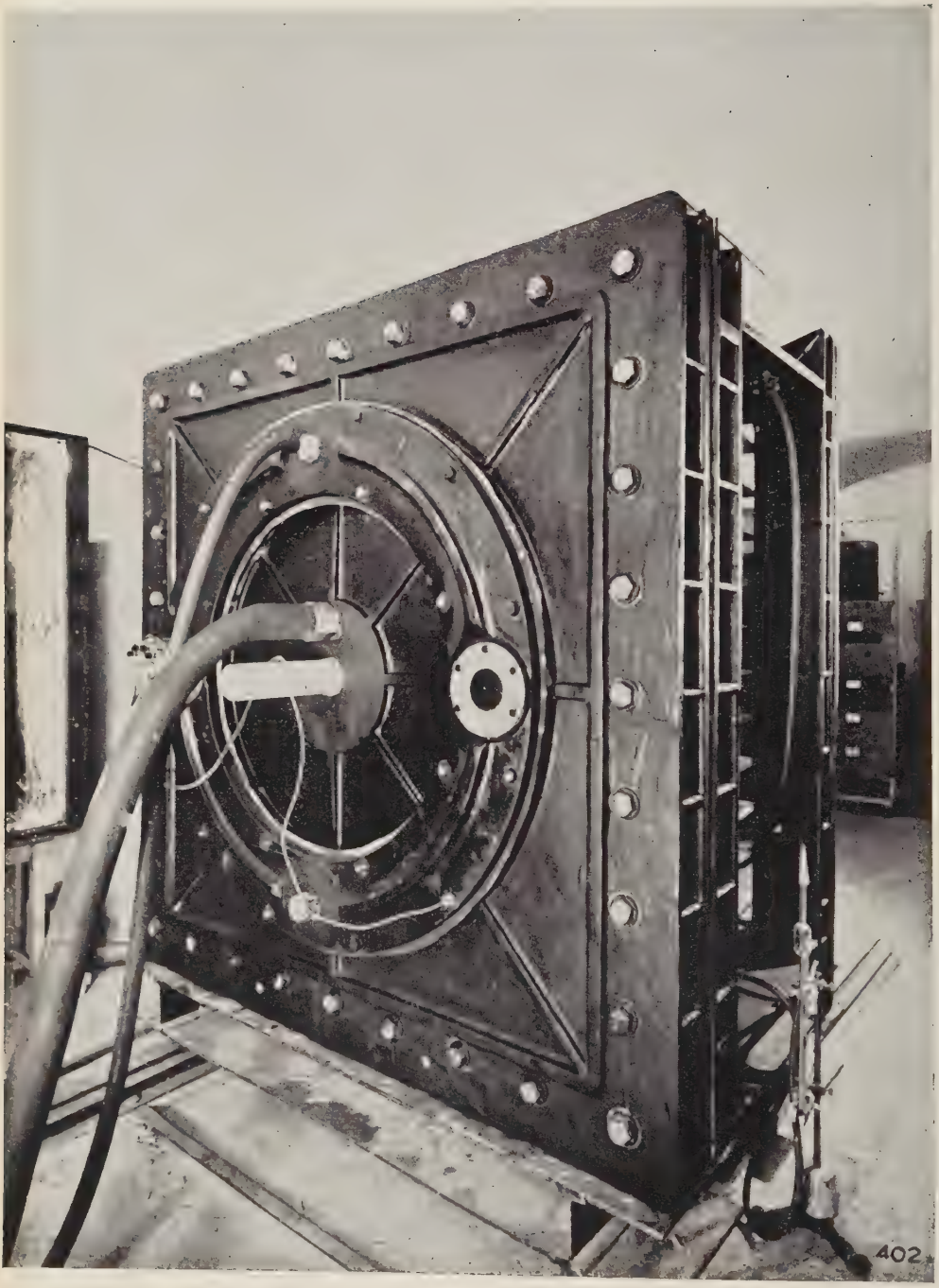

Fig. 3. – Vista posteriore della camera.

Il primo getto è costituito dalla cornice anteriore portavetro che ha una luce di 126×126 cm^2 e pesa circa 90 kg. Il secondo getto costituisce il corpo centrale della camera: la cornice è applicata a questo mediante 32 bulloni 20 MA di 15 cm di lunghezza.

Il corpo centrale della camera è costituito da due lastre piane collegate e rinforzate con grosse travature allegerite con cave in modo da garantire una buona riuscita della fusione; le pareti di separazione tra cava e cava sono state ingrossate per potervi praticare i fori filettati per l'avvitamento dei bulloni. Il peso del corpo centrale della camera, dopo la lavorazione meccanica, è risultato di circa 540 kg.

Il terzo getto, da cui è stato ricavato il fondo della camera, è costituito da una cornice quadrata, allegerita come le travature del corpo centrale, ed accecata da una lastra di 20 mm di spessore, nervata radialmente e munita di una piazzuola anulare di 35 mm di spessore nella quale sono ricavate due corone concentriche di 82 fori da 25 mm di diametro aventi in totale una superficie di circa 800 cm^2. L'intercapedine tra la cornice e la lastra di accecamento, profonda 13 cm, costituisce il retrocamera. Il fondo della camera è applicato al corpo centrale mediante 32 bulloni 20 MA di 24 cm di lunghezza; il suo peso è risultato di circa 320 kg.

Il vetro anteriore ed i vetri laterali sono stati ricavati da lastre di cristallo temperato Vis Securit di 17 mm di spessore, ed hanno rispettivamente dimensioni di 132×132 cm^2 e di 118×54 cm^2: il vetro anteriore è sistemato in una sede ricavata nella cornice anteriore; i vetri delle finestre laterali sono applicati alla camera dall'interno e mantenuti aderenti alle pareti mediante due cornici di duralluminio.

Guarnizioni di gomma di 5 mm di spessore, appositamente preparate dalla Società Pirelli di Milano, interposte tra tutte le superfici a contatto, assicurano la tenuta della camera.

Internamente al corpo centrale della camera, di fianco alle cornici laterali portavetro, sono fissate quattro barre a sezione rettangolare di duralluminio, cui vengono applicate le mensole destinate a sostenere le lastre di materiale da mettere nella camera; la portata massima del portalastre è di 5 tonnellate. Per sgravare la struttura della camera dal grande peso delle lastre sono stati ricavati, in corrispondenza delle basi di appoggio del portalastre, degli appositi sostegni.

Quando il portalastre è in sito, le pareti interne della camera risultano praticamente piane, senza sporgenze tali da creare vortici nel gas durante l'espansione.

La camera può funzionare in ogni posizione: attualmente è montata verticalmente su di un carrello della portata di 10 tonnellate, che scorre su rotaie: il peso complessivo della camera chiusa e senza lastre di materiale, è risultata di circa 15 quintali.

3. – I dispositivi di espansione.

Per evitare le complicazioni meccaniche connesse con la regolazione a volume di una camera di così grandi dimensioni, si è deciso di ricorrere alla regolazione a pressione: in questo caso, infatti, i dispositivi meccanici di espan-

sione si riducono al diaframma mobile, che deve essere rigido, ed alla valvola di espansione.

Il diaframma mobile è stato realizzato impiegando un compensato di balsa di 110×110 cm² di superficie e di 18 mm di spessore sulle cui facce sono stati incollati, con soluzione AC3 Pirelli, due fogli quadrati di gomma di 156 cm di lato. Il foglio affacciato alla camera ha uno spessore di 1 mm ed è ricoperto da un velluto nero di seta; quello affacciato al retrocamera ha uno spessore di 0.5 mm. I due fogli sono fissati, con leggera tensione, ad una cornice quadrata di alluminio serrata tra il corpo centrale della camera ed il fondo. Il peso della parte mobile del diaframma è risultato inferiore a 6.5 kg.

La valvola di espansione è costituita da un grande anello di Silumin dal diametro medio di 118 cm cui sono applicati, da parti opposte, un pneumatico di gomma e due valvole elettromagnetiche a contro campo il cui foro di efflusso ha un diametro medio di 50 mm. Gli emboli di queste valvole sono stati realizzati in lega Atesia « D » di magnesio, dalla Società Italiana per il Magnesio di Bolzano; il loro peso è risultato di soli 50 g.

L'anello di Silumin è montato sulla piazzuola del retrocamera con il pneumatico affacciato ai fori ad una distanza di 20 mm: gonfiando il pneumatico questo si adagia sui fori otturandoli e chiudendo così a tenuta il retrocamera che può venir messo in pressione. L'impulso di espansione, aprendo le valvole elettromagnetiche, sgonfia il pneumatico permettendo alla sovrapressione del retrocamera di scaricarsi all'esterno.

In condizioni normali di funzionamento il retrocamera si scarica in circa 20 ms: per attutire l'urto del diaframma contro la parete di fondo della camera questa è stata rivestita con gomma ondulata, disposta in modo che le ondulazioni possano imprigionare aria durante gli ultimi millimetri di corsa e provvedere ad un sufficiente smorzamento del moto del diaframma.

L'adozione di un sistema di espansione doppio in cascata del tipo ora descritto si è imposto per la necessità di svuotare in un intervallo di tempo molto breve il volume del retrocamera senza dover ricorrere a valvole di espansione di dimensioni eccessive e perciò di più difficile realizzazione meccanica e di meno sicuro funzionamento.

4. – Il sistema pneumatico di alimentazione.

La camera risulta pronta per l'espansione quando il diaframma, sollecitato dalla pressione del retrocamera, ha raggiunto la posizione corrispondente al valore del rapporto di espansione richiesto: in queste condizioni, se il gas impiegato per il riempimento è l'argon, la disposizione attuale è tale che la pressione del retrocamera uguaglia la pressione della camera e la tensione della membrana di gomma è praticamente nulla.

La regolazione del rapporto di espansione si ottiene variando la pressione del retrocamera mediante il sistema pneumatico schematizzato in Fig. 4.

Un compressore, della portata di 24 m³ di aria all'ora, mantiene alla pressione di $8 \div 10$ atmosfere il serbatoio S_1 di 600 dm³ di capacità, e questo, per mezzo del riduttore R_1, alimenta un secondo serbatoio S_2 di 200 dm³ di capacità alla pressione di una atmosfera.

Il riduttore R_2 alimenta permanentemente, attraverso un condotto di piccola portata (diametro interno di 20 mm), il pneumatico alla pressione di 0,7 atmosfere, facendolo adagiare contro i fori del retrocamera.

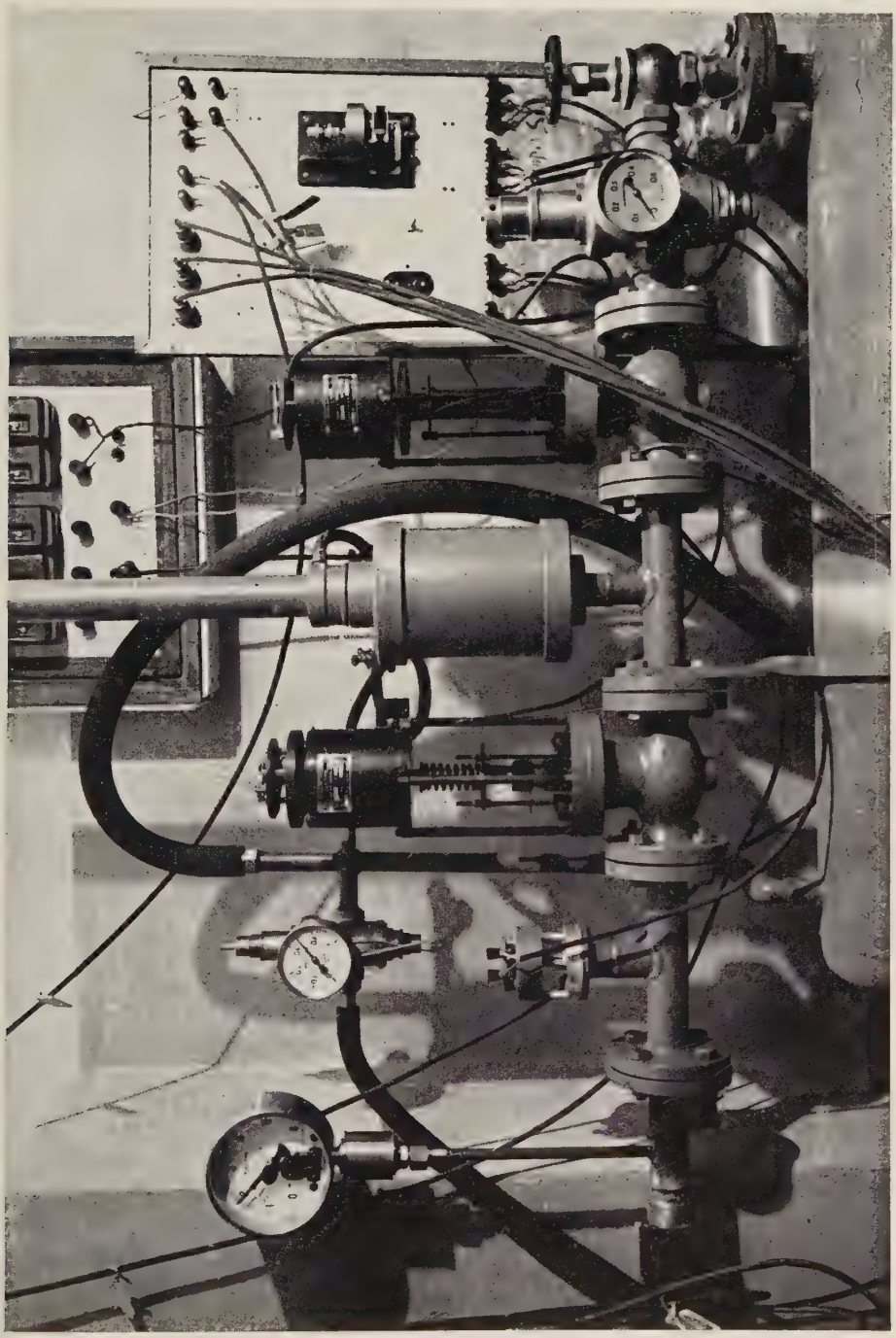

Fig. 5. - Sistema pneumatico.

Il retrocamera può essere rifornito d'aria sia attraverso un condotto di grande portata (diametro interno di 40 mm) costituito dal riduttore R_3 e della valvola elettromagnetica V_1 di compressione e V_2 di sicurezza, sia attraverso il condotto di piccola portata (diametro interno di 10 mm (costituito dal riduttore R_4, dalla valvola a spillo V_s, dal regolatore fine di pressione R_5 e dalla valvola V_2.

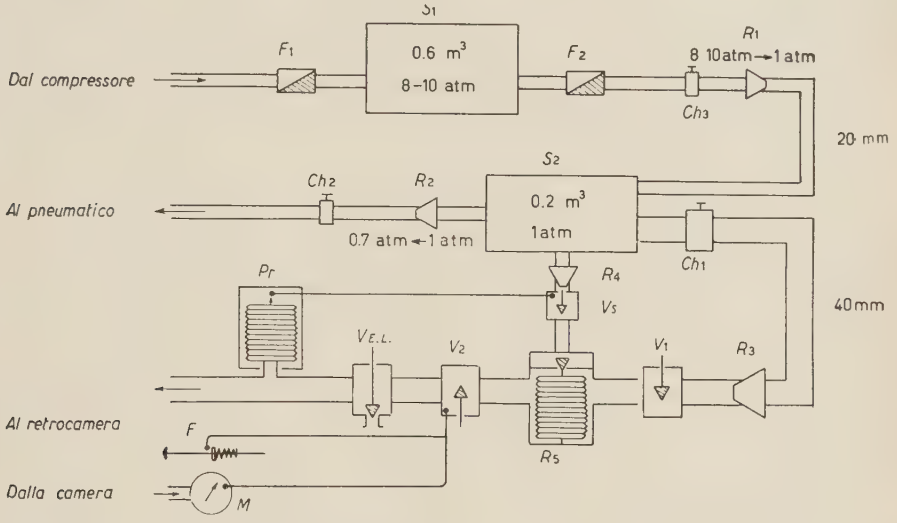

Fig. 4. – Diagramma del sistema pneumatico. F_1-F_2, filtri; S_1-S_2, serbatoi; Ch_1-Ch_2-Ch_3, rubinetti; R_1-R_2-R_3-R_4, riduttori normali; R_5, riduttore fine; V_s, valvola elettromagnetica a spillo; V_1, valvola elettromagnetica di ricompressione rapida; V_2, valvola elettromagnetica di sicurezza; $V_{E.L.}$, valvola espansione lenta; Pr, pressostato fine; F, dispositivo meccanico di sicurezza; M, manometro a massima di sicurezza.

Il primo condotto, inseribile a mezzo del rubinetto Ch_1, permette di effettuare la compressione della camera in meno di 5 s, il secondo in circa due minuti primi.

Il pressostato Pr, pilotando la valvola a spillo V_s, permette di mantenere costante la pressione del retrocamera a meno di tre millesimi di atmosfera, consentendo, a temperatura costante, una buona stabilità di funzionamento.

Il manometro a massima M, in comunicazione con l'interno della camera, pilota la valvola V_2 che in caso di sovrapressione, blocca l'afflusso d'aria al retrocamera. Il dispositivo F è costituito da un embolo che, durante la compressione, segue il diaframma nella sua corsa: nel caso di perdite della camera o di eccessivi abbassamenti di temperatura, esso, chiudendo la valvola V_2, costituisce una sicura garanzia contro eccessivi avanzamenti del diaframma.

Le espansioni lente di chiarificazione vengono eseguite mediante la piccola valvola elettromagnetica $V_{E.L.}$.

5. – Le operazioni di comando.

Le operazioni necessarie al funzionamento della camera si possono classificare in operazioni veloci (espansione rapida, estinzione del campo chiarificatore, blocco dei circuiti d'ingresso, innesco ritardato delle lampade a flash ...) ed in operazioni lente (ricompressione, ricarica macchine fotografiche, espansioni lente e successive ricompressioni, sblocco dei circuiti d'ingresso ...).

Lo schema a blocchi del dispositivo elettronico-meccanico che provvede a queste operazioni è mostrato in Fig. 6. I circuiti elettronici impiegati sono di tipo tradizionale (1).

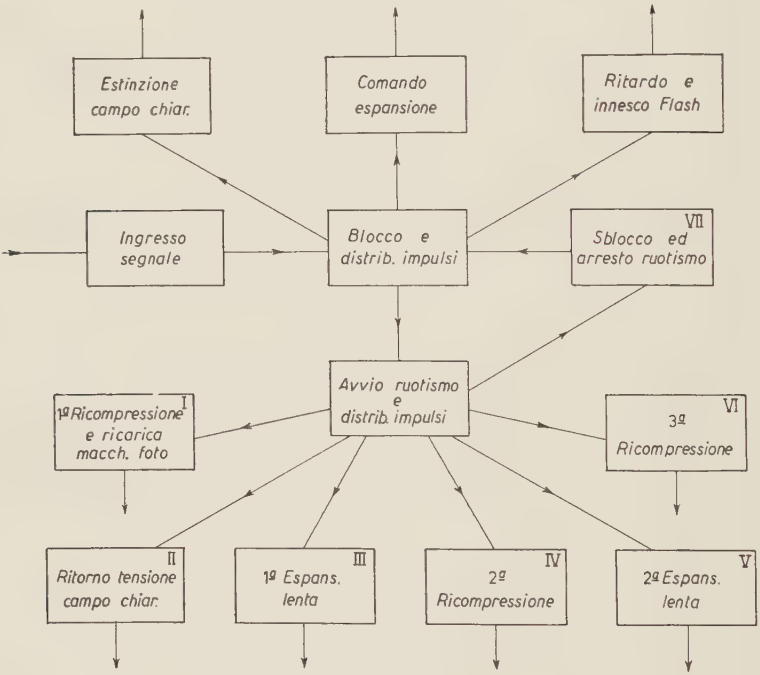

Fig. 6. – Schema del comando.

L'impulso di comando, oltre a far eseguire le operazioni veloci, collega, a mezzo di una frizione elettromeccanica, un motorino ad un distributore di impulsi che, pilotando dei relé, fa eseguire le operazioni lente, arrestandosi automaticamente dopo un giro e sbloccando il circuito d'ingresso.

La durata di un ciclo può venire variata con continuità da un minimo di 1.5 minuti primi ad un massimo di 8 minuti; entro questi limiti l'intervallo di tempo intercorrente tra le varie operazioni può venire variato a piacere.

(1) A. Lovati, A. Mura, G. Tagliaferri e L. Terra: *Nuovo Cimento*, **8**, 713 (1951).

Durante un ciclo normale si possono eseguire zero, una o due espansioni lente; per la pulitura iniziale del gas della camera un altro ruotismo permette di eseguire un numero indefinito di espansioni lente, distanziandole tra loro di tre minuti primi.

6. – Osservazioni sul funzionamento della camera.

La camera è stata impiegata con espansioni casuali e su comando di contatori; buoni risultati di sono ottenuti stabilizzando opportunamente la temperatura del laboratorio (vedi n. 8): di norma una sola espansione lenta per ciclo era sufficiente per una completa chiarificazione.

Benchè dall'entrata in funzione la camera abbia effettuato più di 20000 espansioni, il controllo sistematico del diaframma non ha rivelato alcun logorio.

Durante il funzionamento è stato osservato che se, alla fine di un ciclo, la camera rimaneva in attesa per un tempo relativamente lungo (> 5 minuti primi) la sovrassaturazione raggiunta dal vapore nella successiva espansione risultava leggermente inferiore a quella che si raggiungeva espandendo la camera immediatamente dopo la chiusura del ciclo.

Per studiare più profondamente il fenomeno si sono eseguite serie di espansioni impiegando per la ricompressione o il solo condotto a piccola portata (durata del ciclo circa 6 minuti primi) o il condotto a grande portata (durata del ciclo circa 3 minuti primi): queste prove hanno messo in evidenza che il fenomeno osservato risultava nettamente più rilevante nel primo caso che nel secondo. Dai controlli sistematici eseguiti risultava che la diminuzione della sovrassaturazione osservata non era da imputarsi alla mancata efficienza del sistema pneumatico di regolazione, poichè la pressione si manteneva costante.

Il fenomeno potrebbe forse spiegarsi ammettendo che durante una ricompressione molto lenta avvenga una prolungata evaporazione del liquido costituente la miscela, così che alla fine della ricompressione stessa, data l'assenza dei nuclei di condensazione, il vapore rimanga leggermente sovrassaturo per parecchi minuti: in queste condizioni se la regolazione del rapporto di espansione viene eseguita a fine ciclo, la camera risulta, dopo un certo tempo di attesa, sottoespansa; se al contrario la regolazione viene dilazionata dalla fine del ciclo, il vapore si presenta, in un espansione che segue immediatamente la chiusura del ciclo successivo, eccessivamente sovrassaturo.

Nelle considerazioni precedenti non si è tenuto conto delle variazioni di temperatura subite dal gas della camera durante la ricompressione: al termine di una ricompressione lenta la temperatura finale del gas coincide praticamente con quella all'inizio del ciclo; nel caso di una ricompressione rapida, invece, la temperatura finale risulta superiore a quella iniziale.

Nel primo caso le osservazioni precedenti rimangono valide; nel secondo caso l'aumento di temperatura e la velocità della ricompressione rendono trascurabile il valore della sovrassaturazione alla fine del ciclo.

Con l'apporto di piccole modifiche al sistema pneumatico la camera può funzionare anche con supercompressione [2]: basta regolare i riduttori R_4 ed R_5

[2] E. Fiorini, R. Giacconi, A. E. Sichirollo e C. Succi: *Nuovo Cimento*, **6**, 355 (1957).

al valore della pressione finale di surcompressione, spostando conseguentemente la posizione dell'embolo del dispositivo F di sicurezza.

Il ritorno del diaframma dalla posizione di surcompressione a quella di compressione normale viene ottenuto mediante l'aggiunta di una valvola elettromagnetica di piccola portata, pilotata dal pressostato Pr.

Non essendo stato sino ad ora possibile procurare un vetro di spessore tale da garantire una sufficiente sicurezza, specie per un esercizio prolungato, le prove di surcompressione sono state limitate al minimo indispensabile per controllare il funzionamento della camera.

La camera ha funzionamento soddisfacente con surcompressione regolando la durata del ciclo ad un minuto e mezzo; è prevedibile che migliori risultati si potranno ottenere con uno studio sistematico; si può ritenere infatti che in una camera di così grandi dimensioni i fenomeni connessi con la surcompressione dovrebbero risultare osservabili con grande evidenza.

7. – I dispositivi di illuminazione e di fotografia.

L'illuminazione del volume utile della camera viene effettuata mediante quattro lampade lineari a flash, tipo SF/E 17, della ditta Siemens di Londra, aventi una lunghezza d'arco di 118 cm.

Ciascuna lampada è posta nella linea focale di uno specchio cilindrico a profilo parabolico, di 25 cm di apertura e 120 cm di lunghezza; gli specchi sono montati in coppia in due incastellature metalliche poste ai lati della camera. Davanti alle lampade un sistema di sottili lastre piane, vellutate a spruzzo, provvede a parallelizzare ulteriormente il fascio luminoso.

Gli specchi di ciascuna incastellatura sono montati su una portiera che, aprendosi, permette di accedere alle lampade facilitando le operazioni di controllo. Un sistema di viti micrometriche, manovrabili dall'esterno, permette di spostare gli attacchi delle lampade per disporle lungo la linea focale degli specchi.

Le lampade di ogni gruppo sono eccitate simultaneamente per mezzo di uno spinterogeno; l'energia dissipata da ogni lampada (circa 8000 joule) vien fornita da una batteria di 10 condensatori da 100 μF, tipo Superprotex, della Società ICAR di Milano, caricati alla tensione di 4000 volt per mezzo di un alimentatore elettronico da 500 watt di potenza.

Per evitare i pericoli connessi con l'osservazione diretta della luce dei flash, un dispositivo automatico disinserisce l'alimentatore e collega a terra le batterie di condensatori scaricandole, tutte le volte che un operatore acceda inavvertitamente nel locale in cui è montata la camera (Fig. 7).

L'illuminazione per l'osservazione diretta delle tracce è ottenuta con un gruppo di 40 lampade ad incandescenza, aventi una potenza complessiva di 2400 watt, montate in fila nella linea focale di uno specchio cilindrico a profilo parabolico di 50 cm di apertura e di 120 cm di altezza.

Lo specchio è disposto dietro una delle incastellature dei flash; l'osservazione della camera si esegue semplicemente accendendo la lampada mentre la portiera dell'incastellatura è aperta.

La fotografia viene eseguita con due macchine stereoscopiche ad assi paralleli, rigidamente connesse tra di loro e poste frontalmente alla camera ad una distanza di 4.3 m dal vetro anteriore.

Vengono inpiegati due obbiettivi Xenar Schneider di 150 mm di lunghezza focale aventi un'apertura massima di 1 : 4.5. La pellicola usata è l'ortocromatica tipo Beta della ditta Tensi di Milano, di 46 mm di altezza. Il formato delle fotografie è di 42×55 mm^2; il fattore di riduzione di circa 1/27. Ciascun caricatore delle macchine fotografiche può contenere fino a 30 metri di pellicola.

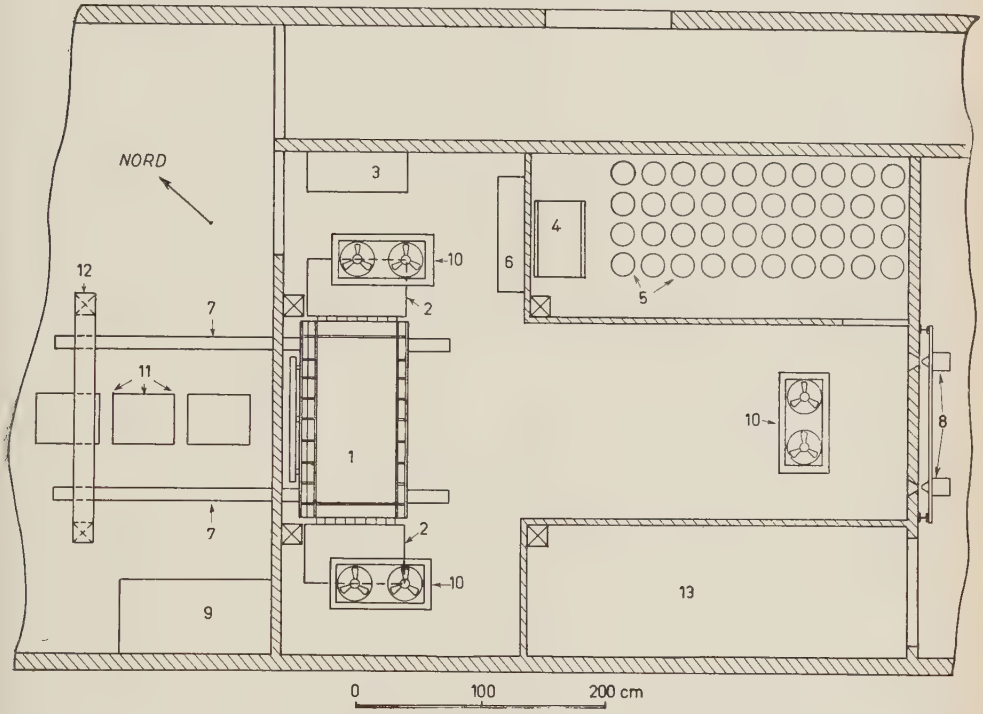

Fig. 7. – Disposizione degli apparecchi nel laboratorio. 1. Camera di Wilson; 2. Lampade a Flash; 3. Lampada per l'illuminazione continua; 4. Alimentatore elettronico; 5. Batterie di condensatori; 6. Scaricatore automatico delle batterie; 7. Rotaie; 8. Macchine fotografiche; 9. Termostato per acqua; 10. Termoconvettori; 11. Apparecchi elettronici; 12. Supporto del paranco; 13. Camera oscura.

Un sistema di marche permette di individuare su ogni fotogramma il punto in cui l'asse di prospettiva del sistema di ripresa incontra la pellicola. Utilizzando il sistema di punti di riferimento riportati in ciascun fotogramma è possibile effettuare la ricostruzione stereoscopica con il metodo analitico e con il metodo di ricostruzione per riproiezione anche impiegando apparecchi di ricostruzione fotogrammetrica (come l'apparecchio Santoni impiegato in geodesia).

Le operazioni di sviluppo sono eseguite mediante un piccolo impianto automatico, capace di restituire, fissato ed essicato, un rotolo di pellicola di 30 metri di lunghezza in 4 ore circa.

8. – La stabilizzazione delle condizioni termiche.

La camera è stata installata con tutte le sue apparecchiature in località « Sabbione » (2518 metri s.m.) in alta Val Formazza, presso la diga della Società Edison-Volta ([3]). La disposizione degli apparecchi è mostrata in Fig. 7.

Poichè una camera di Wilson regolata a pressione è molto sensibile alle variazioni di temperatura, particolare cura è stata rivolta alla sua stabilizzazione ed all'eliminazione dei gradienti termici.

Per raggiungere questo scopo la temperatura dei locali attigui a quello che ospita la camera è stata stabilizzata grossolanamente entro due gradi centigradi, rivolgendo particolare cura all'isolamento termico delle pareti.

Nel locale della camera sono stati installati tre termoconvettori, aventi in totale una superficie di scambio di 60 m^2, attraverso i quali, circa trenta volte all'ora, viene fatta circolare l'aria dell'ambiente mediante sei aspiratori.

Una pompa, della portata di 20 litri al minuto primo, pilotata da un termometro a massima di tipo Vertex, di un decimo di grado di sensibilità, fa circolare nei termoconvettori dell'acqua, mantenuta rigorosamente ad una temperatura di 20 °C in un termostato di 450 litri di capacità.

Impiegando i dispositivi descritti la temperatura del locale della camera è risultata costante entro tre decimi di grado; nelle vicinanze della camera il gradiente orizzontale di temperatura è risultato di circa 0.2 °C/m e quello verticale di circa 0.5 °C/m.

* * *

Dedichiamo con profonda riconoscenza questo scritto alla memoria del nostro indimenticabile maestro ed amico Antonino Mura, che fino alla fine seguì con passione il nostro lavoro.

È poi nostro gradito dovere ringraziare il Prof. G. Polvani, Direttore dell'Istituto di Scienze Fisiche dell'Università di Milano ed il Prof. P. Caldirola, Direttore della Sezione di Milano dell'INFN, per l'appoggio e gli aiuti accordatici durante la progettazione e la realizzazione dello strumento.

Un sentito ringraziamento vogliamo pure esprimere al Prof. G. P. Occhialini ed al Prof. C. Peyrou per le loro preziose informazioni e le interessanti discussioni, ed al Prof. C. Locatelli, al Prof. G. Gotusso, al dott. Ing. V. Zerbini ed al dott. G. Zuppiroli, per i consigli tecnici offertici durante la progettazione di alcune parti dell'apparecchiatura.

Siamo particolarmente grati per la loro cordiale collaborazione ai dott. C. Giori, C. Moravia, A. Sichirollo ed ai tecnici B. Nicolai e G. Gennaro.

La costruzione dell'apparecchio è stata possibile grazie ai generosi contributi finanziari del Gruppo Amici dell'Istituto di Scienze Fisiche dell'Università di Milano, della Sezione di Milano dell'Istituto Nazionale di Fisica Nucleare e dell'ANIDEL; particolare ringraziamento vogliamo ancora esprimere alle Società Innocenti, ICAR, Italiana del Magnesio, Pirelli, Vis Securit, Tensi ed alla Cassa di Risparmio delle Provincie Lombarde.

([3]) E. Fiorini, C. Giori, C. Moriggia e C. Succi: *Il laboratorio per Raggi Cosmici del « Sabbione »*, in *Suppl. Nuovo Cimento* (in corso di pubblicazione).

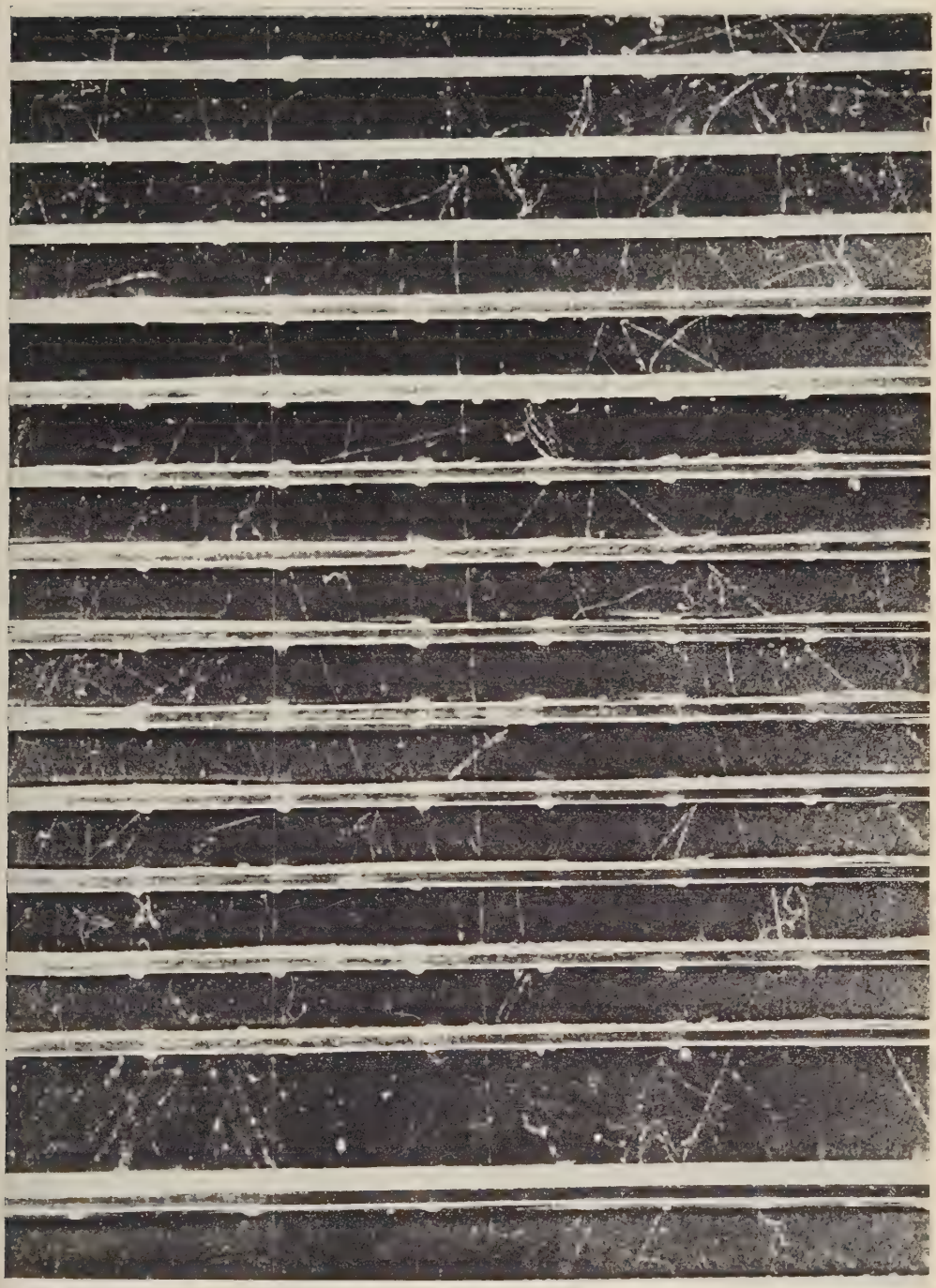

Fig. 8. — Particella penetrante di comando.

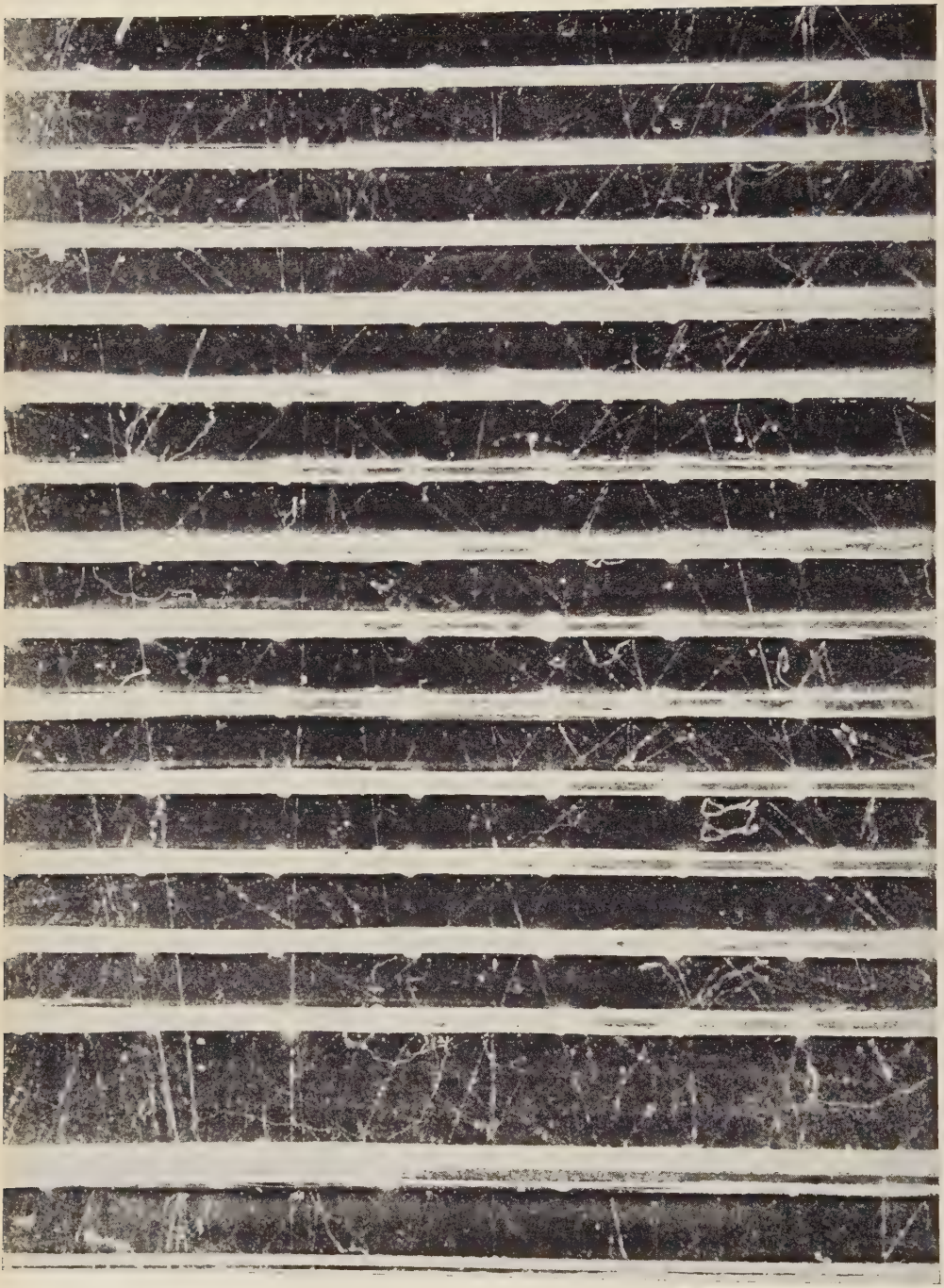

Fig. 9. – Tracce di particelle casuali.

SUMMARY

We describe here a large Wilson cloud chamber with an internal volume of more than a cubic meter and an illuminated volume of $120 \times 114 \times 50$ cm^3. The chamber may contain several plates up to a total weight of some metric tons. The characteristics of the apparatus are of such a kind, that the chamber can be employd either in cosmic rays research or with accelerators. Chambers associated equipment has been projected so as to make possible to work also with overcompression.

Influence de la longueur efficace et du diamètre du cylindre sur la courbe de palier des compteurs de Geiger-Müller à parois de verre et graphitage externe.

D. Blanc

Laboratoire de Physique Corpusculaire, Faculté des Sciences - Toulouse, France

(ricevuto il 6 Maggio 1957)

1. – Introduction.

Dans une récente publication, P. J. Grouse et H. D. Rathgeber [1] ont calculé la longueur efficace de compteurs à parois de verre et graphitage externe, pour leurs diverses tensions de fonctionnement; ils expliquent certains désaccords apparents obtenus antérieurement [2,3]. La longueur efficace L des compteurs du type décrit par D. Blanc et M. Scherer [4] est donc exactement connue (Fig. 1).

Il convient de noter que la distorsion du champ électrique aux extrémités du cylindre à la masse a aussi une influence sur la valeur du seuil de Geiger et la qualité du palier. b étant le diamètre interne de la cathode, l'influence du rapport L/b n'a jusqu'ici été étudiée que dans deux publications relatives à des compteurs à cathode interne métallique.

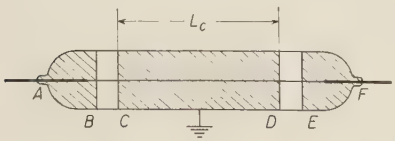

Fig. 1. – Compteur à parois de verre et graphitage externe.

1) M. Chaudhri et A. G. Fenton [5] limitent la partie efficace de l'anode par des tubes capillaires de pyrex ou de laiton de 5 mm de diamètre. Ils utilisent un remplissage d'alcool (pression de 2.3 cm de mercure) et d'argon (pression de 7.7 cm de mercure). Par déplacement des électrodes de garde, L/b peut varier de un à cinq. Le seuil est indépendant de L pour $L/b \geqslant 2$. Avec un capillaire de pyrex, pour $L/b = 2$, la longueur du palier passe par un maximum. Les résultats obtenus avec un capillaire de laiton sont plus difficiles à interpréter.

2) H. L. De Vries et G. M. Barendsen [6] utilisent des électrodes de

(1) P. J. Grouse et H. D. Rathgeber: *Nuovo Cimento*, **5**, 707 (1957).

(2) D. Blanc: *Nuovo Cimento*, **1**, 1280 (1955).

(3) A. M. Baptista et J. P. Galvão: *Nuovo Cimento*, **3**, 647 (1956).

(4) D. Blanc et M. Scherer: *C.R. Acad. Sci.*, **228**, 2018 (1949).

(5) M. Chaudhri et A. G. Fenton: *Proc. Phys. Soc.*, **A-60**, 183 (1948).

garde métalliques de 4 mm de diamètre, placées à la masse et terminées par une partie conique délimitant la longueur efficace avec plus de précision. Par déplacement de ces électrodes, L/b varie de 0.5 à 20. Le seuil n'est constant qu'au dessus de $L/b = 15$. La longueur de palier passe par un maximum pour $L/b = 1.9$. Leur étude portait sur un compteur argon-alcool.

Pour les compteurs à graphitage externe (Fig. 1), les électrodes de garde ont le diamètre de la cathode et sont placées à la haute tension; la répartition des lignes de force est différente, et une étude complète est nécessaire.

2. – Étude experimenatle.

Les expériences ont porté sur des compteurs de grande longueur et de 2 ou 3 cm de diamètre, sous irradiation très faible, pour éviter tout effet électrique parasite sur la paroi interne du cylindre. Les longueurs graphitées L_c voulues étaient obtenues par graphitages successifs de la surface du verre. La longueur isolée totale $L_i = BC + DE$ était maintenue constante et assez grande pour que l'on puisse appliquer la formule:

$$L = L_c + 0.2L_i ,$$

qui donne la longueur efficace L pour le seuil de Geiger [2]. Quatre compteurs ont été étudiés (éthanol sous la pression de 1 cm de mercure, et argon sous la pression de 8.5 cm de mercure), pour des seuils du circuit associé compris entre 0.03 et 1 V.

La Fig. 2 donne la variation des tensions V_D (seuil de démarrage des impulsions correspondant à un seuil du circuit de 0.03 V), V_G (seuil de Geiger) et V_M (tension maximum du palier) en

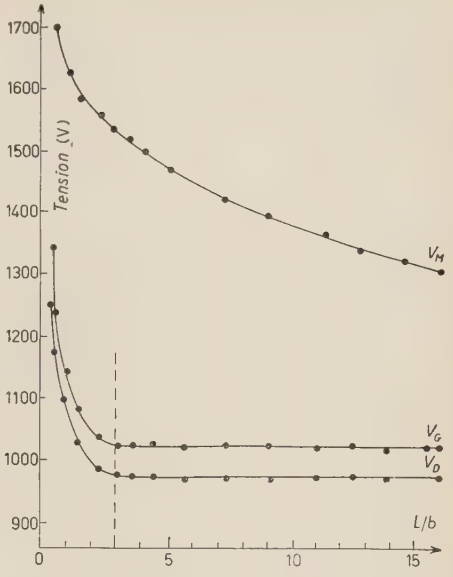

Fig. 2. – V_D, V_G, $V_M = f(L/b)$ pour $b = 3$ cm. Seuil = 0.03 V. Alcool: 1 cm de Hg, argon: 8.5 cm de Hg.

fonction de L/b pour un compteur de 3 cm de diamètre. Cette variation est identique pour $b = 2$ cm.

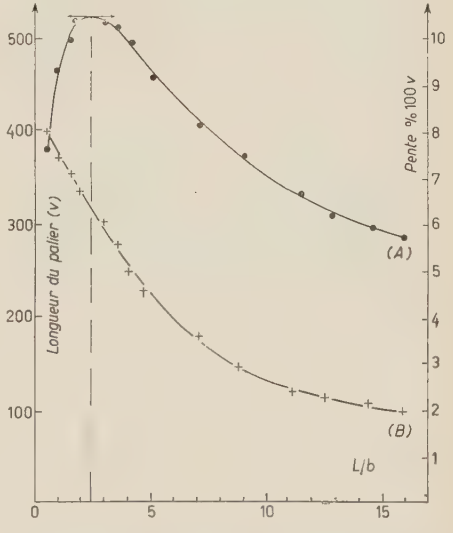

Fig. 3. – Longueur (A) et pente (B) du palier en fonction de L/b pour $b = 3$ cm. Seuil = 0.03 V. Alcool: 1 cm de Hg, argon: 8.5 cm de Hg.

[6] H. L. DeVries et G. W. Barendsen: *Physica*, **18**, 927 (1952).

La Fig. 3 donne la variation de la longueur du palier ($V_M - V_G$) et de sa pente, exprimée en pour-cents par 100 V, pour le même compteur. Les résultats sont les mêmes pour les autres compteurs étudiés.

3. – Conclusion.

1) Les tensions V_D et V_G sont indépendantes de L pour $L/b \geqslant 3$, aux erreurs expérimentales près (5 V).

2) La pente du palier diminue lorsque L augmente. Ceci confirme le résultat connu que la construction d'un compteur est d'autant plus facile que sa longueur est plus grande.

3) La longueur du palier passe par un maximum pour $L/b = 2.5$. Pour $L/b < 2.5$, l'effet prépondérant vient de la distorsion du champ électrique aux extrémités du cylindre. Par contre, pour $L/b > 2.5$, intervient l'augmentation du nombre d'ions arrivant sur le cylindre par impulsion, qui accentue la probabilité d'émission secondaire depuis la cathode.

IL NUOVO CIMENTO Vol. VI, N. 4 1° Ottobre 1957

An Experiment for Polarization of Free Electrons.

S. Yamaguchi

Scientific Research Institute, Tokyo,

(ricevuto l'11 Giugno 1957)

Van der Spuy suggested theoretically a possibility to polarize free electrons [1]. The present author carried out this experiment, as he was excited by the theory.

Powder of permanent magnet (coercive force, about 700 Oe) was attracted onto a substrate of magnet. An electron beam grazed this magnet powder, as is illustrated in Fig. 1. An electron diffraction pattern here obtained (wavelength: 0.0294 Å, camera length: 495 mm) is shown in Fig. 2. In Fig. 3, the central spot found in Fig. 2 is optically enlarged 40 times. It is here of significance that the electron beam is splitted after it has tunneled through a ferromagnetic substance. Fig. 4 shows the electron beam which did not touch the magnet body. Fig. 4 is quite different from Fig. 3, because in Fig. 4 there is no splitting of the electron beam. The splitting discernible in Fig. 3. is distinguishable from the classical Lorentz-effect, i.e., from the spreading of the electron beam.

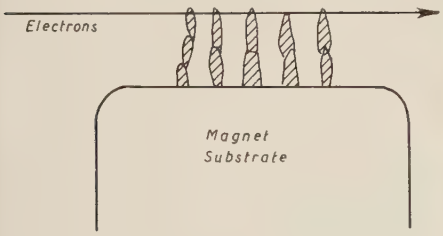

Fig. 1. Process of polarization of free electrons.

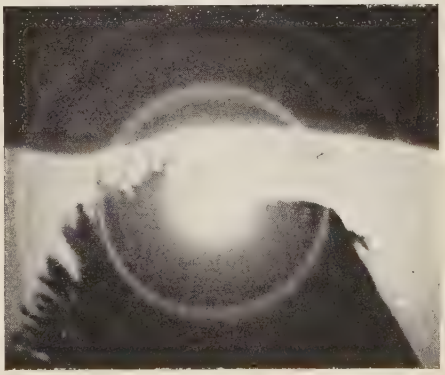

Fig. 2. Diffraction pattern. Body-centred cubic lattice. Wavelength: 0.029$_4$ Å. Camera length: 495 mm. Picture enlarged about 2.2 times.

The author has tried to elucidate the splitting here observed as polarization of free electrons, i.e., as separation of the two types of spin. The spacing ΔZ between the two spots found in Fig. 3

[1] E. Van der Spuy: *Nuovo Cimento*, **4**, 1349 (1956).

is given by

$$\Delta Z = \frac{1}{2} B \left| \frac{\partial H}{\partial Z} \right| m \left(\frac{L\lambda}{h} \right)^2$$

or

$$\Delta Z^2 = \frac{1}{2} B \, \Delta H \, m \left(\frac{L\lambda}{h} \right)^2 , \quad (1)$$

Fig. 3. The central spot found in Fig. 2, optically enlarged 40 times. The splitting of the electron beam is clearly visible.

where: B, magnetic moment of Bohr's magneton; $\partial H/\partial Z$, gradient of the magnetic field applied to the electrons; λ: wavelength of the electrons, and h: Planck's constant. In Fig. 3, we measure

$$\Delta Z = \frac{7}{40} \quad \text{mm},$$

$$\lambda = 0.0294 \quad \text{Å}$$

$$L = 495 \quad \text{mm}.$$

Fig. 4. Electron beam not touching the magnet.

According to the Eq. (1) we obtain

$$\Delta H \fallingdotseq 10^7 \quad \text{gauss}.$$

This strength of magnetic field coincides with the known strength of the Weiss' inner molecular field to be found in ferromagnetic substance.

On the Angular Distribution of Secondary Particles of High Energy Jet Showers.

S. Hasegawa (*), J. Nishimura (+) and Y. Nishimura (×)

Institute for Nuclear Study Tanashi - Tokyo

(ricevuto il 2 Luglio 1957)

It has been suggested by one of us (J.N.), that the transverse momenta of shower secondaries with respect to the shower axis is one of the most important quantities for the study of dynamical properties of high energy jet showers (1). The main results obtained are that the values of transverse momenta, P_T, are nearly constant (about several hundred MeV/c) independent of shower particles and of primary energies.

If these results wi l be confirmed the angular distribution, $F(\theta)\,\mathrm{d}\theta$, of secondary particles in the laboratory system will be closely connected with the momentum distribution of shower particle, $f(P)\,\mathrm{d}P$, by the relation

$$F(\theta)\,\mathrm{d}\theta \simeq F\left(\frac{P_T}{P}\right)\frac{P_T}{P^2}\,\mathrm{d}P \simeq f(P)\,\mathrm{d}P\,,$$

where

$$\theta = P_T/P\,.$$

Thus it seems to be worthwhile to get the information of angular distribution of shower particles of high energy jets in nuclear emulsions especially in the small angle region. It just corresponds to the high energy portion of shower particles, which give the main contrition to the further development of the nucleon cascade in extensive air showers. It seems natural to consider that the angular distribution in such a small angle region represents characteristic features of the meson production in nucleon-nucleon collisions as shown, for example, in the tunnel model (2) or the composite model (3). Furthermore, as shown later (*), it may easily be proved that the shape of the angular distribution in the laboratory system holds even in the centre of mass system t e nucleon-nucleon collision for the power law type of the angular distribution.

(*) Department of Physics, Osaka University.

(+) Institute for Nuclear Study, Tokyo University.

(×) Department of Physics, Kobe University.

(1) The results will be published soon in this journal.

(2) F. C. Roesler and C. B. McCusker: *Nuovo Cimento*, **10**, 127 (1952).

(3) G. Cocconi: *Phys. Rev.*, **93**, 1107 (1954).

(*) Let θ^* be the angle of shower particles with respect to the shower axis in the centre of mass system corresponding to the angle θ in the laboratory system and γ be the Lorentz factor connecting these two systems, the relation $\theta^* = \gamma\theta$ hold for small angles θ.

TABLE I.

No.	Author	Star type	Incident energy per nucleon	Reference
1	KAPLON and RITSON	n_s= 24 (P)	$8.9 \cdot 10^{12}$ eV	*Phys. Rev.*, **88**, 366 (1952)
2	LAL *et al.*	n_s= 210 (Mg)	$\sim 10^{13}$ eV	*Proc. Ind. Acad. Sci.*, **36**, 75 (1952)
3	KAPLON and KOSHIBA	n_s= 36 (P)	$3 \cdot 10^{13}$ eV	*Phys. Rev.*, **97**, 143 (155)
4	DEBENEDETTI *et al.*	n_s= 39 (P)	$4 \cdot 10^{12}$ eV	*Nuovo Cim.*, **4**, 1142 (1956)
5	NAUGLE and FREIER	n_s=110 (N)	$1 \cdot 10^{14}$ eV	*Phys. Rev.*, **104**, 804 (1956)
6	NAUGLE and FREIER	n_s= 38 ($Z \leqslant 5$)	$4.5 \cdot 10^{13}$ eV	*Phys. Rev.*, **104**, 804 (1956)
7	NAUGLE and FREIER	n_s= 25 (α)—	$2.7 \cdot 10^{13}$ eV	*Phys. Rev.*, **104**, 804 (1956)
8	TOKUNAGA (*) *et al.*	n_s= 44 (Na)	$5 \cdot 10^{11}$ eV	—
9	TOKUNAGA (*) *et al.*	n_s=120 (Li)	$5 \cdot 10^{11}$ eV	—

(*) We are indebted to Mr. TOKUNAGA for communicating us his data before publication.

Now, we analyse the spatial distribution of high energy μ-mesons associated with an air shower obtained by the Cornell group [1]. The observations are made at 1600 m w. e, underground, the result of which is that the considering the decay probability of π-mesons in the atmosphere, we get the information of the angular distribution of π-mesons produced in the jets, the result of which is represented by the shape of $(1/\theta)\theta\,\mathrm{d}\theta$ in the small angle region.

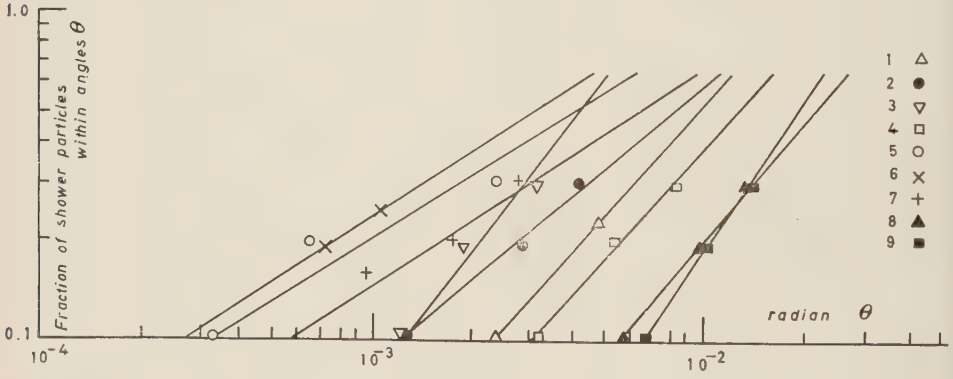

Fig. 1.

spatial distribution of the μ-mesons is almost constant within the circle of radius 10 m.

Using the assumption P_T=const and

It may be possible to take the following two different interpretations, i.e., either the angular distribution of an individual shower follows the above conclusion, or it acquires such a shape only after the superposition of that of many jets. In order to examine these two possibilities and to get more experimental

[1] P. H. BARRETT, L. M. BOLLINGER, G. COCCONI, Y. EISENBERG and K. GREISEN: *Rev. Mod. Phys.*, **24**, 133 (1952).

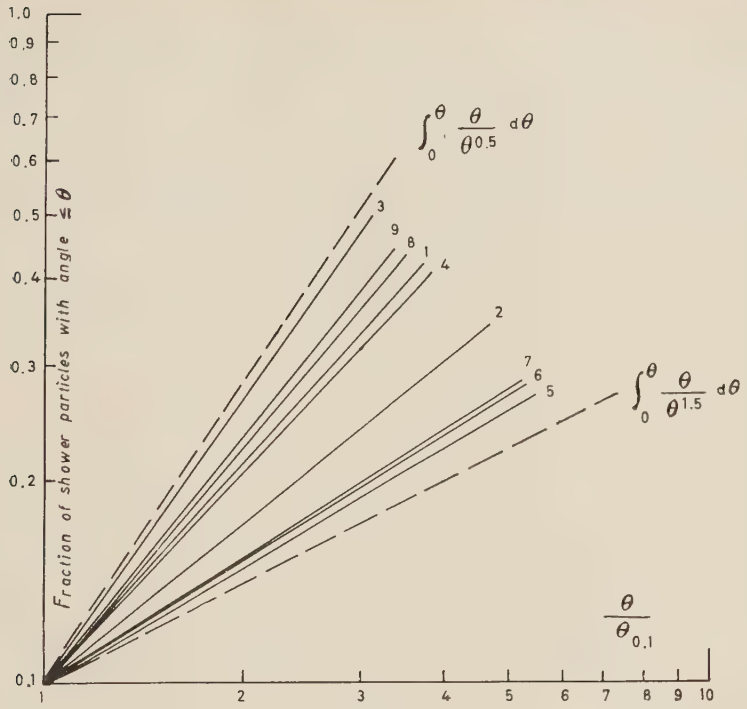

Fig. 2.

information, we analyzed the data obtained in nuclear emulsions, though the energy region of these data is somewhat different from that of the Cornell group. In Table I, we summarize the data used for this analysis. At first we assume the shape of angular distribution as $(1/\theta^{l})\theta\,d\theta$. Then, if we plot the relation of number of shower particles within the angle θ v.s. angle θ in log-log scale, we get the information of the value of l from the slope $(2-l)$ of these curves. The data are plotted in Fig. 1, in which we take the fraction of number of shower particles within the angle θ to n_s to minimize the effect of fluctuation. As shown in Fig. 2, one may conclude that the angular distribution is consistent with the form, $(1/\theta^{1.5})\theta\,d\theta \sim (1/\theta^{1.5})\theta\,d\theta$, though the statistics is not good enough.

The analysis here presented seems to be convenient for the comparison with theories of multiple meson production, because it may not be affected by uncertainties introduced usually by the nucleon cascade in the target nucleons and the Lorentz transformation from laboratory system to centre of mass system. Further analysis will be made in connection with the « Emulsion chamber project » [5] which was carried out last summer in Japan.

* * *

We are greatly indebted to Prof. O. Minakawa and Prof. Y. Fujimoto for their helpful discussions throughout this work.

[5] The details of the project will be published soon in this journal.

Polarization Effects in Beta Decay Accompanied by Internal Bremsstrahlung.

J. Sawicki and J. Szymanski

Institute of Theoretical Physics, University of Warsaw - Warsaw

(ricevuto il 6 Luglio 1957)

The non-conservation of parity in weak interactions gives rise to many specific polarization effects. It is well known, in particular, that β-electrons (-positrons) are longitudinally polarized (see [1,3]) and that γ-rays accompanying the radiative K-capture of electrons (positrons) are circularly polarized [4]. Recently Cutcosky [5] investigated the circularly polarized internal bremsstrahlung associated with the capture of K-electrons. Evidently the internal bremsstrahlung accompanying β-decay must be also circularly polarized. The corresponding β electrons (positrons) are also longitudinally polarized their degree of polarization being, however, different from that corresponding to the case of absence of the internal bremsstrahlung. It appears, at first, reasonable to investigate these polarizations quantitatively. These effects and their mutual relations might appear sensitive to the type of coupling or, eventually, the degree of forbidenness of the reaction.

The calculations were performed under the assumption of the two-component neutrino theory, although the generalization for an arbitrary admixture of the parity non-conserving terms modifies the results for the polarizations only by a constant factor (i.e. $\alpha/(1+\alpha^2)$ for a $(1+\alpha\gamma_5)$ theory α being a real number) (*).

Throughout the paper we use the method and the notation previously applied by Cutcosky [6] to the calculation of the spectra and angular distributions of internal bremsstrahlung γ-rays.

We shall first consider a $n \to p + e^- + \bar{\nu}$ reaction. The degree of circular polarization of the bremsstrahlung rays accompanying this reaction can be shown to be:

$$(1) \qquad P_\gamma^{(i)} = \frac{J_+^{(i)} - J_-^{(i)}}{J_+^{(i)} + J_-^{(i)}} = \mathrm{Sp}\left\{ (i\gamma_\mu g_\mu - m)[m - \gamma_4 E + i(\bar{\gamma}\bar{\varkappa})(\bar{p}\bar{\varkappa})] \cdot \right.$$

$$\left. \cdot (-\bar{\varkappa}\bar{\sigma})(i\gamma_\sigma g_\sigma - m) N^{(i)} \right\} \left[\mathrm{Sp}\left\{ (i\gamma_\mu g_\mu - m)[m - \gamma_4 E + i(\bar{\gamma}\bar{\varkappa})(\bar{p}\bar{\varkappa})](i\gamma_\sigma g_\sigma - m) N^{(i)} \right\} \right]^{-1},$$

(1) T. D. Lee: *Proc. of the Seventh Rochester Conference* (1957).
(2) L. Wolfenstein: *Bull. Am. Phys. Soc.*, Ser. II, **2**, 190 (1957).
(3) L. D. Landau: *Žurn. Éksp. Theor. Phyz.*, **32**, 407 (1957).
(4) R. J. Glauber and P. C. Martin: to be published; see also *Phys. Rev.*, **95**, 572 (1954).
(5) R. E. Cutcosky: to be published.
(*) For a CP conserving theory.

where: (i) denotes the type of coupling involved, the plus (minus) sign of the relative intensity of particles $J^{(i)}$ refers to right (left) circular polarization the polarization vectors being $\boldsymbol{e}_{\pm} = 2^{\frac{1}{2}}(\boldsymbol{\epsilon}_2 \pm i\boldsymbol{\epsilon}_2)$; $\boldsymbol{\epsilon}_1$ and $\boldsymbol{\epsilon}_2$ are two perpendicular unit vectors, which, with a unit vector $\varkappa$ having the direction of the photon propagation form a right handed triad; $\boldsymbol{g}=\boldsymbol{p}+\boldsymbol{k}$, $\boldsymbol{p}$ and $\boldsymbol{k}$, E and ω being, respectively, the electron and the photon momenta and energies; $N^{(i)}=A^{(i)\prime}(\gamma_4 - i\gamma\boldsymbol{q}/q)\bar{A}^{(i)\prime}$, where $A^{(i)}=A^{(i)\prime}(1-\gamma_5)$; $A^{(i)}$ is defined in ref. ([6]) and $\boldsymbol{q}$ is the momentum of the antineutrino.

The polarization $P_\gamma^{(i)}$ was calculated for eleven different couplings $\hat{O}^{(i)}$ for allowed and first forbidden transitions. After performing integrations over the directions of $\boldsymbol{q}$ the following results were obtained:

For the scalar allowed ($\hat{O}\equiv 1$) transition:

$$P(S(1)) = \frac{\omega p^2 \sin^2\theta + E\omega^2\Theta}{(E+\omega)p^2\sin^2\theta + E\omega^2\Theta} = P\,, \tag{2}$$

where $\theta = \sphericalangle(\boldsymbol{p},\boldsymbol{k})$ and $\Theta = 1 - p/E\cos\theta$. The same result follows for the pseudoscalar ($\hat{O}\equiv\gamma_5$) and tensor allowed ($\hat{O}\equiv\boldsymbol{\sigma}$) cases:

$$P_\gamma(P_s(\gamma_5)) = P_\gamma(T(\boldsymbol{\sigma})) = +P\,. \tag{3}$$

The vector allowed ($\hat{O}=\gamma_4$) and pseudovector allowed ($\hat{O}=\boldsymbol{\gamma}\gamma_5$) polarizations are the same in absolute value, but have just the opposite sign:

$$P_\gamma(V(\gamma_4)) = P_\gamma(A(\boldsymbol{\gamma}\gamma_5)) = -P\,. \tag{4}$$

The first forbidden transitions of the « source velocity » type have also the same polarizations in absolute value P. We have for the tensor ($O=\boldsymbol{\alpha}$), vector ($O=\boldsymbol{\gamma}$) and pseudovector ($O=\gamma_4\gamma_5$) cases:

$$P_\gamma(T(\boldsymbol{\alpha})) = -P(V(\boldsymbol{\gamma})) = -P(A(\gamma_5\gamma_4)) = P\,, \tag{5}$$

where the relative signs for T, V and A appear the same as before.

The expressions for the polarization for the first forbidden transitions of the « retardation » type their essential terms containing $i(\boldsymbol{g}+\boldsymbol{q})$ linearly are too complicated to be given here (see ([7])).

For non-oriented nuclei averaging over nuclear orientations cancels interference terms in the expressions for the following mixtures of « pure » couplings:

$$S(1) - T(\sigma),\ Ps(\gamma_5) - T(\bar{\sigma}),\ V(\gamma_4) - A(\boldsymbol{\gamma}\gamma_5),\ Ps(\gamma_5) - A(\bar{\gamma}\gamma_5)\,,$$

for allowed transitions and, similarly, for various other combinations of this type for first forbidden transitions of the « source velocity » type. The expressions for numerators and denominators of P_γ's add then incoherently to each other for such admixtures. In all other admixtures the interference terms confuse the situation. The respective polarizations for reactions involving positrons differ only in signs of the derived expressions.

([6]) R. E. Cutcosky: *Phys. Rev.*, **95**, 1222 (1954).

([7]) J. Sawicki and I. Szymanski: *Bull. Acad. Pol. Sci.*, **5** (1957), in press.

The polarization of the associated e-electrons is:

$$(6) \qquad P_{e^-} = \frac{1}{D} \operatorname{Sp} \left\{ (i\gamma'_\mu q_\mu - m) \sum_r (\boldsymbol{\gamma e}^r) \frac{\boldsymbol{\sigma p}}{p} (m + \gamma_4 E - i(\boldsymbol{\gamma p})(\boldsymbol{\gamma e}^r) \cdot (i\gamma'_\sigma q_\sigma - m) N^{(i)} \right\},$$

the denominator D being the same as that in Eq. (1) (= [ ]).

The same eleven couplings $\hat{O}$ as in the previous section were used to calculate P_{e^-}. The results are:

$$(7) \qquad P_{e^-}(S(1)) = -\frac{(p^2 + \omega E)p \sin^2\theta + \omega^2 p - \omega^2 E \cos\theta}{(\omega + E)p^2 \sin^2\theta + E\omega^2\Theta} = \Pi,$$

$$(8) \qquad P_{e^-}(P_5(\gamma_5)) = P_{e^-}(T(\boldsymbol{\sigma})) = \Pi = -P_{e^-}(V(\gamma_4)) = -P_{e^-}(A(\boldsymbol{\gamma}\gamma_5)),$$

$$(9) \qquad P_{e^-}(T(\boldsymbol{\alpha})) = -P_{e^-}(V(\boldsymbol{\gamma})) = -P_{e^-}(A(\gamma_4\gamma_5)) = \Pi.$$

From Eq. (2)-(5) and (7)-(9) it is seen that the polarizations both of the γ-rays and the electrons for all « pure » allowed and « source velocity » first forbidden transitions are the same in absolute values and differ only in sign. The S, Ps and T-polarizations are equal to P and Π for γ-rays and e^--electrons, respectively, while the V and A-polarizations are of the opposite sign. Only certain mixed couplings, higher order Coulomb corrections and « retardation » type forbidden couplings confuse this situation.

It follows from Eq. (2)-(5) that γ-rays are right (left) circularly polarized, if they accompany electrons (positrons) for the cases S, Ps, T and reversed for V and A. For all the discussed cases $P_\gamma \to 0$ for $\omega \to 0$. For small ω the « retardation » first forbidden transitions give:

$$(10) \qquad \begin{cases} P_\gamma(S(\boldsymbol{r})) = P_\gamma(P_5(\boldsymbol{r}\gamma_5)) \cong \dfrac{\omega(p^2 + q^2)}{E(p^2 + q^2) - \frac{2}{3}p^2 q}, \\ P_\gamma(V(\gamma_4 \bar{r})) \cong -\dfrac{\omega(p^2 + q^2)}{E(p^2 + q^2) + \frac{2}{3}p^2 q}. \end{cases}$$

Since for small ω: $P \cong \omega/E$, the difference between the « retardation » type polarization $P(S(\boldsymbol{r}))$ and P is positive and vanishing for $q = 0$. For small ω the polarizations P_γ are isotropic.

If we do not measure the (β, γ) coincidence, but only the electron polarization, we have to integrate over θ. The asymptotic expression for the integrated Π for small ω is:

$$(11) \qquad \Pi_{\text{int.}} \cong -\frac{p^2 + E\omega}{pE + p\omega}.$$

Hence we see that the bremsstrahlung effect tends to increase the effect of the electron polarization, quite independently of the coupling assumed.

On the Charge Distribution of the Nucleon.

Y. Nogami

Department of Physics, University of Osaka Prefecture - Sakai, Japan

(ricevuto il 7 Luglio 1957)

According to the recent experiments on the electron-neutron interaction and on the high energy electron-proton scattering, the mean square radii of the charge distribution of the proton and the neutron, except the Foldy terms, are found to be [1]

$$\langle r^2 \rangle_p = (0.77 \pm 0.10) \cdot l^2 ,$$

$$\langle r^2 \rangle_n = (0.00 \pm 0.08) \cdot l^2 ,$$

respectively. Here and henceforth

$$l = 10^{-13} \text{ cm} .$$

Pion-theoretical calculations of the charge distribution of the nucleon, especially with respect to the electron-neutron interaction, have been carried out by several authors, using the covariant perturbation method [2] and, recently, using the static cut-off theory [3]. The latter, with a reasonable coupling constant and a cut-off momentum, gives $\langle r^2 \rangle_p = -\langle r^2 \rangle_n \approx 0.3 \cdot l^2$, which is far from the experimental values [4]. The static theory associates only with the pion current. It is therefore necessary to examine the relativistic corrections and the nucleon current contribution. We examine these points using the covariant perturbation method combined with the cut-off method.

Applicability of the perturbation method to the pion-nucleon interaction is open to question. However, it was shown by Goto [5] that for the anomalous magnetic moment of the nucleon and for the γ-decay of the neutral pion the discrepancies between the results of the perturbation method and experiments are considerably diminished by using the cut-off method. On the other hand annoying behaviors of the propagation functions in the large momentum region have recently been pointed out [6]. These circumstances may indicate that the

(1) D. R. Yennie, M. M. Lévy and D. G. Ravenhall: *Rev. Mod. Phys.*, **29**, 144 (1957). In their notation these are $\langle r^2 \rangle_{1,p}$ and $\langle r^2 \rangle_{1,n}$ Earlier literatures on the electromagnetic structure of the nucleon are listed in this paper.

(2) B. D. Fried: *Phys. Rev.*, **88**, 1142 (1952).

(3) G. Salzman: *Phys. Rev.*, **99**, 973 (1955); **105**, 1076 (1957). S. B. Treiman and R. G. Sachs: *Phys. Rev.*, **103**, 435 (1956). F. Ando and H. Miyazawa: *Progr. Theor. Phys.*, **17**, 607 (1957).

(4) In the conventional way of expression of the electron-neutron interaction, this implies the potential strength of about -10 keV, whereas the experimental value is $+0.2 \sim -0.2$ keV.

(5) S. Goto: *Progr. Theor. Phys.*, **12**, 699 (1954).

(6) E.g., H. Lehmann: *Nuovo Cimento*, **11**, 342 (1954).

present cut-off method is an approximation of a correct theory and can be trusted semiquantitatively.

Now we divide $\langle r^2 \rangle_p$ and $\langle r^2 \rangle_n$ into two parts:

$$\langle r^2 \rangle_p = \langle r^2 \rangle_s + \langle r^2 \rangle_v ,$$

$$\langle r^2 \rangle_n = \langle r^2 \rangle_s - \langle r^2 \rangle_v .$$

Since the anomalous magnetic moment comes from the same diagrams as the charge distribution, it should be examined also in parallel. Then we write the anomalous magnetic moments of the proton and the neutron similarly:

$$\Delta\mu_p = \Delta\mu_s + \Delta\mu_v ,$$

$$\Delta\mu_n = \Delta\mu_s - \Delta\mu_v .$$

The terms with the indices s and v will be referred to as scalar and vector parts, respectively. The scalar part comes from the nucleon current. The vector part comes from both the nucleon and pion currents. The lowest order perturbation calculation in the pseudoscalar theory with the pseudoscalar coupling is readily performed. To cut-off the high momentum contributions of the virtual pion, we use Feynman's method ([7]). Namely, from the result calculated without cut-off, we subtract the corresponding quantity, but with the pion mass μ replaced by $(\mu^2 + \lambda^2)^{\frac{1}{2}}$. This procedure does not spoil the gauge invariance. In the static limit the pion current contribution to $\langle r^2 \rangle$ coincides with Salzman's result ([8]), with the coupling constant g replaced by $f(\mu/2M)$. M is the nucleon mass and f is the coupling constant of the pseudoscalar interaction.

Using the values of the masses $\mu = 273\, m_e$, $M = 1\,840\, m_e$, a coupling constant $f^2/4\pi = 0.08(2M/\mu)^2 = 14.6$, and a cut-off parameter $\lambda = M$, the results of calculations are listed in the first column of Table I. The results without cut-off are also shown in the parentheses. For the convenience of comparison the results of the static theory are quoted in Table II, where a coupling constant $g^2/4\pi = 0.08$, and a cut-off momentum is 6μ ([9]). Comparing these results, we see that relativistic corrections are remarkable and the pion current contribution to $\langle r^2 \rangle_v$ is considerably reduced compared, with the result of the static theory ([10]). The nucleon current is sensitive to the cut-off, while the pion current is not.

It may be expected that the higher order effects will improve the situation. At present, we have no reliable and feasible means to estimate the higher order effects. However, an approximate estimation will be given by supplementing an anomalous magnetic moment to the virtual nucleon ([11]). Namely, we further associate the Pauli term to the nucleon-photon vertex. For the anomalous magnetic moment of the virtual nucleon we substitute that of the real nucleon, i.e., $\Delta\mu_p = 1.79$ or $\Delta\mu_n = -1.91$ (nuclear magneton). The bulk of this effect appears as an isotopic vector, which is subtractive for $\langle r^2 \rangle_v$ and additive for $\Delta\mu_v$. The scalar parts are almost unchanged. In the static theory higher order corrections are also subtractive for $\langle r^2 \rangle_v$ and additive for $\Delta\mu_v$, and the order

([7]) R. P. Feynman: *Phys. Rev.*, **76**, 769 (1946).

([8]) This static limit does not include the Foldy term. Yennie *et al.* ([1]) inferred that non-relativistic theories are ambiguous in the treatment of the Foldy term. But, no ambiguity seems to arise in the actual procedure to take the non-relativistic limit.

([9]) For $\langle r^2 \rangle$, Treiman and Sachs, cited in ref. ([3]). For $\Delta\mu$, H. Miyazawa: *Phys. Rev.*, **101**, 1565 (1956). $\Delta\mu_v$ quoted here is Miyazawa's μ_1, which is the pion current contribution. $\Delta\mu$ was calculated also by S. Fubini: *Nuovo Cimento*, **3**, 1425 (1956).

([10]) Relativistic effects on the charge distribution have been independently investigated by Mr. K. Ishida: private communication.

([11]) M. Yamada: *Progr. Theor. Phys.*, **13**, 124 (1954). The charge distribution of the virtual nucleon gives no contribution in the perturbation of the lowest order with respect to the electromagnetic interaction.

TABLE I. – $\langle r^2\rangle_{s,v}$ *and* $\Delta\mu_{s,v}$ *in units of* l^2 *and nuclear magneton, respectively*

	Lowest order perturbation		Including Pauli term		Experimental value
$\langle r^2\rangle_s$	0.048	(0.108)	0.043	(0.095)	0.3
$\langle r^2\rangle_v$	0.190	(0.192)	0.149	(0.057)	0.3
$\Delta\mu_s$	− 0.64	(− 1.65)	− 0.60	(− 1.55)	− 0.06
$\Delta\mu_v$	1.31	(2.17)	1.70	(3.19)	1.85

of magnitude of the corrections is in agreement with our results. This agreement suggests that, for the higher order corrections of the vector parts, the present recipe will be not very wrong.

Owing to these corrections, agreement with the experiments becomes somewhat better for $\Delta\mu_v$, while it becomes far worse for $\langle r^2\rangle_v$. This dilemma would probably persist if a correct calculation could be done. As for the scalar part, though the experiment requires $\langle r^2\rangle_s \approx \langle r^2\rangle_v$,

TABLE II. – *The results of the static theory. The units are the same as in Table I.*

	Lowest order perturbation	with higher order correction
$\langle r^2\rangle_v$	0.383	0.309
$\Delta\mu_p$	1.80	2.05

it would be rather natural to expect that the theory gives $\langle r^2\rangle_s \ll \langle r^2\rangle_v$, because $M \gg \mu$. Thus it seems unlikely that a correct calculation would bring good agreement with the experiments for these quantities simultaneously.

One might conceive that the effect of the new particles is important. The effect on the anomalous magnetic moment was examined by ISO and IWAO [12]. We now briefly examine the charge distribution, confining the considerations to the virtual processes; $p \rightleftarrows \Sigma^+ + K^0$, $p \rightleftarrows \Sigma^0 + K^+$, and $n \rightleftarrows \Sigma^- + K^+$. Concerning the electron-neutron interaction SANDRI [13] has pointed out that the K-meson cloud cancels the pion cloud around the neutron. He estimated this by the static theory. But, because of the large mass of the K-meson, the relativistic effects are important and considerably reduce the contribution. In Table III the results of the lowest order covariant perturbation calculation are listed. $\langle r^2\rangle_K$ and $\langle r^2\rangle_\Sigma$ mean the K-meson and Σ-hyperon current contributions, respectively. The contribution to the proton is $\frac{1}{2}\langle r^2\rangle_K - \langle r^2\rangle_\Sigma$, and that to the neutron is $\langle r^2\rangle_K + \langle r^2\rangle_\Sigma$. The spins of the K-meson and the Σ-hyperon are assumed to be 0 and $\frac{1}{2}$, respectively. The (NΣK) interaction is assumed to be scalar or pseudoscalar coupling. The values of the masses of the K-meson and the Σ-hyperon are taken to be 966 m_e and 2330 m_e, the coupling constant $G^2/4\pi = 1$, and the

TABLE III.
$\langle r^2\rangle_K$ *and* $\langle r^2\rangle_\Sigma$ *in unit of* $10^{-4}\cdot l^2$.

	Scalar	Pseudoscalar
$\langle r^2\rangle_K$	94 (118)	18 (30)
$\langle r^2\rangle_\Sigma$	− 26 (− 72)	− 11 (− 46)

(12) C. ISO and S. IWAO: *Progr. Theor. Phys.*, **16**, 417 (1956).

(13) G. SANDRI: *Phys. Rev.*, **101**, 1616 (1956).

cut-off parameter $\lambda = M$. The values in the parentheses are the results obtained without cut-off. As for the coupling constant, it is estimated as $G^2/4\pi \approx 1$ from the K^+-p scattering ([14]), and as $2 \sim 3$ from the mass difference of the $\Sigma^{\pm}$ ([15]). At any rate $\langle r^2 \rangle_K$ and $\langle r^2 \rangle_\Sigma$ are of negligible magnitude in view of the extent of accuracy of the present calculation of the pion-nucleon interaction. Their contribution to the electron-neutron interaction is, in the conventional expression, at most several hundred eV. Effects of other possible processes, e.g. $p \rightleftarrows \Lambda + K^+$, are of the same order of magnitude, and do not alter this conclusion.

Thus, summarizing the preceding arguments, we may say that the electromagnetic structure of the nucleon will not satisfactorily be explained by the conventional theory of the pion-nucleon interaction. The effects of the new particles are too small to rescue the present discrepancies. As YENNIE *et al.* ([1]) discussed, this may require some deep-lying changes in the present formalism of the field theory, or indicate that the physical model used is wrong.

([14]) S. MIYACHI: *Progr. Theor. Phys.*, **1,7** 515 (1957).

([15]) E. C. G. SUDARSHAN and R. E. MARSHAK: *Phys. Rev.*, **104**, 267 (1957).

The Liquid Helium Bubble Chamber as Analyzer of Proton Polarization.

G. Jona Lasinio and G. C. Moneti

Istituto di Fisica dell'Università - Roma
Istituto Nazionale di Fisica Nucleare - Sezione di Roma e
Laboratori Nazionali di Frascati

(ricevuto il 31 Luglio 1957)

It is well known that the knowledge of the polarization of the products of nuclear reactions can yeld some information which cannot be obtained from measurements of the total and differential cross-section.

The standard method to detect the polarization of protons and neutrons consists in having them scattered by an analyzer nucleus and in measuring the ratio of the intensities scattered in two directions symmetrical relatively to the direction of the incident nucleons at a well-defined energy (1). This ratio is connected with the unknown nucleon polarization $\boldsymbol{P}_i$, by

$$\frac{I_+}{I_-} = \frac{1 + \boldsymbol{P}_i \cdot \boldsymbol{P}_0}{1 - \boldsymbol{P}_i \cdot \boldsymbol{P}_0},$$

where $\boldsymbol{P}_0$ is the polarization induced by the nucleus analyzer (supposed to have 0 spin) on unpolarized nucleons (2).

Several experiments have been performed using ^{4}He as nucleus analyzer since $\boldsymbol{P}_0$ for this nucleus can be calculated from the phase-shifts which are now well known in the low energy range (3). Since $\boldsymbol{P}_0$ is a rapidly varying function of incident nucleons energy and of scattering angle, in this kind of experiments it was necessary to have incident nucleons strictly collimated and of well defined energy. For this

(1) See for instance L. Marshall and J. Marshall: *Phys. Rev.*, **98**, 1398 (1955); M. J. Brinkworth and B. Rose: *Nuovo Cimento*, **3**, 195 (1956).

(2) See for instance L. Wolfenstein: *Phys. Rev.*, **75**, 1664 (1949); J. V. Lepore: *Phys. Rev.*, **79**, 137 (1950).

(3) G. Freier, E. Lampi, W. Sleator and J. H. Williams: *Phys. Rev.*, **75**, 1345 (1949); C. L. Critchfield and D. C. Dodder: *Phys. Rev.*, **76**, 602 (1949); C. H. Braden: *Phys. Rev.*, **84**, 762 (1951); W. E. Kreger, W. Jentschke and P. G. Kruger: *Phys. Rev.*, **93**, 837 (1954); T. M. Putnam: *Phys. Rev.*, **87**, 932 (1952); R. G. Freemantle, T. Grotdal, W. M. Gibson, R. McKeague, D. J. Prowse and J. Rotblat: *Phil. Mag.*, **45**, 1090 (1954); B. Cork and W. Hartsough: *Phys. Rev.*, **96**, 1267 (1954); I. I. Levintov, A. V. Miller and V. N. Shamshev: *Nucl. Phys.*, **3**, 221 (1957).

reason only a very small fraction of the polarized nucleons produced in the nuclear reaction under study is used. This fact represents a limitation for this type of experiments when the number of polarized nucleons produced per unit of time is very low. This is the case, for instance, of all reactions induced by pions and γ-rays.

We want to suggest here a method for analyzing polarized protons for which no such limitation should exist and which presents additional advantages. If indeed the protons to be analyzed are scattered in a liquid helium bubble chamber (*) the collimation of the beam is by no means necessary, the analysis of each event being performed independently from the scattering angle and energy. Besides for the p-^{4}He scattering almost the whole solid angle is useful and a broad energy range can be exploited. Let us now develop these points quantitatively.

* * *

As a basis for our discussion we have considered the recoil protons from $\pi^+ + p$ scattering for π^+ of 165 MeV in the laboratory system. It is well known that even a rough polarization measurement should allow to distinguish between Fermi phase shifts and Yang phase shifts ([4]). Besides if we consider the formula giving the polarization of recoil protons as a function of the π^+ scattering angle in the centre of mass system:

$$P_i(\theta) = -\frac{4 \sin\theta \sin(\alpha_{33} - \alpha_{31}) \{\sin\alpha_3 \sin(\alpha_{33} + \alpha_{31} - \alpha_3) + 3\cos\theta \sin\alpha_{33} \sin\alpha_{31}\}}{a + b\cos\theta + c\cos^2\theta},$$

it is easy to realize that even a 50% measurement of this polarization for convenient scattering angles leads to a measurement of α_{31} with less than 10% error, which precision is far from being approached when this phase is deduced from cross-section measurements. The liquid helium bubble chamber, under development at the Rome University will be used also for performing said measurement, and the geometrical data, that will come in afterwards, refer to said bubble chamber. Our aim is here to evaluate whether the time that would be required for such an experiment is reasonably short and the number of photographs reasonably low.

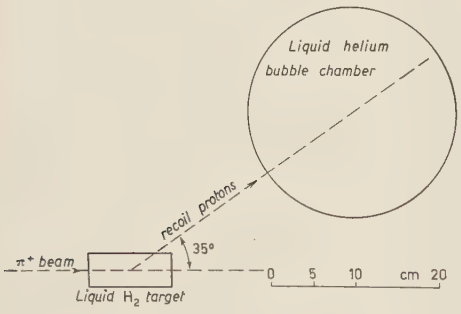

Fig. 1.

* * *

To visualize the idea let us now consider an experimental setting as shown in Fig. 1.

The beam of π^+ strikes a liquid Hydrogen cylindrical target having the axis parallel to the beam, the target being about 4 cm in diameter and 10 cm in length. By said dimensions the beam of π^+ may be fully employed while reducing to a minimum the energy loss

(*) Liquid helium bubble chambers have been constructed at the Duke University. A small experimental bubble chamber has been constructed at the Rome University where a larger liquid helium bubble chamber of about 6 litres is now at the study.

([4]) E. FERMI: *Phys. Rev.*, **91**, 947 (1953).

of the protons in the liquid H. The liquid helium bubble chamber supposed to be cylindrical, 25 cm diameter and 12 cm depth, would be placed at about 20 cm from the target. This short distance between the target and the bubble chamber implies a special design for both, but the short distance is necessary to assure that the bubble chamber receives the recoil protons emitted inside the maximum possible solid angle.

With the disposition shown into the bubble chamber are received at least all the protons emitted between 25° and 45°, which correspond to scattering angles of the π^+ between 90° and 130° in the center of mass system. The corresponding solid angle would be about .12 sr. By suitably calibrating the thickness to be passed over by the protons (the equivalent of about 2 mm of Al) things may be arranged so that their residual ranges when entering the useful space of the helium bubble chamber are between 6.4 and 26 cm of liquid helium. In this way all protons are stopped in the chamber. The energies of π^+ scattered in the same angular interval are found to be between 89 and 118 MeV, while the corresponding ranges are longer than 1 m.

Let us suppose now that we are able to detect all scattering events in the bubble chamber in which the proton is left with a residual range not less than 1 mm at angles between 15° and 170° in the laboratory. With said hypothesis it is possible to calculate the probability of observing a double scattering event, with the proton scattered in the liquid helium between 5 and 10 MeV (energies less than 5 MeV cannot be utilized since the residual range of the scattered protons would be too small; on the other hand for energies greater than 10 MeV sufficient data are not yet available).

We maintain that 200 events are sufficient for a 25% measurement of P_i. This can be seen from the approximated formula giving the asimmetry in our case:

$$\frac{N + P_i(N_1 - N_2)}{N - P_i(N_1 - N_2)},$$

where P_i is the mean polarization of protons in the accepted angular interval and N, N_1, N_2 are defined as follows

$$N = \int_{5\ \mathrm{MeV}}^{10\ \mathrm{MeV}} \frac{\mathrm{d}x}{\mathrm{d}E}\,\mathrm{d}E \int_{\theta_{\min}}^{\theta_{\max}} \left(\frac{\mathrm{d}x}{\mathrm{d}\Omega}\right)_0 \sin\theta\,\mathrm{d}\theta\,,$$

$$N_1 = \int_{5\ \mathrm{MeV}}^{10\ \mathrm{MeV}} \frac{\mathrm{d}x}{\mathrm{d}E}\,\mathrm{d}E \int_{\theta_{\min}}^{\theta_{\mathrm{invers.}}} \left(\frac{\mathrm{d}\sigma}{\mathrm{d}\Omega}\right)_0 P_0 \sin\theta\,\mathrm{d}\theta\,, \qquad N_2 = \int_{5\ \mathrm{MeV}}^{10\ \mathrm{MeV}} \frac{\mathrm{d}x}{\mathrm{d}E}\,\mathrm{d}E \int_{\theta_{\mathrm{invers.}}}^{\theta_{\max}} \left(\frac{\mathrm{d}\sigma}{\mathrm{d}\Omega}\right)_0 P_0 \sin\theta\,\mathrm{d}\theta\,.$$

$\theta_{\min}$ and $\theta_{\max}$ are the minimum and maximum angles that can be detected and θ_{invers} is the angle at which P_0 changes its sign. $(\mathrm{d}\sigma/\mathrm{d}\Omega)_0$ is the differential cross-section for an unpolarized beam.

P_0, the polarization induced by ^{4}He on unpolarized protons, has been calculated by several authors in the energy range $E_p = 1 \div 10$ MeV (E_p = protons energy in the laboratory system) ([5]). Since recently it has been published a cross-sec-

([5]) L. Marshall and J. Marshall: loc. cit.; M. J. Brinkworth and B. Rose: loc. cit.; A. C. Juveland and W. Jentschke: *Zeits. f. Phys.*, **144**, 521 (1956).

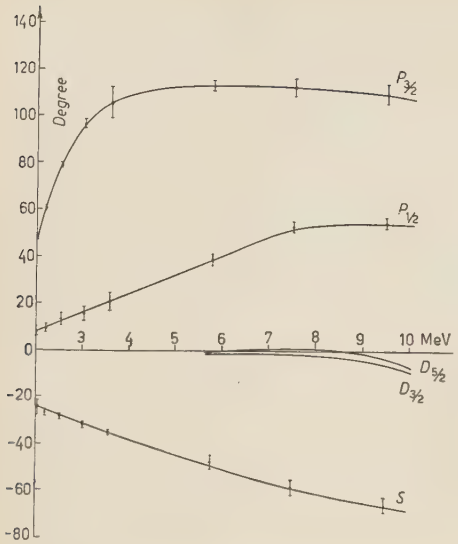

tion measurement improving considerably the information on phase shifts about 10 MeV ([6]), we have re-calculated $P_0(\theta)$ and $(d\sigma/d\Omega)_0$ in the interval between 5 and 10 MeV, after graphical interpolation of the phases taking in consideration this new measurement. For $E_p = 8$, 9, 10 MeV we have also included D phases. In Figs. 2, 3 and 4 we give our graphical interpolation of the phases and the curves from them obtained.

We have also calculated the polarization induced in the $\pi^+ + p$ scattering using the following figures for the two different phase types ([7]).

Fig. 2. – Graphical interpolation of $p + {}^4He$ scattering phase-shifts. ←

FERMI	$\alpha_3 = -20.0°$	$\alpha_{33} = 63.0°$	$\alpha_{31} = 3.7°$
YANG	$\alpha_3 = -19.0°$	$\alpha_{33} = 32.7°$	$\alpha_{31} = 94.2°$

Regarding to the pion flux that can be obtained from accelerating machines, it would appear that the CERN synchrocyclotron may supply a beam of π^+ considerably intense about the energy considered, namely of about 200 π^+/pulse distributed on a 2 sq. in. area.

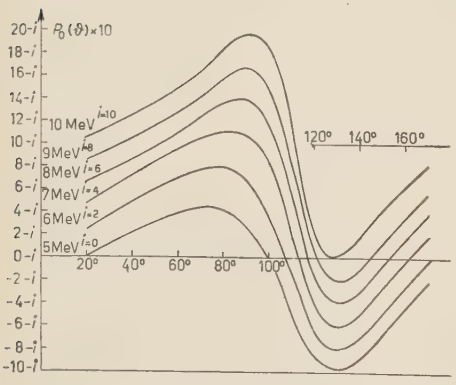

Fig. 3. – Polarization P_0 induced on protons by ${}^4He$ as function of scattering angle in center of mass system for $E_p = 5$, 6, 7, 8, 9, 10 MeV.

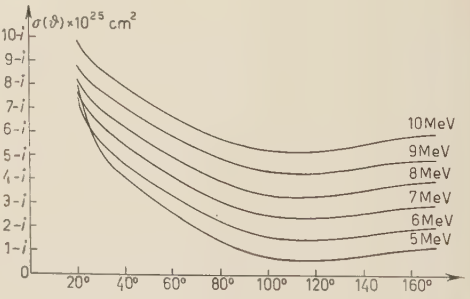

Fig. 4. – Differential cross-section for $p + {}^4He$ scattering for the same values of E_p.

([6]) T. M. PUTNAM, J. E. BROLLEY Jr. and L. ROSEN: *Phys. Rev.*, **104**, 1303 (1956).
([7]) The figures are taken from H. L. ANDERSON and M. GLICKSMAN: *Phys. Rev.*, **100**, 268 (1955).

Finally let us suppose—what looks reasonable—that the repetition time of the bubble chamber is one second.

With the above hypothesys we obtained:

Total number of double scattering events per unit of time . . .	$= .4 \cdot 10^{-3}$ events/s
Time necessary to detect 200 events	= 23 h
Number of photographs necessary to detect 200 events	= 83 000
$N =$	$2.03 \cdot 10^{-25}$ cm^3/rad
$N_1 =$	$-.69 \cdot 10^{-25}$ cm^3/rad
$N_2 =$	$.14 \cdot 10^{-25}$ cm^3/rad
Left - right asimmetry for Fermi phase-shifts	= 1.44
Left - right asimmetry for Yang phase-shifts	= 1/2.17

To distinguish between Fermi and Yang phase-shifts it is necessary to detect an asymmetry of $1.44 \cdot 2.17 = 3.12$.

From the above results it looks reasonable to draw the following conclusions:

1) The time of experiment necessary to detect 200 events in order to have a 25% measurement of P_i is not exceedingly long. Therefore the value of the pion flux available and the repetition time of the chamber are not critical.

2) The time of experiment given above can be greatly reduced by using $p+{}^4He$ scattering also at an energy greater than 10 MeV. Of course preliminary measurements are required to extend the knowledge of $p+{}^4He$ scattering at the energies higher than 10 MeV.

3) It is easily seen that if it were necessary to collimate the beam of protons to be analyzed the solid angle should be reduced at least by a factor 100. Therefore the time of experiment would be lengthened by a factor 100 under the same conditions of experiment.

4) The number of photographs to be scanned is rather high. This number could be considerably reduced with the camera operated by the coincidences between the recoil proton and the corresponding pion.

* * *

We wish to thank Prof. G. Morpurgo who first suggested this work. To him to Profs. G. Salvini and C. Franzinetti and Dr. E. Di Capua we are grateful for helpful advice.

Life Time Estimate of Λ^0 and θ^0 Particles.

C. Ballario (*), R. Bizzarri (+), B. Brunelli, A. De Marco (*), E. Di Capua, A. Michelini, G. C. Moneti, E. Zavattini (*) and A. Zichichi (+)

Istituto di Fisica dell'Università - Roma
Istituto Nazionale di Fisica Nucleare - Sezione di Roma

(ricevuto il 1° Agosto 1957)

Among about 30000 photographs taken at the « Laboratorio della Testa Grigia » (3500 m a.s.l.) with a multiplate cloud chamber triggered for penetrating showers (1), 115 V^0 events with a coplanar shower (×) have been found. In Fig. 1 the geometrical characteristics of the apparatus, most interesting in this paper, are shown.

For all these 115 events the angles between the two secondary tracks and between these and the line of flight of the V^0 have been measured, and the ionizations of the secondaries have been visually estimated; in some cases it has also been possible to have information about the range of one or both secondaries. All these measurements are in many cases sufficient to distinguish between the two decaying particles:

$$\Lambda^0 \to p + \pi^- + 37 \text{ MeV},$$

$$\theta^0 \to \pi^+ + \pi^- + 214 \text{ MeV}.$$

Neglecting the existence of other types of unstable neutral particles with a two body decay, it has been possible to classify our 115 V^0 particles as shown in Table I.

Table I.

Number of events	Identification
27	Λ^0
42	θ^0
38	Λ^0 or θ^0
8	neither Λ^0 nor θ^0

A detailed discussion of the selection criteria and of the methods of analysis will be published (2) later.

(*) Now at C.E.R.N., Geneva.

(+) Now at Enrico Fermi Institute for Nuclear Studies, University of Chicago.

(1) C. Ballario, B. Brunelli, A. De Marco and E. Zavattini: to be published in the *Nuovo Cimento*.

(×) The maximum non coplanarity angle admitted is 3°.

(2) G. Alexander, C. Ballario, R. Bizzarri, B. Brunelli, E. Di Capua, A. Michelini and G. C. Moneti: to be published on the *Nuovo Cimento*.

It is nevertheless convenient to make clear that for the lifetime estimate only V^0-decays have been considered which have the following properties:

1) The decay occurs in the « useful zone », i.e. in that zone of the V^0 line of flight in which the scanning efficiency can be assumed to be constant.

This zone has to be defined separately for each event because the scanning efficiency may be influenced by the presence of other tracks obscuring the vertex of the decay. In this connection it has been convenient to fix a fiducial region in the illuminated portion of the chamber.

This region has been defined, in each space between the plates, by the planes projecting, from the optical centers of the camera lenses, two horizontal straight lines which, on the front glass of the chamber, are distant 2 mm from the upper visibility limit, and 9 mm from the lower one, respectively.

In most cases this region defines the above mentioned « useful zone ».

It is worth noting that owing to the particular inclination of our plates, the minimum distance between the vertex of the V^0 and the plates is, under the above given conditions, always larger than 3 mm: we think that at such a distance there are neither reduction in the degree of supersaturation and illumination, nor appreciable distorsions. It is therefore practically impossible that in the « useful zone » a chance coincidence of two tracks mask a V^0 event.

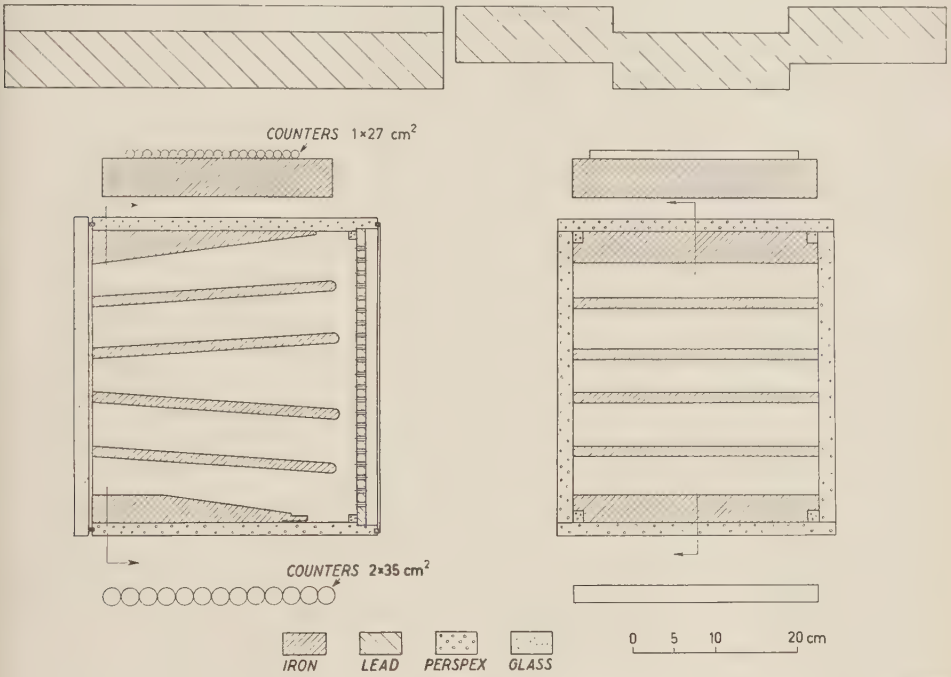

Fig. 1.

2) The associated shower originates in the iron plates and its origin is coplanar to the decay.

3) The nature is established unambiguously (some events have been excluded because in their interpretation an information about the range of one of the secondaries was essential, but the one we had was ambiguous).

With these above mentioned restrictions the number of Λ^0 and θ^0 given in Table I are reduced to 25 and 38 respectively.

For what regards the constance of the measurability conditions, each event has been analized following the suggestion given by NEWTH (3).

Our mean lifetime estimates are usual maximum likelihood estimates; to give the statistical errors the confidence intervals have been calculated following the method of Bartlett (4) for a multiplate chamber.

We obtain for 25 Λ^0 particles:

$$\tau_{\Lambda^0} = (2.14^{+.80}_{-.47}) \cdot 10^{-10} \text{ s}$$

and for 38 θ^0 particles:

$$\tau_{\theta^0} = (.92^{+.30}_{-.18}) \cdot 10^{-10} \text{ s} ,$$

where the errors are given with the usual confidence level of 32% (5).

To show the influence of the skewness correction on the confidence intervals we have calculated these intervals for the confidence level of 4.5%. We obtain for the Λ^0 particles with the correction $(1.29 \div 4.32) \cdot 10^{-10}$ sa nd without it $1.37 \div 4.67$; for the θ^0 particles with the correction $(.59 \div 1.74) \cdot 10^{-10}$ s and without it $(.62 \div 1.81) \cdot 10^{-10}$ s.

The errors in the lifetime due to momentum errors have been calculated using Bartlett's formula (3), but inserting in it, instead of the relative standard deviation of the momentum measurements, the mean relative maximum errors corresponding to our errors in the angular measurements.

Following this procedure we overestimated the mean lifetime errors; we obtain however:

$$\Delta\tau_{\Lambda^0} = .06 \cdot 10^{-10} \text{ s} ,$$

$$\Delta\tau_{\theta^0} = .01 \cdot 10^{-10} \text{ s} .$$

These errors are completely negligible compared with the statistical errors (6).

Concerning the errors due to the length measurements along the line of flight, relating to the effective and potential paths, it can be said that they are still smaller than those due to momentum errors (6).

* * *

Thanks are due to Dr. R. S. SALMERON for discussions.

(3) J. A. NEWTH: *Proc. Roy. Soc.*, A **221**, 406 (1954).

(4) M. S. BARTLETT: *Phil. Mag.*, **44**, 249, 1407 (1953).

(5) For a summary of earlier results and literature see: I. C. GUPTA, W. Y. CHANG and A. L. SNYDER: *Phys. Rev.*, **106**, 149 (1957).

(6) D. I. PAGE: *Phil. Mag.*, **45**, 863 (1954).

On Gauge Invariance of Second Kind.

B. Ferretti
CERN - Genève

(ricevuto il 2 Agosto 1957)

In a previous letter (1) about baryons conservation, I had the occasion to remark that gauge invariance of second kind seems to be not only a sufficient, but a necessary condition for the existence of local conservation laws expressed by the vanishing of the divergence of a four current.

As I became aware that this fact is not generally known, I think it not completely useless to give, together with the precise meaning, a brief proof of this statement.

We shall restrict ourselves to the cases in which the « matter » to which the current is due, is described by a fermion field only and we shall suppose therefore that in the four current are not contained time derivatives of the matter field.

It seems, however, likely that the theorem and the proof may be extended quite easily to the boson case.

Supposing then that we have any system in which a four fermionic current j_μ is defined with the property:

$$\partial j_\mu / \partial x_\mu = 0$$

and supposing that a Hamiltonian description of this system is possible, we do not change in any way, from the point of view of physics, our system if we add to the Lagrangian of the system itself the Lagrangian of a scalar, zero mass, not interacting field A. In fact we might even suppose that all physical states are vacuum with respect to the field A, and this condition will always be respected as A is not interacting.

Similarly, we do not change anything to our system if we further add to the Lagrangian a pseudo-interaction term of the form

$$\mathcal{L}' = j_\mu \frac{\partial A}{\partial x_\mu} .$$

In fact, as it is well known, this pseudo-interaction may be eliminated by means of canonical transformation *under the only condition*

$$\partial j_\mu / \partial x_\mu = 0$$

and does not represent any real interaction at all.

We now remark that for the modified system we may construct a first integral of the motion given by

$$\delta F = \int \delta \mathcal{F} \, \mathrm{d}\boldsymbol{x}$$

(1) B. Ferretti: *Nuovo Cimento*, **4**, 951 (1956).

where

$$\delta\mathcal{F} = i\alpha j_4 + \alpha\pi - \dot{\alpha}\Lambda\,,$$

π is the canonical conjugate to Λ, and α is an arbitrary infinitesimal function satisfying the d'Alembert equation and vanishing at infinity in the ordinary space.

In fact we have

$$\pi = \dot{\Lambda} - ij_4$$

and therefore

$$\delta\mathcal{F} = \alpha\dot{\Lambda} - \dot{\alpha}\Lambda\,.$$

It is then easy to verify that

$$\frac{\mathrm{d}}{\mathrm{d}t}\,\delta F = 0$$

keeping into account that

$$\Box\,\Lambda = \partial j_\mu / \partial x_\mu = 0\,.$$

But applying now a very well known general theorem, we can construct the group of transformations which is generated by the first integral of the motion δF and we know that the equations of motion are invariant for this group of transformations. It is now easily seen that this group of transformations is just the second kind gauge group.

We have shown therefore that under the only condition $\partial j_\mu/\partial x_\mu = 0$ is it possible to describe the given physical system without changing at all its physical properties, in such a way that the resulting equation of motion admits the second kind gauge invariance.

In this sense we may state that the second kind gauge invariance is a necessary condition for the local conservation law. This property is due to the fact that the local conservation laws allow the construction of an infinite number of first integrals of motion which, on the other hand, could be easily connected with an integral expression of the charge conservation law itself.

On the Conservation of Lepton Number.

B. Ferretti
CERN - Geneva

(ricevuto il 2 Agosto 1957)

Pauli has shown recently [1] that in the case in which one considers only interactions between leptons and nucleons, the conservation law for light particles is independent from the other invariance properties of the theory of weak interactions and depends only from certain expressions of the second degree in the coupling constants which are invariant with respect to a canonical transformation which may mix the neutrino and anti-neutrino states.

It is now possible to show that this theorem of Pauli holds even in the case in which one considers not only the lepton-nucleon interaction, but the interaction which leads to the μ decay.

Due to the existence of the canonical transformation of Pauli, it is convenient to eliminate the neutrino from the statement of the leptonic charge conservation law limiting this statement to the case in which there are no neutrinos in the initial and final states.

One has then in general to consider «a priori» two cases even in the hypothesis that the law holds:

a) μ^+ and e^+ of the same leptonic charge;

b) μ^+ and e^- of the same leptonic charge.

If we indicate with $p_{(NNe^-e^-)}$ the probability of the process $NN \to NNe^-e^-$ describing the emission of two electrons and no neutrinos by two nucleons, and similarly with $p_{\mu^\pm\mu^\pm e^\pm e^\pm}$ the probability of the process $\mu^\pm\mu^\pm \to e^\pm e^\pm$, indicating the annihilation of two muons with emission of two electrons only, a set of necessary and sufficient conditions for leptons charge conservation is given by the following relation:

$$\alpha) \quad p_{(NNe^-e^-)} = p_{(PPe^+e^+)} = 0$$

$$\beta) \quad p_{(NN\mu^-\mu^-)} = \ldots = 0$$

$$\gamma) \quad p_{(\mu^\pm\mu^\pm e^\pm e^\pm)}\, p_{(NNe^\pm\mu^\pm)} = 0$$

$$\delta) \quad p_{(NNe^\pm\mu^\pm)}\, p_{(NNe^\pm\mu^\mp)} = 0 .$$

For the condition γ) one has to study:

$$p_{(\mu^\pm\mu^\pm e^\pm e^\pm)}$$

which is related to the μ decay process. For this purpose one may write the interaction which leads to the decay of μ in the following manner:

$$H_\mu = \sum i_{q'q''p} (iq'q''p) \cdot$$

$$\cdot (\bar{\nu}^{(q')} 0_i \mu)(\bar{\nu}^{(q'')} \gamma_p 0_i \psi) + \text{h.c.} ,$$

[1] W. Pauli: *Nuovo Cimento*, **6**, 204 (1957).

where

$$\nu^{(1)} = \nu$$

(neutrino field function)

$$\nu^{(2)} = \nu^c$$

$$p = \begin{cases} + \\ - \end{cases}$$

$$\gamma_+ = 1$$

$$\gamma_- \quad \gamma^5 .$$

It is possible to show now that the interaction constant $(iq'q''p)$ may be expressed by means of quantities which transform in a simple way with respect to the canonical group of transformations of Pauli. One has in fact:

$$(i+) = \tfrac{1}{4}\,(S_i - (-1)^{q''} R_i \; - \\ - (-1)^{q'} B_i + (-1)^{q'+q''} A_i)$$

$$(i-) = \tfrac{3}{4}\,(S_i + (-1)^{q''} R_i \; \cdot \\ - (-1)^{q'} B_i - (-1)^{q'+q''} A_i)$$

where

$S_{q'q''}$	transforms	as	$F_{q'}F_{q''}$
$A_{q'q''}$	»	»	$G_{q'}G_{q''}$
$R_{q'q''}$	»	»	$F_{q'}G_{q''}$
$B_{q'q''}$	»	»	$G_{q'}F_{q''}$

(F and G are the quantities already considered by Pauli) and furthermore if:

$$\boldsymbol{i} = (15)(24)i$$

one has:

$$S_i = S_{\boldsymbol{i}}$$

$$A_i = A_{\boldsymbol{i}}$$

$$R_i = \quad R_{\boldsymbol{i}}$$

$$B_i = -B_{\boldsymbol{i}} .$$

One may then put:

$$S_{q'q''} = K^{\mathrm{I}}_{q'} F^{\mathrm{I}}_{sq''} + K^{\mathrm{II}}_{q'} F^{\mathrm{II}}_{sq''}$$

$$A_{q'q''} = L^{\mathrm{I}}_{q'} G^{\mathrm{I}}_{aq''} + L^{\mathrm{II}}_{q'} G^{\mathrm{II}}_{aq''}$$

$$R_{q'q''} = K^{\mathrm{I}}_{q'} G^{\mathrm{I}}_{rq'} + K^{\mathrm{II}}_{q'} G^{\mathrm{II}}_{rq''}$$

$$B_{q'q''} = L^{\mathrm{I}}_{q'} F^{\mathrm{I}}_{gq''} + L^{\mathrm{II}}_{q'} F^{\mathrm{II}}_{bq''} .$$

where K^{I} and K^{II} transform as F, L^{I} and L^{II} transform as G, are independent from i, and in a certain frame of the neutrino–anti-neutrino space have the components:

$$\begin{cases} K^{\mathrm{I}}_1 = 1 \\ K^{\mathrm{I}}_2 = 0 \end{cases} \quad \begin{cases} K^{\mathrm{II}}_1 = 0 \\ K^{\mathrm{II}}_2 = 1 \end{cases} \quad \begin{cases} L^{\mathrm{I}}_1 = 1 \\ L^{\mathrm{I}}_2 = 0 \end{cases} \quad \begin{cases} L^{\mathrm{II}}_1 = 0 \\ L^{\mathrm{II}}_2 = 1 \end{cases}$$

It is then possible to form all the invariants with respect to the Pauli transformation group from which

$$\mathrm{p}_{(\mu^{\pm}\mu^{\pm}\mathrm{e}^{\pm}\mathrm{e}^{\pm})}$$

may depend (absolute or relative invariant).

This is possible in an easy manner, noting that any relative invariant of the full group of Pauli must be an absolute invariant of the sub-group (I) of Pauli and, on the other hand, a typical integrity basis for the invariants of such a group may be found exactly as for the uni-modular group and is

$$(F^*F) = F^*_1 F_1 + F^*_2 F_2$$

and

$$(F' \wedge F'') = F'_1 F''_2 - F'_2 F''_1 .$$

One may proceed then exactly as in Pauli's paper and it is easy then to arrive to the conclusion which we have already stated.

* * *

I have the pleasure of thanking Professor W. Pauli for sending me a preprint of his paper on leptons conservation.

IL NUOVO CIMENTO Vol. VI, N. 4 1° Ottobre 1957

On the Existence of Large Intensity Modulations in the Spectra of Protons from Some Nuclear Reactions.

L. Colli

Laboratori CISE - Milano
Istituto Nazionale di Fisica Nucleare - Sezione di Milano

S. Micheletti

Istituto di Scienze Fisiche dell'Università - Milano
Istituto Nazionale di Fisica Nucleare - Sezione di Milano

(ricevuto il 4 Agosto 1957)

In the study of the energy spectrum of protons emitted in n, p reactions induced by neutrons of 14 MeV energy, we have found that some of the spectra show bumps or large peaks, as clearly seen in the case of Mg (n, p) ([1-3]), and Rh (n, p) ([4]).

This result being rather interesting, and since it seemed that some other mechanism than evaporation was involved in such reactions, we examined the spectra of particles, mainly protons emitted in nuclear reactions explained by a mechanism of the kind of direct interaction, as in the case of stripping (d, p) and inelastic proton scattering (pp'), at incident proton energies of the same order used by us in (n, p) reactions.

The purpose of this study was to see whether there is any evidence of the existence of large peaks in the spectra of the protons.

We shall first examine the results on d, p reactions.

In many experiments, the spectrum of protons coming from (d, p) reactions induced by deuterons having energies of a few MeV was measured with a magnetic spectrograph, an instrument of a very good resolution, so that all the proton groups corresponding to the excited levels of the residual nucleus are well separated.

By observing the intensity of the proton lines corresponding to the different levels it is easily noticed that some groups of lines are more strongly excited

([1]) C. Badoni, L. Colli and U. Facchini: *Nuovo Cimento*, **4**, 1618 (1956).

([2]) L. Colli and U. Facchini: *Nuovo Cimento*, **5**, 309 (1957).

([3]) L. Colli, U. Facchini and S. Micheletti: *Nuovo Cimento*, **5**, 502 (1957).

([4]) L. Colli, U. Facchini, G. Marcazzan, M. Pignanelli and A. Sona: to be published on the *Nuovo Cimento*.

so that the whole spectrum shows some kind of modulation in the intensity of the lines, in which the maxima are at a distance of about one MeV from each other. This effect may be easily seen in the proton spectra of Al (d, p) and Na (d, p) reactions shown in Fig. 1 and 2 ([5,6]).

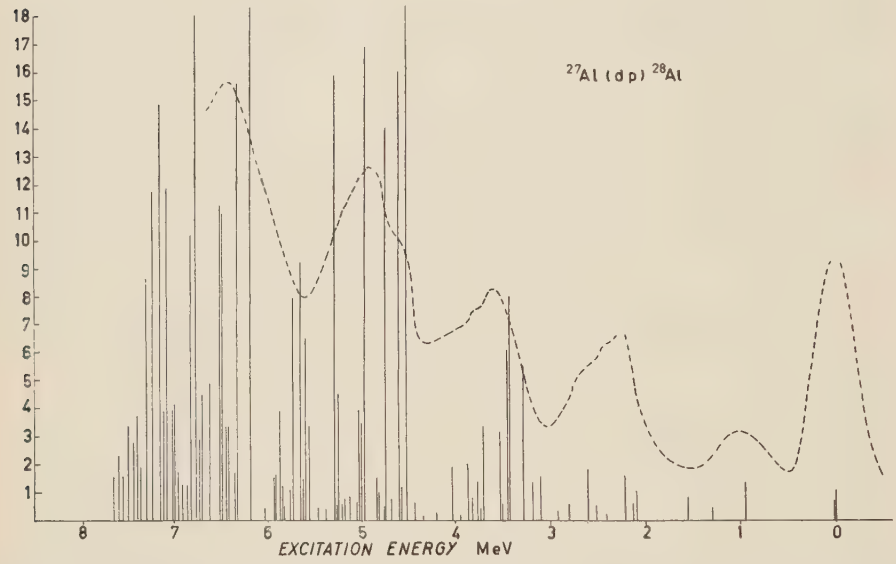

Fig. 1. – Schematic aspect of the proton spectrum from the ^{27}Al(d, p)^{28}Al reaction measured with a high-resolution magnetic spectrometer. The dashed curve shows the same spectrum measured with a counter.

It is quite obvious that when the proton spectrum is measured with an instrument of a lower resolving power than the magnetic spectrograph, such as a gas or scintillating counter, the result will be a spectrum with bumps or large peaks as it is indeed in the case of the Al (d, p) measurement done by GOVE ([7]) also reported in Fig. 1. Such spectra presenting large peaks and bumps, have been found more or less clearly in all the elements studied.

Particularly in the case of heavy nuclei measurements have always been done with the counter (bad resolution) technique. A very interesting group of measurements on proton spectra from (d, p) reactions have been done by HARWEY ([8]) for the three separated isotopes of lead and bismuth.

The spectra of all these elements show well defined large peaks at a distance of the order of 1 MeV or less from each other which are also clearly defined even for residual nucleus excitation energies of about 6÷7 MeV. One of these spectra is shown in Fig. 3.

These measurements have been done with deuteron energy of 14 MeV. Com-

([5]) W. W. BUECHNER, M. NAZARI and A. SPERDUTO: *Phys. Rev.*, **101**, 188 (1956).

([6]) A. SPERDUTO and W. W. BUECHNER: *Phys. Rev.*, **88**, 574 (1952).

([7]) H. E. GOVE: *Phys. Rev.*, **81**, 364 (1951).

([8]) J. A. HARVEY: *Canad. Journ. of Phys.*, **31**, 278 (1953).

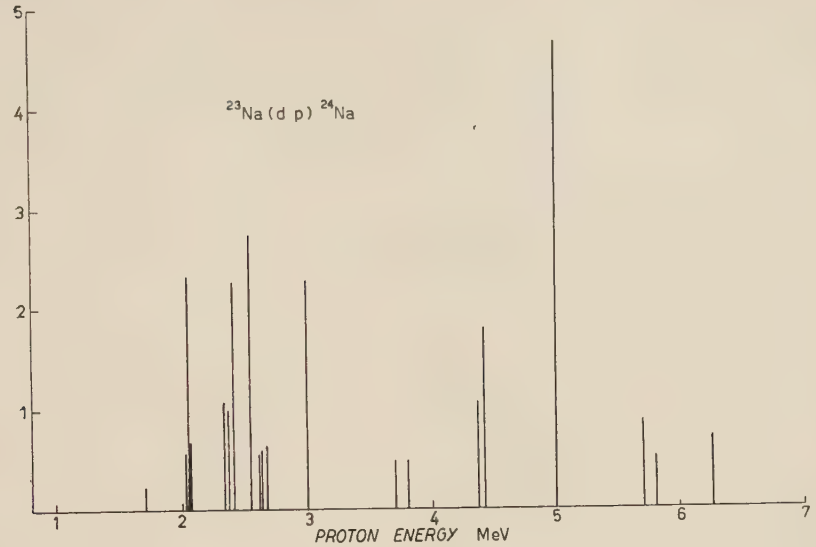

Fig. 2. – Schematic aspect of the proton spectrum from ^{23}Na(d, p)^{24}Na reaction measured with a high-resolution magnetic spectrometer.

Fig. 3. – A typical spectrum of a (d, p) reaction on a heavy element measured with a low-resolution spectrometer.

paring these results for heavy elements with those for light elements reported above it is easily shown that the peaks found in the spectra of lead cannot be explained as single levels of the residual nucleus, because it would be necessary in that case to assume that the level density of lead is much lower than that of aluminium, or that only a few levels of the residual nucleus are excited in (d, p) reactions on lead while most of them or all are excited in the (d, p) reaction on aluminium.

At this point therefore we draw the conclusion that the peaks shown in the spectra of protons from (d, p) reactions on heavy elements contain many nuclear levels and that they correspond to a modulation of the intensity of the excitation of residual nucleus levels, as shown in the light element spectra.

The measurements of (pp′) reactions done by GUGELOT [9] with 18 MeV protons and by COHEN [10] with 23 MeV protons show a pronounced forward asymmetry in the angular distribution particularly for the heavier nuclei; according to these results, it seems that such reactions involve some mechanism other that the compound nucleus evaporation.

These measurements, done by means of counters have shown the existence of peaks having about the same characteristics as found in the (d, p) reactions, in other words, they have distances on the energy scale of the same order of magnitude, they are rather large and are clearly defined even at rather high excitation energy of the residual nucleus.

Moreover, a measurement of (pp′) scattering on copper [11] done by means of the magnetic spectrograph, shows that in the place of the first bump of the spectrum given by COHEN there is a group of 5 lines. This measurement has been done at 6 MeV proton energy (Fig. 4).

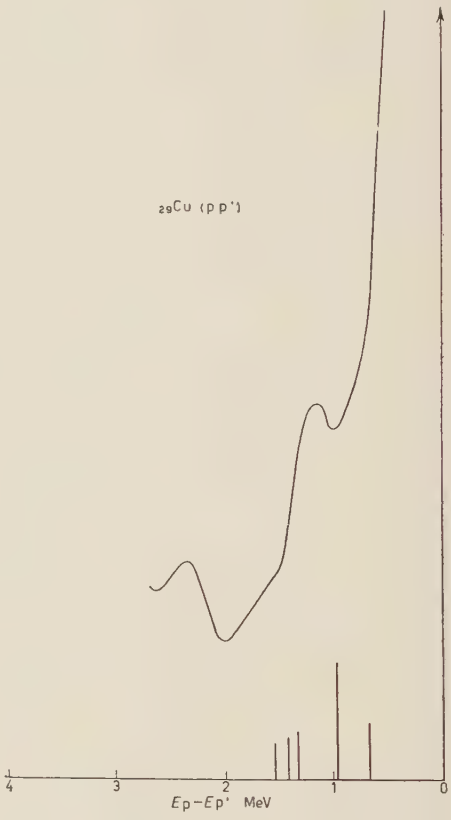

Fig. 4. – Comparrion between proton spectra of the ^{29}Cu(p, p′)^{29}Cu reaction measured with instruments of different resolution.

In view of the above considerations, all these peaks or bumps in proton spectra of heavy nuclei observed in (d, p) and (pp′) reactions can be looked upon as intensity modulations of the proton group corresponding to many levels of the residual nucleus, and not as proton groups from a single level.

It is very interesting to note that such intensity modulations seem to have simple regularities throughout the perio-

(9) P. C. GUGELOT: *Phys. Rev.*, **93**, 425 (1954).
(10) B. L. COHEN: *Phys. Rev.*, **105**, 1549 (1957).
(11) P. M. WINDHAM, C. R. GOSSET, G. C. CHILLIPS and T. E. YOUNG: *Phys. Rev.*, **103**, 1321 (1956).

dical system, as the experiments by COHEN show.

Moreover, in the case of the $^{23}Na(d, p)^{24}Na$ reaction, as it has been shown by BLOK ([12]) the two groups of lines correspond rather well on the energy scale of the residual nucleus excitation energy to the bumps that we found in the proton spectrum from the reaction $^{24}Mg(n, p)^{24}Na$. This is to be expected because these two reactions have the same residual nucleus.

At this stage it is not possible to give any interpretation of such intensity modulations in the proton spectra. Nevertheless the discovery of this effect could throw some light on the mechanism of nuclear reactions.

([12]) J. BLOK: private communication, and J. BLOK, C. C. JONKER: *Nuovo Cimento*, **6**, 378 (1957).

ERRATA-CORRIGE

S. NARANAN, P. V. RAMANAMURTY, A. B. SAHIAR and B. V. SREEKANTAN – **Interaction of μ-mesons Underground** (190 MeV): *Nuovo Cimento*, **5**, 1773 (1957).

Page	*Column*	*Line*	*Read*	*for*
1773	Title		190 MWE	190 MeV
»	1	1	workers ([1-12])	workers ([1,12])
»	1	6	10^{-30}	10^{-3}
»	2	3	10^{-29}	10^{-2}
1775	1	9	190 m w.e.	190 m e.w.

Parity Non Conservation and the $\Delta I = \frac{1}{2}$ Rule in Hyperon Decays.

C. Ceolin

Istituto di Fisica dell'Università - Padova
Istituto Nazionale di Fisica Nucleare - Sezione di Padova

(ricevuto il 12 Agosto 1957)

As is known in the Gell-Mann and Pais (1) scheme the decays of hyperons and heavy mesons are characterized by the selection rule $\Delta I = \pm\frac{1}{2}$ and $\Delta I_3 = \pm\frac{1}{2}$. Recent measurings (2) of the lifetime of the particles Σ^+ and Σ^- and the branching ratio $R_I = \mathrm{P}(\Sigma^+ \to \mathrm{P} + \pi^0)/\mathrm{P}(\Sigma^+ \to \mathrm{N} + \pi^+)$ give the value of about 1 for R_I and the value 2.3 for the ratio R_2 of the mean life. It is difficult to make these values agree with those calculated with the above rule. Many Authors, however, have suggested that this disagreement may be traced back to the parity non-conservation of the hyperon decay, similarly to what happens in processes involving neutrinos.

It has been believed to be of some interest to calculate the degree of parity non-conservation necessary to re-establish agreement with the experimental data. This calculation may be made without specifying the details of the interaction. In fact, according to Wentzel (3), the above selection rule may be considered as formally equivalent to the assumption that in every vertex, involving weak interaction, a spurious particle carrying isotopic spin $\frac{1}{2}$ is emitted and that the global interaction is charge-independent. Therefore, the wave functions for Σ^+ and Σ^- after the decay can be written as:

$$(1) \qquad Y_1^{\prime} = C^{\prime} a_{\frac{1}{2}} \chi_{\frac{1}{2}}^{\frac{1}{2}} S_{\frac{1}{2}}^{\frac{1}{2}} + C^{\prime\prime} a_{\frac{3}{2}} \chi_{\frac{3}{2}}^{\frac{1}{2}} S_{\frac{1}{2}}^{\frac{1}{2}}, \qquad Y_1^{-1} = C^{\prime\prime\prime} a_{\frac{3}{2}} \chi_{\frac{3}{2}}^{-\frac{3}{2}} S_{\frac{1}{2}}^{\frac{1}{2}},$$

where the C's are the Clebsch-Gordan coefficients, and the

$$\chi_{\frac{1}{2}}^{\frac{1}{2}} = -\sqrt{\tfrac{1}{3}}\mathrm{P}\pi^0 + \sqrt{\tfrac{2}{3}}\mathrm{N}\pi^+; \qquad \chi_{\frac{3}{2}}^{\frac{1}{2}} = \sqrt{\tfrac{2}{3}}\mathrm{P}\pi^0 + \sqrt{\tfrac{1}{3}}\mathrm{N}\pi^+; \qquad \chi_{\frac{3}{2}}^{-\frac{3}{2}} = \mathrm{N}\pi^-.$$

The a_1's are the decay amplitudes, and the spurious particle wave function $S_{\frac{1}{2}}^{\frac{1}{2}}$ will not be explicitely written down in the following formulas. According to Takeda, (4)

(1) M. Gell-Mann and A. Pais: *Procedings of the Glasgow Conference.*
(2) Alvarez and Rosenfeld: *Procedings of the Rochester Conference,* 1957.
(3) Wentzel: *Procedings of the Sixth Annual Rochester Conference.*
(4) Takeda: *Phys. Rev.,* **101,** 1547 (1956).

the a_I's are proportional to $\exp[i\delta_I]$, where the δ_I's are the pion-nucleon scattering phase shift, at pion energies corresponding to the Q-value of the hyperon.

If parity non-conservation in the hyperon decay occurs and if we assume the hyperon spin to be $\frac{1}{2}$, the pion can be created in S and in P state and therefore the phase shifts $\delta_{\frac{1}{2}}$; $\delta_{\frac{3}{2}}$; $\delta_{\frac{1}{2}1}$; $\delta_{\frac{3}{2}1}$ will come into the picture. Then, eq. (1) becomes:

$$Y_1' = -\sqrt{\frac{1}{3}}\left(\alpha_{\frac{1}{2}}\exp[i\delta_{\frac{1}{2}}]+\eta_{\frac{1}{2}}\alpha_{\frac{1}{2}}\exp[i\delta_{\frac{1}{2}1}]+\frac{1}{\sqrt{2}}\beta_{\frac{3}{2}}\exp[i\delta_{\frac{3}{2}}]+\frac{1}{\sqrt{2}}\eta_{\frac{3}{2}}\beta_{\frac{3}{2}}\exp[i\delta_{\frac{3}{2}1}]\right)\mathrm{P}\pi^0+$$

$$+\sqrt{\frac{1}{3}}\left(\sqrt{2}\,\alpha_{\frac{1}{2}}\exp[i\delta_{\frac{1}{2}}]+\sqrt{2}\,\eta_{\frac{1}{2}}\alpha_{\frac{1}{2}}\exp[i\delta_{\frac{1}{2}1}]-\frac{1}{2}\beta_{\frac{3}{2}}\exp[i\delta_{\frac{3}{2}}]-\frac{1}{2}\eta_{\frac{3}{2}}\beta_{\frac{3}{2}}\exp[i\delta_{\frac{3}{2}1}]\right)\mathrm{N}\pi^+,$$

$$Y_1^{-1} = -\frac{\sqrt{3}}{2}(\beta_{\frac{3}{2}}\exp[i\delta_{\frac{3}{2}}]+\eta_{\frac{3}{2}}\beta_{\frac{3}{2}}\exp[i\delta_{\frac{3}{2}1}])\mathrm{N}\pi^-,$$

where the degree of parity non-conservation is indicated by η_1.

In the simplifying hypothesis that $\eta_{\frac{1}{2}}^2=\eta_{\frac{3}{2}}^2=\eta^2$ it is easy to obtain for R_1 and R_2 the following expressions:

$$R_1 = \frac{\mathrm{P}(\Sigma^+\to \mathrm{P}+\pi^0)}{\mathrm{P}(\Sigma^-\to \mathrm{N}+\pi^+)} =$$

$$= \frac{\alpha_{\frac{1}{2}}^2(1+\eta^2)+\frac{1}{2}\beta_{\frac{3}{2}}^2(1+\delta^2)+\sqrt{2}\alpha_{\frac{1}{2}}\beta_{\frac{3}{2}}[\cos(\delta_{\frac{1}{2}}-\eta_{\frac{3}{2}})+\eta_{\frac{1}{2}}\eta_{\frac{3}{2}}\cos(\delta_{\frac{1}{2}1}-\delta_{\frac{3}{2}1})]}{2\alpha_{\frac{1}{2}}^2(1+\eta^2)+\frac{1}{4}\beta_{\frac{3}{2}}^2(1+\eta^2)-\sqrt{2}\alpha_{\frac{1}{2}}\beta_{\frac{3}{2}}[\cos(\delta_{\frac{1}{2}}-\delta_{\frac{3}{2}})+\eta_{\frac{1}{2}}\eta_{\frac{3}{2}}\cos(\delta_{\frac{1}{2}1}-\delta_{\frac{3}{2}1})]},$$

$$R_2 = \frac{\mathrm{P}(\Sigma^+\to \mathrm{P}+\pi^0)+\mathrm{P}(\Sigma^+\to \mathrm{N}+\pi^+)}{\mathrm{P}(\Sigma^-\to \mathrm{N}+\pi^-)} = \frac{4}{3}\frac{\alpha_{\frac{1}{2}}^2}{\beta_{\frac{3}{2}}^2}+\frac{1}{3}.$$

Therefore, in order to obtain the experimental values indicated above for R_1 an R_2 we must place $\eta^2=0.3$.

We observe that η^2 depends very critically on the experimental data and, as these are affected by an error of about 15%, the value of η^2 may vary considerably; in any case we may conclude that, if the lack of agreement between the experimental data and the selection rules of Gell-Mann and Pais must be attributed to a certain degree of parity non-conservation, this ought to be considerable and easily detected experimentally by measuring the angular distribution.

* * *

I wish to thank Prof. N. Dallaporta for useful discussions.

LIBRI RICEVUTI E RECENSIONI

Symposium du Cern sur la physique des mesons π, vol. II.

Il C.E.R.N. ha curato l'edizione di due eleganti volumi che raccolgono le comunicazioni presentate durante il Symposium tenutosi a Ginevra dall'11 al 23 Giugno 1956. Il primo volume è dedicato agli acceleratori di particelle elementari e il secondo per la massima parte alla fisica dei mesoni π.

Il II volume inizia colle comunicazioni relative alle tecniche di rivelazione: camere a bolle, camere di Wilson supercompresse, contatori Čerenkov, emulsioni nucleari.

Alcune comunicazioni forniscono risultati sperimentali sullo scattering nucleone-nucleone e nucleone-deutone intorno a 500 MeV di energia.

Le comunicazioni teoriche della fisica dei mesoni π sono centrate attorno alla teoria della dispersione e alla teoria della sorgente fissa per l'urto elastico pione-nucleone; speculazioni sulla struttura del nucleone sono state fatte in connessione alla produzione di mesoni π da parte di nucleoni veloci, alla bremsstrahlung di pioni veloci su nuclei, e allo scattering di elettroni su protoni.

La sezione sperimentale della fisica dei π presenta ulteriori risultati sperimentali dello scattering $\pi+p$ a bassissima energia e in prossimità della risonanza; interazione di mesoni π coi nuclei delle emulsioni nucleari; una nuova misura del rapporto di Panofsky e misure di raggi X ottenuti da atomi mesici.

La seconda metà del volume raccoglie le numerose comunicazioni relative alla fotoproduzione di mesoni su idrogeno, deuterio, e nuclei complessi; l'effetto Compton su protone oltre la soglia mesonica; e la produzione di mesoni nell'urto p-p e nell'urto di nucleoni su nuclei leggeri.

L'opera si presenta quindi molto interessante in quanto raccoglie risultati aggiornati fino alla prima metà del 1956.

A. Minguzzi

Handbuch der Physik, herausgegeben von S. Flügge. Band XXXV. Atome I, con 61 figure, Springer, 1957, pp. 1-454.

Questo volume dell'*Handbuch* contiene i seguenti articoli:

1) *The fundamental constants of physics* di E. R. Cohen e J. W. DuMond (pp. 1-87); 2) *Quantum mechanics of one and two electron systems* di H. A. Bethe e E. E. Salpeter (pp. 88-436).

Il primo articolo contiene un resoconto delle esperienze e dei metodi statistici per determinare le costanti fondamentali; viene presentata la situazione

nel 1955. Si può rilevare qui come negli ultimi dieci anni i metodi di risonanza sviluppati particolarmente alla Columbia University hanno raggiunto precisioni tali da influenzare in maniera sensibile la valutazione delle costanti fondamentali.

Il secondo articolo è una edizione completamente rifatta della rassegna di BETHE apparsa sul volume XXIV dell'*Handbuch* del 1933. Tale rassegna è stata sfrondata di molti dettagli attualmente sorpassati mentre sono stati inseriti un gran numero di risultati sperimentali nuovi e di metodi teorici recenti. Basterà notare qui il metodo di Foldy Wothuysen per passare al limite non relativistico dell'equazione di Dirac; i problemi delle correzioni radiative a vari processi (Lamb shift, momento magnetico dell'elettrone); il positronio e una trattazione molto estesa dell'atomo di elio.

L'articolo di BETHE e SALPETER ci sembra avere una duplice utilità; in primo luogo quella di articolo di consultazione dove si può trovare rapidamente una informazione necessaria; e d'altro canto la base per un organico corso di « esercitazioni » (in senso elevato) di meccanica quantistica.

G. MORPURGO

Handbuch der Physik, herausgegeben von S. FLÜGGE, Band XXXVI. Atome II, con 152 figure, Springer, 1956, pp. VI+424.

Questo volume dell'*Handbuch* contiene i seguenti articoli:

1) *Quantenmechanik der Atome* (HUND); 2) *Statistische Behandlung der Atome* (GOMBAS); 3) *Theory of Atomic Collisions* (MASSEY); 4) *Excitation and ionization of atoms by electron impact* (MASSEY).

Come indicato dai titoli i primi due sono scritti in tedesco, gli ultimi due in inglese. Cercheremo in quanto segue di dare un resoconto quanto più possibile completo del contenuto di ciascun articolo.

Il primo (pp 1-108) di HUND, contiene le basi quantistiche della descrizione degli atomi. Esso può dividersi essenzialmente in due parti: la prima è richiamo di meccanica atomica elementare ed occupa circa metà dell'articolo. La seconda, sebbene essa pure a carattere elementare descrive alquanto più in dettaglio i fondamenti della meccanica quantistica dei sistemi ad uno, due e più elettroni; con particolare riferimento a quelle proprietà che seguono da considerazioni generali di simmetria; in particolare viene esposta la teoria elementare di Hund dei caratteri di simmetria. Si tratta di un articolo generale di fisica ormai classica, dove i riferimenti bibliografici ad articoli posteriori al 1930 o 1935 sono rarissimi.

L'articolo di GOMBAS « La teoria statistica dell'atomo » (pp. 109-231) è più attuale, sebbene ormai classici ne siano i fondamenti. L'articolo segue abbastanza da vicino il ben noto libro dello stesso Gombas sull'argomento. Tuttavia mentre il libro è del 1949 l'articolo contiene una bibliografia aggiornata fino al 1955. Si noti che i riferimenti bibliografici ad articoli apparsi tra il 1949 e il 1955 sono oltre 200. L'articolo è particolarmente notevole in quanto fornisce un resoconto completo delle applicazioni che del metodo statistico sono state fatte, oltre che per gli atomi, anche per le molecole, i cristalli, e la materia sotto alte pressioni.

L'articolo di MASSEY « Teoria delle collisioni atomiche » (pp. 232-306) contiene una trattazione abbastanza moderna dei metodi che si usano per calcolare il problema di collisione di elettroni con atomi o molecole oppure di atomi con atomi. Naturalmente parte del materiale è quello ormai classico del trattato di Mott e Massey, ma parte è nuovo: ad es. la discussione della convergenza dell'approssimazione di Born, la causalità alla Wigner, e un lungo paragrafo

sui metodi variazionali, in particolare quelli di Hulthén, Kohn e Schwinger.

L'ultimo articolo infine (pp. 307-408) « Eccitazione e ionizzazione di atomi per urto di elettroni » contiene un resoconto dei risultati sulle sezioni d'urto per eccitazione e ionizzazione di atomi da parte di elettroni e dei metodi per determinarle. Tali sezioni d'urto vengono paragonate nei casi più semplici con le previsioni teoriche, facendo anche uso dei metodi sviluppati nell'articolo precedente. Infine in un paragrafo si mostrano le varie applicazioni ai fenomeni di scarica e ionizzazione nei gas, alla fisica della corona solare, ecc., che può avere la conoscenza delle sezioni d'urto per eccitazione.

G. Morpurgo

M. Born – *Physics in my generation.* 1 vol. in-16° di pp. 232. Pergamon Press, London-New York, 1956.

Si tratta di una raccolta di vari scritti divulgativi o di circostanza, pubblicati da Born tra il 1921 e il 1951, cioè in un periodo particolarmente « avventuroso » per la fisica. Tra la prefazione del volume sulla relatività einsteiniana e l'appendice di quello sul « Restless Universe », che costituiscono rispettivamente il primo e l'ultimo degli scritti qui riportati in ordine cronologico, vengono toccati gli argomenti che più spesso hanno costituito oggetto di accesi dibattiti intorno alla fisica moderna: dai riflessi filosofici della meccanica quantistica, della relatività e delle nuove cosmologie, alle conseguenze politiche e sociali dell'avvento dell'era atomica.

Sull'interpretazione statistica della funzione d'onda di Schrödinger, da Born stesso proposta nel 1926, egli fornisce interessanti dettagli storico-critici, che chiariscono il passaggio dai tentativi prima compiuti da lui e Wiener per rendere applicabile ai processi aperiodici il metodo delle matrici, a tale riuscita estensione dell'idea avuta da Einstein, di interpretare i quadrati delle ampiezze d'onda ottiche come densità di probabilità della presenza di fotoni.

Altri saggi di notevole valore didattico sono quelli dedicati a « Causa, fine ed economia nelle leggi di natura » (cioè ai principi di minimo e di massimo della meccanica analitica e della meccanica statistica), alle teorie statistiche di Einstein ed a varie questioni concettuali del genere di quelle trattate, in forma più approfondita, nel volume « Natural Philosophy of Cause and Chance », pubblicato da Born nel 1949.

V. Somenzi

L. Bieberbach – *Einführung in die Theorie der Differentialgleichungen im reellen Gebiet.* Die Grundlehren der matematischen Wissenschaften in Einzeldarstellungen, Band LXXXIII. Springer-Verlag, Berlin-Göttingen, Heidelberg, 1956, pagine 281 con 9 figure.

Questo volume consta di un'introduzione e di cinque paragrafi. L'introduzione ed il § 1 sono dedicati ai teoremi di esistenza e di unicità per il problema di Cauchy relativo ad un'equazione differenziale ordinaria o ad un sistema di tali equazioni. È usato dapprima il metodo delle approssimazioni successive e successivamente, con ampiezza di dettagli e di osservazioni critiche, il metodo di Cauchy-Lipschitz. Viene anche studiata la questione della dipendenza degli integrali dai valori iniziali e da parametri figuranti nell'equazione o nel sistema di equazioni. Complessivamente la trattazione segue gli indirizzi ormai classici, ma non mancano cenni o notizie su risultati recenti.

Il § 2 ha carattere elementare e contiene quelle nozioni sulle equazioni differenziali ordinarie che vengono esposte nei nostri corsi universitari del primo

biennio (equazioni del 1° ordine integrabili per quadrature, equazioni lineari, ecc.).

Nel § 3 sono studiate le equazioni differenziali ordinarie nelle quali non figura esplicitamente la variabile indipendente (*equazioni stazionarie*). Soprattutto si studia il sistema $dx/dt=f(x, y)$, $dy/dt=g(x, y)$ in relazione al comportamento delle *caratteristiche* (curve $x=x(t)$, $y=y(t)$ del piano xy) in prossimità di un *punto critico* (punto ove $f=g=0$). Dapprima si esamina il caso lineare $f = ax + by$, $g=cx+dy$ e si procede alla nota classificazione dei punti critici in nodi, colli, fuochi, centri; successivamente si passa al caso $f=ax+by+p(x, y)$, $g=cx+dy+q(x, y)$, con p, q infinitesimi per $x^2+y^2\to 0$, che viene studiato con grande accuratezza. Si considerano anche altri casi ed in particolare quello contemplato dal noto teorema di Bendixon. Segue una parte ove si accenna alla possibile esistenza di caratteristiche chiuse, dando in proposito interessanti esempi (equazioni di van der Pol, di Lièнard, ecc.). Questo § 3 si conclude con un breve studio di certe equazioni dette *quasi-stazionarie*.

Nel § 4 sono considerati i problemi ai limiti per le equazioni differenziali ordinarie. La maggior parte di esso concerne lo studio di tali problemi per le equazioni lineari del 2° ordine, che si svolge nell'indirizzo classico (teoremi di Sturm, esistenza degli autovalori e loro proprietà, comportamento asintotico delle autosoluzioni, ecc.). Sono inserite nel paragrafo stesso alcune altre questioni; per esempio nel § 4.2 viene studiato con una certa ampiezza il problema (non lineare) di Duffing e nel § 4.4 sono raccolti dei notevoli complementi sulle equazioni differenziali lineari del 2° ordine.

Il § 5 infine è dedicato alle equazioni a derivate parziali del primo ordine. Sono esposte le classiche teorie di Cauchy (delle caratteristiche) e di Lagrange (degli integrali completi), con cenni a questioni di carattere critico.

Da quanto precede risulta che il libro è redatto con scopi essenzialmente didattici. I paragrafi che più direttamente possono interessare le applicazioni fisiche o tecniche sono il terzo ed il quarto. La redazione è sempre molto chiara e precisa ed in essa non si fa mai ricorso a nozioni elevate; il volume riesce perciò di lettura attraente e di facile consultazione.

A. GHIZZETTI

Mechanism for Diffusion in Metals, fascicolo della « Series of Selected Papers in Physics », pubblicato a cura della Società Giapponese di Fisica (Physical Society of Japan, 1957).

In questo volume sono raccolti ventidue tra i più importanti articoli nel campo della diffusione nei metalli.

Un primo gruppo di articoli è a carattere prevalentemente teorico e concerne lo studio del meccanismo atomico di diffusione: potremmo dire che ne riassume la storia recente. I meccanismi di diffusione sono di tre tipi: scambio atomico diretto, migrazione interstiziale, migrazione dovuta a posti vacanti. Queste possibilità sono tutte prese in esame per il caso del Rame nel lavoro di HUNTINGTON e SEITZ del 1942. Gli autori concludono che il meccanismo di diffusione per posti vacanti è energeticamente favorito. Successivi lavori di HUNTINGTON sul Rame confermano questo punto di vista. La possibilità di diffusione ad anello (ring diffusion), avanzata da ZENER in un lavoro del 1950, viene studiata da SEITZ in un articolo successivo e viene dimostrata almeno poco probabile rispetto alla diffusione per posti vacanti. In un recente lavoro FUMI riesce a calcolare le energie di formazione di posti vacanti nei metalli nobili e nei metalli alcalini e a dare una stima delle energie di migrazione. I risultati ottenuti sono in accordo con i dati sperimentali e questo sembra indicare che la diffusione per posti vacanti è un fatto abbastanza

generale nei metalli. Nei successivi articoli di DIENES, HUNTINGTON, LE CLAIRE e SHEWMON e BECHTOLD si considera l'influenza dell'entropia di attivazione sul valore del coefficiente di diffusione.

Un secondo gruppo di articoli riguarda direttamente le misure sperimentali di coefficienti di diffusione con la tecnica dei traccianti radioattivi. Sono descritte in dettaglio misure di coefficienti di autodiffusione e della loro dipendenza dalla temperatura in Cu, Ag e Na. Il fenomeno della dipendenza del coefficiente di diffusione di un'impurità dal numero atomico della impurità stessa viene messo in evidenza e se ne tenta una spiegazione semiquantitativa. Tutti questi articoli appartengono ad un gruppo di ricercatori dell'Università dell'Illinois: LAZARUS, SLIFKIN, TOMIZUKA, BLATT ed altri. Un altro lavoro di interesse qui riprodotto è una comunicazione di SLICHTER su misure di coefficienti di diffusione in Na e Li con la tecnica della risonanza magnetica nucleare. Altri lavori ancora riguardano cambiamenti di volume e comparsa di porosità durante la diffusione, ossia l'effetto Kirkendall.

Concludendo, questo volumetto presenta una scelta molto equilibrata di articoli teorici e sperimentali; da essi ci si può formare un'idea accurata della situazione in questo campo della fisica dei solidi e se ne possono prevedere ulteriori importanti sviluppi.

F. BASSANI

Direttore responsabile: G. POLVANI

Tipografia Compositori - Bologna

Questo fascicolo è stato licenziato dai torchi il 28-IX-1957